CHANGES TO THE INNERVATION OF THE RAT UTERUS DURING PREGNANCY AND POST-PARTUM

Greta Jane Elizabeth Gnanamanickam

April 2015

A thesis submitted for the degree of Doctor of Philosophy

Cardiovascular Neuroscience Group

Cardiovascular Medicine and Centre for Neuroscience

Flinders University of South Australia

Declaration

I certify that this thesis does not incorporate without acknowledgement any material previously submitted for a degree or diploma in any university; and that to the best of my knowledge and belief it does not contain any material previously published or written except where due reference is made in the text.

Greta J. E. Gnanamanickam

April 2015

Abstract

Pre-eclampsia is a hypertensive disorder affecting 5 to 8% of all pregnancies. One of the main characteristics of pre-eclampsia is a reduction in blood flow to the placenta and other maternal organs. Because sympathetic and parasympathetic nerves control blood vessel diameters, I examined the innervation of the uterus during pregnancy and post-partum using whole mount preparations. Whole mounts provide a complete picture of the innervation of all layers of the uterus compared to sections where only small samples can be studied. In my Master's thesis, I showed that uterine horns from rats at 20 day (E20) of a 21-22 day pregnancy have almost no sympathetic, parasympathetic or sensory nerves. In non-pregnant uterine horns, all uterine layers and uterine blood vessels receive significant sympathetic, parasympathetic and sensory innervation.

In this project, I examined and quantified the loss of uterine sympathetic, parasympathetic and sensory nerves during late pregnancy and their reappearance during the first 4 weeks after delivery. Immunoreactivity for tyrosine hydroxylase (TH) and neuropeptide Y (NPY) were used as markers for sympathetic nerves; vesicular acetylcholine transporter (VAChT), for parasympathetic nerves; and calcitonin gene-related peptide (CGRP), for sensory nerves. I assessed uterine horns from non-pregnant rats at oestrus, rats at pregnancy days E14, E16, E18 and E20 and rats at post-partum (P) days P1, P3, P5, P7, P10, P14 and P28.

In pregnant uterine horns, there was a steady decline in the density of TH-, NPY-, VAChT- and CGRP-immunoreactive axons as pregnancy progressed until innervation had almost completely disappeared near term. By E18, blood vessels were scarcely innervated. By E20 there were only rare axons around blood vessels

and virtually none deep in the endometrium or in the longitudinal muscle. Quantification using an unbiased stereological method showed that the density of TH-, CGRP- and VAChT-immunoreactive axons had decreased by over a 99.9% in the E20 uterus compared to the uterus at oestrus. Re-innervation began immediately after delivery; rare TH-, NPY-, VAChT- and CGRP-immunoreactive axons were present in uterine horns at P1. There was a steady increase in the number of TH, NPY, VAChT and CGRP-immunoreactive axons between P1 and P28. Axons with growth cones were abundant in P3 and P5 uterine horns; rare uterine axons still had growth cones at P28. The densities of uterine nerves at P28 were still lower than in the uterus at oestrus, indicating that even at 4 weeks post-partum uterine innervation had not returned to normal.

To investigate a possible mechanism underlying uterine innervation changes, I compared expression of microRNAs extracted from rat major pelvic ganglia (MPG), the source of uterine sympathetic and parasympathetic innervation from rats at oestrus, E20 pregnant rats and P5 and P14 post-partum rats. MicroRNA samples were analysed by microarrays and real time relative quantitation reverse transcription PCR. Expression levels of microRNAs in the intact MPG did not differ among any of the time points examined.

This thesis describes the time course of uterine sympathetic, parasympathetic and sensory denervation during pregnancy and re-innervation post-partum using whole mount preparations and presents the first reliable quantitative assessment of these changes. The molecular biological studies suggest that microRNAs from the MPG may not be involved in uterine innervation changes. The immunohistochemical data will provide a foundation for future studies on the involvement of uterine nerves in pre-eclampsia.

Acknowledgements

I would like to thank my supervisor, Professor Ida Llewellyn-Smith, for her support and assistance throughout this project and the previous years spent as a Masters student and as a research assistant in her laboratory. Thank you for being an inspiration and for your time, patience and the opportunities you have given me. I consider myself privileged to have learnt so much about the process of research under her supervision.

Thank you also to Associate Professor Nick Spencer for his support and help throughout my PhD. I am grateful to Dr. Michael Michael for giving me the opportunity to work on miRNAs in his lab and for his guidance and advice. I am also very grateful to Dr. Shahid Ullah for his time and help with the statistical analysis. Thank you also to the team of Biostatisticians from Flinders Centre for Epidemiology and Biostatistics in addition to Shahid, Dr. Susan Kim and Prof Richard Goodman for their advice on the best way to quantify the innervation of the uterus. Thanks to Mark van der Hoek and Rosalie Kenyon from the Adelaide Microarray centre for their assistance with the microarrays. I'm also grateful to Prof. Rainer Haberberger for his advice about miRNA experiments. Mr. David Summerhayes took the beautiful photographs of the whole mount preparations that was used for quantification and he also printed the final thesis figures, I'm thankful that he has made time whenever requested in spite of his busy schedule.

I would also like to thank Mr. Lee Travis who has always been available to help and is the master of finding MPGs. I am also grateful for members of Michael's lab, especially Ms. Letitia Pimlott and Dr. Karen Humphreys for their time and

advice. Thank you to members from the Department of Ophthalmology especially Dr. Veronika Bandara and Dr. Sarah Martin for their friendship and encouragement when times were tough. Thank you to Ms. Roxanne Collingwood, Kate, Jess and Leah from the School of Medicine Animal Facility for looking after my animals.

I am also grateful for my wonderful church family, those that gave me hugs, those that brought us chocolate and meals, those that prayed and everyone who was generally available to help. I couldn't have done this so far away from my own family without their constant encouragement. I am also grateful for my amazing family, my parents and parents-in-law for their love, support and encouragement. Especially grateful for my parents who decided to fund and encourage a young girl with dreams that were different to their own, thank you for believing in me all those years ago. And I'm also grateful for my lovely husband, for his love and encouragement especially in the last 4 years while trying to complete a PhD thesis himself. I couldn't have gotten so far without his support. I will miss our late night and weekend study dates. Finally I thank God for giving me this opportunity and the ability to complete it.

I am extremely grateful for all the people mentioned above for their support and help especially over the past 4 years. A PhD is a lot of work and I couldn't have made it without your support.

Table of Contents

List of Figures and Tables

Chapter 1

Introduction

1.1 ANATOMY OF THE UTERUS

1.1.1 General Features

In rodents and other mammalian species, the wall of the uterus contains three layers, the outer mesometrium, the intermediate myometrium and the inner endometrium (Figure 1.1; (Papka et al., 1985). A layer of longitudinal smooth muscle cells and a layer of circular smooth muscle cells comprise the myometrium (Figure 1.1); between these two smooth muscle layers, there is a layer of connective tissue that contains an extensive network of blood vessels. In rats, a thick bundle of longitudinal smooth muscle cells forms a ridge opposite to the mesometrium (Figure 1.2). This ridge of longitudinal muscle is called the linea uteri (Melton and Saldivar, 1967) and it has functional, pharmacological and morphologically properties that differ from the rest of the uterine smooth muscle (Borda et al., 1978). The inner circular smooth muscle layer of the myometrium abuts the endometrial layer (Latini et al., 2008; Zoubina and Smith, 2000), which acts as a lining for the myometrium (Jones and Lopez, 2006). The endometrium consists of two layers, the stratum functionalis and the stratum basalis. The stratum functionalis contains epithelial cells and uterine glands; blood vessels are concentrated in the stratum basalis. At its distal end, the uterus is connected to the ovary via the oviduct. At its proximal end, the uterus is continuous with the cervix as it passes through the pelvic wall. Supportive ligaments link the uterus, ovaries and cervix in humans (Jones and Lopez, 2006).

FIGURE 1.1: DIAGRAM OF A CROSS SECTION THROUGH A RODENT UTERUS SHOWING THE MAIN LAYERS

Diagram based on the mouse uterus. The diagram does not show the linea uteri, which is a thick band of longitudinal smooth muscle cells that lies opposite to the mesometrium. Uterine horns in rats have linea uteri. Whether or not mouse uterine horns have linea uteri is not known.

Modified from Finn & Porter. (1975)

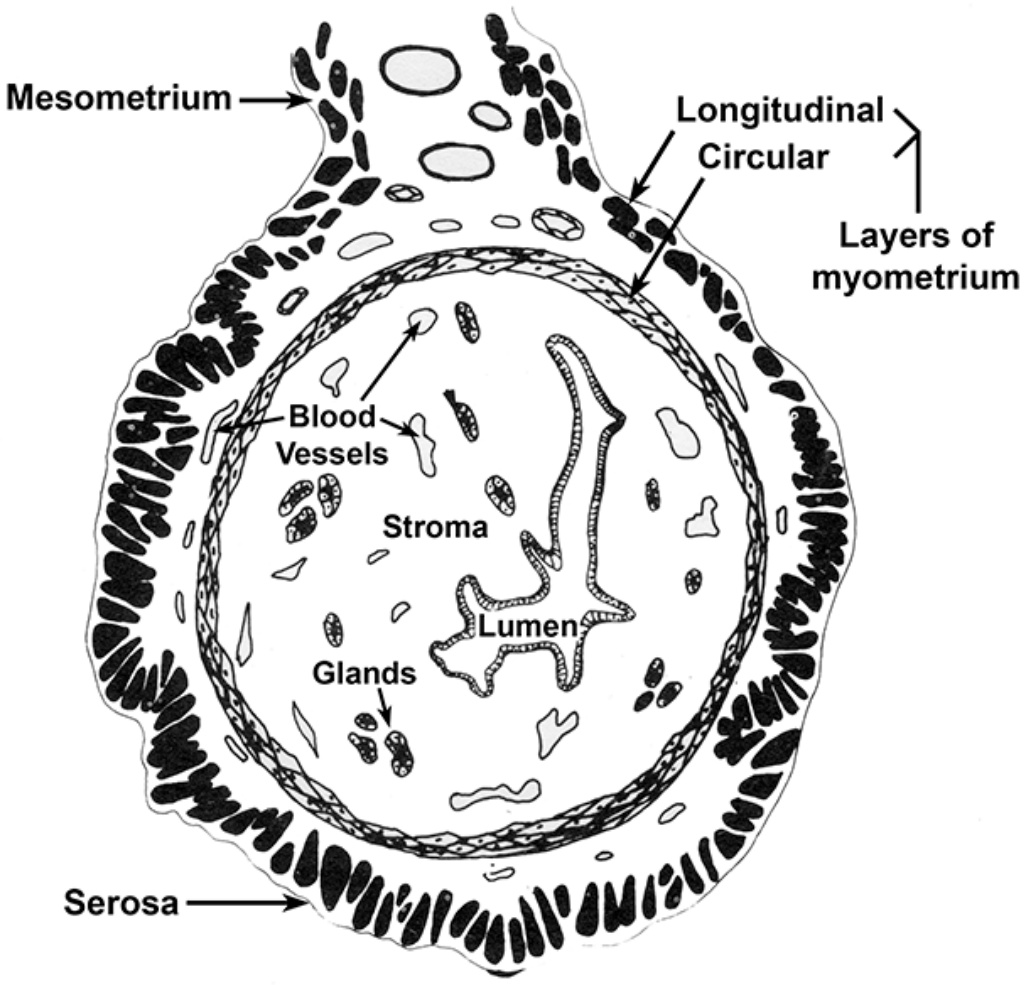
Mesometrium
Longitudinal
Circular
Layers of
myometrium
Blood
Vessels
Stroma
Lumen
Glands
Serosa

FIGURE 1.2: LINEA UTERI IN VIVO IN DIFFERENT RAT STRAINS

Linea uteri are visible to the naked eye in the non-pregnant uterus in all rat strains that have been examined. Linea uteri (arrows) occur opposite the mesometrium in Sprague Dawley (A), Fisher 344 (B) and Hooded Wistar (C) rats.

Reproduced from Gnanamanickam & Llewellyn-Smith. (2011)

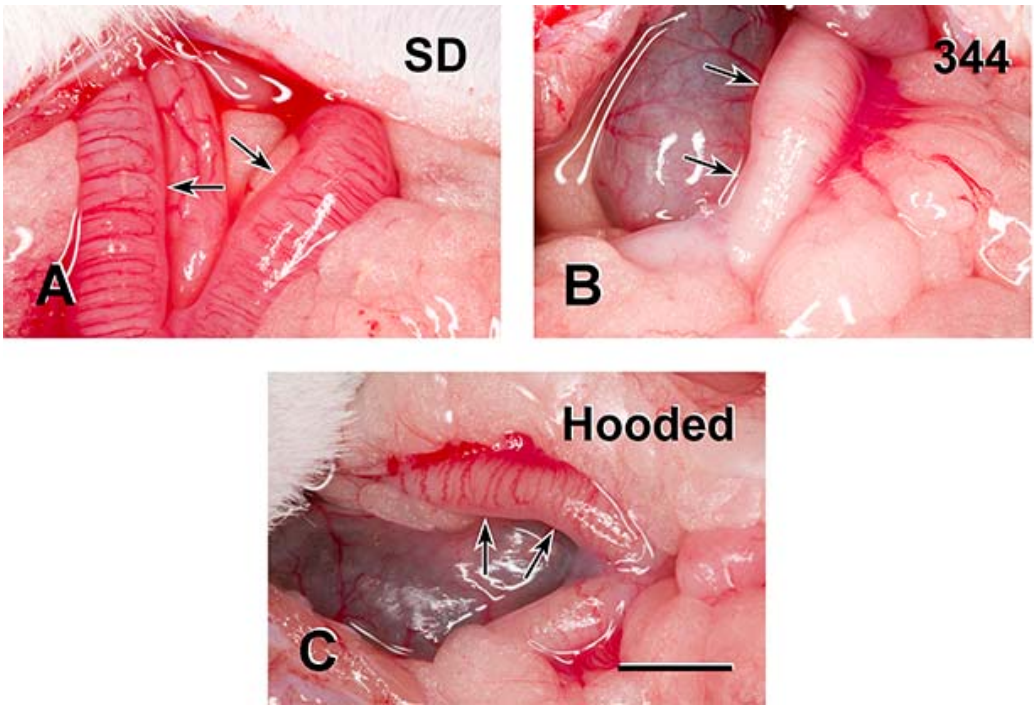
SD
A
344
B
Hooded
C

Blood vessels and nerves enter the uterus through a sheet of connective tissue called the mesometrium (also known as the broad ligament in humans).

1.2 FUNCTIONS, ORIGINS AND IDENTIFICATION OF NERVES THAT SUPPLY THE UTERUS

Sympathetic, parasympathetic and sensory nerves comprise the three types of nerves that are present in the non-pregnant uterus (Figure 1.3).

1.2.1 Sympathetic Nerves

Sympathetic post-ganglionic neurons synthesize and release the classical neurotransmitter, noradrenaline (NA), and the neuropeptide transmitter, neuropeptide Y (NPY) (Papka et al., 1996). Sympathetic nerves in the uterus regulate vasoconstriction and contraction of the myometrial smooth muscle. In the uterus, NA influences myometrial contractions and can either relax or contract the myometrium (Traurig and Papka, 1993). Both NA and NPY can also constrict blood vessels (Fried and Thoresen, 1990; Traurig and Papka, 1993). In the female reproductive system, NPY affects blood flow and contraction of the non-vascular uterine smooth muscle and is influenced by steroid hormones (Markiewicz et al., 2003; Papka et al., 1996). Although NPY can act as a vasoconstrictor along with NA (Traurig and Papka, 1993), NPY is also capable of vasodilation when released from parasympathetic nerves (Markiewicz et al., 2003).

Sympathetic post-ganglionic neurons that supply the uterus have been identified in the paracervical ganglia (Owman and Stjernquist, 1988), which lie between the uterine cervix and vagina (Papka et al., 1987). Sympathetic post-ganglionic neurons from the inferior mesenteric ganglia (Owman and Stjernquist,

1988; Papka et al., 1996), superior mesenteric ganglia (Vera et al., 1997) and suprarenal ganglia (Houdeau et al., 1998; Vera et al., 1997) also supply the uterus. Suprarenal ganglia and paravertebral sympathetic chain ganglia from T10 to L3 supply the ovarian region of the rat uterus while the cervical region of the uterus and the cervix is supplied by ganglia from T13 to S2 paravertebral sympathetic chain (Houdeau et al., 1998).

Originally, sympathetic nerves were detected with formaldehyde- or glyoxylic acid-induced fluorescence (Cowen and Burnstock, 1980; Falck et al., 1982; Tervo et al., 1978). Now, sympathetic nerves are usually visualized with immunohistochemistry either for tyrosine hydroxylase (TH), the rate-limiting enzyme in the biosynthesis of noradrenaline, for dopamine β hydroxylase (DβH), and another enzyme involved in the NA synthesis, or for NPY. However, NPY-immunoreactivity is also present in some parasympathetic nerves (Markiewicz et al., 2003) so NPY-immunoreactive axons in the uterus may be a mixed population of sympathetic and parasympathetic nerves.

1.2.2 Parasympathetic Nerves

All parasympathetic nerves release the classical neurotransmitter, acetylcholine (ACh). ACh is synthesized by the enzyme, choline acetyltransferase (ChAT), and then transported into synaptic vesicles by the vesicular acetylcholine transporter (VAChT) (Arvidsson et al., 1997). Parasympathetic nerves can cause uterine contractions and vasodilation (Traurig and Papka, 1993). ACh is a vasodilator and contracts the myometrium (Papka et al., 1999; Traurig and Papka, 1993). Uterine parasympathetic nerves also contain vasoactive intestinal peptide (VIP), a neuropeptide transmitter that promotes vasodilation (Traurig and Papka, 1993).

Parasympathetic nerves in the uterus also release the gaseous transmitter, nitric oxide (NO), which can relax vascular and non-vascular smooth muscle. NO is produced by the enzyme, nitric oxide synthase (NOS). In the uterus, there are three different types of NOS, inducible NOS (iNOS), vascular endothelial constitutive NOS (eNOS) and neuronal constitutive NOS (nNOS) or brain NOS (bNOS) (Bansal et al., 1997; Massmann et al., 1999; Norman et al., 1999; Riemer et al., 1997).

Like uterus-projecting sympathetic post-ganglionic neurons, parasympathetic post-ganglionic neurons that supply the uterus lie in the paracervical ganglia (Papka and Traurig, 1993). The dorsal motor vagal nucleus also provides parasympathetic innervation to the rat uterus through the vagus nerve (Ortega-Villalobos et al., 1990). Immunoreactivity for ChAT, VAChT, VIP and nNOS have been used to identify uterine parasympathetic nerves. The presence of ChAT- or VAChT-immunoreactivity, which occur only in cholinergic neurons, is the most reliable way to identify parasympathetic innervation. However, many of the antibodies directed against ChAT or VAChT stain peripheral cholinergic axons poorly or not at all so it is fortuitous when researchers find an anti-ChAT or anti-VAChT antibody that stains well. The lack of good antibodies that specifically mark cholinergic nerves in the periphery has meant that uterine parasympathetic axons have often been studied with immunohistochemistry for nNOS or histochemistry for NADPH-diaphorase. However, immunoreactivity for nNOS has been observed in neurons not only in the paracervical ganglia but also in dorsal root ganglia that supply sensory innervation to the uterus (Papka et al., 1995). Hence, nNOS-immunoreactivity and NADPH-diaphorase activity could be present not only in uterine parasympathetic but also uterine sensory nerves (Alm et al., 1995).

FIGURE 1.3: DIAGRAM OF THE NEUROANATOMY OF THE RAT UTERINE HORN

The diagram illustrates the general distribution of all classes of axons that innervate a rat uterine horn. The location and orientation of the mesometrial smooth muscle layers are also shown. The diagram was derived from whole mount preparations in which the wall of the uterine horn was cut open at the mesometrium and stretched flat.

Modified from Papka et al. (1985)

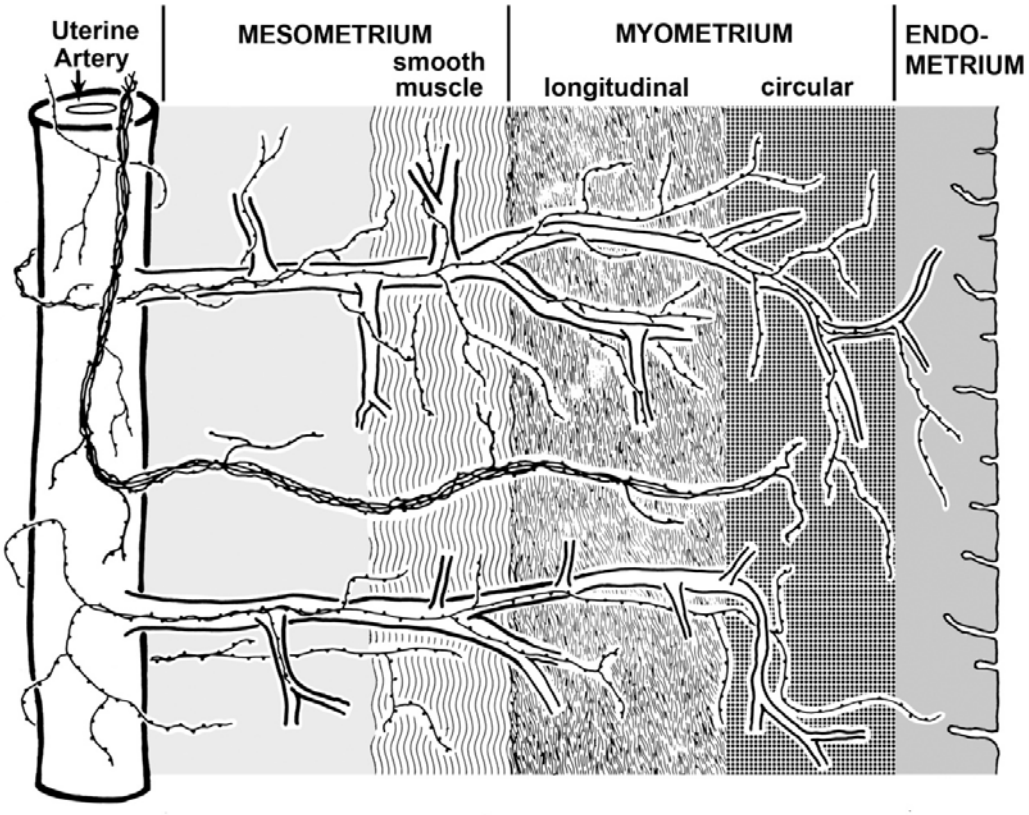
Uterine Artery
MESOMETRIUM
smooth muscle
MYOMETRIUM
longitudinal
circular
ENDO-METRIUM

NPY also occurs in some parasympathetic post-ganglionic neurons (Markiewicz et al., 2003) but is not a reliable marker for this nerve type because it is also synthesized by sympathetic post-ganglionic neurons. Acetylcholinesterase (AChE) staining has also been used to study uterine innervation. However, this method is not specific for parasympathetic axons because AChE is expressed not only by cholinergic neurons but also by non-cholinergic neurons. For example, the cell bodies and dendrite of sympathetic post-ganglionic neurons in the superior cervical ganglion (SCG) stain for AChE (Davis and Koelle, 1978).

1.2.3 Sensory Nerves

Sensory nerves relay information about sensory modalities (e.g., pain, mechanical stretch) from the uterus to the spinal cord (Traurig and Papka, 1993). Sensory neurons supplying the uterus contain the neuropeptide transmitters, calcitonin gene related peptide (CGRP) and substance P (SP). CGRP is known to be a vasodilator (Shew et al., 1990; Shew et al., 1991; Traurig and Papka, 1993) and also relaxes smooth muscle. CGRP also inhibits SP-stimulated contractions in the rat uterus (Shew et al., 1991). Like CGRP, SP contracts myometrial smooth muscle and promotes vasodilation (Traurig and Papka, 1993).

The uterus receives sensory innervation from the dorsal root ganglia (DRG) at thoracic segmental level 13 and lumbar segmental level 1 (Traurig et al., 1991).

Immunoreactivity for SP and CGRP have been used to study the sensory innervation of the uterus. As in other organs, CGRP and SP have been found to co-exist in uterine sensory nerves in both guinea-pigs and rats (Alm and Lundberg, 1988; Shew et al., 1991). Double immunofluorescent staining showed that all SP-immunoreactive axons in the uterus also contained CGRP but not all CGRP-

immunoreactive axons contained SP (Shew et al., 1991). nNOS-immunoreactivity also occurs in some DRG neurons that innervate the uterus. However, nNOS is not a specific marker for uterine sensory nerves because it also occurs in parasympathetic neurons that supply the uterus (Papka et al., 1995; Alm et al., 1995).

1.3 INNERVATION OF THE NON-PREGNANT UTERUS

1.3.1 Sympathetic Innervation of the Non-pregnant Uterus

1.3.1.1 Non-pregnant Rats

We have previously detailed the sympathetic innervation of the non-pregnant rat uterus using full-thickness whole mount preparations that were immunoperoxidase stained for TH (Gnanamanickam and Llewellyn-Smith, 2011), providing the most comprehensive analysis of uterine sympathetic innervation published to date. These whole mount preparations showed that varicose TH-immunoreactive axons entered the uterus along with blood vessels and that blood vessels were surrounded by dense plexuses of TH-positive axons. Many TH-immunoreactive axons ran parallel to the smooth muscle cells of the linea uteri and of the longitudinal and circular muscle layers. The linea uteri had more TH-immunoreactive axons than the rest of the smooth muscle. Rarely TH-immunoreactive axons were seen near uterine glands in the endometrium. Glyoxylic acid-induced catecholamine fluorescence reveals a similar distribution of sympathetic nerves (Papka et al., 1985). -Fluorescent NA nerves entered the rat uterus through the mesometrium, either unaccompanied or along with the arteries that supply the uterus. Significant numbers of NA axons also occurred around blood vessels in the mesometrium.

Although a subset of NPY-immunoreactive axons are likely to be parasympathetic (Markiewicz et al., 2003), immunoreactivity for NPY has often been used as a marker for sympathetic nerves. In our study on whole mount preparations (Gnanamanickam and Llewellyn-Smith, 2011), we found a significant number of NPY-immunoreactive axons in the non-pregnant rat uterus. The innervation was similar to the TH innervation of non-pregnant rat uterine horns, with extensive plexuses of NPY-immunoreactive axons occurring around blood vessels. Many NPY-immunoreactive axons were also present in the linea uteri and the longitudinal and circular smooth muscle layers. The linea uteri had more NPY-immunoreactive innervation than the rest of the smooth muscle. Many fine varicose axons were present at the base of the circular muscle layer, forming a circular muscle plexus similar to that seen in the gut (Christensen and Rick, 1987; Llewellyn-Smith et al., 1988). Sometimes NPY-immunoreactive axons occurred near uterine glands. In an earlier study using NPY immunohistochemistry, AChE histochemistry and glyoxylic acid-induced fluorescence (Papka et al., 1985), NPY-positive axons were found to have a similar density to AChE-positive nerves. Like NA nerves, NPY-immunoreactive axons entered the uterus either on their own or along with the arteries that supply the uterus. In the myometrium, NPY-containing axons followed the orientation of longitudinal and circular muscle cells and many NPY-immunoreactive axons were also found around blood vessels.

1.3.1.2 Non-pregnant guinea pigs

In the guinea pig uterus, nerves identified by catecholamine fluorescence were present in the longitudinal and circular muscle layers and around blood vessels. Fluorescent nerves were higher in density at the ovarian end of the uterine horn than

in the rest of the uterus (Thorbert et al., 1977). Many TH- and DβH- immunoreactive axons have also been found in the guinea pig uterus (Mitchell and Ahmed, 1992). Nerves immunoreactive for TH, DβH or NPY showed a similar distribution in the non-pregnant guinea pig uterus but there were more TH and DβH-positive axons than NPY-positive axons (Alm and Lundberg, 1988). Fine varicose TH-, DβH- and NPY-immunoreactive axons were found in the muscle layers, around blood vessels and sometimes following them deep into the endometrium (Alm and Lundberg, 1988).

1.3.1.3 Non-pregnant humans

In human uteri, many TH- and NPY-immunoreactive axons occur around blood vessels (Fried et al., 1986; 1986). Nerve bundles containing TH- and NPY-positive axons were also occasionally present in the human uterus (Fried et al., 1986). Formaldehyde-induced fluorescence showed nerves containing NA associated with both uterine vascular and non-vascular smooth muscle in humans (Owman et al., 1986).

1.3.1.4 Other species

In non-pregnant mares, TH-immunoreactive axons run parallel to the smooth muscle cells of the myometrium and alongside uterine blood vessels (Bae et al., 2001). More TH-positive axons were present in the myometrium than in the endometrium and sympathetic axons also occurred close to the endometrial glands (Bae et al., 2001). DβH-immunoreactive axons had a distribution similar to that of TH-immunoreactive axons (Bae et al., 2001). In mare uterus, NPY-immunoreactive axons were less dense than TH-immunoreactive axons, travelled parallel to circular and longitudinal

smooth muscle cells and were associated with blood vessels. More NPY-immunoreactive axons were seen in the myometrium than the endometrium. NPY-positive axons were also present near the endometrial glands (Bae et al., 2001).

The non-pregnant cat uterus also contains many catecholamine nerves identified using the Falck and Hillarp method. Fluorescent nerves were present in the muscle layers and around blood vessels (Alm et al., 1986).

In summary, sympathetic nerves are found in abundance in the non-pregnant uterus and occur in all regions and all layers, including the longitudinal muscle, circular muscle and endometrium.

1.3.2 Parasympathetic Innervation of the Non-pregnant Uterus

1.3.2.1 Non-pregnant rats

We identified parasympathetic innervation by immunoreactivity for VAChT in full-thickness whole mount preparations of uterine horns and showed that the rat uterus contained a significant density of parasympathetic nerves that were present in all uterine layers (Gnanamanickam and Llewellyn-Smith, 2011). VAChT-immunoreactive axons occurred around blood vessels but their density was lower than the density of perivascular TH-, NPY- and nNOS-immunoreactive axons. The density of VAChT-positive axons in the myometrium was similar to the density of SP- and nNOS-positive axons. The linea uteri was more densely innervated than the rest of the smooth muscle. In sections of rat uterus (Papka et al., 1999), ChAT- and VAChT-immunoreactive axons were found around blood vessels, in the longitudinal and circular muscle layers and in the endometrium, often accompanying blood

vessels. ChAT- (Papka et al., 1999) and VAChT- (Gnanamanickam and Llewellyn-Smith, 2011; Papka et al., 1999) immunoreactive axons enter the uterus alone at the mesometrium or along with blood vessels.

Immunoperoxidase staining of full-thickness whole mount preparations has also revealed many nNOS-immunoreactive axons in the rat uterus (Gnanamanickam and Llewellyn-Smith, 2011). These axons densely innervated uterine blood vessels. The myometrium contained many nNOS-immunoreactive axons. The density of nNOS-immunoreactive innervation was similar to the density of uterine SP-immunoreactive innervation. Many nNOS-immunoreactive axons were present in the endometrium. Thick nerve bundles containing nNOS-immunoreactive axons were also present in the non-pregnant rat uterus.

1.3.2.3 Other species

In the non-pregnant mare uterus, VIP-immunoreactive axons were present in the muscle layers, in the endometrium and around blood vessels. The density of VIP-immunoreactive axons was higher in the cervix than in the uterus (Bae et al., 2001).

The non-pregnant cat uterus contained AChE-stained nerve fibers and VIP-immunoreactive axons, which were concentrated in the muscle and also around blood vessels. Innervation density was higher in the cervix than in the uterus (Alm et al., 1986).

In summary, the non-pregnant uterus receives a significant innervation from parasympathetic nerves, which are present in all uterine layers.

1.3.3 Sensory Innervation of the Non-pregnant Uterus

1.3.3.1 Non-pregnant rats and guinea-pigs

Our study on CGRP-immunoreactive axons in full-thickness whole mount preparations of rat uterine horns is the most thorough description of sensory innervation of the uterus. We found CGRP-positive axons innervating all uterine layers (Gnanamanickam and Llewellyn-Smith, 2011). CGRP-immunoreactive axons occurred around blood vessels but their density was lower than that of perivascular TH- and NPY-immunoreactive axons. CGRP-positive axons ran parallel to the smooth muscle cells of the longitudinal and circular muscle layers and of the linea uteri. The linea uteri had more CGRP-containing axons than the rest of the smooth muscle. Many CGRP-immunoreactive axons were seen in the endometrium and sometimes came close to the uterine glands. Earlier studies on whole mount preparations and cryostat sections of the rat genital tract obtained similar results (Shew et al., 1990; Shew et al., 1992). CGRP-immunoreactive axons entering the uterus usually travelled near or adjacent to blood vessels but sometimes were not associated with the vasculature. Within the uterus, CGRP-positive axons followed blood vessels, ran alongside smooth muscle cells and travelled to the endometrium from the myometrium.

SP immunoreactive axons are also present in all layers of the rat uterus (Gnanamanickam and Llewellyn-Smith, 2011; Papka et al., 1985). Like CGRP-containing axons, SP-immunoreactive axons entered the rat uterus in association with blood vessels or by themselves. SP-positive axons occurred in the circular and longitudinal muscle layers and in the endometrium. A few SP-positive axons were found close to uterine glands (Gnanamanickam and Llewellyn-Smith, 2011; Shew et

al., 1991); some of these axons travelled to the endometrium from blood vessels (Gnanamanickam and Llewellyn-Smith, 2011). SP-immunoreactive axons formed perivascular plexuses around blood vessels but there were fewer SP-positive perivascular axons than perivascular TH- and NPY-immunoreactive axons (Gnanamanickam and Llewellyn-Smith, 2011).

In rats and guinea-pigs, the densities of SP- and CGRP-immunoreactive axons were higher in the endometrium compared to the rest of the uterus (Alm and Lundberg, 1988; Gnanamanickam and Llewellyn-Smith, 2011; Haase et al., 1997). In rat uterus, there were fewer CGRP- and SP-immunoreactive axons than NPY-immunoreactive axons (Papka et al., 1985).

1.3.3.2 Other species

In mares, CGRP-immunoreactive axons were occasionally found associated with uterine blood vessels and there was more CGRP innervation of the vasculature in the cervix than uterus (Bae et al., 2001). The numbers of CGRP- and SP-immunoreactive axons were less than the number of NPY-immunoreactive axons in the mare uterus (Bae et al., 2001).

In summary, the non-pregnant uterus of all species examined to date receives many sensory nerves containing immunoreactivity for CGRP or SP. These sensory nerves are present in all layers of the uterus.

1.4 CHANGES IN INNERVATION OF THE UTERUS DURING THE OESTRUS CYCLE

The density of uterine innervation changes during the oestrus cycle (Zoubina et al., 1998; Zoubina and Smith, 2000) and this cyclical change relates to variations in the level of oestrogen (Zoubina et al., 2001; Zoubina and Smith, 2001).

Changes in immunoreactivity for protein gene product 9.5 (PGP 9.5, a marker that identifies all nerves), DβH, CGRP and VIP have been assessed during the estrous cycle. PGP 9.5 and DβH immunofluorescence varied during the estrous cycle while CGRP, VIP (Zoubina et al., 1998) and SP (Traurig et al., 1984) did not change. In contrast, another study using immunohistochemistry on both sections and whole mounts found no differences during the estrous cycle in peptide-containing nerves in rat uterine horns (Papka et al., 1985).

1.5 CHANGES TO UTERINE INNERVATION DURING PREGNANCY

1.5.1 Changes in Sympathetic Innervation during Pregnancy

1.5.1.1 Pregnant Rats

Catecholamine innervation of the pregnant rat uterus has been studied with glyoxylic acid-induced fluorescence and with immunohistochemistry at day 5, 10, 15, 18 and 22 days of a 21-22 day pregnancy (Chavez-Genaro et al., 2006; Klukovits et al., 2002). At 5, 7 and 10 days of pregnancy, the density of catecholaminergic axons was similar to the density in the non-pregnant rat uterus (Chavez-Genaro et al., 2006; Klukovits et al., 2002). At day 15, axons in the myometrium and axons associated with blood vessels were degenerating. These degenerating nerves were fragmented and had swollen varicosities. At day 18, there was significant denervation. There

were hardly any sympathetic axons in the myometrium and very few axons associated with blood vessels (Klukovits et al., 2002). At day 19, one study saw no sympathetic axons in the pregnant rat uterus (Chavez-Genaro et al., 2006) whereas another study reported that at day 22, the uterus was almost devoid of axons and the rare remaining axons were degenerating (Klukovits et al., 2002). In our unpublished studies using whole mount preparations, we have found that at day 20 of a 21-22 day pregnancy, there was significant sympathetic denervation. TH-immunoreactive axons were rare in uterine horns from near-term pregnant rats and almost no immunoreactive axons occurred around uterine blood vessels. Occasional TH-positive axons entered the uterus along with a blood vessel and disappeared as they travelled towards the side of the uterus opposite the mesometrium. Haase et al (1997) also documented a reduction in TH-immunoreactive axons in the pregnant rat uterus (Haase et al., 1997). The loss of sympathetic axons in the uterus correlates with a decrease in the size of TH-immunoreactive, uterus-projecting neurons in the thoraco-lumbar sympathetic chain in the rat (Richeri et al., 2005).

In rats, the decrease in the density of sympathetic innervation during pregnancy apparently relates to the presence of foetuses. In unilateral pregnancies in rats, glyoxylic acid-induced fluorescence showed that horns containing foetuses showed a similar innervation density to horns of pregnant rats with foetuses in both horns. However, during pregnancy and post-partum, uterine horns that lacked foetuses showed a density of sympathetic innervation that was similar to non-pregnant uteri (Chavez-Genaro et al., 2006).

Unpublished work from our laboratory using whole mount preparations has also demonstrated a massive reduction in the number of NPY-immunoreactive axons in the pregnant compared to non-pregnant rat uterus.

1.5.1.2 Pregnant guinea pigs

In pregnant guinea pig uterus, there are no TH-, NPY- or DBH-immunoreactive axons at term (Alm and Lundberg, 1988). Ultrastructural studies using 5-hydroxydopamine to identify catecholaminergic nerves showed a significant decrease in catecholaminergic nerves in the pregnant compared to the non-pregnant uterus (Sporrong et al., 1981). Up to pregnancy day 10, there were many catecholaminergic nerves. However, between 10 and 30 days of pregnancy, there were signs of axonal degeneration with the content of the axons becoming condensed. Degeneration of axons progressed as pregnancy proceeded and at term no catecholaminergic nerves were present (Sporrong et al., 1981). Immunofluorescence studies have shown that the numbers of both NPY-immunoreactive and TH-immunoreactive axons were significantly reduced in the guinea pig uterus during pregnancy (Fried et al., 1985). The few axons that remained were single and were present in both the myometrium and endometrium (Fried et al., 1985).

Fluorescence histochemistry to detect catecholaminergic nerves in pregnant guinea pig uteri showed that there were differences in the innervation of uterine tissue immediately surrounding the foetus compared to the rest of the uterus (Thorbert et al., 1978). In early pregnancy, uterine tissue immediately surrounding a foetus showed a reduction in catecholamine-fluorescent nerves. In addition there were microscopic changes to axon terminals, i.e., they lacked the distinct varicosities characteristic of fluorescent terminals in the non-pregnant uterus. In uterine tissues between foetuses (i.e., at the ovarian end of the horn as well as in horns that did not contain foetuses) there was no change to the fluorescent nerves during early

pregnancy. By mid-gestation (35-40 days of pregnancy), there were no catecholamine-fluorescent nerves in the uterine tissue surrounding a foetus. In uterine tissue between foetuses, there were reductions in the number and density of fluorescent nerves. Empty uterine horns showed varying results, with either no change or a reduction in fluorescent nerves. During late gestation (60 to 64 days of pregnancy), most of a uterine horn that contained foetuses lacked catecholamine-fluorescent nerves although a few nerves persisted at the ovarian end. In empty horns, a small amount of catecholaminergic innervation persisted in the body of the uterus and the ovarian end still received a dense array of catecholamine-fluorescent axons (Thorbert et al., 1978).

Immunofluorescence for neurofibrillary protein (NF) and neuron-specific enolase (NSE), general markers that identify all nerves, as well as immunofluorescence for TH and NPY has been used to study the innervation of the guinea pig uterus during pregnancy (Alm et al., 1988). At day 25 of a 65 day pregnancy, the tissue surrounding foetuses had very few axons of any type in the myometrium. NSE-, NF-, TH- and NPY-immunoreactive nerves were found in the endometrium and appeared to be degenerating. In uterine tissue away from foetuses, the number of nerves in the myometrium was reduced but there were more nerves than in tissue surrounding foetuses. Most of the axons in tissue away from foetuses were degenerating. The space between the longitudinal and circular muscle layers, which contains many blood vessels, did not show any change in the number of nerves present; but TH- and NPY-immunoreactive axons associated with blood vessels showed signs of degeneration. There was no change in innervation of the endometrium. At 37-40 days of pregnancy (mid-pregnancy), the tissue surrounding foetuses showed no immunoreactive structures and there were no immunoreactive

axons in the endometrium. The myometrium of uterine tissue not immediately surrounding foetuses showed many fewer varicose TH- and NPY-immunoreactive axons, which showed signs of degeneration. Between 45 days and term, foetus-containing uterine horns remained completely devoid of NF-, NSE-, TH- and NPY-immunoreactive axons. However, horns without foetuses contained a few nerves immunoreactive for TH, NPY, NSE and NF (Alm et al., 1988).

In guinea pigs with unilateral pregnancies, enzyme activity for TH and 3, 4-dihydroxy-L-phenylalanine (DOPA) decarboxylase, an enzyme that converts dopamine into NA, has been assessed in both foetus-containing horns and horns without foetuses (Alm et al., 1979). Compared to activity in non-pregnant uterine horns, TH activity in foetus-containing horns was reduced to 50% at day 25 and to 25% at day 40 of a 65-day pregnancy (Alm et al., 1979). The decline in TH activity in horns without foetuses was similar to that in horns with foetuses. In unilateral pregnancies at term, however, there was no TH activity in foetus-containing horns but horns without foetuses showed 10% of the TH activity found in non-pregnant horns (Alm et al., 1977; Alm et al., 1979).

NA content has also been measured in uterine horns containing foetuses and horns without foetuses in the guinea pig. In horns with and without foetuses, NA content increased to twice the amount found in non-pregnant horns within the first 10 days of gestation. In horns with foetuses, NA content slowly decreased to almost zero between day 10 and near-term (65 days). In horns without foetuses, after the initial doubling of NA content, the levels were steady and only dropped to near zero two weeks before term (Owman et al., 1975).

1.5.1.3 Pregnant cats

In the cat uterus, there is a marked reduction in catecholamine nerves identified by the Falck and Hillarp method. During early and mid-pregnancy, a few nerves are present only in areas of uterine horns devoid of foetuses. Where foetuses were present, there were no fluorescent nerves. By late pregnancy, all catecholamine fluorescent axons had disappeared from the cat uterus (Alm et al., 1986).

1.5.1.4 Pregnant humans

In a study comparing the innervation of the human uterus in the non-pregnant state, in the second trimester of pregnancy and at term using the Falck and Hillarp method (Thorbert et al., 1979), many catecholamine fluorescent nerves were found in the non-pregnant uterus (Thorbert et al., 1979). However, during the second trimester, the number of fluorescent nerves was greatly reduced and almost none were present at term (Thorbert et al., 1979). In contrast, another study using a similar method found that there were very few nerves containing NA in the myometrium and around blood vessels in the pregnant uterus (Nakanishi et al., 1969). The absence of TH- and NPY-immunoreactive axons in the pregnant human uterus has also been reported (Fried et al., 1986).

Biochemical measurements support the loss of sympathetic innervation in human pregnancy. The concentration of NA in human uterine tissue is reduced during the second trimester compared to the non-pregnant uterus. At term, the decrease is significant (Nakanishi et al., 1969). Measurements of the activities of TH, DOPA decarboxylase and ChAT revealed that, at term, TH and DOPA decarboxylase activity were only 13% and 14%, respectively, of the activity seen in the non-pregnant state while the activity of ChAT was virtually unchanged at 97% of

the activity in the non-pregnant state (Thorbert et al., 1979). In non-pregnant human uterus, the concentration of NA measured by high-performance liquid chromatography in two different studies was 536.0±95.0 ng/g (Zuspan et al., 1981) and 410±82 pmol/g w/w (Fried et al., 1986). In women undergoing normal labour, the NA concentration decreased to 20.8±4.6 ng/g (Zuspan et al., 1981) and 23.7±6.3 pmol/g w/w in pregnant women (Fried et al., 1986). In humans, the uterine NPY concentration was also reduced, 0.17±0.05 pmol/g w/w in pregnant women compared to 2.14±0.91 pmol/g w/w in non-pregnant women (Fried et al., 1986).

Taken together, these anatomical and biochemical data indicate that sympathetic innervation in three species, rats, guinea pigs and humans, massively decreases during pregnancy. In the pregnant uteri of rats, guinea pigs and humans, almost no sympathetic nerves are present at term. Degenerating sympathetic axons, which showed fragmentation, swollen varicosities and/or uneven and irregularly distributed immunoreactivity, have been identified in uteri from pregnant rats and guinea pigs. Furthermore, in unilateral pregnancies in the guinea pig, foetus-containing horns had different innervation and denervation patterns from horns that lacked foetuses.

1.5.2 Changes in Parasympathetic Innervation during Pregnancy

1.5.2.1 Pregnant rats

Our unpublished data from whole mount preparations of rat uterine horns have shown that at day 20 of a 21-22 day pregnancy, VAChT- and nNOS-immunoreactive axons are greatly reduced in number. The pregnant rat uterus had almost no VAChT-

and nNOS-immunoreactive axons. Only on rare occasions were single VAChT- or nNOS-immunoreactive axons encountered.

Both immunodetection of nNOS protein and localization of axonal nNOS-immunoreactivity in a very small sample of rat uterine tissue indicated that the pregnant rat uterus lacked nNOS innervation whereas there were nNOS-immunoreactive axons in the non-pregnant rat uterus (Riemer et al., 1997). NADPH-diaphorase staining showed that in the rat uterus, the number of nNOS-containing axons was lower at parturition than in the non-pregnant uterus (Natuzzi et al., 1993). In early pregnancy (7-10 days) in the rat, AChE -positive axons detected by the Karnovsky and Roots method showed low staining intensity around foetuses but higher intensity in other parts of the uterus. By late pregnancy (15-20 days), there was a significant reduction in AChE-stained nerve fibers in the rat uterus (Moustafa, 1988).

1.5.2.2 Pregnant humans

In humans, western blots and immunohistochemistry have shown that the amount of nNOS protein was higher pre-term compared to the non-pregnant uterus (Norman et al., 1999). However, another immunohistochemical study of nNOS did not show any change in innervation of the myometrium, placenta, and fetal membranes during human pregnancy (Thomson et al., 1997).

1.5.2.3 Other species

There is a large reduction in VIP-immunoreactive and AChE-positive axons in the cat uterus during early and mid-pregnancy although a few nerve fibers were present in areas of uterine horns lacking foetuses. During late pregnancy, there were no VIP-

positive or AChE-positive fibers in the uterus. However, horns without foetuses contained a few AChE-positive and VIP-positive axons (Alm et al., 1986).

Western blotting on the sheep uterus showed that the expression of nNOS protein did not change during pregnancy; however, nNOS mRNA was reduced in the sheep myometrium at day 100 of a 144-145-day pregnancy (Massmann et al., 1999).

Our unpublished studies in the rat have used anti-VAChT antibodies to study uterine parasympathetic innervation and shown a massive reduction in parasympathetic nerves supplying the pregnant compared to the non-pregnant uterus. Studies in rats and other species have shown a decrease in the parasympathetic supply to the pregnant uterus using staining for AChE and VIP. Studies targeting parasympathetic innervation using the less reliable markers nNOS or NADPH-diaphorase have shown that nNOS protein and/or nNOS innervation either decrease or are absent near term in pregnancy, with the exception of one study in humans that found nNOS protein increased pre-term. Some biochemical studies also support the loss of parasympathetic nerves during pregnancy.

1.5.3 Changes in Sensory Innervation during Pregnancy

1.5.3.1 Pregnant Rats

In our unpublished study on whole mount preparations of uterine horns from pregnant rats, we used both SP- and CGRP-immunoreactivity to identify sensory nerves. We found that there were almost no sensory axons in the uterus at day 20 of a 21-22 day pregnancy so that the uterus was virtually devoid of sensory innervation. Immunoreactivity for SP measured by radioimmunoassay in rat uterine horns showed

a decrease in the concentration of SP at day 14 and day 19 of pregnancy (Traurig et al., 1984).

1.5.3.2 Pregnant Guinea pigs

In a small sample of uterine horns from late pregnant guinea pigs (15μm thick sections, 8-10 sections each from 6 to 10 guinea pigs), no SP- or CGRP-immunoreactive axons were found (Alm and Lundberg, 1988).

The data above suggest that in rats, uterine sensory innervation is dramatically decreased in the pregnant compared to the non-pregnant uterus. The observations in guinea-pigs, although limited, suggest that sensory innervation also disappears during pregnancy in this species. There is currently no data available on sensory innervation of the pregnant human uterus.

1.6 CHANGES TO UTERINE INNERVATION POST-PARTUM

1.6.1 Post-partum Changes in Uterine Sympathetic Innervation

1.6.1.1 Post-partum Rats

In rats, the density of sympathetic innervation 3-5 days post-partum was similar to early pregnancy in uterine horns processed for glyoxylic acid fluorescence (Chavez-Genaro et al., 2006). At 24 to 48 hours after delivery, there were nerves immunostained by PGP 9.5 and TH in the rat uterus (Haase et al., 1997). The densities of PGP 9.5- and TH-immunoreactive axons were higher in horns from early post-partum rats than in horns from full term pregnant rats; however, there were no axons in the endometrium in the early post-partum period (Haase et al., 1997).

Between 1 and 3 weeks after delivery, most of the rat uterus lacked axons showing glyoxylic acid-induced fluorescence but there were some fluorescent axons in its ovarian and cervical ends (Moustafa, 1988). At 3 weeks post-partum, a few more axons were present than at earlier times post-partum.

Measurements of NA uptake and release by electric field stimulation in pregnant and post-partum rat myometrium and cervix have shown that activity was highest in the non-pregnant myometrium and cervix and that activity decreased as pregnancy progressed (Zupko et al., 2005). In the post-partum rat uterus, there was a slow increase in uterine NA uptake that was statistically significantly different between 14 and 21 days post-partum. In the non-pregnant uterus, electrical field stimulation resulted in the release of a significant amount of NA, which slowly decreased during pregnancy. In the post-partum period, there was a slow increase in NA release but this change was not statistically significant relative to the amount of NA released in late pregnant uterus (Zupko et al., 2005).

1.6.1.2 Post-partum guinea pigs

By 3 weeks post-partum, the ovarian end of the guinea pig uterus was completely re-innervated whereas the rest of the uterine horn that contained foetuses had either no or a very small number of catecholamine-florescent nerves even at 6-12 weeks post-partum (Thorbert et al., 1978). Empty uterine horns contained some fluorescent axons at 6 weeks after delivery and these nerves were higher in density at 12 weeks (Thorbert et al., 1978). Foetus-containing uterine horns had very small numbers of axons immunoreactive for TH, NPY, NF and NSE at 3, 6 and 9 months post-partum so that innervation was not completely restored even at this late time (Alm et al., 1988). Three months after delivery in horns that did not contain foetuses, innervation

was similar to that seen at full term. At 6 and 9 months after delivery, sympathetic innervation in uterine horns lacking foetuses was restored and resembled the innervation of a non-pregnant horn (Alm et al., 1988).

In guinea pigs 3 and 12 weeks after delivery, TH enzyme activity was only 10% of that in non-pregnant guinea pigs (Alm et al., 1977). Even at 6 months post-partum, TH activity in horns that had contained foetuses was only 14% or 40% of the activity seen in non-pregnant guinea-pigs (Alm et al., 1977; Alm et al., 1979).

1.6.1.3 Post-partum sheep

The results for re-innervation in the post-partum (74-91 days) sheep uterus were variable (Sigger et al., 1986). In two of five sheep, sympathetic innervation detected with glyoxylic acid-induced fluorescence was high in both the myometrium and around blood vessels but in two other sheep very few axons were present in the myometrium. In the fifth animal, the innervation density was even lower.

In summary, sympathetic re-innervation begins very soon after delivery in all species examined to date but it remains unknown whether or not innervation of a foetus-containing horn ever returns to the level present in the non-pregnant uterus. Biochemical studies in animals have also provided support for an increase in sympathetic innervation post-partum. There is currently no data available on sympathetic re-innervation of the human uterus post-partum.

1.6.2 Post-partum Changes in Uterine Parasympathetic Innervation

Changes to uterine parasympathetic innervation post-partum have been examined in only two studies. These reports were based on AChE staining (Haase et al., 1997;

Moustafa, 1988), which is unlikely to be specific for parasympathetic nerves (see Section 1.2.2). In the early post-partum period (24 to 48 hours after delivery), AChE-stained nerve bundles were present in the rat uterus along with axons around blood vessels in the myometrium (Haase et al., 1997). In uteri from rats sacrificed within a week after delivery, there was a reduction in the number of axons that stained for AChE and the persisting axons appeared fragmented. Two to three weeks after delivery, large AChE-positive nerve trunks were present (Moustafa, 1988).

Currently, details about the parasympathetic re-innervation of the uterus post-partum are sparse but suggest that the process may begin shortly after delivery. Parasympathetic re-innervation has not been examined in post-partum human uteri.

1.6.3 Post-partum Changes in Uterine Sensory Innervation

Again, there is very limited information about re-innervation of the uterus by sensory nerves in the post-partum period. Axons immunostained for CGRP were present in the rat uterus 1-2 days after delivery and their number was higher in early post-partum uterine horns than in late pregnant uterine horns (Haase et al., 1997). Aside from this study in rats, there is no published work on sensory innervation in post-partum uteri from other mammalian species, including humans.

From this one study, we know that sensory re-innervation of the uterus begins immediately after delivery but there is no detailed description about the re-innervation process. It is also unclear whether or not after pregnancy uterine sensory innervation returns to the density seen in the non-pregnant state.

1.7 PREGNANCY RELATED CHANGES TO UTERINE BLOOD VESSELS

Blood flow to the reproductive organs increases massively during pregnancy. Blood flow to the uterus has been reported to be 23 times higher in pregnant rats (Bruce, 1976), 15 times higher in pregnant guinea pigs (Guenther et al., 1988) and 10 times higher in humans (Page et al., 2002) than in the non-pregnant state in the same species. This increase in blood flow is necessary to provide adequate supplies of nutrients and oxygen to the developing foetus.

Pregnancy results in significant remodelling of uterine blood vessels in order to accommodate the increase in uterine blood flow. In pregnant rats the uterine artery is two or three times longer than in non-pregnant rats (Osol and Mandala, 2009). During pregnancy in the guinea pig, the uterine artery increases in length from 3.5±0.5 cm to 11.1±2.0 cm and in diameter from 1.5±0.5 mm to 3.5±0.5 mm (Mione et al., 1988). The luminal area of uterine arteries increases about 2.5 times in pregnant compared to non-pregnant guinea pigs (Mione et al., 1990). In rats, there is also an increase in the luminal diameter of uterine veins (Page et al., 2002).Increases in mitotic indices, which are measures of cell division and therefore growth, suggest that there are more vascular smooth muscle cells and endothelial cells in pregnant versus non-pregnant uterine veins In rats (Page et al., 2002).

Changes in perivascular innervation accompany the structural changes in uterine blood vessels. In the non-pregnant guinea pig, NPY- and VIP-immunoreactive axons densely innervate the uterine artery while the density of perivascular CGRP-immunoreactive axons is moderate and the density of perivascular SP-immunoreactive axons is low. During a guinea-pig pregnancy, uterine veins become denervated (Page et al., 2002). Results on the innervation of the

uterine artery in pregnant guinea pigs have varied, with two studies finding decreases in innervation (Guenther et al., 1988; Mione et al., 1988) and one study showing increases (Mione et al., 1990). In the 1988 study by Mione et al. perivascular NPY-immunoreactive axons decreased by 42% and CGRP-immunoreactive axons by 45% compared to the non-pregnant uterine artery whereas decreases in the numbers of VIP- and SP-immunoreactive axons were not so pronounced (26% and 25%, respectively). However, a 1990 study by the same group found an increase in the density of NPY-immunoreactive axons and no significant difference in the numbers of VIP-, SP- and CGRP-immunoreactive axons in pregnant versus non-pregnant uterine arteries (Mione et al., 1990). However, NA axons showing glyoxylic acid-induced fluorescence decreased during pregnancy along with NA levels measured by high performance liquid chromatography (Mione et al., 1990). In pregnant rat uterine veins, the density of nerves showing glyoxylic acid-induced fluorescence were 50% lower compared to non-pregnant veins (Page et al., 2002). In contrast, in the uterine artery of the guinea pig, an increase in the number of perivascular axons has been reported. There were also increases in the numbers of nerve bundles, axons and varicosities in the pregnant guinea pig artery compared to the non-pregnant artery at the ultrastructural level (Mione and Gabella, 1991). NA content in the uterine artery of pigs (Yorkshire gilts) decreased from day 20 of pregnancy to day 80 of pregnancy and had increased a small amount by pregnancy day 110 (Guenther et al., 1988).

In non-pregnant guinea pigs, NPY increases blood pressure and NA increases blood flow in the uterine artery (Fried and Thoresen, 1990). In contrast, the arterial system of the pregnant uterus is unresponsive to both NA and NPY (Traurig and Papka, 1993).

In summary, during pregnancy blood flow increases massively in all species and blood vessels undergo substantial structural remodelling. The data related to the innervation of uterine blood vessels is not consistent but mostly suggest that perivascular innervation decreases during pregnancy.

1.8 HYPERTENSION IN PREGNANCY

Hypertension in pregnancy is classified into three categories: gestational hypertension, chronic hypertension and pre-eclampsia.

Blood pressure of 140/90 mm Hg or more before mid-gestation and persisting for more than 12 weeks after delivery is defined as chronic hypertension (Leeman and Fontaine, 2008; Roberts et al., 2003; Swiet, 2003). Elevated blood pressure without proteinuria (presence of protein in the urine) after mid-gestation is defined as gestational hypertension (Leeman and Fontaine, 2008; Roberts et al., 2003; Swiet, 2003). Half of the women with gestational hypertension develop pre-eclampsia (see next section) later in pregnancy (Leeman and Fontaine, 2008). Women with chronic hypertension can also develop pre-eclampsia (Leeman and Fontaine, 2008).

1.9 PRE-ECLAMPSIA

Pre-eclampsia is defined as the presence of high blood pressure (≥140/90 mm Hg) along with proteinuria (≥300 mg protein per 24 hours) after mid-gestation (Leeman and Fontaine, 2008; Roberts, 2003; Roberts et al., 2003; Swiet, 2003). Pre-eclampsia proceeds to eclampsia when there are seizures, which can be life-threatening (Roberts et al., 2003). These seizures can happen after mid gestation, during labour and within 48 hours after delivery (Roberts et al., 2003).

Pre-eclampsia is considered a multi-organ disease and has severe outcomes for both mother and child. It affects 3 to 5 % of all pregnancies (Quinn, 2005) and up to 18% of pregnancies in some African countries (Villar et al., 2003). About 40,000 women die each year in developing countries due to pre-eclampsia and 20% of babies born to pre-eclamptic women are stillborn or die perinatally (Villar et al., 2003). According to the World Health Organization, about 30 million babies are born with growth restrictions each year in developing countries (Villar et al., 2003). In developed countries, maternal death from pre-eclampsia is prevented by early delivery. Babies born to pre-eclamptic women can not only die but also suffer other consequences, including intrauterine growth restriction, low birth weight and preterm birth (Roberts et al., 2003).

Risk factors for pre-eclampsia include maternal age (<20 years, >35 years), obesity, genetic predisposition, previous pre-eclampsia, primiparity (birth of the first child), a long interval between births, multiple pregnancy, hydatidiform mole, hydrops (abnormal accumulation of fluid in body tissues or cavities), triploidy (presence of 3 chromosomes in each cell), in vitro fertilization, hypertension, diabetes and renal disease (Nelson-Piercy, 2003).

1.9.1 Theories regarding the pathophysiology of pre-eclampsia

The exact cause(s) of pre-eclampsia remain unknown. However, the following factors have been suggested as contributing to the development of pre-eclampsia (adapted from (Leeman and Fontaine, 2008).

- Abnormal placental implantation
- Angiogenic factors
- Cardiovascular maladaptation and vasoconstriction

- Genetic predisposition
- Immunologic intolerance between fetoplacental and maternal tissue
- Platelet activation
- Vascular endothelial damage or dysfunction

1.9.2 Pathophysiology of pre-eclampsia

There are two stages in the pathophysiology of pre-eclampsia Stage one is characterized by reduced blood flow to the placenta (Page, 1939; Roberts, 2003). The placenta is required for the development of pre-eclampsia (Redman, 1991; Roberts et al., 2003). For example, pre-eclampsia persisted in one woman even after delivery because the placenta had not been completely removed (Roberts, 2003). During normal human pregnancy, spiral arteries that supply blood to the placenta undergo extensive remodelling. Invasion of trophoblast cells into the placenta results in highly distended arteries that are unresponsive to vasoactive stimuli (VanWijk et al., 2000). In pre-eclampsia, this remodelling does not occur normally, resulting in reduced perfusion of the placenta (Roberts et al., 2003). In pre-eclamptic pregnancies, trophoblast invasion of the spiral arteries is impaired or absent leading to narrow arteries that still react to vasoactive stimuli (VanWijk et al., 2000).

In the second stage of pre-eclampsia, blood flow to other maternal organs is reduced (Roberts, 2003; Roberts et al., 2003). In addition to the reduction in perfusion, other pathological changes occur in pre-eclampsia, including haemorrhage and necrosis in the liver, petechial haemorrhage in the brain, subendocardial necrosis in the heart and glomerular endotheliosis in the kidney, a condition unique to pre-eclamptic hypertension (Roberts, 2003). Vasoconstriction, micro-thrombi (small blood clots) and reduced plasma volume may explain the reduction in perfusion of

maternal organs (Roberts et al., 2003). Following placental ischemia in pre-eclampsia, the angiogenic factors, soluble FMS-like tyrosine kinase (sFlt-1) and soluble endoglin (sEng), increase. Administration of sFlt-1 to pregnant and non-pregnant rats has produced pre-eclamptic symptoms (Maynard et al., 2003). In addition to higher levels of sFlt-1 and sEng, there is also an increase in angiotensin type II receptor (AT2R) in pre-eclampsia. However, placental growth factor (PIGF) and vascular endothelial growth factor (VEGF) show decreases (Noori et al., 2007; Young et al., 2010).

1.9.3 Vasoconstriction in pre-eclampsia

The narrowing of blood vessels (vasoconstriction) may be responsible for the reduced blood flow seen in pre-eclampsia. Sympathetic nerves are responsible for vasoconstriction and parasympathetic nerves are responsible for vasodilation. The opposing functions of these two types of nerves lead to the hypothesis that disruption to the normal process of sympathetic denervation during pregnancy may be responsible for some of the symptoms of pre-eclampsia. Consistent with this hypothesis, the myometrial radial arteries have reduced luminal diameter and wall thickness in women with pre-eclamptic pregnancies compared to women with normal pregnancies (Ong et al., 2005).

1.9.3.1 Cardiovascular changes in normal vs pre-eclamptic pregnancies

In normal pregnancy, plasma volume and red cell volume increase. In pre-eclampsia, this increase is not as large as in a normal pregnancy; and in some cases of pre-eclampsia, plasma volume and red blood cell volume are the same as in non-pregnant women (Chesley, 1975). In women with severe pre-eclampsia and eclampsia,

hemoconcentration (a rise in the concentration of cells and a decrease in the fluid content of blood) results in an increase in plasma viscosity; but hemoconcentration is not considered a key cause of hypertension in pre-eclampsia. Vascular reactivity as well as responses to the vasoconstrictors, vasopressin, NA and angiotensin, increase in pre-eclampsia (Chesley, 1975). Increased responses to these substances could contribute to the vasoconstriction that is a hallmark of pre-eclampsia (Croiset et al., 2000; Li et al., 1996; Traurig and Papka, 1993).

1.9.3.2 Uterine sympathetic function in normal vs pre-eclamptic pregnancies

As detailed above, there is likely to be an almost complete loss of uterine innervation during normal pregnancy in humans and other mammals. Nothing is known about how uterine innervation changes in animal models of pre-eclampsia. However, one study comparing innervation in uteri from women with pre-eclamptic versus normal pregnancies (Fried et al., 1986) suggests that the denervation process induced by pregnancy is defective in pre-eclampsia, Immunohistochemistry for TH and NPY revealed no axons at all in uteri from normal pregnancies whereas in a small sample of pre-eclamptic uteri, a few axons persisted in the myometrium and around blood vessels. If this observation can be generalized, then pre-eclamptic pregnant uteri may retain more sympathetic innervation than normal pregnant uteri. This idea is supported by measurements of the content of sympathetic neurotransmitters in the uterus. In women with normal pregnancies, uterine NA and NPY levels were 23.7±6.3 pmol/g w/w and 0.17±0.05 pmol/g w/w, respectively, while in pre-eclamptic pregnancies uterine levels of these transmitters were greater (98.8±9.9 pmol/g w/w for NA and 0.88±0.16 pmol/g w/w for NPY; (Fried et al., 1986).

Interestingly, sympathetic nerve activity was higher in pre-eclamptic women than in normal pregnant women (Schobel et al., 1996).

Differences in the plasma concentrations of markers for sympathetic neurotransmission have also been found between women with normal and pre-eclamptic pregnancies; but the data have not always been consistent. One study showed that plasma NA levels in pre-eclamptic women were significantly higher than in normal pregnant women (Manyonda et al., 1998). However, another study found that plasma NA levels were lower in the pre-eclamptic group than in the normal pregnant group (Aune et al., 2000). Pregnant women who had hypertension but not proteinuria, i.e., who did not have pre-eclampsia, had plasma NA concentrations that were not different from the normal pregnant group (Manyonda et al., 1998). NA levels in cord blood were also higher in the pre-eclamptic versus normal pregnant groups (Manyonda et al., 1998). Plasma levels of NPY, another transmitter released by sympathetic nerves, are four-fold higher in women with eclampsia and two-fold higher in women with pre-eclampsia than in women with normal pregnancies (Khatun et al., 2000). Adrenaline levels in the plasma also vary. Pre-eclamptic women have higher plasma adrenaline than women having normal pregnancies (Oian et al., 1985). In women with eclampsia, plasma adrenaline and noradrenaline levels have been reported to be much higher than in women having normal pregnancies (Khatun et al., 1997).

NA levels were also elevated in women 5-6 years after a pre-eclamptic pregnancy. When NA was measured using high performance liquid chromatography in blood samples from women who had pre-eclampsia 5 to 6 years earlier and those who had normal pregnancies, there was a significant increase in NA in those had been diagnosed with pre-eclampsia (Lampinen et al., 2014).

There are also differences in sympathetic markers in the placenta between normal and pre-eclamptic pregnancies. Placental tissue from women with pre-eclampsia and eclampsia showed higher enzyme activity for TH than placental tissue from women with normal pregnancies (Manyonda et al., 1998). The expression of TH mRNA in pre-eclamptic placental tissue was also higher than in placental tissue from normal pregnancies (Manyonda et al., 1998).

The findings summarized above indicate that there are many significant differences between pre-eclamptic and normal human pregnancies in indicators for sympathetic innervation. These differences suggest that maladaptations in sympathetic function may occur during a pre-eclamptic pregnancy; possibly because sympathetic denervation is incomplete by the end of pregnancy (Figure 1.4). The failure of normal adaptations in sympathetic functions to the pregnant state could be responsible for some of the symptoms of pre-eclampsia.

1.9.4 Animal models of pre-eclampsia

Several animal models of pre-eclampsia have been developed over the past two decades. These models include the reduced uterine perfusion pressure (RUPP) (Granger et al., 2006) and uteroplacental ischaemia (UPI) (Makris et al., 2007) models, models based on anti-angiogenic factors that are increased in pre-eclampsia (Maynard et al., 2003; Venkatesha et al., 2006), inflammatory models (Sunderland et al., 2011b) and a transgenic model (Sunderland et al., 2011a).

FIGURE 1.4: TROPHOBLAST INVASION INTO THE SPIRAL ARTERIES IN THE PLACENTAL BED IN NORMAL PREGNANCY AND IN PRE-ECLAMPSIA.

Trophoblast invasion differs between normal and pre-eclamptic pregnancies. Failure of trophoblast cells to invade the spiral arteries in pre-eclampsia results in increased vascular resistance, which may be due to the persistence of sympathetic nerves.

From VanWijk, M. J et al. Cardiovascular Research 2000 47:38-4.8

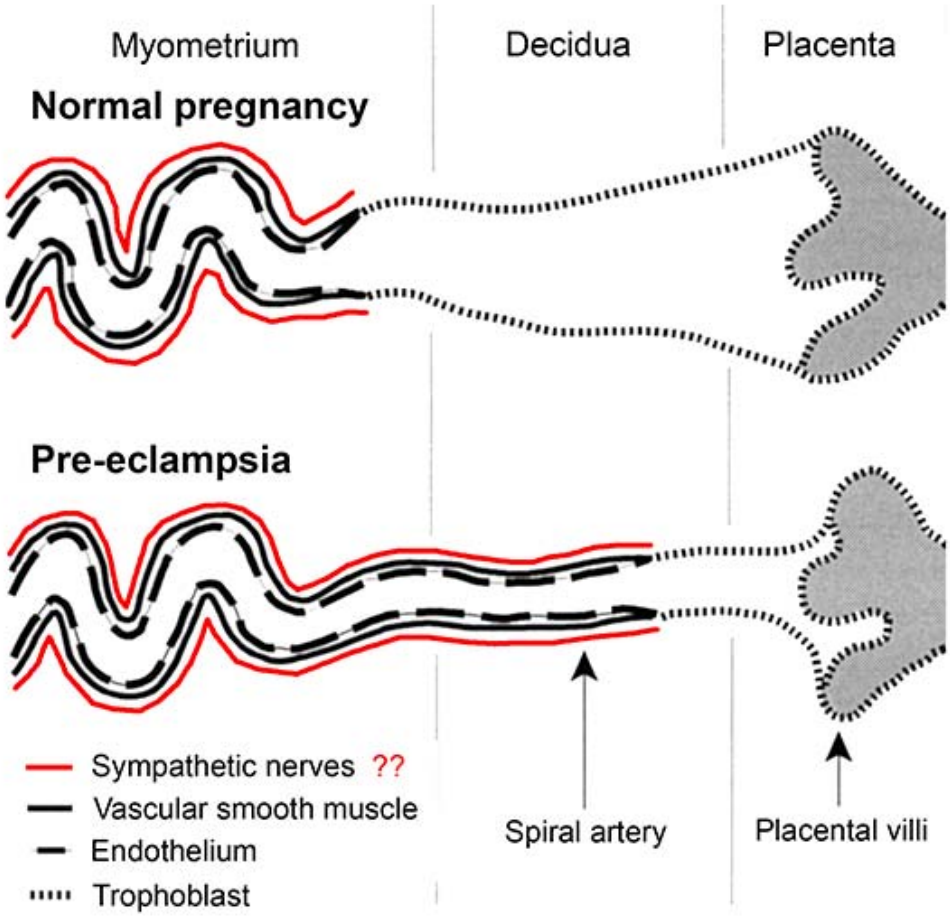
Myometrium
Decidua
Placenta
Normal pregnancy
Pre-eclampsia
Sympathetic nerves ??
Vascular smooth muscle
Endothelium
Trophoblast
Spiral artery
Placental villi

1.9.4.1 RUPP and UPI models of pre-eclampsia

In the RUPP model of pre-eclampsia, the aorta below the renal arteries and the main uterine artery are occluded with silver clips. The occlusion results in high blood pressure, proteinuria, reduced renal plasma flow, a reduced glomerular filtration rate and intrauterine growth restriction, all of which are features of a human pre-eclamptic pregnancy (Granger et al., 2006). However, blockage of blood vessels does not occur in human pre-eclampsia so this model is not truly physiological. The UPI model involves ligation of one of the uterine arteries, which reduces placental perfusion by 30-50%. Symptoms of pre-eclampsia, including hypertension, proteinuria, renal histological and plasma biochemical changes and elevation of sFlt-1, occur in this model (Makris et al., 2007). However, the UPI model can be criticized as unphysiological for the same reason as the RUPP model, i.e., the UPI model also involves blocking the uterine artery, which does not occur in human pre-eclampsia. In pre-eclampsia, vasoconstriction, i.e., narrowing of blood vessels, is the cause of reduced placental flow.

1.9.4.2 Models of pre-eclampsia based on anti-angiogenic factors

When injected into pregnant animals, the anti-angiogenic factors, sFlt-1 and s-Eng, cause pre-eclamptic symptoms, including high blood pressure, foetal growth restriction, renal and liver changes, hemolysis and vascular damage (Venkatesha et al., 2006). Injection of sFlt-1 into non-pregnant rats also resulted in high blood pressure and proteinuria (Maynard et al., 2003). Elevation of these anti-angiogenic factors has been suggested to be related to stage two in the pathophysiology of pre-eclampsia (Redman and Sargent, 2009). It is currently unknown how these factors

relate to vasoconstriction in pre-eclampsia and whether they are a cause or consequence of restricted blood flow.

1.9.4.3 Models of pre-eclampsia based on inflammation

Many models of pre-eclampsia are based on the induction of inflammation. These include infusion of inflammatory substances, such as tumour necrosis factor α (TNF-α), interleukin-6 (IL-6) and low-doses of bacterial endotoxin. Pre-eclamptic symptoms have also been evoked by treatment with TNF-α plus progesterone and by infusions of Th1/Th2 splenocytes. The RUPP model has also been done in combination with TNF- α blockade (Sunderland et al., 2011a). Infusion of TNF-α into pregnant baboons has resulted in some of the symptoms of pre-eclampsia, including high blood pressure, proteinuria and elevated levels of sFlt-1 and sEng. However, there were no pre-eclamptic symptoms in foetuses apart from one instance of stillbirth, which was reported to be related to birth trauma (Sunderland et al., 2011b). It is not known how the inflammatory response in pre-eclampsia is related to vasoconstriction. Infusion of the cytokine IL-6 into pregnant rats resulted in high blood pressure and a rise in protein in the urine whereas IL-6 infusion into non-pregnant rats did not significantly change blood pressure (Orshal and Khalil, 2004). In IL-6 infused pregnant rats, there was also a decrease in endothelial NO-mediated vascular relaxation and an increase in vascular contraction. Pups of IL-6-treated pregnant rats showed intrauterine growth restriction and were smaller than pups of untreated pregnant rats. Administration of endotoxin to pregnant rats raised blood pressure and increased the amount of albumin in the urine (Faas et al., 1994). Pregnant rats that had been given endotoxin also had defects in platelet coagulation and deposits of fibrinogen in renal glomeruli whereas untreated pregnant rats did not.

The number and weight of foetuses did not vary between treated and untreated groups; but in the group treated with high dose endotoxin, more pups were reabsorbed.

1.9.4.4 Transgenic mouse model of pre-eclampsia

When female transgenic mice expressing angiotensinogen were mated with male transgenic mice expressing renin, secretion of renin during late pregnancy resulted in high blood pressure in the pregnant female mouse. Increased protein in the urine, myocardial hypertrophy and placental necrosis and oedema was also seen in this transgenic mouse model of pre-eclampsia (Takimoto et al., 1996).

1.10 POSSIBLE ROLE OF MICRORNAS IN UTERINE INNERVATION CHANGES DURING PREGNANCY AND POST-PARTUM

MicroRNAs (miRNAs) are small, single-stranded, non-coding RNAs that are 18-24 nucleotides in length. They are post-transcriptional regulators of gene expression(Bicker and Schratt, 2008) and most can affect more than one gene (Morales Prieto and Markert, 2011). MiRNAs are involved in the development of the nervous system as well as influencing function within the mature nervous system (Bicker and Schratt, 2008; Christensen and Schratt, 2009). MicroRNAs are important in the development of the nervous system as the regulate the differentiation and proliferation of neural stem cells, neuronal maturity and function (Sun et al., 2013). Many diseases of the nervous system, such as Parkinson's disease and Alzheimer's disease, have been associated with differential expression of miRNAs (Bicker and Schratt, 2008).

1.10.1 MicroRNA synthesis

MicroRNA synthesis begins in the nucleus and ends in the cytoplasm (Figure 1.5). Long primary transcripts (pri-miRNAs) are derived from polyadenylated RNA polymerase II transcripts. The nuclear ribonuclease (RNAase III) enzyme, Drosha, cleaves the pri-miRNAs to form 70-100 nucleotide hairpin precursor-miRNAs. Pre-miRNAs are then transported to the cytoplasm by exportin 5. In the cytoplasm, another RNAase III enzyme, Dicer, cleaves the pre-miRNA to produce a duplex of ~22 nucleotides. One strand of this duplex, the mature miRNA, is incorporated into the RNA-induced silencing complex (RISC) and acts as a guide for the RISC to target and prevent the translation of specific mRNA transcripts (Kosik, 2006; Saba and Schratt, 2010).

1.10.2 MicroRNA mode of action

For a specific gene to be expressed, a process of transcription and translation takes place within the cell. The specific portion of DNA that codes for the gene is copied into mRNA transcripts in the nucleus of the cell. The mature mRNA sequence is then transported into the cytoplasm, where translation into protein occurs (Alberts et al., 2014b). MicroRNAs can regulate gene expression by interfering with the translation of mRNA into protein (Figure 1.5). By base pairing with specific mRNAs, miRNAs in RISCs can either degrade mRNA or inhibit its translation. After the mRNA is degraded, RISC is released and can move on to another mRNA. Hence, a single miRNA molecule in a RISC can block the translation of many mRNA molecules (Alberts et al., 2014a), (Kosik, 2006).

FIGURE 1.5: DIAGRAM SHOWING THE SYNTHESIS AND MODE OF ACTION OF MICRORNAS.

Long primary transcripts (pri-miRNAs), derived from polyadenylated RNA polymerase II transcripts, are cleaved by the enzyme, Drosha, to form 70-100 nucleotide hairpin pre-miRNAs. Exportin 5 transports the pre-miRNAs to the cytoplasm, where another enzyme, Dicer, cleaves the pre-miRNA to produce a duplex of ~22 nucleotides. One strand of this duplex, the mature miRNA, is incorporated into an RNA-induced silencing complex (RISC) and acts as a guide for the RISC to target and prevent the translation of specific mRNA transcripts.

Reproduced from Hebert et al (2009)

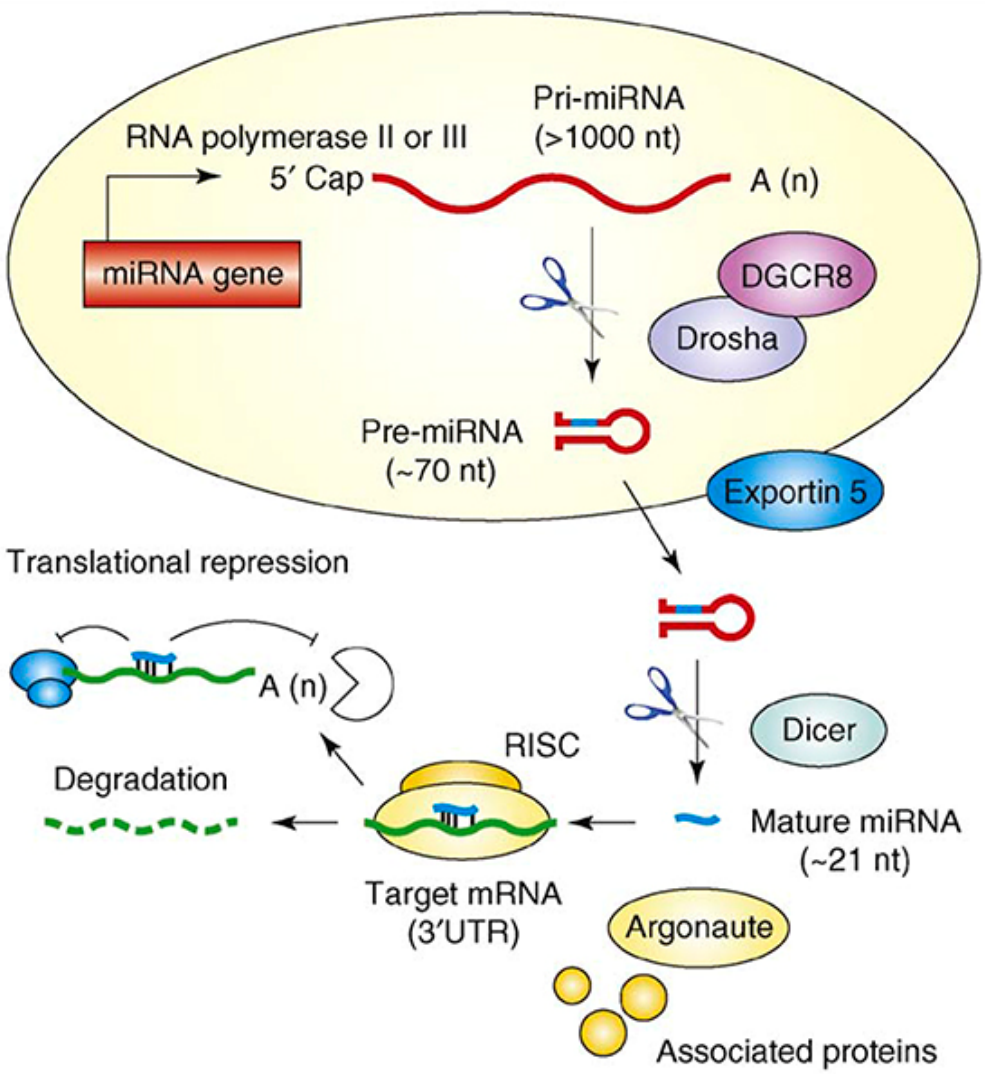
RNA polymerase II or III
Pri-miRNA
(>1000 nt)
5′ Cap
A (n)
miRNA gene
DGCR8
Drosha
Pre-miRNA
(~70 nt)
Exportin 5
Translational repression
A (n)
Dicer
RISC
Degradation
Mature miRNA
(~21 nt)
Target mRNA
(3′UTR)
Argonaute
Associated proteins

1.10.3 MicroRNAs in development and degeneration/regeneration of the nervous system[1]

MicroRNAs participate in the development of the nervous system and also have roles in the mature nervous system (Christensen and Schratt, 2009; Li and Jin, 2010; Schratt and Greenberg, 2008; Schratt et al., 2006; Visvanathan et al., 2007). MicroRNAs control the fate of neural stem cells. For example, miR-124 is important for the proliferation of neural stem cells (Sun et al., 2013) and miR-9 promotes neuronal differentiation and migration (Kawahara et al., 2012). Both miR-9 and mi-124 expression are high during neurogenesis (Christensen and Schratt, 2009). Experimental suppression of miRNA biogenesis supports the idea that miRNAs are essential for neuronal development. Dicer is necessary for the maturation of miRNAs. In dicer mutant zebrafish, there are serious defects in the morphology of the brain and other organs, confirming that miRNAs are necessary for the normal development of the nervous system (Giraldez et al., 2005). Deletion of Dicer in mice has shown that miRNAs are necessary for normal development of neurones and their polarity. When Dicer is inactivated in Purkinje cells of mouse cerebellum, there is progressive loss of miRNA expression followed by a slow neuronal degeneration and ultimately cell death (Schaefer et al., 2007).

---

[1] This subsection has been reproduced from the Background section of an application for a Faculty of Health Sciences Seeding Grant, which was funded in 2013. The title of the project was "microRNAs change during pregnancy and post-partum in ganglia supplying uterine innervation".

Dicer deletion in the dividing zone of the mouse cerebral cortex causes abnormal differentiation of neural stem cells and apoptosis. These effects are mediated both by reductions in the levels of proteins responsible for survival and protection against apoptosis and by increases in proteins responsible for apoptosis (Kawase-Koga et al., 2010). Conditional dicer knock-out mice also produce many more axons than normal control mice, supporting a role for miRNAs in generation of neuronal polarity (Li et al., 2012).

MiRNAs regulate adult neurogenesis and synaptic plasticity and influence axonal growth (Strickland et al., 2011; Wu et al., 2012; Yu et al., 2011). Over-expression of miR-134 decreases the size of dendritic spines in cultured hippocampal neurons (Schratt et al., 2006) and miR-124 regulates adult neurogenesis of stem cells in the subventricular zone (Cheng et al., 2009). Neurite outgrowth is more extensive in cultures of DRG neurons from mice that overexpress miR-21 than in DRG cultures from control mice. MiR-21 is also upregulated in DRGs after sciatic nerve transaction (Strickland et al., 2011). In contrast, increased expression of miR-1 in rat DRG neurons decreases neurite outgrowth (Bastian et al., 2011) and miR-541 reduces neurite outgrowth in PC12 cells (Zhang et al., 2011b), a model for mature sympathetic neurons. Another miRNA, miR-338, negatively regulates axon growth. MiR-9, which targets a protein, Map1b, that regulates microtubule stability, is expressed in the somata, dendrites and axons of primary cultures of embryonic day 17 (E17) mouse cortex. A decrease in axon length but an increase in axonal branching occurs when miR-9 is overexpressed, while inhibiting miR-9 expression increases axonal length and decreases branching (Dajas-Bailador et al., 2012). Neurons in *Xenopus* embryos and growth cones in *Xenopus* neuronal cultures express miR-134, suggesting a role for miR-134 in axonal development (Han et al., 2011).

Following sciatic nerve injury, an increase in miR-222 expression promotes neurite outgrowth in rat DRGs (Zhou et al., 2012). In contrast, there is no regeneration of axons after sciatic nerve injury in DRG cultures from dicer-deficient mice (Wu et al., 2012). DRGs from rats with sciatic nerve transections show a decrease in expression of miR-144, 145 and 214. MiR-145 also inhibits neurite outgrowth in cultured neurons (Zhang et al., 2011a). Following transection of the zebrafish spinal cord, regenerating brainstem neurons upregulate miR-133b, which inhibits the small GTPase RhoA to inhibit axonal growth (Yu et al., 2011). Some miRNAs are also differentially expressed in diseases of the nervous system, such as Parkinson's disease, Huntington's disease and Alzheimer's disease (Bicker and Schratt, 2008; Bushati and Cohen, 2008; Harraz et al., 2011; Hebert et al., 2008; Lee et al., 2011; Li et al., 2011; Satoh, 2010).

Post-ganglionic neurons in the MPG, inferior mesenteric ganglia (Owman and Stjernquist, 1988; Papka et al., 1996), superior mesenteric ganglia (Vera et al., 1997) and suprarenal ganglia (Houdeau et al., 1998; Vera et al., 1997) provide sympathetic innervation to the uterus. MiRNAs have been identified in axons in the SCG (Natera-Naranjo et al., 2010), which contains sympathetic post-ganglionic neurons that supply innervation to the head and neck. In cultured SCG neurons, overexpression of miR-338 decreases neurite outgrowth whereas inhibition of miR-338 increases outgrowth (Oliveira et al., 2013). These observations are consistent with the idea that miRNAs may be involved in retraction and outgrowth of sympathetic axons innervating the uterus.

1.10.4 MicroRNAs in pregnancy[2]

In non-neuronal tissue, miRNAs are differentially expressed during pregnancy and in pre-eclampsia (Enquobahrie et al., 2011; Morales Prieto and Markert, 2011; Pineles et al., 2007). Conditional deletion of Dicer in uterine epithelium and endometrial connective tissue resulted in mice that were sterile and had serious uterine defects, suggesting that miRNAs are important for normal development of the uterus (Hawkins et al., 2012). MiRNAs have been demonstrated in human plasma and expression levels differ during pregnancy and after parturition, when expression of miR-141, miR-221, miR-29a and miR-144 is lower (Pan et al., 2012). In the placentas of women with pre-eclampsia and those with pre-eclampsia and small for gestational age infants, there were differences in the expression of seven miRNAs compared to the control group of women undergoing spontaneous preterm labour without pre-eclampsia (Pineles et al., 2007). Two studies have found that miR-210 is more highly expressed in placentas from pre-eclamptic compared to normal pregnancies (Enquobahrie et al., 2011; Pineles et al., 2007) although another study found miR-210 expression to be lower in pre-eclamptic placentas (Mayor-Lynn et al., 2011). Pre-eclamptic placentas have also been reported to express lower levels of

---

[2] This subsection has been reproduced from the Background section of an application for a Faculty of Health Sciences Seeding Grant, which was funded in 2013. The title of the project was "microRNAs change during pregnancy and post-partum in ganglia supplying uterine innervation".

miR-328, miR-584, miR-139-5p, miR-500, miR-1247, miR-34C-5p, miR-1, miR-15b, miR-483-5p and miR-181a compared to normal placentas while expression of miR-493 is slightly higher (Enquobahrie et al., 2011; Mayor-Lynn et al., 2011).

MiRNAs also change in other disorders of pregnancy. For example, in placentas from pregnancies with fetal growth restriction, miR-141 was upregulated and its target mRNAs were downregulated compared to placentas from normal pregnancies (Tang et al., 2013). Growth restriction probably occurs because miR-141 suppresses the expression of the transcription factor E2F3, which is important for normal placental development, and of the gene PLAG1, which is essential for normal embryonic growth (Tang et al., 2013).

The information summarized above shows that miRNAs are important for normal development and growth of central and peripheral neurons and that miRNAs change during pregnancy. Sympathetic and parasympathetic innervation of the uterus is supplied by neurons in the MPG (Baljet and Drukker, 1980), inferior mesenteric ganglia (Owman and Stjernquist, 1988; Papka et al., 1996), superior mesenteric ganglia (Vera et al., 1997) and suprarenal ganglia (Houdeau et al., 1998; Vera et al., 1997) and the dorsal motor vagal nucleus through the vagus nerve (Ortega-Villalobos et al., 1990). We have shown that both types of innervation disappear during pregnancy and reappear after birth. Currently, there is no information available about the miRNAs that are expressed in the MPG and we were interested to determine whether MPG neurons express any miRNAs associated with axonal growth and whether their levels differ at oestrus, during pregnancy and post-partum.

Rationale, Aims and Hypotheses

1.11 RATIONALE

While there is a reasonable amount of data on uterine sympathetic denervation during pregnancy (see Section 1.5.1), only a handful of published papers have examined pregnancy-related parasympathetic and sensory denervation of the uterus (see Sections 1.5.2 and 1.5.3). Knowledge of the denervation process that the uterus undergoes during a normal pregnancy is critical for understanding why uterine denervation appears to be incomplete in human pre-eclamptic pregnancies. There is also very little information about the re-innervation of the uterus that occurs post-partum (see Section 1.6). A further limitation of published work is that almost all of the studies on uterine innervation have been done on sections of uterine tissue, which are generally less than 30 micrometres thick. Only a very small portion of a uterine horn can be examined in sections and therefore sections cannot provide a complete picture of innervation or how it changes during pregnancy and post-partum. We have previously developed a method to study immunohistochemically-characterized nerves in full-thickness whole mount preparations of the rat uterus (Llewellyn-Smith and Gnanamanickam, 2011). Using these whole mounts, we can track the course of axons from their entry into the uterus until they terminate in one of the uterine layers, characterize the perivascular nerve plexuses associated with blood vessels and examine axons that travel on their own through the uterus. Chapters 3-5 of this thesis consists of a detailed description of the time course of denervation and re-innervation of the rat uterus by sympathetic, parasympathetic and sensory nerves at various time points during pregnancy and post-partum. I have also quantified the density of

sympathetic, parasympathetic and sensory innervation in the non-pregnant stage and at various time points during pregnancy and post-partum. These results provide the first complete picture of how nerves supplying the rat uterus change during pregnancy and in the first month after delivery.

The studies summarized in Section 1.10 above suggest that miRNAs play specific roles during pregnancy and that disruption of miRNA function can lead to abnormal pregnancies. The data presented in Section 1.5 indicate that there is an almost complete disappearance of nerves in the uterus during a normal pregnancy (Thorbert et al., 1979). However, in pre-eclamptic pregnancies, more nerves persist in the uterus than in normal pregnancies (Fried et al., 1986). The mechanisms that underlie the changes in innervation of the uterus during pregnancy and in pre-eclampsia are currently unknown. Section 1.10 shows that miRNAs are involved in the development, degeneration and regeneration of neurons. However, it is not known whether miRNAs play a role in the innervation changes induced by pregnancy. This information could be critical for understanding the normal regulation of the denervation process during pregnancy and the maladaptation seen in pre-eclampsia. As a first step towards understanding whether miRNAs play a role in innervation changes during pregnancy and post-partum, this project determined if there were any differences in the expression of miRNAs in the major pelvic ganglion during pregnancy and post-partum.

1.12 AIMS

- To define the sympathetic, parasympathetic and sensory innervation of the uterus at 4 time points during pregnancy and 7 time points post-partum and to quantify the density of each type of innervation at each time point using whole mount preparations and immunohistochemical detection of neurochemical markers that identify the three different functional types of uterine nerves.
- To compare levels of microRNAs (miRNAs) influencing neuronal structure in the major pelvic ganglion (MPG) at oestrus, pregnancy (E) day 20 (E20) and post-partum (P) day 5 (P5) in order to assess whether miRNAs may influence the loss of uterine nerves during pregnancy and their regrowth post-partum.

1.13 HYPOTHESES

- The sympathetic, parasympathetic and sensory innervation of the rat uterus changes during pregnancy and post-partum.
- The expression levels of microRNAs in the major pelvic ganglion change during pregnancy and post-partum.

Chapter 2

Materials and Methods

2.1 ANIMALS

A total of 122 female rats were used in this project. Ninety-nine rats were perfused for the immunohistochemical studies in Chapters 3-5 and 40 rats provide data for the molecular biological studies in Chapter 6. Non-pregnant rats were purchased from Laboratory Animal Services (LAS) at the University of Adelaide. Pregnant and post-partum rats were either time-mated in the School of Medicine Animal Facility at Flinders University or purchased from LAS. All experimental protocols were approved by the Animal Welfare Committee, Flinders University.

Twenty non-pregnant rats were sacrificed at oestrus. The day on which either sperm were detected in a vaginal smear or a vaginal plug was present indicated that a rat was pregnant and was termed pregnancy (E) day 0. For immunohistochemical studies, pregnant animals were sacrificed at E14 (7 rats), E16 (7 rats), E18 (6 rats) or E20 (10 rats) of a 21-22 day pregnancy. The day of delivery was considered post-natal (P) day 0. Post-partum rats for immunohistochemistry were sacrificed at P1 (6 rats), P3 (7 rats), P5 (7 rats), P7 (9 rats), P10 (7 rats), P14 (9 rats) or P28 (13 rats). For studies on miRNA changes in the major pelvic ganglia (MPG) during pregnancy and post-partum, rats were sacrificed at oestrus (n=12), E20 (n=10), P5 (n=9) and P14 (n = 8). E20 was chosen because uterine denervation is most extensive at this stage, which is near term in a 21-22 day pregnancy. P5 was chosen because growth cones are abundant at this time. P14 was chosen because growth cones were much less common and a significant amount of re-innervation had occurred. All rats except

those at P28 were primiparous. The P28 rats used were ex-breeders so some of them had given birth more than once.

2.2 VAGINAL SMEARING

Vaginal smearing was done to determine the stage of the oestrus cycle. A few drops of sterile water were flushed into and out of the rat's vagina several times. The water was placed on glass slides and dried on a slide warmer. The dried smear was stained using Quick Dip Fixative (Fronine Laboratory Supplies, Riverstone, Australia). The slides were immersed consecutively in fixative, stain 1 and stain 2 and rinsed twice in distilled water between each step. All incubations in the fixative and stains were done for 15 seconds each. Rinses in distilled water were done for a few seconds. Once the slides were dry, the morphology of vaginal cells was assessed to determine the stage in the oestrus cycle (Figure 2.1). A smear in which the majority of cells were non-nucleated indicated that rat was in the oestrus stage of the oestrus cycle. Vaginal smears were taken for at least 2 complete cycles before the rats were either sacrificed at oestrus or mated overnight.

2.3 PERFUSION

Each rat was given an intraperitoneal injection of pentobarbitone sodium (Ilium Pentobarb, Virbac, Australia Pty Limited, Milperra, Australia) diluted 1:5 in sterile distilled water (AstraZeneca, North Ryde, Australia).to a give a final concentration of 60 mg/ml. Each rat received a 60 mg/kg dose of the diluted anaesthetic. Once the rat was unconscious, an incision was made along the abdominal midline to expose the intestines, kidneys and uterine horns.

FIGURE 2.1: CYTOLOGY OF VAGINAL SMEARS AT DIFFERENT STAGES OF THE OESTRUS CYCLE.

Figure modified from one kindly provided by Dr Thelma Lovick, School of Physiology and Pharmacology, University of Bristol, UK. PRO, proestrous; OEST, Oestrus; ED, early diestrous; LD, Late diestrous.

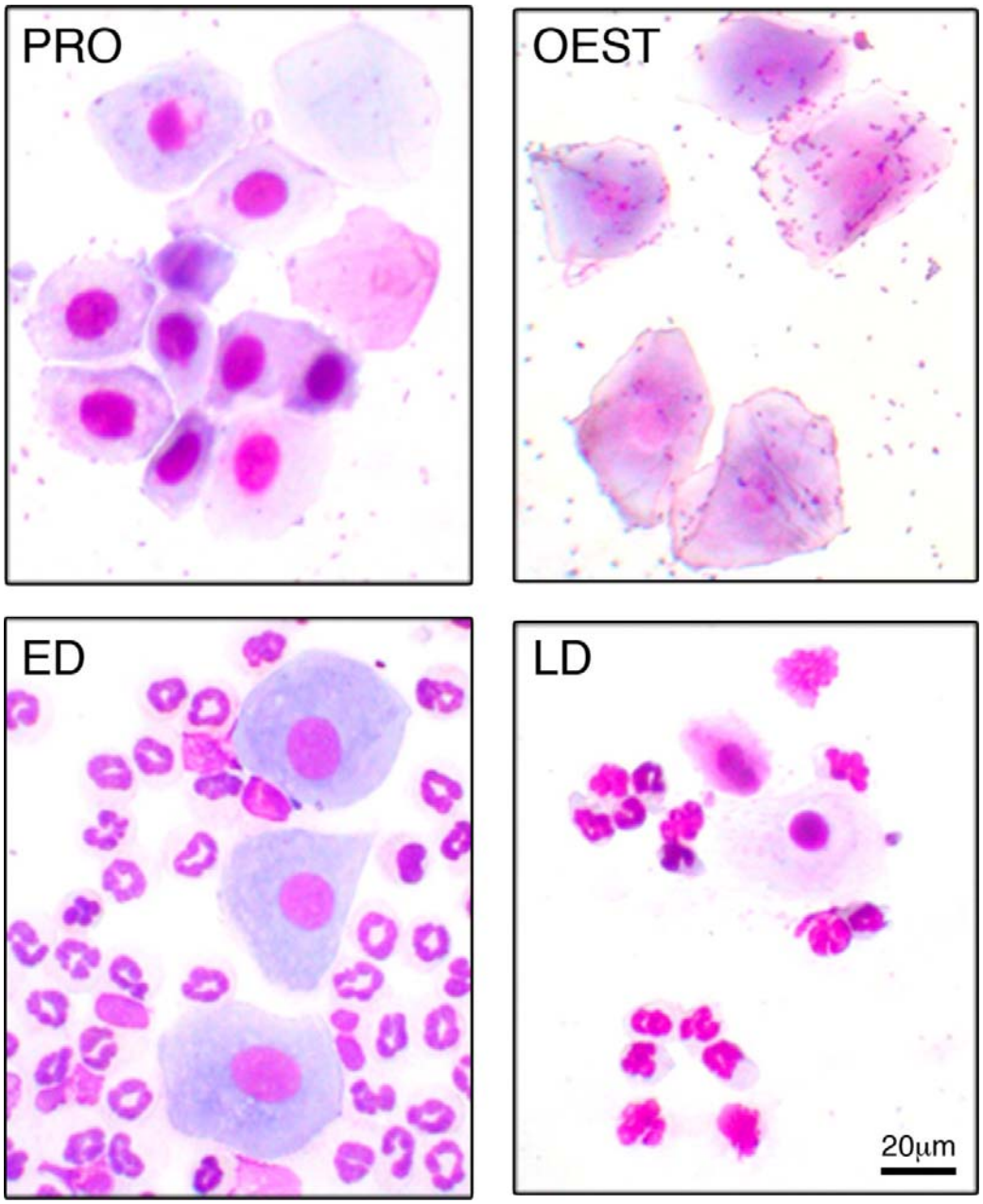
PRO
OEST
ED
LD
20µm

The kidneys and intestines were clamped with haemostats. The sternum was held with another haemostat and the diaphragm was opened to expose the heart. A blunt needle was then inserted through the left ventricle into the aorta and 1ml of heparin (1000 IU in 1 ml; Hospira, Melbourne, Australia) was injected through a 3-way tap to prevent clotting of blood. The left atrium was snipped and 500 ml of phosphate-buffered saline, pH 7.4, (PBS, see Appendix) or tissue culture medium (Dulbecco's modified Eagle's medium, Catalogue #: D8900, Sigma-Aldrich, St Louis, USA) was flushed through the rat to remove blood. If a significant amount of blood remained in the uteri, removing the haemostats on the renal arteries sometimes allowed enough PBS or tissue culture medium to flow to the uteri to clear more of the blood. All rats except for post-partum rats at P28 were perfused using PBS. P28 rats were perfused with tissue culture medium because P28 uterine horns flushed with tissue culture medium had less background staining after immunohistochemistry than P28 horns flushed with PBS.

Three randomly chosen pups from each horn were weighed at E16, E18 and E20 in order to test whether or not pup weights were appropriate for the pregnancy time point. For consistency, six randomly chosen pups were weighed from post-partum rats.

2.4 IMMUNOHISTOCHEMISTRY

2.4.1 Tissue Preparation

After perfusion, uterine horns were removed, bubbled with Carbogen in Ca^{+2}-free Krebs or tissue culture medium (Dulbecco's Modified Eagle's Medium, Sigma-Aldrich) for 30 minutes, cut through the mesentery and pinned flat on Sylgard (Dow

Corning Corporation, USA)-coated Petri dishes (ProScitech, Kirwan, Australia), which were either8.5 cm and 14 cm in diameter. Uterine horns from rats at oestrus, P3, P5, P7, P10, P14 and P28 were stretched and pinned intact onto Sylgard-coated Petri dishes. Uterine horns from rats at E14 and P1 were cut in half and stretched to 2 cm wide during pinning. Uterine horns from rats at E16 were also halved and stretched to 2.5cm during pinning. Halved horns from E18 and E20 rats were stretched to 3 cm wide and pinned. The ovary remained connected to each uterine horn as a marker for its ovarian end. The cervical end was marked with a suture. The uterine horns were immersion-fixed in 4% formaldehyde in 0.1M phosphate buffer, pH 7.4, for 3-4 days at room temperature.

After fixation, all non-pregnant, pregnant and post-partum uterine horns were rinsed in 0.1M phosphate buffer, pH 7.4, at least 3 times. Each uterine horn was placed on a gauze pad to remove as much liquid as possible and weighed. To measure its length, width and area, each uterine horn was placed in a Petri dish on a scanner, the Petri dish was covered with a piece of black cardboard to exclude light and the uterine horn was scanned using a CanonScan Lide25 (Canon, Sydney, Australia). The scanned images were saved as TIFF files. Length and width were measured on the TIFF files produced by the scanner using Adobe PhotoShop CS2. A TIFF file was opened in PhotoShop and guides were placed at the ovarian and cervical edges of the image of the uterine horn. The length of the uterine horn was then measured using the ruler. The width of each horn was measured similarly using guides placed at the two mesometrial edges of the image of the uterine horn.

After fixation, each horn from rats at oestrus, P5, P7, P10, P14 or P28 was cut in half into ovarian and cervical segments, which were then placed together in a 20 ml vial for storage. Uterine horns from rats at E14, E16, E18, E20, P1 and P3 were

cut into 3cm wide strips and each strip was transferred into a 5 ml plastic vial. Once dissected, the uterine tissue was stored in 0.1 M phosphate buffer, pH 7.4, containing 0.05% sodium azide at 4^{o}C until used for immunohistochemical staining.

2.4.2 Immunoperoxidase staining

Peroxidase immunohistochemistry was used to label axons in the whole mount preparations of rat uterine horns. At E14, E16, E18, E20, P1 and P3, one 3 cm strip from the ovarian, middle and cervical uterine segments from each rat were stained for tyrosine hydroxylase (TH; n = 29), calcitonin gene-related peptide (CGRP; n = 27) or vesicular acetylcholine transporter (VAChT; n = 30) and from each of 3 rats for neuropeptide Y (NPY). For the other time points (i.e., oestrus, P5, P7, P10, P14 and P28), staining for was done on whole uteri, an ovarian segment or a cervical segment from each rat (n = 27 rats for TH; n = 28 rats for CGRP; n = 24 rats for VAChT). Two ovarian and two cervical segments from different rats were stained for NPY at P7 and P14 (i.e., n=4 rats at each time point).

The primary and secondary antibodies used in this study are detailed in Table 2-1. In order to determine optimal dilutions, primary antibodies were titrated on 1 cm x 1 cm pieces of uterine whole mounts from staged or un-staged non-pregnant rats (Table 2.2). The optimal dilution was considered to be the dilution at which immunoreactive axons were best stained and background staining was minimal. VAChT was generally used at a dilution of 1:10,000. However, uterine horns from some rats were faintly stained so other uterine samples from these rats were stained with anti-VAChT at a dilution of 1:2500.

TABLE 2.1: PRIMARY AND SECONDARY ANTIBODIES USED

Antigen	Immunogen	Manufacturer, Species antibody was raised in, Mono- vs. polyclonal, Catalogue & Lot number	Dilution used
PRIMARY ANTIBODIES			
Tyrosine Hydroxylase (TH)	Tyrosine hydroxylase from rat pheochromocytoma (denatured with sodium dodecyl sulfate)	Chemicon International, rabbit, polyclonal, Catalogue # AB152, Lot # LV1375881, LV1382810	1:2,000
Neuropeptide Y (NPY)	Synthetic Neuropeptide Y	Kind Gift of Dr Bevan Jarrott, Monash University	1:10,000
Calcitonin gene related peptide (CGRP)	Synthetic rat Tyr-CGRP (23-37)	Biogenesis (UK), goat, polyclonal, Catalogue # 1720-9007, Lot # 22110851	1:5,000
Calcitonin gene related peptide (CGRP)	Synthetic rat alpha-CGRP coupled to bovine thyroglobulin with glutaraldehyde	Immunostar, rabbit, polyclonal, Catalogue # 24112, Lot # 1223001	1:20,000
Vesicular acetylcholine transporter (VAChT)	Strep-Tag fusion protein of the C-terminal part of rat VAChT (aa 475-530)	Synaptic Systems, rabbit, polyclonal, Catalogue # 139 103, Lot # 139103/22	1:10,000
SECONDARY ANTIBODIES			
Biotinylated anti-rabbit IgG	Rabbit Immunoglobulin G purified by immunoaffinity chromatography	Jackson ImmunoResearch Laboratories Inc.	1:500
Biotinylated anti-goat IgG	Goat Immunoglobulin G purified by immunoaffinity chromatography	Jackson ImmunoResearch Laboratories Inc.	1:500

The protocol for immunohistochemistry on whole mount preparations was identical to the one that I have published (Gnanamanickam and Llewellyn-Smith, 2011; Llewellyn-Smith and Gnanamanickam, 2011). The whole mounts were incubated in 30% methanol and 1% hydrogen peroxide in distilled water for 30 minutes to block endogenous peroxidise activity. This step was followed by 3 washes of 20 minutes each in immunobuffer (see Appendix) to remove cell membranes and then 30 minutes in 10% normal horse serum (Gibco Heat-Inactivated Horse Serum; Life Technologies, Mulgrave, Australia) diluted in immunobuffer (see Appendix) to prevent non-specific antibody binding. The whole mounts were then incubated in primary antibody diluted with 10% normal horse serum (Life Technologies, Mulgrave, Australia) in immunobuffer (see Appendix), secondary antibody diluted 1:500 with 1% normal horse serum (Life Technologies, Mulgrave, Australia) diluted in immunobuffer (see Appendix) and finally in ExtrAvidin peroxidase (Sigma Aldrich, St Louis, MO, USA) diluted 1:1500 in immunobuffer. All steps were carried out at room temperature. All incubations in immunoreagents were for at least 3 days. The whole mounts were washed 3 x 30 minutes in Tris-phosphate buffered saline (TPBS, see Appendix) after each incubation in an immunoreagent. Depending on the sizes of the pieces of uterine tissue, staining was done in 70 ml specimen containers using 8 ml of each immunoreagent or in glass crystallizing dishes using 12 ml of each immunoreagent.

Immunoreactive structures were visualized with a nickel-intensified diaminobenzidine (DAB) reaction (Llewellyn-Smith et al., 2005). Reactions were monitored using a dissecting microscope. The whole mounts were reacted until well-labelled axons with minimal background staining could be seen, which took 8-20 minutes. The whole mounts were then washed twice in TPBS to stop the reaction.

Reactions were followed by a 5 minute wash in TPBS and three x 10 minute washes in 0.1M phosphate buffer, pH 7.4. Whole mounts were stored in 0.1M phosphate buffer at 4^{o}C until they were processed into resin.

2.4.3 Controls for Antibody Specificity

To test antibody specificity, absorption controls were carried out on the anti-CGRP antibody and the anti-VAChT antibody used in this project.

The anti-CGRP antibody was absorbed with CGRP (Cat #2112, Auspep, Tullamarine, Victoria, Australia). A 200µg/ml solution of CGRP was prepared by dissolving 100 µg of CGRP in 500 µl of 0.1M glacial acetic acid. Unabsorbed anti-CGRP, anti-CGRP + 10 µg/ml CGRP, anti-CGRP + 1 µg/ml CGRP and anti-CGRP + 0.1 µg/ml CGRP were prepared and stored at 4^{o}C overnight. The final dilution of the anti-CGRP was 1:10,000. Pieces of uterine tissue 0.5 cm x 1 cm from non-pregnant rats were immunostained with the absorbed and unabsorbed antibody solutions. No CGRP-immunoreactive axons were found in uterine tissue stained with anti-CGRP absorbed with 10 µg/ml CGRP whereas staining with the unabsorbed antibody showed the expected distribution of CGRP-immunoreactive axons in the uterus.

The anti-VAChT antibody was absorbed with VAChT (Catalogue # 139-1P, Synaptic Systems, Goettingen, Germany). A 200 µg/ml solution of VAChT was prepared by dissolving 100 µg of VAChT in 500 µl of filtered deionized water. Unabsorbed anti-VAChT, anti-VAChT + 25 µg/ml VAChT, anti-VAChT + 10 µg/ml VAChT, anti-VAChT + 1 µg/ml VAChT and anti-VAChT + 0.1 µg/ml VAChT were prepared and incubated at 4^{o}C overnight. The final dilution of the anti- VAChT antibody was 1:5000.

TABLE 2.2: ANTIBODY TITRATIONS

Antibody	Dilutions tested	Dilution used
rabbit anti-TH	1:1000, 1:2000, 1:5000, 1:10,000	1:2,000
rabbit anti-NPY	1:1000, 1:2000, 1:5000, 1:10,000	1:10,000
goat anti-CGRP	1:2000, 1:5000, 1:10,000, 1:20,000	1:5,000
rabbit anti-CGRP	1:2,000, 1:5,000, 1:10,000, 1:20,000	1:20,000
rabbit anti-VAChT	1:2,000, 1:5,000, 1:10,000, 1:20,000	1:2,500 [a] 1:10,000 [b]

[a] E14 (n=3), E16 (n=1), E18 (n=1), P7 (n=1), P10 (n=1), P14 (n=2), P28 (n=4); experiments that had to be repeated due faint staining at a dilution of 1:10,000 were repeated with a dilution of 1:2500.

[b] OEST (n=4), E14 (n=1), E16 (n=3), E18 (n=3), E20 (n=4), P1 (n=4), P3 (n=4), P5 (n=4), P7 (n=3), P10 (n=3), P14 (n=2).

Pieces of non-pregnant uterine tissue were immunostained with the unabsorbed and absorbed antibody solutions using the same immunostaining protocol as for the anti-CGRP absorption control above. Absorption of the anti-VAChT antibody with 25 µg/ml VAChT abolished staining of uterine VACHT- immunoreactive axons whereas staining with the unabsorbed antibody showed the expected staining pattern for VAChT in the uterus.

Absorption controls have previously been carried out on the anti-NPY antibody used here (Llewellyn-Smith et al., 1990). No NPY staining was present with anti-NPY absorbed with 10^{-6} M NPY while the unabsorbed anti-NPY stained neurons and fibers as expected in the spinal cord. The antibody also labels neurons in the expected locations in the medulla.

The anti-TH antibody also shows the expected labelling pattern for medullary neurons and axons in the spinal cord. The specificity of this anti-TH antibody has been tested by the supplier using western blotting; a single band at ~62k Da (reduced) was labelled, corresponding to molecular weight of TH.

2.4.4 Processing uterine whole mounts into resin

After immunostaining, the whole mounts were processed into epoxy resin (Llewellyn-Smith and Gnanamanickam, 2011). The stained whole mounts were washed 2 x 15 minutes in distilled water to remove salts. The whole mounts were then placed in crystallizing dishes under weighted wire meshes to keep the whole mounts flat (Figure 2.2) and then dehydrated by 2 x 15 minute washes in graded acetone solutions (30%, 50%, 70%, 90%, 95%, and 100% acetone).

FIGURE 2.2: PROCESSING FULL-THICKNESS UTERINE WHOLE MOUNTS INTO RESIN

A, Purpose-built weighted wire meshes were used to keep the immunostained whole mount preparations of uterine horns flat while they were being dehydrated in crystallizing dishes. B, A uterine whole mount being infiltrated with resin in a Petri dish. Arrows, meniscus of the resin. C, A uterine whole mount has been embedded on a glass slide under an Aclar coverslip and polymerized at 60^{o}C. Dotted lines, corners of the Aclar coverslip.

Reproduced from Llewellyn-Smith and Gnanamanickam (2011 (Llewellyn-Smith and Gnanamanickam, 2011)).


A

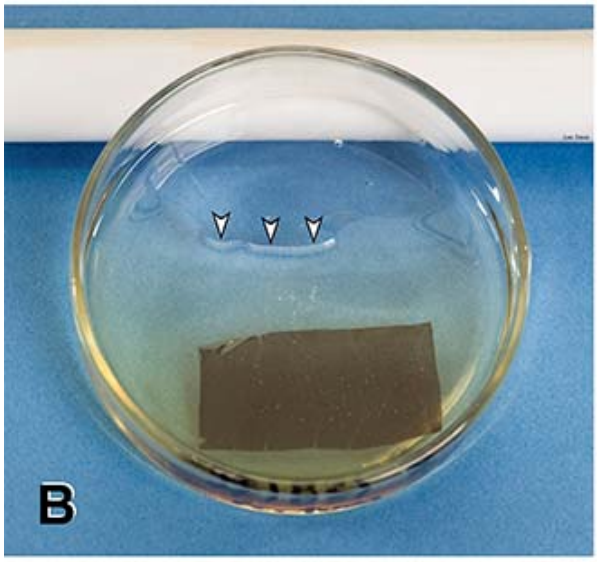
B


C

After 2 x 10 minute washes in propylene oxide, the whole mounts were infiltrated with 1:1 propylene oxide: resin for at least 30 minutes. Before the resin was used for infiltration, it was degassed under vacuum for at least 30 minutes. For infiltration with resin, the whole mounts were placed in glass petri dishes in pools of resin, heated for 10 minutes at 60^{o}C and then left overnight under vacuum at room temperature. The whole mounts were then placed on glass slides in resin, degassed under vacuum for at least 30 minutes, coverslipped with Aclar cover slips and finally polymerized at 60^{o}C for 24 to 48 hours.

2.4.5 Data Collection and Analysis

Quantification of the density of TH-, CGRP- and VAChT-immunoreactive axons at E14, E16, E18, E20, P1 and P3 was done on one 3 cm strip from the ovarian, middle and cervical uterine segments from each of 4 rats. To collect data at oestrus, P5, P7, P10, P14 and P28, the densities of TH-, CGRP- and VAChT-positive axons were quantified on two whole uteri, one ovarian segment and one cervical segment from 4 different rats for each antigen at each time point.

2.4.5.1 Photography

Photographs of the immunostained, resin-embedded whole mounts of uterine horns were taken with a Canon digital camera by Mr. David Summerhayes, Media and Illustration Department, Flinders Medical Centre, and saved as TIFF files. Digital photomicrographs of the whole mounts were collected using an Olympus BH2 brightfield microscope and a SPOT Insight Model 18.2 firewire colour camera controlled by SPOT software version 5.2 (Diagnostic Instruments Inc., Sterling Heights, MI, USA).

2.4.5.2 Quantifying Innervation Density

The slides and corresponding Canon photographs of the immunostained uterine whole mount preparations were blinded and numbered by Prof Ida Llewellyn-Smith. Innervation density was quantified in the middle third of the middle segment of each uterine horn using an unbiased stereological method. For each marker (i.e., TH, VAChT and CGRP), uterine horns from each of 4 rats at each time point were analyzed.

To determine the locations where innervation density would be quantified, a new layer was added to the Canon digital image of each uterine whole mount in Adobe PhotoShop and the area for quantification was marked out using guides, rulers and the line tool. On photographs of uterine horns from non-pregnant and post-partum rats at P5, P7 (Figure 2.3), P10, P14 and P28, lines were drawn to divide the uterine horn into thirds, which contained the ovarian, middle and cervical segments. The middle segment of the horn was then divided into thirds around its circumference. For quantifying innervation density at E14, E16, E18, E20, P1 and P3, the immunostained 3 cm strip from the middle segment of each uterine horn was divided into thirds around its circumference. A locating grid with 500μm x 500 μm squares was constructed in Adobe Photoshop and saved as a TIFF file. The file containing the locating grid was added to the photograph of the stained uterine horn as a new layer and the locating grid was positioned so that the middle third of the middle segment where innervation density was to be quantified was completely covered by grid squares. The squares of the locating grid that overlay the middle third of the middle segment were then numbered (Figure 2.3A).

FIGURE 2.3: QUANTIFYING INNERVATION DENSITY

A, Digital photograph of an entire uterine horn immunostained for TH from a rat at P7. The horn was divided into thirds to give ovarian, middle and cervical segments and then the middle segment was divided into thirds circumferentially. To define areas for quantifying innervation density, a locating grid with 500 μm x 500 μm squares was placed over the middle third of the middle segment. The higher magnification views show the squares of the locating grid after numbering. The 5 randomly chosen squares in which axonal intersection were counted (Squares 4, 30, 37, 56 and 126) are n in pink. B, Brightfield photomicrograph of Box 30 in the locating grid to which the counting grid containing 50 μm x 50 μm squares has been added as another layer in Adobe Photoshop. Montage of 6 micrographs. C, Brightfield photomicrograph of Box 37 in the locating grid to which the counting grid containing 50 μm x 50 μm squares has been added as another layer in Adobe Photoshop. Montage of 2 micrographs.

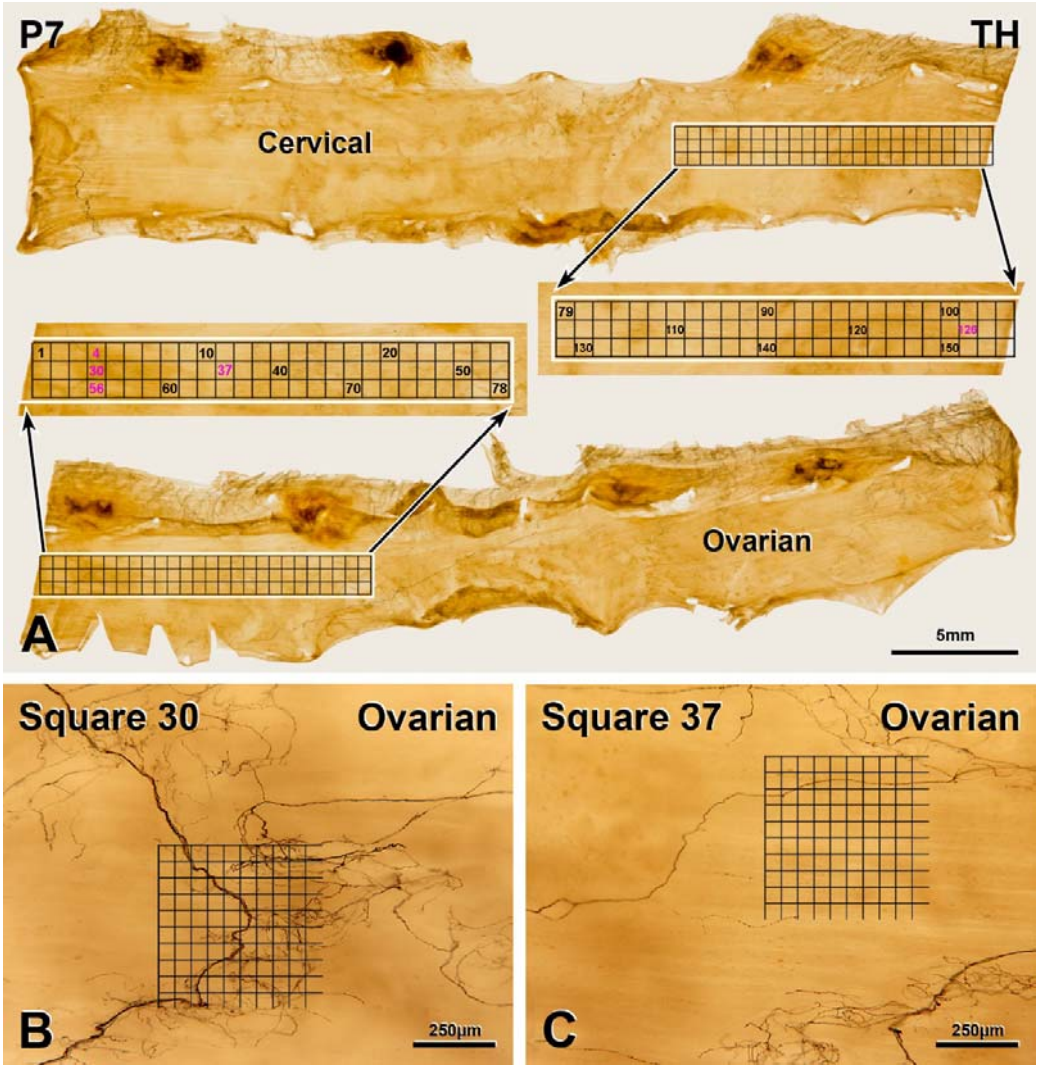
P7
TH
Cervical
Ovarian
A
5mm
Square 30
Ovarian
B
250µm
Square 37
Ovarian
C
250µm

In uterine horns that had been divided in half before immunostaining, grid squares that were less than 80% filled with uterine tissue were excluded. To define locating grid squares for counting, the RANDBETWEEN(1,total number of boxes) function in Microsoft Excel was used to generate five random numbers from the total number of squares in the locating gird for each uterine horn (for example, =RANDBETWEEN(1,250) for a horn in which the middle region of the middle segment was completely covered by 250 squares of the locating grid). The five randomly-chosen squares were then marked on the Canon photograph of the resin-embedded whole mount (Figure 2.3A).

Brightfield photomicrographs of each area of the immunostained uterine horn overlaid by one of the five randomly-chosen squares in the locating grid were taken using an x10 objective (Figure 2.3B and 2.3C). In each randomly-chosen square of the locating grid, every focal plane containing axons was photographed throughout the thickness of the entire uterine wall. All the micrographs from each selected square in the locating grid were then layered on top of each other in Adobe Photoshop to produce a single TIFF file.

Innervation density in each TIFF file containing a stack of micrographs was quantified by counting intersection of immunoreactive axons with the bars of a 500 µm x 500 µm counting grid that consisted of 50 µm x 50 µm squares. The counting gird was constructed in Adobe Photoshop and saved as a TIFF file. The file containing the counting grid was added as a layer to the file containing the stack of images through all the focal planes of each randomly-selected locating square. A new layer called “Counts” was added and each intersection of an axon with a grid bar was marked on the “Counts” layer with a dot made by the pencil tool. All counts were done at very high magnification in Photoshop (x400, using the zoom tool). Axonal

intersections that occurred anywhere within the thickness of the uterine wall were recorded and the TIFF file was saved. When bundles of axons were encountered, each axon that was individually visible on high magnification (x400, using the zoom tool) in Photoshop was counted separately. When it was not possible to clearly distinguish how many axons were in an axon bundle, only one intersection was counted.

Intersections of immunoreactive axons with grid bars were counted using Image J. The "Counts" layer generated above was saved as a new TIFF file in Adobe Photoshop and converted to grayscale. The grayscale image was opened in Image J and the dots (representing axonal intersections that had been marked with the pencil tool in Adobe Photoshop) were counted using the Analyze Particle function. The total number of axonal intersections from each counting square was saved to an Excel worksheet and the intersection data from the twenty randomly selected counting squares (5 counting squares / rat x 4 rats) at each time point were averaged.

From a statistical perspective, axonal intersections as a measure of innervation density in the rat uterus during pregnancy and post-partum is considered a count measurement because there are many independent variables (i.e., time points) that affect the outcome or the dependant variables (number of intersections of axons with grid bars). To analyze these data statistically, it is therefore necessary to do Poisson Regression Analysis, which was performed using the statistical package, STATA, by Dr Shahid Ullah, Flinders Centre for Epidemiology and Biostatistics, Flinders University). Excel files containing details about time point, rat number, total number of locating grid squares in each uterine horn, the numbers given to the five squares randomly-chosen from the total number of locating grid squares in each horn and the

total number of intersections in each square counted was sent to Dr Ullah, for analysis. Incidence rate ratio (IRR) is a relative measure of the effect of a particular time point on the number of intersections. IRR was generated by STATA when Poisson Regression Analysis was performed. Because there were sizeable differences in the areas of the uterus between the different time points; counts were normalized by total number of locating grid squares for each horn during the statistical analysis.

2.5 MICRORNAS IN THE MAJOR PELVIC GANGLION

2.5.1 Tissue Preparation

Rats at oestrus, pregnancy day 20 day (E20), post-partum day 5 (P5) and post-partum day 14 (P14) were used to examine changes in miRNA expression during pregnancy and post-partum. Rats were anesthetized with isoflurane in oxygen administered through a nose cone and a horizontal incision was made in the pelvic area. Retractors were used to move organs aside, exposing the area around the cervix and bladder, where the major pelvic ganglia (MPG) are located. Stitches were placed in the connective tissue close to the right and left MPGs in order to mark their locations and the nose cone was removed. To maintain anesthesia, the rat was immediately injected with Lethabarb diluted to 60 mg/ml with distilled water (dose = 60 mg/kg) and then perfused transcardially with saline as described in Section 2.3. Once the perfusion had been completed, both MPGs were removed from each rat and placed in PBS. The MPGs were pinned on a Sylgard coated Petri dish and as much extraneous tissue as possible was removed with the aid of a dissecting microscope. The MPGs were then stored in RNA Later (Life Technologies, Mulgrave, Australia) at 4^{o}C overnight in labelled 1.5ml Eppendorf tubes. The following day, the RNA Later was drained

from the MPGs and they were transferred to a -80^{o}C freezer. One non-pregnant rat at oestrus was perfused as above and the hypothalamus was removed for the collection of total RNA. The hypothalamus was also stored in RNA Later overnight at 4^{o}C and transferred to the -80^{o}C freezer the following day.

2.5.2 RNA Extraction

MPGs were transported on dry ice from the -80^{o}C freezer to the laboratory of Dr Michael, Flinders Centre for Innovation in Cancer. Each MPG was transferred into 0.2 ml of Trizol (Life Technologies) and homogenized using a power homogenizer and homogenization pestles (Sigma Aldrich; Z359947-100EA, Castel Hill, NSW, Australia). To prevent the degradation of RNA, MPGs were not allowed to thaw prior to homogenization. Once ganglia had been homogenised, an additional 0.3 ml of Trizol was added and the samples were incubated at room temperature for 5 minutes. After the addition of 0.1 ml of chloroform, each sample was shaken vigorously by hand for 15 seconds and then incubated at room temperature for 2-3 minutes. Samples were then centrifuged with a Sigma 1-14 microfuge (Sigma Laborzentrifugen GmbH, Osterode, Germany) for 15 minutes at 12,000g at 2-8^{o}C. The aqueous phase containing extracted RNA was transferred to a sterile Eppendorf tube to which 250 µl of isopropanol and 2 µl of 20 µg/ml glycogen were added. The samples were stored overnight at -20^{o}C to allow RNA to precipitate and then centrifuged at 20,000g for 20 minutes using a Sigma 1-14 centrifuge. After centrifugation, the supernatant was carefully removed without disturbing the pellet. One ml of chilled 75% ethanol was added to the supernatant; the solution was vortexed and centrifuged using a Sigma 1-14 centrifuge for 5 minutes at 7500g. The supernatant was carefully removed without disturbing the pellet, which was left to air

dry for approximately 5 minutes and then dissolved in 10 µl of sterile distilled water. One microlitre of the dissolved RNA was used to determine the total amount of RNA in each of the MPG samples using a Nanodrop 8000 spectrophotometer (Thermoscientific, Wilmington, DE, USA).

A. RNA was also extracted from the hypothalamus of the one non-pregnant rat at oestrus using the protocol above. Total RNA from this hypothalamus was used to generate standard curves for the PCR experiments.

2.5.3 Microarray Analysis

Total RNA from MPGs extracted using Trizol, as above, was sent to Mr. Mark van der Hoek, Adelaide Microarray Centre, Adelaide, Australia. RNA quality was determined using a Bioanalyzer (Agilent Technologies, Santa Clara, CA, USA). MicroRNA v4 arrays (Affymetrix, Santa Clara, CA, USA) were used for the microarray analysis. In summary, RNA samples were labelled with FlashTag Biotin HSR and hybridised overnight on an Affymetrix miRNAv4 array. After hybridisation, the arrays were washed and stained following the Fluidics protocol. Finally, the arrays were scanned using GeneChip Scanner 3000 7G. The resulting intensity data was analysed using Partek software (Partek Inc. St. Louis, Missouri, USA). Data was normalised using the RMA normalisation method with mean probeset summarisation. Analysis of Variance (ANOVA) was used to determine differential expression.

2.5.4 Quantitative Real-Time Polymerase Chain Reaction (qRT-PCR)

MicroRNA-specific cDNA was synthesized from samples of total RNA extracted from MPGs. Forty nanograms of each total RNA sample were diluted with 20 µl of sterile distilled water to give a final RNA concentration of 2 ng/µl.

Serial dilutions of total RNA from the hypothalamus were used to construct standard curves. Eight hundred nanograms of hypothalamic total RNA was diluted to 100 µl with sterile distilled water to give a final RNA concentration of 8 ng/µl. For PCR reactions, each well contained 3.5 µl of master mix, 2.5 µl of diluted RNA and 1.5 µl of Taqman microRNA assay primer (Applied Biosystems, Foster City, CA, USA). A Taqman reverse transcription kit (Catalogue # 4366596, Applied Biosystems) was used to make up the master mix, which contained 0.095 µl of RNAse inhibitor, 0.75 µl of 10X reverse transcription buffer, 0.50 µl of reverse transcriptase and 0.075 µl of 100 mM nucleoside triphosphates containing deoxyribose (dNTPs). The reverse transcription PCR reaction was done in Axygen sterile 8 strip tubes (Adelab Scientific, Therbaton, South Australia) in a thermal cycler (Applied Biosystems). cDNA was synthesized by incubating the reaction mixture at 16^{o}C for 30 minutes, 42^{o}C for 30 minutes and 85^{o}C for 5 minutes. The solution containing synthesized cDNA was maintained at 4^{o}C until use.

Following the preparation of cDNA, real time PCR was done. The master mix for Real Time PCR contained 3.84 µl nuclease free water, 5 µl Taqman 2x Universal master mix (Applied Biosystems,) and 0.50 µl Taqman Assay Primer per reaction (Applied Biosystems). Real time PCR reactions were done in Axygen sterile 4-strip 0.1 ml tubes (Adelab Scientific) using 1 µl of cDNA plus 9.34 µl of master mix. The tubes were loaded into a thermal cycler (Qiagen Rotogene Q, Chadstone Centre,

Victoria, Australia) and incubated for 10 minutes at 95^{o}C then cycled for 15 seconds at 95^{o}C and 60 seconds at 60^{o}C for 50 cycles. Samples were tested in triplicate.

As this is the first study to examine miRNAs in MPGs, it was necessary to test different housekeeping genes to establish the best one for assessing levels of miRNA in MPGs. U6snRNA, U87 and sno234 were chosen as test house-keeping genes based on literature examining miRNA in various neuronal tissue and advice from Prof Rainer Haberberger, Department of Anatomy and Histology, Flinders University. The expression level of U87 was high in the RNA samples from MPGs and showed minimal variation across the different time points examined. U87 was therefore chosen as the housekeeping gene for all RT-PCR reactions on RNA extracted from MPGs.

Taqman miRNA assays (Table 2-3) were used to assess changes in miRNA expression levels in the MPG during pregnancy and post-partum. The cycle threshold (Ct) values, i.e. the number of cycles required for the fluorescent signal to increase above threshold/background level, were determined for RNA from MPGs by Rotor-gene 6000 series software (Version 5.0.61; Corbett Research, Mortlake, NSW, Australia). Qgene software (Simon, 2003) was used to calculate relative miRNA expression levels from Ct values. GraphPad Prism (GraphPad Software, Inc., La Jolla, CA, USA) was used for statistical analysis and for the generation of graphs. Statistical significance was established using unpaired Student t tests. A P value of <0.05 was considered statistically significant.

TABLE 2.3: TAQMAN MIRNA ASSAYS

MiRNA	Assay ID (Catalogue Number)	Mature miRNA sequence
RNU6B	001093	CGCAAGGATGACACGCAAATTCGTGAAGC GTTCCATATTTTT
U87	001712	ACAATGATGACTTATGTTTTTGCCGTTTAC CCAGCTGAGGGTTTCTTTGAAGAGAGAAT CTTAAGACTGAGC
miR-221	000524	AGCUACAUUGUCUGCUGGGUUUC
miR-222	002276	AGCUACAUCUGGCUACUGGGU

Chapter 3

Changes in sympathetic innervation of the rat uterus during pregnancy and postpartum

3.1 INTRODUCTION

As detailed in Chapter 1, the non-pregnant rat uterus is richly supplied with sympathetic nerves. Sympathetic axons identified by immunoreactivity for tyrosine hydroxylase (TH) or neuropeptide Y (NPY) occur in the longitudinal and circular muscle layers, the endometrium, around blood vessels and rarely near the endometrial glands (Alm and Lundberg, 1988; Bae et al., 2001; Gnanamanickam and Llewellyn-Smith, 2011; Owman et al., 1986; Papka et al., 1985). The linea uteri, a thick band of longitudinal muscle lying opposite the mesometrium, has more TH- and NPY- immunoreactive axons than the rest of the uterine smooth muscle (Gnanamanickam and Llewellyn-Smith, 2011). During pregnancy, there is a significant reduction in the sympathetic innervation of the uterus in rats (Chavez-Genaro et al., 2006; Klukovits et al., 2002), guinea pigs (Alm et al., 1979; Alm and Lundberg, 1988; Fried et al., 1985; Sporrong et al., 1981) and humans (Thorbert et al., 1979); but the extent of the denervation has not been quantitatively assessed. Re-innervation of the uterus begins immediately after birth (24 to 48 hours) (Haase et al., 1997) but very little is known about the process or time course of re-innervation of the uterus that occurs post-partum (see Chapter 1). Therefore, the aim of this chapter was to describe in detail the sympathetic denervation and re-innervation of the rat uterus during pregnancy and postpartum and to quantify the density of TH-immunoreactive sympathetic axons at oestrus, at pregnancy days E14, E16, E18, E20

and at postnatal days P1, P3, P5, P7, P10, P14, P28. Immunostaining for NPY was also done on uteri from rats at pregnancy days E14, E16 and E18 and at postpartum days P1, P3, P7 and P14. Because NPY is also present in some parasympathetic nerves (Markiewicz et al., 2003), the densities of uterine NPY-immunoreactive axons were not quantified at any of the times points examined.

3.2 RESULTS

3.2.1 Changes in the dimensions of the uterus during pregnancy and postpartum

Before fixation, uterine horns were pinned into Sylgard-coated Petri dishes. In order to obtain an estimate of how much the uterus changed in size during pregnancy and post-partum, I measured the lengths and widths of stretched uterine horns after they were fixed. These size data for all of the stretched and fixed uterine horns examined during the course of this project are summarised in Table 3.1.

Stretched uterine horns increased in size as pregnancy progressed and decreased in size as time after delivery increased. From oestrus to E20, the length of stretched and fixed uterine horns quadrupled and their lengths increased approximately 3-fold. By P28, the lengths and widths of the horns had returned to approximately those of stretched and fixed horns from rats at oestrus.

TABLE 3.1: DIMENSIONS OF PREGNANT AND POST-PARTUM UTERINE HORNS

Time	Average length (cm ± SE)	Average width (cm ± SE)
Oestrus	6.12 ± 0.11	0.95 ± 0.10
E14	16.14 ± 0.70	2.18 ± 0.06
E16	16.96 ± 1.15	2.34 ± 0.09
E18	18.81 ± 0.84	2.92 ± 0.06
E20	24.3 ± 1.89	3.37 ± 0.06
P1	11.29 ± 0.58	2.22 ± 0.04
P3	8.58 ± 0.23	1.09 ± 0.03
P5	6.99 ± 0.17	0.82 ± 0.02
P7	7.61 ± 0.15	0.69 ± 0.02
P10	7.45 ± 0.17	0.58 ± 0.02
P14	7.59 ± 0.19	0.50 ± 0.03
P28	6.64 ± 0.13	0.79 ± 0.04

3.2.2 Changes in uterine sympathetic innervation revealed by immunostaining for TH

As mentioned in Chapter 2, TH innervation was assessed at twelve different time points were examined during pregnancy and post-partum, E14 (n=5), E16 (n=4), E18 (n=4), E20 (n=4), P1 (n=6), P3 (n=5), P5 (n=4), P7 (n=5), P10 (n=4), P14 (n=4), P28 (n=10). TH innervation of the non-pregnant rat uterus at oestrus (n=4) was also analyzed.

3.2.2.1 Oestrus : Figure 3.1

I have previously described the TH-immunoreactive innervation of the non-pregnant rat uterus at oestrus (Gnanamanickam and Llewellyn-Smith, 2011). At this stage of the oestrus cycle, non-pregnant uterine horns receive a significant number of TH-immunoreactive axons, which enter the uterus through the mesometrium, usually in association with blood vessels. At their entry points, the TH-positive axons are present mainly in thick nerve bundles but also occur as single axons. Within the uterus, thick nerve bundles containing many TH-positive axons are also present. In the non-pregnant uterus at oestrus, all blood vessels are innervated by TH-immunoreactive axons, which form dense perivascular plexuses around the blood vessel walls (Figure 3.1A). Many TH-stained axons are present in the longitudinal and circular muscle layers. The linea uteri has more TH-immunoreactive axons than the rest of the longitudinal smooth muscle (Figure 3.1B). Some TH axons travel to the endometrium from the myometrium. On rare occasions, these endometrial TH-immunoreactive axons travel close to uterine glands.

FIGURE 3.1: TH-IMMUNOREACTIVE INNERVATION OF THE NON-PREGNANT RAT UTERUS AT OESTRUS

A and B show different focal planes through the same region of a rat uterine horn at oestrus. A, A blood vessel is surrounded by a dense plexus of TH-immunoreactive axons. B, TH-immunoreactive axons in the linea uteri.

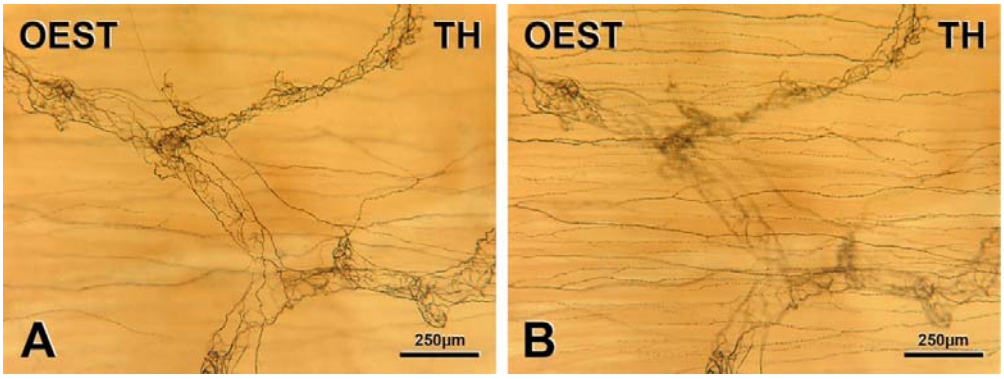
OEST
TH
A
250µm
OEST
TH
B
250µm

FIGURE 3.2: TH-IMMUNOREACTIVE INNERVATION OF THE PREGNANT RAT UTERUS AT E14

A, The perivascular plexus of TH-immunoreactive axons around a blood vessel is less dense than at oestrus. B, Individual TH-immunoreactive axons in the longitudinal muscle layer. C, Whole mount preparation of a strip from the middle segment of an E14 uterine horn. Letters indicate the location of the micrographs in D-F. D & E, Fragmented degenerating axons. F, An area in the E14 uterus with no TH-positive innervation.

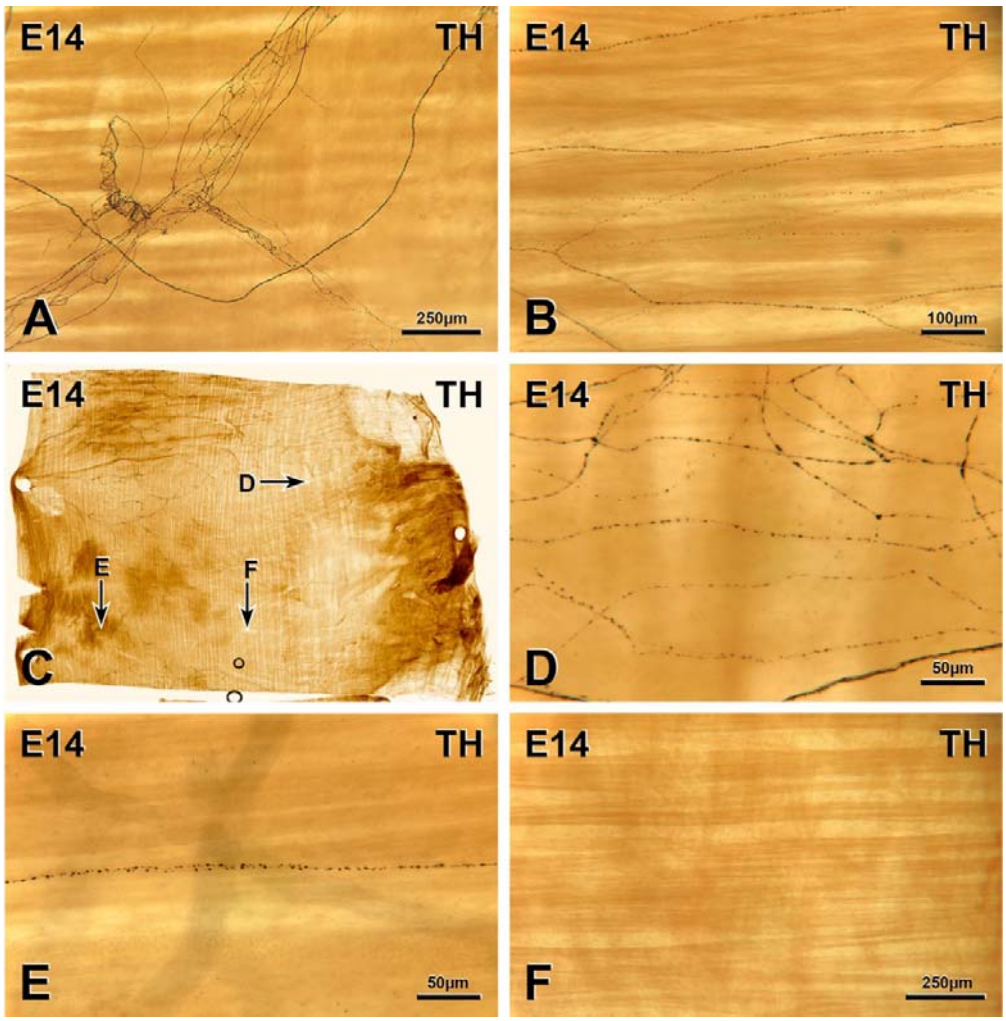
E14
TH
A
250µm
E14
TH
B
100µm
E14
TH
D
E
F
C
E14
TH
D
50µm
E14
TH
E
50µm
E14
TH
F
250µm

3.2.2.2 Pregnancy day 14 (E14) : Figure 3.2

On pregnancy day E14, the density of TH-immunoreactive axons was much lower for all types of tissue in all uterine layers (longitudinal muscle, circular muscle and endometrium) and all uterine regions (ovarian, cervical and middle) than in the non-pregnant uterus at oestrus. The ovarian region of each uterine horn was more densely innervated than the middle and cervical regions.

Some TH-positive axons entered the uterus along with blood vessels and followed the blood vessels as they branched and connected with other blood vessels. Many but not all blood vessels received TH innervation; but the density of innervation was usually less than in the non-pregnant uterus (Figure 3.2A). Rare blood vessels were lacking in TH innervation. A few thick nerve bundles containing some TH-immunoreactive axons were present throughout the uterus. In the middle region of the uterine horn in one rat, a thick nerve bundle travelled from the mesometrium to the anti-mesometrium and showed signs of degeneration in the anti-mesometrium. The innervation of the myometrium was much less at E14 than at oestrus. Very few single TH axons were present in the longitudinal muscle layer (Figure 3.2B). Rare TH-immunoreactive axons not associated with blood vessels occurred in the circular smooth muscle. At E14, there were no TH-immunoreactive axons in the linea uteri. Rare TH-immunoreactive axons were present in the endometrium; these axons travelled to the endometrium from around blood vessels in the myometrium. Areas lacking TH innervation were present in E14 uterine horns (Figure 3.2F). Areas without innervation were more common on the anti-mesometrial side compared to the mesometrial side. Areas without TH innervation were never seen in non-pregnant uterine horn at oestrus.

Degenerating TH-immunoreactive axons were present throughout the E14 uterus (Figure 3.2D&E). Axons that were clearly fragmenting or swollen with condensed axonal content were classified as degenerating (Klukovits et al., 2002; Sporrong et al., 1981). The density of degenerating axons was similar in ovarian, middle and cervical regions of the uterus.

3.2.2.3 Pregnancy day 16 (E16) : Figure 3.3

The TH innervation of the uterus at E16 was less dense than at E14 in all regions and all layers. Ovarian segments of E16 uterine horns had the most TH-immunoreactive axons and middle segments had very few TH-positive axons compared to the ovarian and cervical segments.

Blood vessels received less TH innervation at E16 than at E14 (Figure 3.3A&B). Although some blood vessels received TH-immunoreactive axons, blood vessels without any TH innervation were also present. In the middle and cervical segments, the number of perivascular TH-immunoreactive axons was lower than in ovarian segments. A few thick nerve bundles containing some TH-positive axons were present throughout the uterus (Figure 3.3C). In the myometrium, there were very few single TH axons not associated with blood vessels, especially in the longitudinal muscle. In the ovarian-most region of uterine horns from two rats, more TH-immunoreactive axons were present in the linea uteri compared to the rest of the smooth muscle. There were no TH-immunoreactive axons in the linea uteri in the other rats examined. Rare TH-immunoreactive axons associated with blood vessels travelled in a loop to the endometrium.

FIGURE 3.3: TH-IMMUNOREACTIVE INNERVATION OF THE PREGNANT RAT UTERUS AT E16

A, TH innervation in the middle region of an E16 uterine horn. B, A blood vessel (arrow) has a perivascular plexus of TH-immunoreactive axons but the plexus is less dense than at oestrus. C, A thick nerve bundle in the myometrium contains some TH-immunoreactive axons. D, An area without any TH innervation in the middle region of an E16 uterine horn. E, Degenerating TH-immunoreactive axons that are beginning to fragment (arrows). F, A degenerating TH-immunoreactive axon that is swollen (arrow).

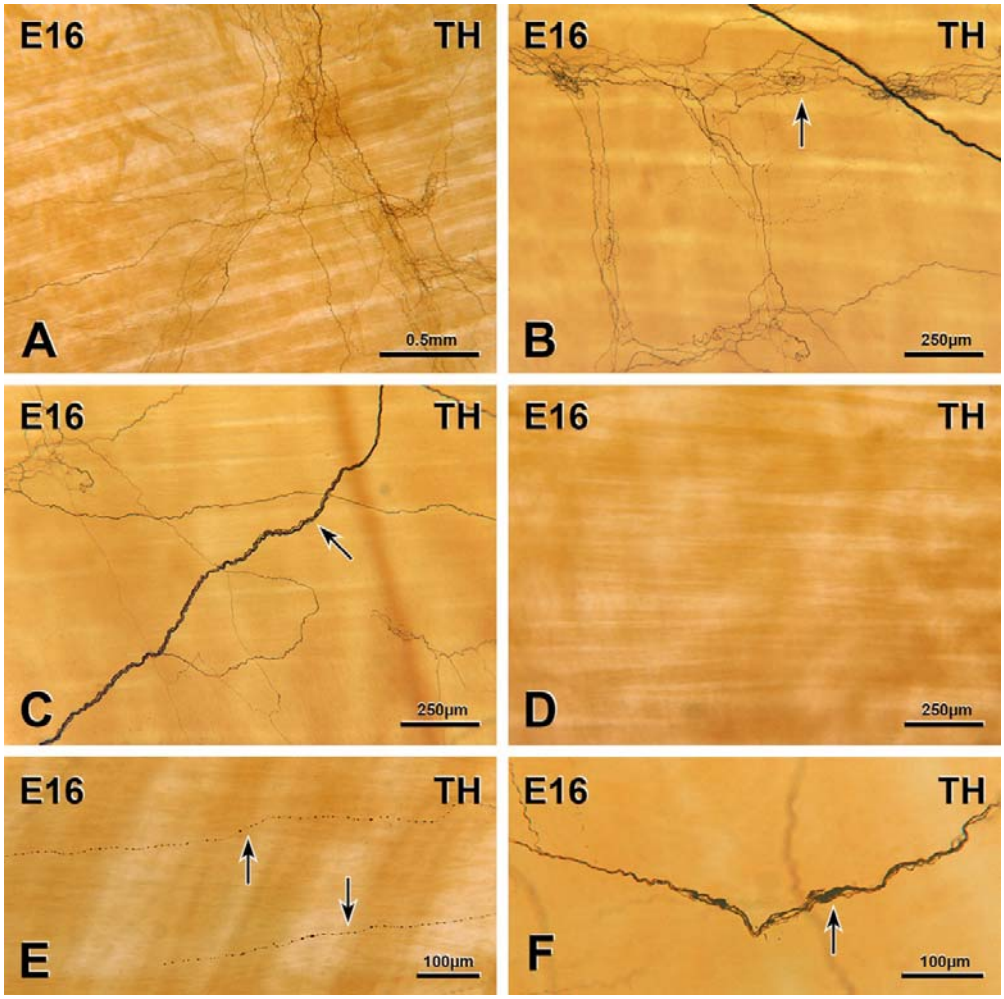
E16
TH
A
0.5mm
E16
TH
B
250µm
E16
TH
C
250µm
E16
TH
D
250µm
E16
TH
E
100µm
E16
TH
F
100µm

Degenerating TH-immunoreactive axons (Figure 3.3E&F) were present at E16; they were common throughout the uterus and present in all regions i.e., ovarian, middle, cervical, mesometrial and anti-mesometrial. Many areas were not innervated by TH-positive axons (Figure 3.3D). Areas without innervation were common throughout the E16 uterus.

3.2.2.4 Pregnancy day 18 (E18) : Figure 3.4

E18 uterine horns had fewer TH-immunoreactive axons in all regions and layers than E14 and E16 horns. At E18, the ovarian regions of uterine horns were more densely innervated than the middle and cervical regions. The middle segments of E18 uteri received the least TH innervation.

The density of TH-immunoreactive axons around blood vessels and the number of innervated blood vessels was lower at E18 compared to E14 and E16. Many uterine blood vessels lacked TH innervation at E18 and only a few blood vessels had TH-immunoreactive axons associated with them (Figure 3.4A&B). In the ovarian region, occasional blood vessels were surrounded by a few more TH-immunoreactive axons than in the other regions. Few thick nerve bundles containing few TH-immunoreactive axons were present in E18 uterine horns and only a few individual TH-positive axons occurred in the myometrium. The innervation of the linea uteri varied among E18 rats. In one rat, there were more TH-positive axons in the linea uteri at its ovarian-end compared to the rest of the smooth muscle whereas there were no TH-immunoreactive axons in the linea uteri in the other rats. Very rare TH-immunoreactive axons travelled to the endometrium from blood vessels in the myometrium.

Most of the TH-stained axons in E18 uterine horns were fragmented and degenerating (Figure 3.4C). Axons with this appearance were present throughout the E18 uterus. Many areas in the E18 uterine horns also lacked any TH innervation (Figure 3.4D); these regions were more common at E18 than at E16.

3.2.2.5 Pregnancy Day 20 (E20) : Figure 3.5

E20 uterine horns had the lowest density of TH-immunoreactive axons of any of the time points examined. E20 horns had fewer TH-positive axons in all layers and regions than E18 horns.

In my Master's thesis, I described in detail the innervation of the rat uterus at pregnancy day 20. To summarize, the number of TH-immunoreactive axons was very substantially reduced in E20 compared to non-pregnant uterine horns. Very few TH-immunoreactive axons entered the uterus through the mesometrium and there were hardly any TH-positive axons in the horns themselves. Occasionally, TH-immunoreactive axons ran alongside a blood vessel but did not appear to wrap around the blood vessel and perivascular axons were rarely present (Figure 3.5B&C). Almost no TH-stained axons were present on the anti-mesometrial side of the E20 uterus. Overall, almost every areas of E20 uterine horns completely lacked any TH innervation so that the horn was virtually denervated (Figure 3.5D,H,L).

FIGURE 3.4: TH-IMMUNOREACTIVE INNERVATION OF THE PREGNANT RAT UTERUS AT E18

A, A blood vessel (BV) is surrounded by a sparse perivascular plexus of TH-immunoreactive axons. B, A few TH-immunoreactive axons run alongside a blood vessel (BV on right) but the blood vessel lacks a perivascular plexus of TH-immunoreactive axons. C, A degenerating TH-immunoreactive axon that is fragmenting. D, An area of an E18 uterine horn without any TH innervation.

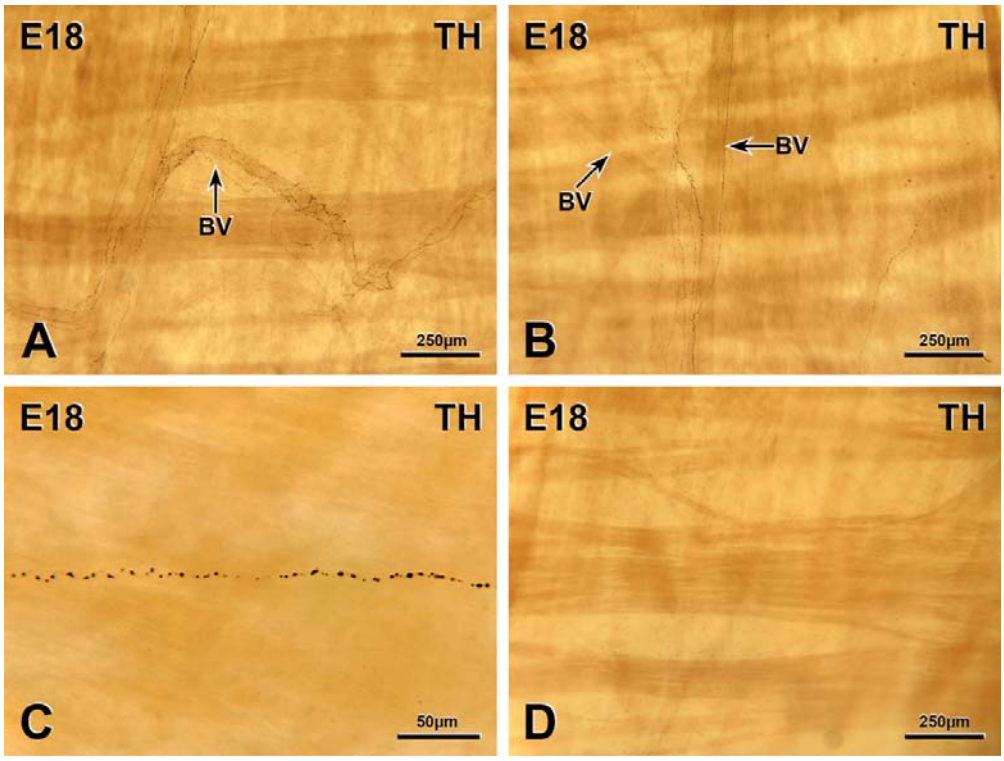
E18
TH
BV
A
250µm
E18
TH
BV
BV
B
250µm
E18
TH
C
50µm
E18
TH
D
250µm

FIGURE 3.5: TH-IMMUNOREACTIVE INNERVATION OF THE PREGNANT RAT UTERUS AT E20

A, Whole mount preparation of a strip from the cervical end of a 20-day pregnant uterine horn. Letters indicate the location of the micrographs in B-D. Bar, 5 mm. B, Nerve bundles contain TH-immunoreactive axons. Two blood vessels (BV) are surrounded by spares plexuses of TH-immunoreactive axons. Bar, 250 μm. C, A thick, wavy nerve bundle contains several non-varicose, TH-immunoreactive axons. Bar, 250 μm. D, A cervical area with no TH-positive innervation. A blood vessel (BV) lacks a TH-positive perivascular plexus. Bar, 250 μm. E, Whole mount preparation of a strip from the middle region of a 20-day pregnant uterine horn. Letters indicate the location of the micrographs in F-H. Bar, 5 mm. F, A TH-immunoreactive axon. Arrow G, portion of the axon shown in G. Bar, 100 μm. G, The TH-immunoreactive axon in F at higher magnification. The axon has varicosities that are variable in size and a branch with two round varicosities. Globs of immunoreactivity close to the axon suggest that other axons branches may be dying back. Bar, 25 μm. H, An area in the middle region that contains no TH-positive innervation. A blood vessel (BV) lacks a TH-positive perivascular plexus. Bar, 250 μm. I, Whole mount preparation of strip from the ovarian region of a 20-day pregnant uterine horn. Letters indicate the location of the micrographs in J-L. Bar, 5 mm. J, Small nerve bundles containing TH-immunoreactive axons. Two blood vessels (BV) have perivascular plexuses of faintly-stained TH-positive axons. Bar, 250 μm. K, A thick, wavy nerve bundle contains several non-varicose, TH-positive axons. Bar, 100 μm. L, An ovarian area with no TH-positive innervation. Blood vessels (BV) lack TH-positive perivascular plexuses. Bar, 250 μm.

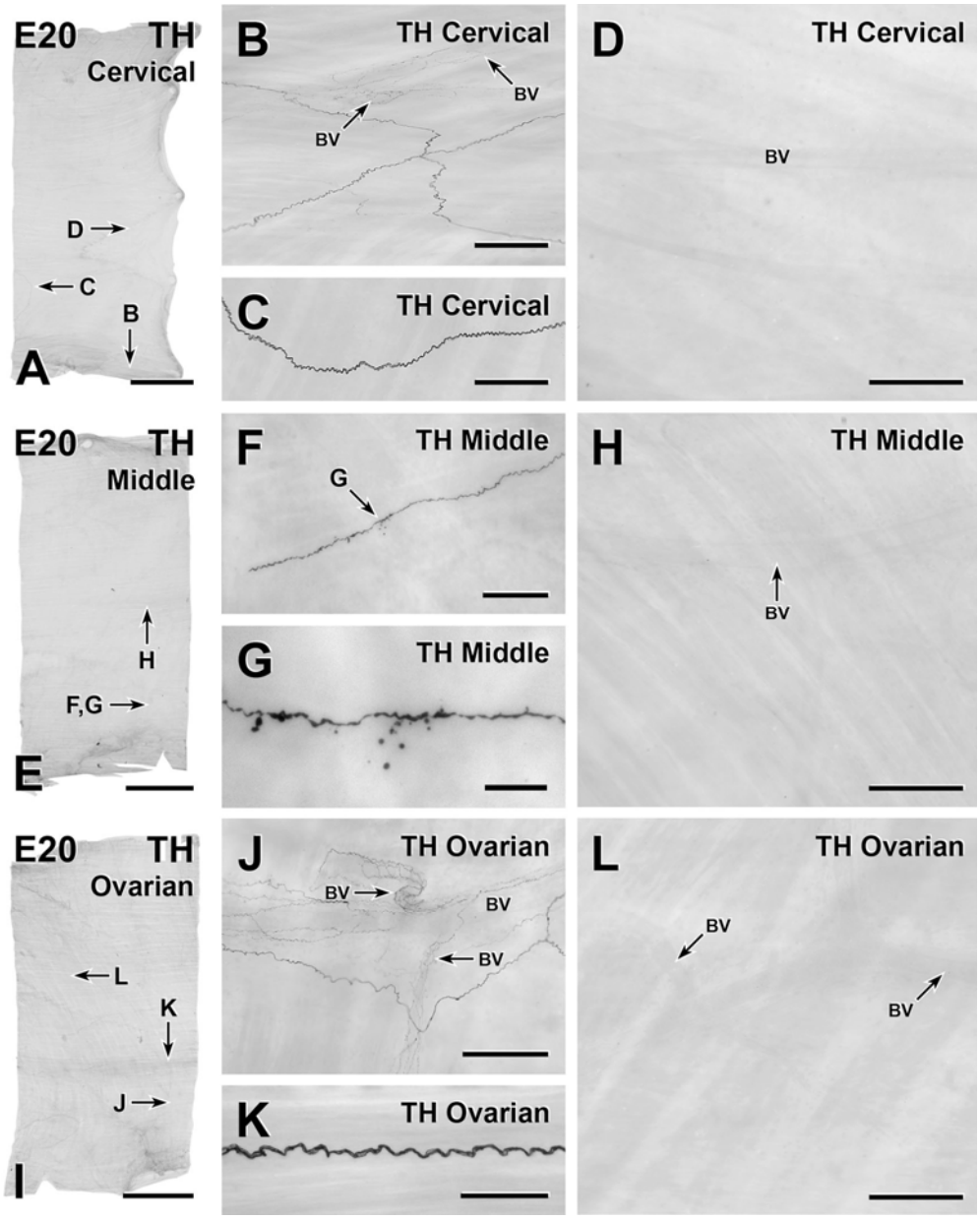
E20 TH Cervical
D
C
B
A
B TH Cervical
BV
BV
C TH Cervical
D TH Cervical
BV
E20 TH Middle
H
F,G
E
F TH Middle
G
G TH Middle
H TH Middle
BV
E20 TH Ovarian
L
K
J
I
J TH Ovarian
BV
BV
BV
K TH Ovarian
L TH Ovarian
BV
BV

3.2.2.6 Postpartum Day 1 (P1) : Figure 3.6

At P1, the density of TH-immunoreactive axons in rat uterine horns was low but axons were more numerous than at E20. Within a uterine horn, the density of TH-immunoreactive axons was slightly higher in the cervical and ovarian segments than in middle segments. The ovarian-most region contained the highest density of TH-immunoreactive axons and also more thick nerve bundles with TH-positive axons.

Very few TH-immunoreactive axons entered at the mesometrium either along with blood vessels or on their own, A few TH-positive axons entered along with blood vessels at the ovarian and cervical ends. There were more TH-immunoreactive axons around blood vessels at P1 than at E20. Nevertheless, very few uterine blood vessels were innervated and innervation around blood vessels was sparse (Figure 3.6A), except at the ovarian-most region where blood vessels were somewhat more heavily supplied with TH-positive axons (Figure 3.6B). Sometimes TH-immunoreactive axons left one blood vessel and travelled to another blood vessel. P1 uterine horns contained more thick nerve bundles than E20 horns. These bundles were present in similar numbers throughout the uterine horn and contained variable numbers of TH-immunoreactive axons. In all regions of the P1 uterus, rare single TH axons were present in the longitudinal and circular muscle layers of the myometrium; their number was higher than in the E20 uterus. There was no difference in the density of TH-positive axons between the linea uteri and the rest of smooth muscle. Very rarely, TH-immunoreactive axons were observed to travel from nerve bundles in the myometrium to the endometrium. No TH-immunoreactive axons were observed near uterine glands. Like at E20, there were many areas in each uterine horn that did not receive any TH innervation.

Most TH-stained axons showed signs of regrowth as evidenced by the presence of growth cones (Figure 3.6C&D). Growth cones appeared as bulbous sprouts or fine finger-like processes or fine film of immunoreactivity that arose from axons. Simple growth cone had one or two sprouts or fine processes. A complex growth cone had several spouts, processes or a fine film. The ovarian end of P1 uterine horns had more growth cones than other regions. Sometimes individual TH-immunoreactive axons showed signs of undergoing extensive regrowth, giving off complex arrays of growth cones at many points along their lengths. Many perivascular TH-immunoreactive axons had growth cones, some of which were simple and some of which were complex.

FIGURE 3.6: TH-IMMUNOREACTIVE INNERVATION OF THE POST-PARTUM RAT UTERUS AT P1

A & B, TH-immunoreactive axons innervate blood vessels on the mesometrial side of P1 uterine horns. The P1 uterus also contains thick nerve bundles with TH-immunoreactive axons. Inset in A, Growth cones on the axons associated with the blood vessel, which are at the arrow in A. C & D, TH-immunoreactive axons with growth cones (arrows) in the P1 uterus

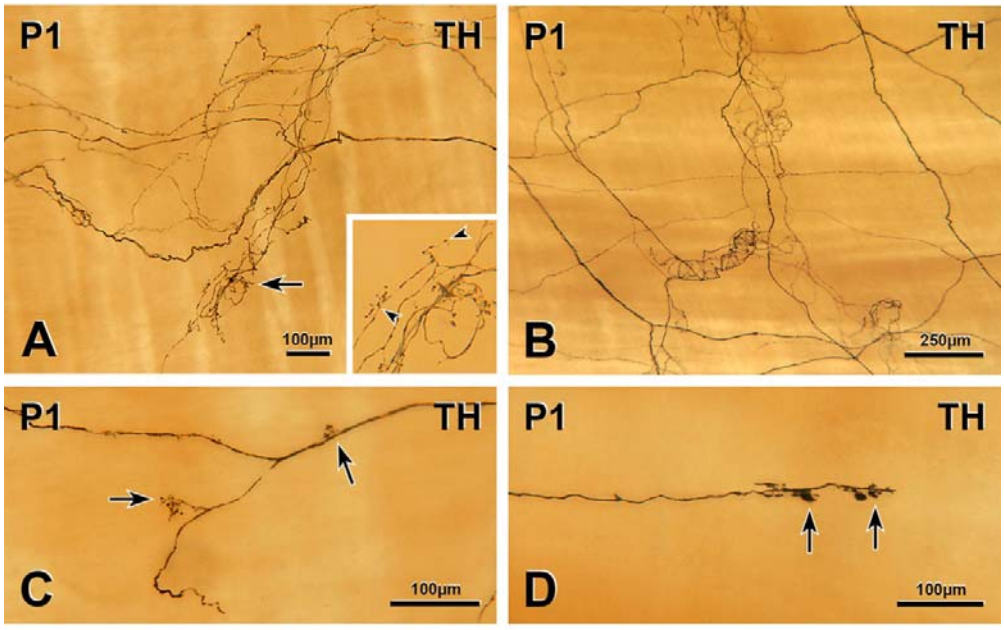
P1
TH
A
100µm
P1
TH
B
250µm
P1
TH
C
100µm
P1
TH
D
100µm

FIGURE 3.7: TH-IMMUNOREACTIVE INNERVATION OF THE POST-PARTUM RAT UTERUS AT P3

A, TH innervation at the ovarian-most end of a P3 uterine horn. TH-immunoreactive axons enter the uterus at the mesometrium (bottom of micrograph). B, In the middle region of a P3 uterine horn, TH innervation is less dense than at the ovarian-most end and fewer TH-immunoreactive axons enter at the mesometrium (bottom of micrograph). C, An area with a sparse TH innervation near the mesometrium (bottom of micrograph) in the middle region of a P3 uterine horn. .

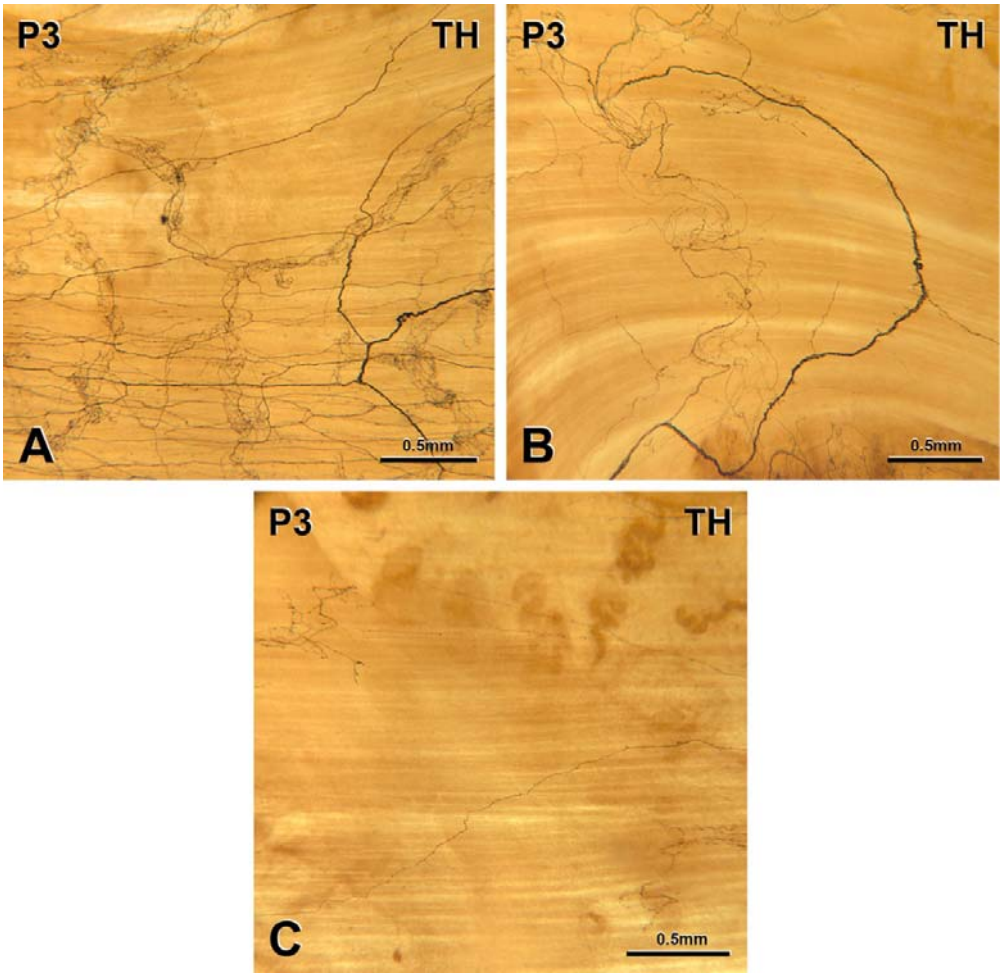
P3
TH
A
0.5mm
P3
TH
B
0.5mm
P3
TH
C
0.5mm

FIGURE 3.8: TH-IMMUNOREACTIVE INNERVATION OF THE POST-PARTUM RAT UTERUS AT P3

A, A blood vessel in the myometrium is moderately innervated by TH-immunoreactive axons. B, At the ovarian-most end of a P3 uterine horn, many TH-immunoreactive axons in thick nerve bundles have growth cones. C & D, TH-immunoreactive axons with growth cones in the myometrium. Inset in D, higher magnification of the complex growth cone indicated by the arrow in D.

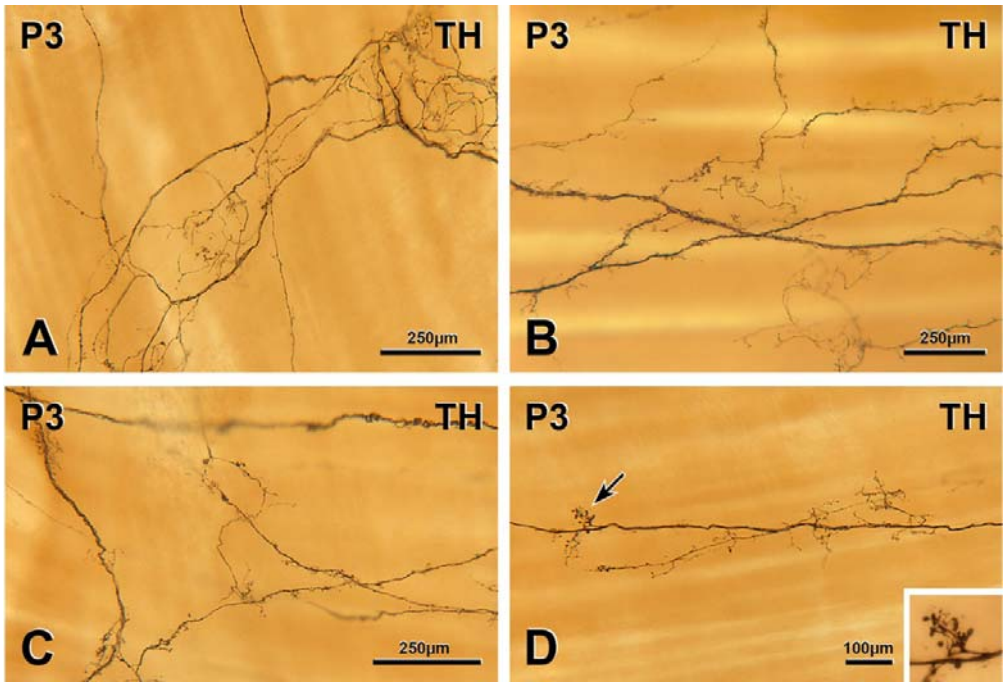
P3
TH
A
250µm
P3
TH
B
250µm
P3
TH
C
250µm
P3
TH
D
100µm

3.2.2.7 Postpartum day 3 (P3) : Figure 3.7&8

The density of TH-immunoreactive axons in rat uterine horns was higher at P3 than at P1. The ovarian-most end was more heavily innervated than the rest of the uterus.

At P3, more TH-immunoreactive axons entered the uterus at the mesometrium than at P1with some axons entering at the ovarian end. Compared to P1, more blood vessels were innervated and the density of perivascular innervation was higher (Figure 3.7A). Nevertheless, TH innervation of blood vessel was still very low compared to non-pregnant uterine horns. At P3, rare blood vessels at the mesometrium received a reasonable amount of innervation from TH-immunoreactive axons and some smaller branches of blood vessels also received innervation. A few thick nerve bundles containing TH-immunoreactive axons were present in the myometrium throughout the length of the horn (Figure 3.7B). Outside the myometrium, nerve bundles with TH-positive axons were more numerous at P3 than at P1 and more common in the ovarian-most region of uterine horns compared to the rest of the uterus. The longitudinal and circular smooth muscle contained rare single TH-immunoreactive axons that were not associated with blood vessels or thick nerve bundles, mostly in the ovarian and cervical segments. Generally at P3, the linea uteri was not innervated. However, in some parts of the ovarian segment in two rats, the density of TH-immunoreactive axons was higher in the linea uteri than in rest of the longitudinal muscle. At P3, rare TH-immunoreactive axons travelled from blood vessels in the myometrium to the endometrium. There were slightly more TH-stained axons in the endometrium at P3 than at P1. Similar to P1, no TH-immunoreactive axons were present near uterine glands.

FIGURE 3.9: TH-IMMUNOREACTIVE INNERVATION OF THE POST-PARTUM RAT UTERUS AT P5

A, A blood vessel that receives a heavier innervation from TH-immunoreactive axons from a P5uterine horn. B, In the myometrium of a P5 uterine horn, complex growth cones arise from TH-immunoreactive axons give rise to C, TH-immunoreactive axons with growth cones grow out from a nerve bundle.

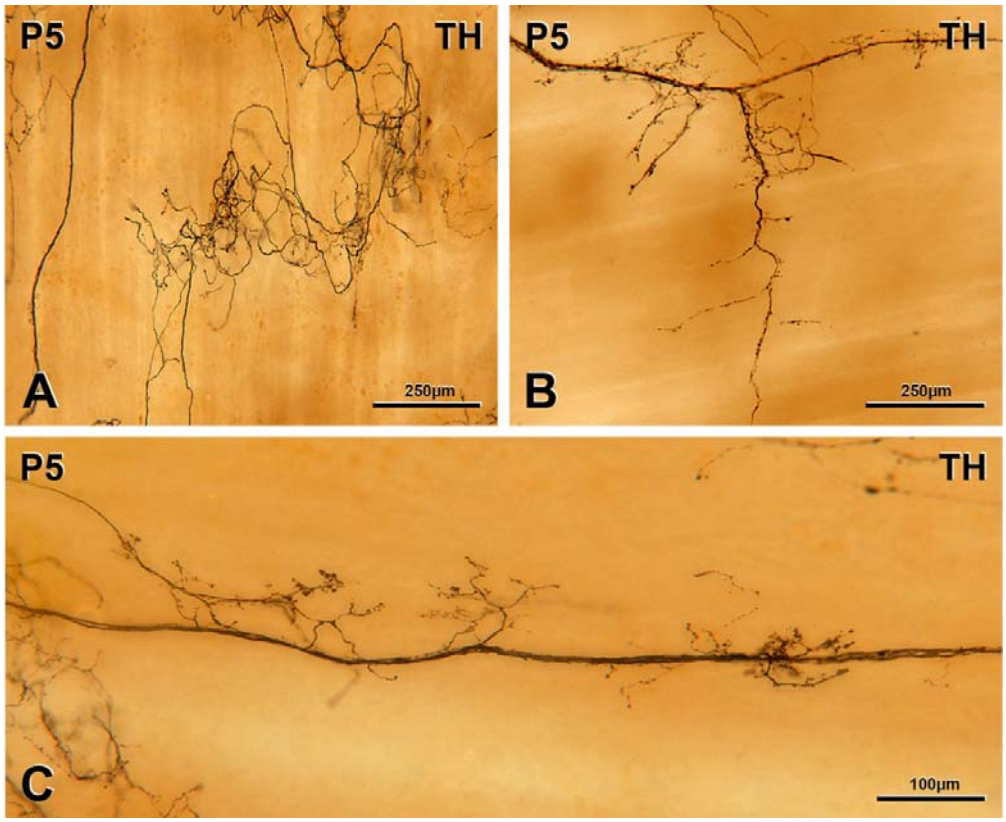
P5
TH
A
250µm
P5
TH
B
250µm
P5
TH
C
100µm

At P3, there were many areas of the uterus without any TH innervation, mostly on the anti-mesometrial side but also sometimes on the mesometrial side.

There were many more growth cones, both simple and complex, on TH-immunoreactive axons at P3 compared to P1 (Figure 3.7D). Growth cones were also common on perivascular TH-positive axon. One TH-immunoreactive axon was observed to branch off from the perivascular plexus, branch again and then form an array of growth cones. Growth cones also occurred on TH-positive axons in thick nerve bundles (Figure 3.7B).

3.2.2.8 Postpartum day 5 (P5) : Figure 3.9

The density of TH innervation in all layers of P5 uterine horns was higher than at P3. Some TH-immunoreactive axons entered the uterus along with blood vessels or in thick nerve bundles. Only a few blood vessels received a supply of TH-positive axons at P5. Although TH-immunoreactive perivascular plexuses were still sparse compared to non-pregnant uterine horns, the number of innervated blood vessels was slightly higher and their innervation was more dense at P5 than at P3 (Figure 3.9A). Thick nerve bundles with TH-immunoreactive axons were present across the P5 uterus, mostly on the mesometrial side (Figure 3.9B). Most of the TH innervation in the longitudinal and circular muscle layers was in the form of perivascular axons or axons in thick nerve bundles although rare single TH axons were present in the muscle layers. In all of the P5 uterine horns examined, there was no difference in the TH innervation of the linea uteri compared to the rest of the uterine smooth muscle. Occasional TH-immunoreactive axons originating from blood vessels travelled into the endometrium and rare TH-positive axons travelled close to glands. One TH-immunoreactive axon could be followed as it branched from the perivascular plexus

around a small blood vessel and travelled into the endometrium to terminate close to a uterine gland. Like the earlier post-partum time points, there were areas of P5 uterine horns that lacked innervation and other areas that received some TH-immunoreactive axons. These uninnervated areas were less common at P5 than at the earlier post-partum time points.

Both simple and complex growth cones on TH-immunoreactive axons were abundant at P5 and more common than at P3 (Figure 3.9C). Many TH-positive axons in thick nerve bundles had complex growth cones; simple and complex growth cones also occurred on TH-positive axons around blood vessels.

3.2.2.9 Postpartum day 7 (P7) : Figure 3.10 & 11

Throughout the uterus, the density of TH-immunoreactive axons was higher at P7 than at P5. The ovarian-most end was more densely innervated compared to the middle and cervical regions.

TH-immunoreactive axons entered P7 uterine horns along with blood vessels or in thick nerve bundles. There were more TH-positive axons in plexuses around blood vessels at P7 than at P5 (Figure 3.11A). The number of blood vessels that were innervated by TH-immunoreactive axons was also higher at P7. A few blood vessels, particularly at the ovarian end, received a moderate TH innervation. Thick nerve bundles containing TH-immunoreactive axons were present across the uterus (Figure 3.11B). Their number was similar to the number at P5. The innervation of the myometrium at P7 was similar to P5, consisting of perivascular TH-positive axons and TH-positive axons in thick nerve bundles. At the ovarian-most end in three rats, the linea uteri had more TH-immunoreactive axons compared to the rest of the smooth muscle; apart from this innervation, there were almost no single TH-

immunoreactive axons in either the longitudinal or circular muscle layers. The density of TH innervation in the endometrium at P7 was similar to P5. On very few occasions, TH-immunoreactive axons travelled from a perivascular plexus to the endometrium; and very rarely, a TH-immunoreactive axon was found close to an uterine gland. As at P5, TH innervation density was not consistent across P7 uterine horns. In some areas, there was little or no TH innervation whereas in other areas there was denser innervation (Figure 3.10). The number and size of denervated areas were smaller at P7 than at P5.

In P7 uterine horns, many simple and complex growth cones were present on TH-immunoreactive axons (Figure 3.11C&D). Often, single TH-positive axons terminated with a growth cone shortly after branching off from a perivascular plexus or from a thick nerve bundles. Many of the TH-immunoreactive axons in thick nerve bundles had growth cones. Growth cones on TH-immunoreactive axons were more numerous at the ovarian-most end but overall there were still fewer growth cones at P7 than at P5.

3.2.2.10 Postpartum day 10 (P10) : Figure 3.12&13

There were more TH-immunoreactive axons in P10 uterine horns than in P7 horns. Some TH-immunoreactive axons entered the uterus either alongside blood vessels or in thick nerve bundles. Some blood vessels had a low to moderate TH innervation (Figure 3.13A). Compared to P7, there were generally a few more TH-immunoreactive axons around innervated blood vessels than at P10. Thick nerve bundles containing TH-positive axons were present in the P10 uterus and were similar in number and distribution to the nerve bundles in P7 uterine horns (Figure 3.13D).

FIGURE 3.10: TH-IMMUNOREACTIVE INNERVATION OF THE POST-PARTUM RAT UTERUS AT P7

A & B, A whole mount preparation of a P7 uterine horn stained for TH. Box B is shown at higher magnification in B. Letters indicate the location of the micrographs shown in C and D. C & D, The densities of TH-immunoreactive axons in two neighbouring areas of the same P7 horn vary substantially. Area C has a high density of TH innervation whereas the density of TH innervation in area D is low.

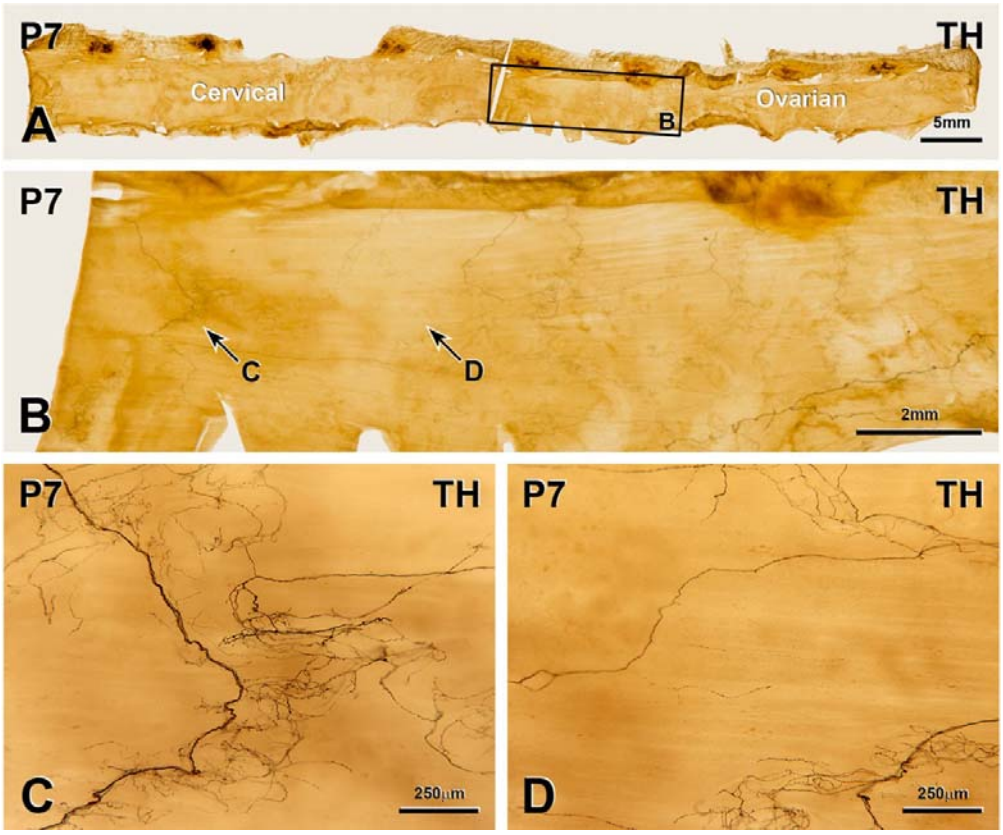
P7
TH
Cervical
Ovarian
A
B
5mm
P7
TH
C
D
B
2mm
P7
TH
C
250μm
P7
TH
D
250μm

FIGURE 3.11: TH-IMMUNOREACTIVE INNERVATION OF THE POST-PARTUM RAT UTERUS AT P7

A, A Blood vessel is moderately innervated by TH-immunoreactive axons. B, TH-immunoreactive axons and growth cones in the endometrium on the mesometrial side of a P7 uterine horn. C, TH-immunoreactive axons with growth cones in the circular muscle layer on the anti-mesometrial side of a P7 uterine horn. D, TH-immunoreactive axons with growth cones in the circular muscle layer on the mesometrial side of a P7 uterine horn.

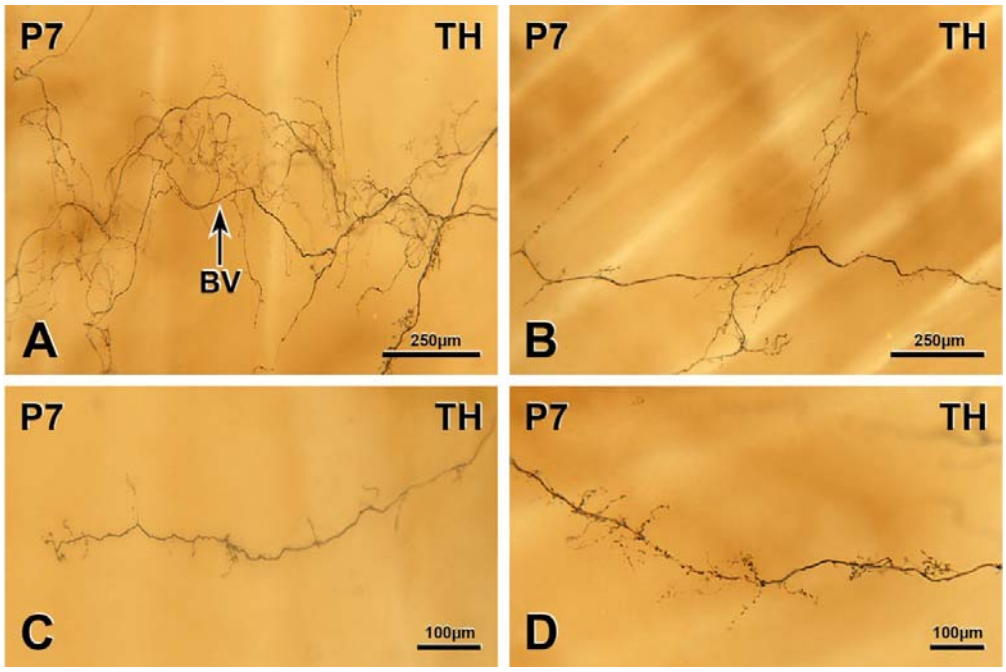
P7
TH
BV
A
250µm
P7
TH
B
250µm
P7
TH
C
100µm
P7
TH
D
100µm

FIGURE 3.12: TH-IMMUNOREACTIVE INNERVATION OF THE POST-PARTUM RAT UTERUS AT P10

A, At the ovarian-most end of a P10 uterine horn, there are many TH-immunoreactive axons around blood vessels, in thick nerve bundles and in the linea uteri. B, In one area from the middle region of a P10 uterine horn, there is less TH innervation than at the ovarian most end. C, In another area from the middle region of a P10 uterine horn, TH innervation density is much lower.

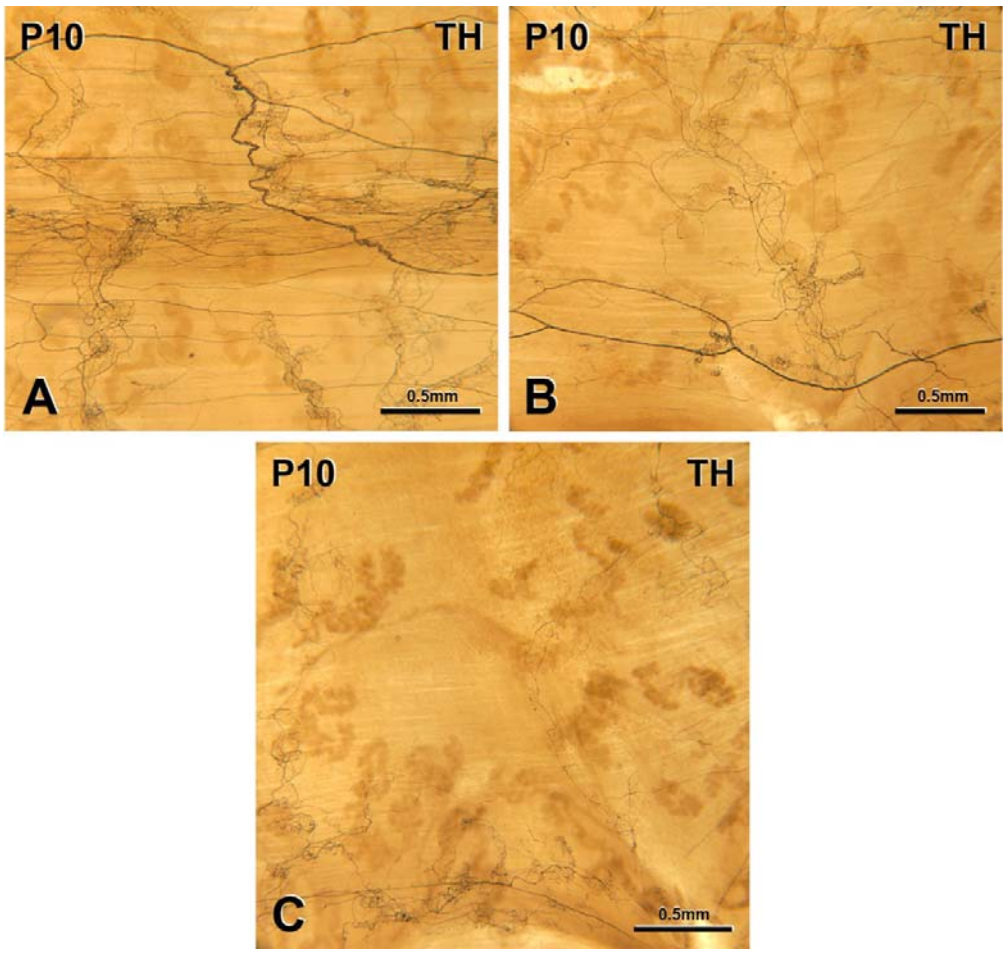
P10
TH
A
0.5mm
P10
TH
B
0.5mm
P10
TH
C
0.5mm

FIGURE 3.13: TH-IMMUNOREACTIVE INNERVATION OF THE POST-PARTUM RAT UTERUS AT P10

A, Around a blood vessel TH-immunoreactive axons form a perivascular plexus that is moderately dense r. B, Some TH-immunoreactive axons are present in the linea uteri at the ovarian most end of a P10 uterine horn. C, TH-immunoreactive axons with growth cones. D, Thick nerve bundles containing TH-immunoreactive axons that are giving off growth cones.

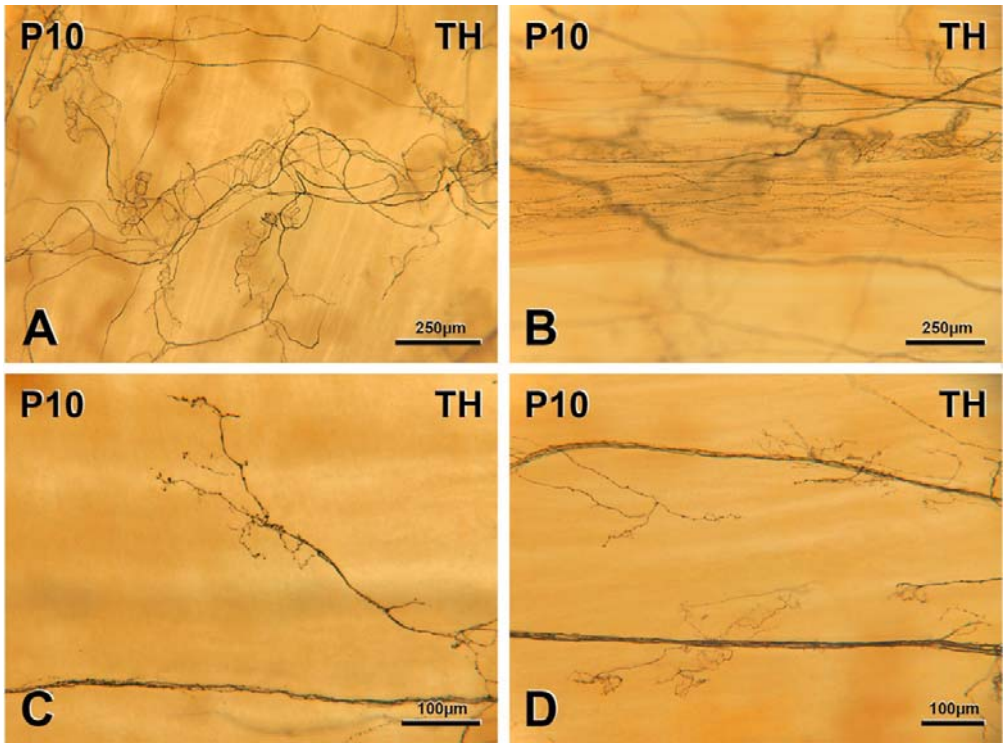
P10
TH
A
250µm
P10
TH
B
250µm
P10
TH
C
100µm
P10
TH
D
100µm

The density of innervation in the myometrium was slightly higher at P10 than at P7. The longitudinal muscle contained very few single axons that were not associated with blood vessels or in thick nerve bundles. The TH innervation of the circular muscle layer consisted of perivascular axons and axons in thick nerve bundles. In general, the linea uteri lacked TH innervation. However, in the ovarian region of the uterine horn from two rats, the linea uteri had more TH-immunoreactive axons than the rest of the smooth muscle (Figure 3.13B). A few TH-positive axons were present in the endometrium, some of which originated from perivascular plexuses in the myometrium. The density of TH innervation in the endometrium was mostly similar to the P7 uterus. Sometimes, TH-immunoreactive axons originating from blood vessels travelled deep into the endometrium following a torturous path; on some occasions these axons also had growth cones. Rare TH-immunoreactive axons ended close to a uterine gland. There were still areas with little or no TH innervation (Figure 3.13B&C) in P10 uterine horns although these areas were much smaller and less common than at earlier post-partum time points. They were also regions with a higher innervation density, particularly at the ovarian most end (Figure 3.10A)

Growth cones were still present on TH-immunoreactive axons in P10 uterine horns but there were fewer than at P7 (Figure 3.13C). Perivascular TH-positive axons had simple and complex growth cones. Growth cones were also present on TH-immunoreactive axons that innervated the linea uteri. One TH-immunoreactive axon originating from a small blood vessel travelled into the endometrium and had many growth cones.

3.2.2.11 Postpartum day 14 (P14) : Figure 3.14

The density of TH-immunoreactive axons in P14 uterine horns was higher than at P10 but still much lower than in non-pregnant horns. The ovarian end was more densely innervated by TH-immunoreactive axons than the rest of the uterus.

TH-immunoreactive axons entered the uterus along with blood vessels or in thick nerve bundles. Many blood vessels were moderately innervated by TH-positive axons (Figure 3.14A). Other blood vessels entering the uterus at the mesometrium were sparsely innervated. As blood vessels spilt into smaller branches inside the uterus, the TH-immunoreactive axons innervating them followed and sometimes ended with growth cones. The innervation density of the blood vessels was higher at P14 than at P10. In P14 uterine horns, thick nerve bundles containing some TH-immunoreactive axons entered through the mesometrium and were more common at the mesometrial side but occasionally travelled to the anti-mesometrial side. The myometrium received slightly more TH innervation at P14 than at P10. In three rats, the linea uteri was more densely innervated by TH-stained axons in the ovarian region compared to the rest of the smooth muscle. In one rat, some portion of the middle region of the uterine horn also had a few TH-immunoreactive axons in the linea uteri. Apart from those in the linea uteri, there were few single TH-immunoreactive axons in rest of the longitudinal muscle layer (Figure 3.14B). The innervation of the circular muscle layer consisted of perivascular TH axons and axons in thick nerve bundles. At P14, the TH innervation density in the endometrium was still low, similar to P10. A few TH-immunoreactive axons travelled to the endometrium from blood vessels in the myometrium; occasionally these axons ended in growth cones. Rare TH-immunoreactive axons travelled close to uterine glands.

FIGURE 3.14: TH-IMMUNOREACTIVE INNERVATION OF THE POST-PARTUM RAT UTERUS AT P14

A, TH-immunoreactive axons around blood vessels and in thick nerve bundles in a P14 uterine horn. Axons at arrow C are shown in C. B, A few TH-immunoreactive axons in the longitudinal muscle. C & D, TH-immunoreactive axons in thick nerve bundles in the myometrium give rise to growth cones.

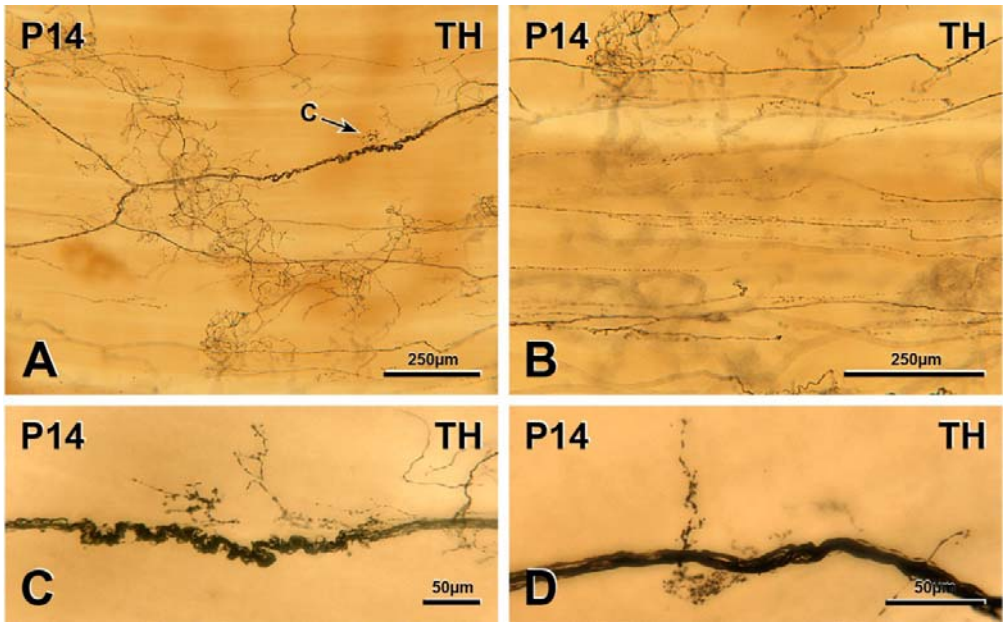
P14
TH
C
A
250µm
P14
TH
B
250µm
P14
TH
C
50µm
P14
TH
D
50µm

FIGURE 3.15: TH-IMMUNOREACTIVE INNERVATION OF THE POST-PARTUM RAT UTERUS AT P28

A, In the ovarian region of a P28 uterine horn, there are many TH-immunoreactive axons around blood vessels, in thick nerve bundles and in the linea uteri. B, There is less TH innervation in the middle region of a P28 horn than at the ovarian end. C, A blood vessel (arrow) in the ovarian-most region is surrounded by many TH-immunoreactive axons. Thick nerve bundles containing TH-positive axons (arrowhead) are also prominent. D, Many TH-immunoreactive axons (arrows) in the linea uteri in the ovarian most end. E, A blood vessel that receives a less dense TH-immunoreactive axons. F, Several of the TH-immunoreactive axons that have entered a P28 horn at the mesometrium (bottom of the micrograph) have growth cones (arrowheads). Inset, The growth cone on the axon indicated by the arrow in D. BV, blood vessel.

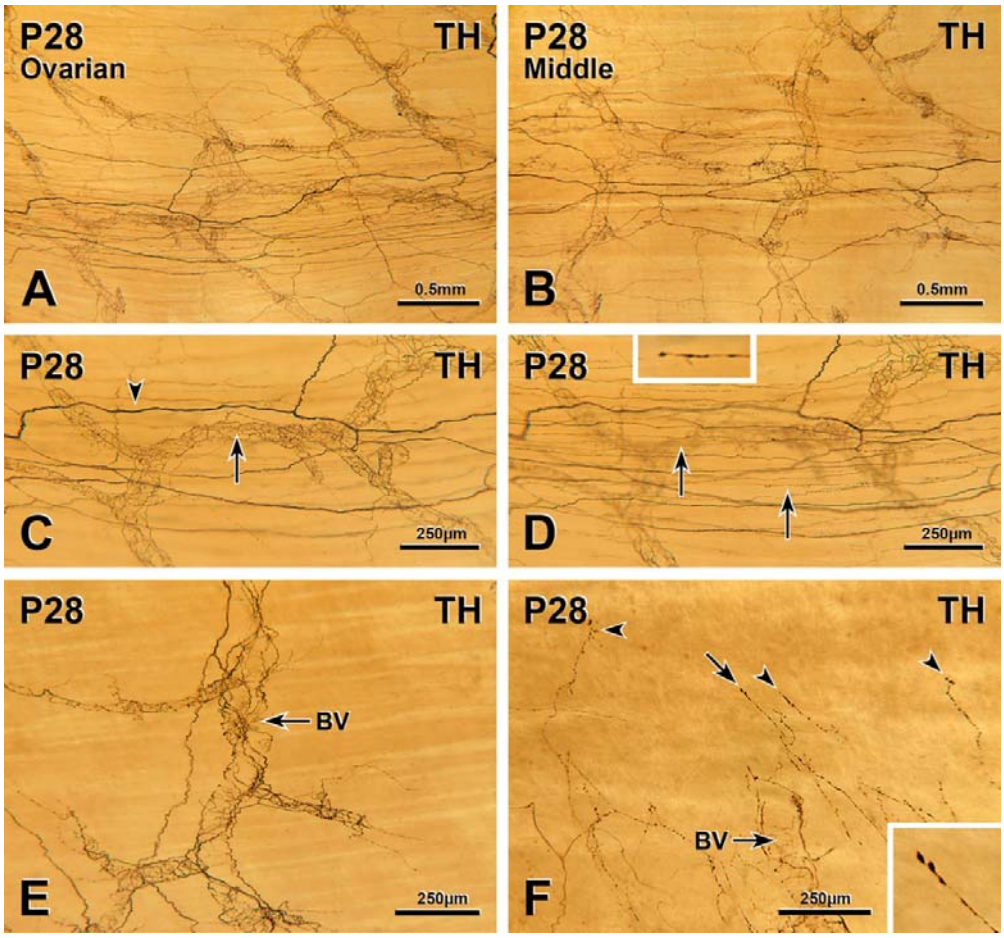
P28
Ovarian
TH
A
0.5mm
P28
Middle
TH
B
0.5mm
P28
TH
C
250μm
P28
TH
D
250μm
P28
TH
BV
E
250μm
P28
TH
BV
F
250μm

Variability in innervation density across a uterine horn persisted at P14. Small areas in the P14 uterus received fewer TH-immunoreactive axons than most of the rest of the uterus.

TH-immunoreactive axons in P14 uterine horns still had growth cones but they were less numerous than at earlier post-partum time points. Some of the TH-positive axons associated with blood vessels ended with growth cones. Growth cones also occurred on TH-immunoreactive axons in thick nerve bundles (Figure 3.14C&D) and TH-positive axons innervating the linea uteri.

3.2.2.12 Postpartum day 28 (P28) : Figure 3.15

TH innervation in P28 uterine horns was denser than in P14 horns but the density was still lower than the density at oestrus (Figure 3.15A&B).

Many TH-immunoreactive axons entered the uterus along with blood vessels or in thick nerve bundles. Compared to P14 uterine horns, more blood vessels were innervated by TH-immunoreactive axons. Perivascular TH innervation was generally denser at P28 than at P14. Most blood vessels were moderately innervated (Figure 3.15C). However, occasional vessels at the ovarian end had a significant TH innervation and some vessels had innervation comparable to that seen at P14 (Figure 3.15E). Thick nerve bundles containing many TH-immunoreactive axons were present throughout P28 uterine horns (Figure 3.15C). The density of TH-immunoreactive axons in the myometrium was slightly higher at P28 than at P14 but still lower than at oestrus. There were some single TH-immunoreactive axons in the longitudinal muscle. TH-immunoreactive axons in the circular muscle layer were perivascular or associated with or originating from blood vessels. In the ovarian end of uterine horns from all rats examined, the linea uteri was more densely innervated

by TH-immunoreactive axons than the rest of the smooth muscle (Figure 3.15D). In other regions of P28 horns, the TH innervation of the linea uteri was similar to that of the rest of the longitudinal smooth muscle. At P28, the innervation density of the endometrium was similar to P14. A few TH-immunoreactive axons travelled to the endometrium from blood vessels in the myometrium and sometimes came close to a uterine gland.

In P28 uterine horns, TH-positive axons with growth cones were present but rare (Figure 3.15F).

3.2.3 Quantification of TH-immunoreactive axons in the pregnant and post-partum uterus

TH-immunoreactive axons were quantified at 12 different time points: in non-pregnant rats at oestrus (OEST), in rats at pregnancy days 14 (E14), 16 (E16), 18 (E18) and 20 (E20) and in rats at post-partum days 1 (P1), 3 (P3), 5 (P5), 7 (P7), 10 (P10), 14 (P14) and 28 (P28).

Entire uterine horns from four rats at oestrus were stained for TH. E14, E16, E18 and E20 uterine horns were divided into 1.5cm strips and one segment from each third (ovarian, middle and cervical) of the uterus from 4 different rats was stained for TH. The P1 and P3 uteri were also divided into 1.5cm strips and one segment from each third (ovarian, middle and cervical) of the uterus from 4 different rats was stained for TH. At P5, P7, P10, P14 and P28, immunostaining for TH was done on an entire uterine horn from each of two rats, on an ovarian half horn from a third rat and on a cervical half horn from a fourth rat.

TABLE 3.2: POISSON REGRESSION ANALYSIS OF INTERSECTIONS OF TH-IMMUNOREACTIVE AXONS DURING PREGNANCY AND POST-PARTUM

Time point	Average intersections	Incidence Rate Ratio (%)	95% Confidence Interval	P value	% innervation at OEST
OEST	321.95	Reference	-	-	
E14	53.3	5.74	2.02 – 16.32	<0.001	16.56
E16	45.85	3.30	1.16 – 9.41	<0.001	14.24
E18	20.45	1.56	0.55 – 4.45	<0.001	6.35
E20	6.65	0.23	0.08 – 0.72	<0.001	2.07
P1	9.10	0.84	0.29 – 2.42	<0.001	2.83
P3	39.20	10.20	3.59 – 29.03	<0.001	12.18
P5	63.55	14.23	4.99 – 40.54	<0.001	19.74
P7	50.20	11.47	4.03 – 32.64	<0.001	15.59
P10	112.40	38.82	13.67 – 110.21	0.07	34.91
P14	132.95	43.75	15.41 – 124.21	0.12	41.30
P28	157.35	46.13	16.25 – 130.93	0.15	48.87

Incidence Rate Ratio is a relative measure of the effect of a particular time point on the number of intersections generated by STATA during Poisson Regression Analysis. Oestrus was considered the reference; therefore IRR=100%.

FIGURE 3.16: DENSITY OF SYMPATHETIC INNERVATION DURING PREGNANCY AND POST-PARTUM

The graph shows the difference in sympathetic innervation density in the non-pregnant (OEST), pregnant day 14 (E14), 16 (E16), 18 (E18), 20 (E20), day 1 post-partum (P1), 3 (P3), 5 (P5), 7 (P7), 10 (P10), 14 (P14) and 28 (P28) uteri.

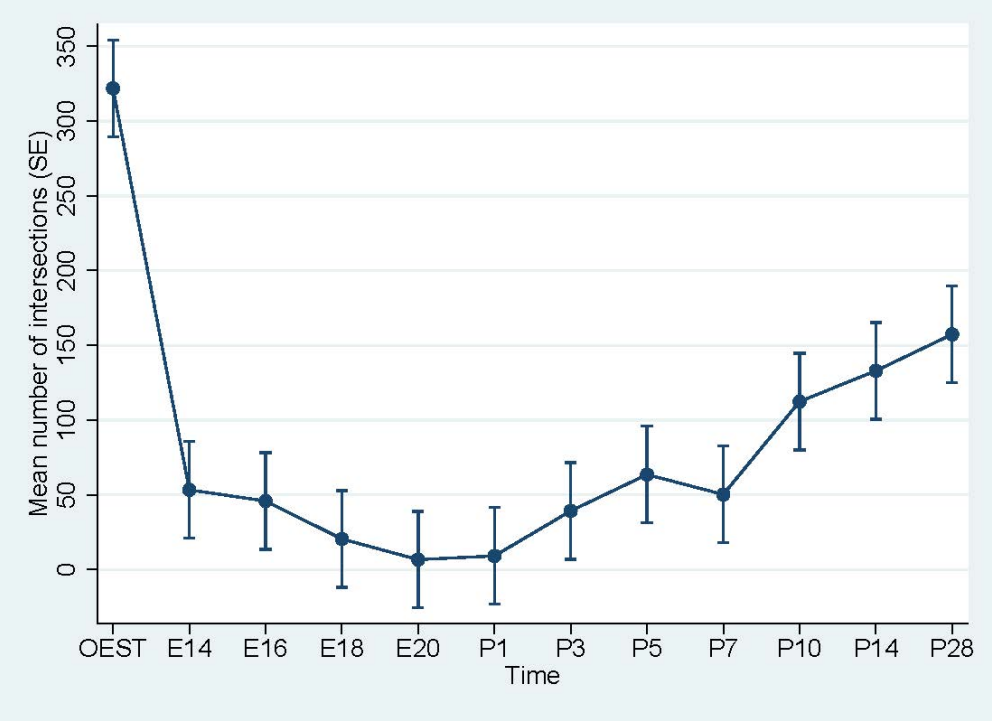
Mean number of intersections (SE)
0
50
100
150
200
250
300
350
OEST
E14
E16
E18
E20
P1
P3
P5
P7
P10
P14
P28
Time

The quantification procedure is detailed in Section 2.4.5.2 of Chapter 2. Poisson Regression Analysis was performed by Dr Shahid Ullah, Flinders Centre for Epidemiology and Biostatistics, Flinders University, and took into account the differences in the total number of boxes in the locating grid for each uterine horn.

The data from this analysis are summarized in Table 3.2 and graphed in Figure 3.14. At oestrus, the mean number of intersections of TH-immunoreactive axons with the bars of the counting grid was 321.95. During pregnancy, the number of intersections decreased to 53.30 at E14, 45.85 at E16, 20.45 at E18 and 6.65 at E20. After delivery, there was an increase in the mean number of axonal intersections from 9.10 at P1 to 157.35 at P28.

Compared to oestrus, Poisson Regression Analysis showed that there were statistically significant differences in Incidence Rate Ratio (IRR) for sympathetic innervation density at all time points during pregnancy. At E14, sympathetic innervation density was already much lower than at oestrus, with an IRR of 5.74%. The IRR at later time points during pregnancy were 3.30% at E16, 1.56% at E18 and 0.23% at E20. In the post-partum period, sympathetic innervation density had increased slightly from 0.23% at E20 to 0.84% at P1. IRR continued to increase as the number of post-partum days increased, ultimately reaching 46.13% at P28. When compared to the non-pregnant rat at oestrus, there were statistically significant differences in sympathetic innervation density at E14, E16, E18, E20, P1, P3, P5 and P7. There were large differences in IRR between post-partum time points P10, P14, P28 compared to oestrus. Nevertheless, the IRR values for these time points did not differ significantly from oestrus. One reason for the lack of significant differences could be the small number of samples in which innervation density was quantified at P10, P14 and P28. This is the first study to quantify uterine innervation density in

whole mount preparations and axonal intersections were counted at each time point in a total of 20 squares measuring 500mm x 500mm (5 counting grids for each uterine horn in each of 4 rats). From the data generated in this analysis, the required sample size to yield statistically significant differences in IRRs was calculated to be 74 counting squares per time point. Squares with dense TH innervation could take 1-2 hours to count and therefore counting 74 squares at each of the 12 different time points was beyond the scope of this project. The high degree of variability in innervation density within individual horns is also the likely cause of the large confidence intervals seen in Table 3.1.

Figure 13.3 suggests that there is a decline in the density of TH innervation at P7 compared to P5. If regeneration of TH=immunoreactive axons that supply the uterus was occurring throughout the post-partum period, the numbers of intersections of TH-immunoreactive axons with the bars of the counting grid would be expected to increase with increasing time after delivery. However, there is a small decrease in the IRR at P7. As mentioned in the descriptions above of the distribution of TH-immunoreactive axons at post-partum time points, there was a high degree of variability in innervation density within each TH-stained uterine horn. Consequently, post-partum uterine horns contained areas that received very little or no TH innervation as well as areas that had a high density of innervation, particularly if blood vessels supplied by TH-immunoreactive axons were present in that area. As a result, the number of axonal intersections counted was completely dependent on where the randomly-located counting squares fell within any given uterine horn (see Figures 2.3 and 3.14).

3.2.4 Changes in uterine sympathetic innervation as revealed by immunostaining for NPY

While NPY has been used here as a sympathetic marker, it must be noted that immunoreactivity to NPY occurs in both sympathetic or parasympathetic post-ganglionic neurons (Markiewicz et al., 2003). Entire uterine horns from 4 different rats at oestrus were stained for NPY. Studies on NPY innervation in E14, E16, E18, E20, P1 and P3 uterine horns used one segment from the ovarian, middle and cervical regions of horns from each of three rats. To assess NPY innervation at P7 and P14, ovarian halves of uterine horns from 2 rats and cervical halves from another 2 rats were used.

3.2.4.1 Oestrus : Figure 3.17

I have previously described the NPY-immunoreactive innervation of the non-pregnant rat uterus at oestrus (Gnanamanickam and Llewellyn-Smith, 2011). In summary, many NPY-immunoreactive axons supplied non-pregnant uterine horns. Blood vessels received a significant NPY innervation (Figure 3.17B&C). Thick nerve bundles containing NPY-immunoreactive axons were present throughout the uterus. Fine varicose axons following the orientation of the circular muscle (the circular muscle plexus or CMP) were present in the mesometrial side of the non-pregnant uterus; these axons were found at the bottom of the circular muscle layer and absent in the anti-mesometrial side (Figure 3.17D). The linea uteri had more NPY axons compared to the rest of the uterine smooth muscle (Figure 3.17A). Rare NPY axons were present in the endometrium close to glands

3.2.4.2 Pregnancy day 14 (E14)

The distribution of NPY-immunoreactive axons in E14 uterine horns was similar to the innervation pattern of uterine TH-immunoreactive axons at E14. NPY innervation density at E14 was much lower than at oestrus. NPY-immunoreactive axons entered the uterus mostly alongside blood vessels but sometimes in thick nerve bundles. Blood vessels containing NPY-immunoreactive axons were present throughout E14 uterine horns. Some blood vessels were innervated and smaller branches also received NPY-immunoreactive axons. Occasionally, NPY-immunoreactive axons associated with blood vessels in the myometrium travelled to other blood vessels or to another muscle layer. Very few thick nerve bundles containing some NPY-positive axons occurred throughout the uterus, mostly on the mesometrial side. The density of NPY innervation in the myometrium and endometrium was much lower at E 14 than at oestrus. A few NPY-immunoreactive axons ran through the longitudinal muscle. There was no noticeable difference in the innervation of linea uteri by NPY-stained axons compared to the rest of the longitudinal muscle. The fine varicose NPY axons present at oestrus in the circular muscle (circular muscle plexus) close to the endometrium in the mesometrial side were not observed at E14**.** NPY-immunoreactive axons were very rare in the endometrium. There were areas of the E14 uterus that did not receive any innervation from NPY-positive axons; areas without innervation were present throughout the E14 uterus.

Degenerating NPY axons were present in all regions of the E14 uterus, the ovarian, middle cervical, mesometrial and anti-mesometrial sides. They were common in the E14 uterus.

FIGURE 3.17: NPY-IMMUNOREACTIVE INNERVATION OF THE NON-PREGNANT RAT UTERUS AT OESTRUS

A & B and C & D show different focal planes through the same regions of a uterine horn at oestrus. A, NPY-immunoreactive axons in the linea uteri. B, NPY-immunoreactive axons in the circular muscle plexus (top of micrograph), around blood vessels and in a thick nerve bundle. C, NPY-immunoreactive axons around blood vessels and in a thick nerve bundle. D, Fine varicose NPY-immunoreactive axons in the circular muscle plexus.

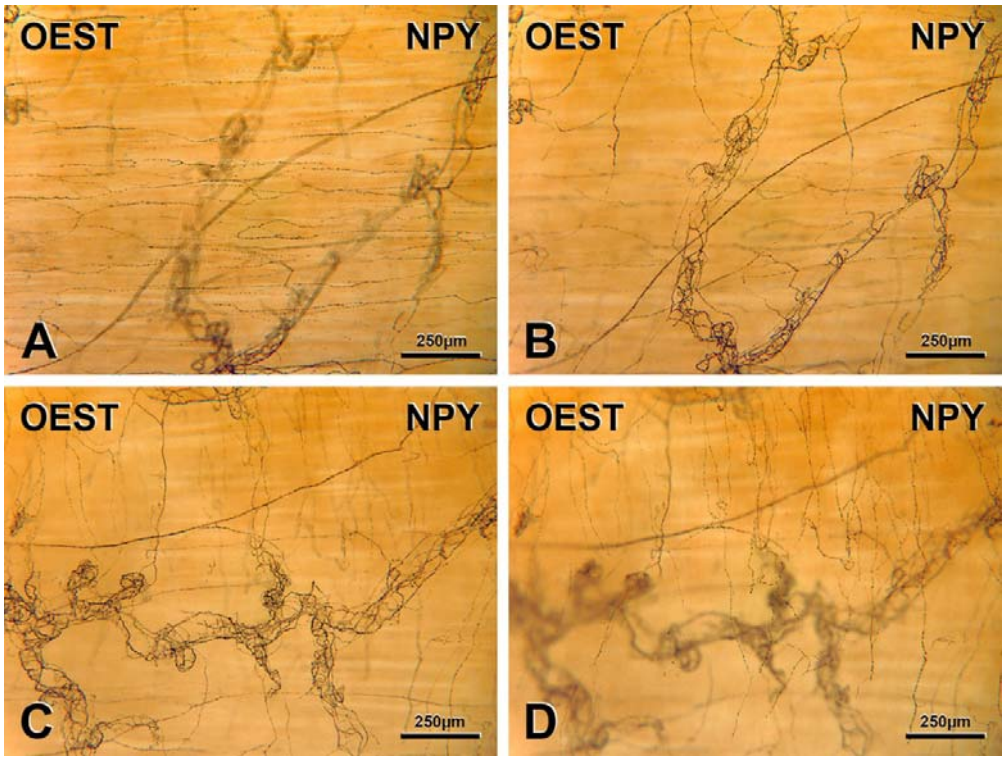
OEST
NPY
A
250µm
OEST
NPY
B
250µm
OEST
NPY
C
250µm
OEST
NPY
D
250µm

FIGURE 3.18: NPY-IMMUNOREACTIVE INNERVATION OF THE PREGNANT RAT UTERUS AT E16

A, A sparsely innervated blood vessel (BV) in an E16 uterine horn. B, An Area in an E16 uterine horn that lacks NPY innervation. C-F, Degenerating NPY-immunoreactive axons in the E16 uterus. Some degenerating axons are fragmented (C, D) and others are swollen (E, F). Inset in C, swollen and fragmented NPY-immunoreactive axons in the region of the nerve bundle in C indicated by the arrow.

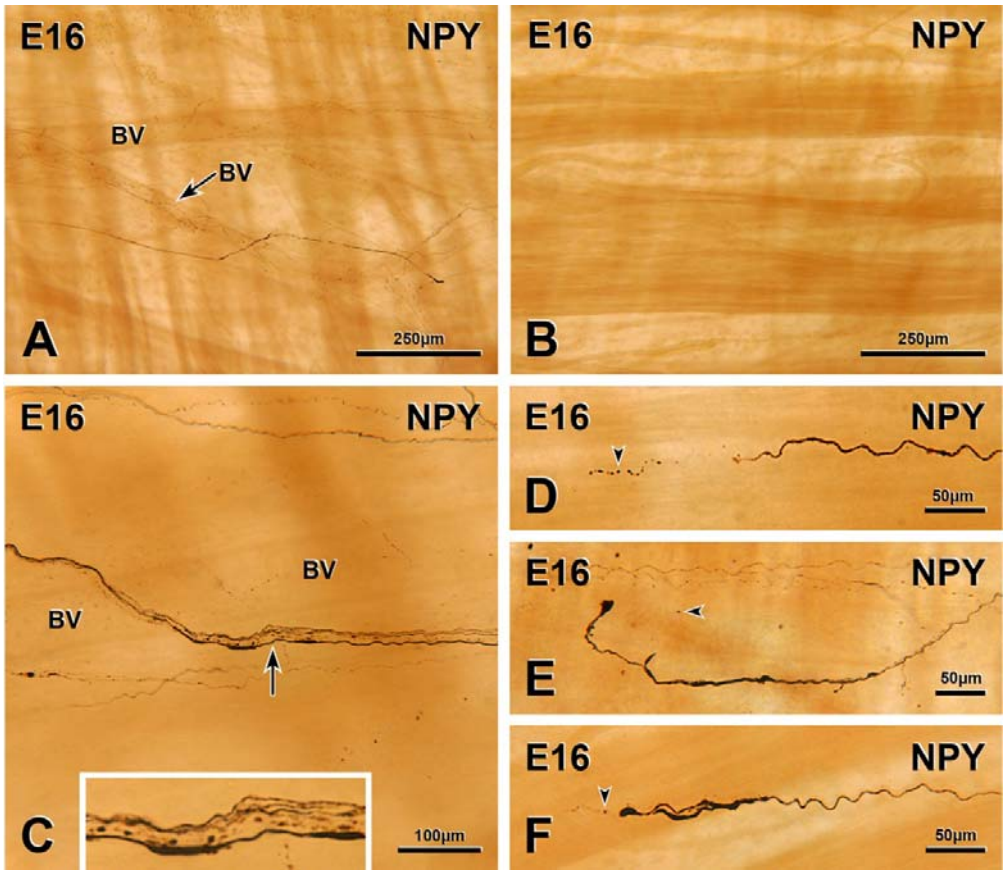
E16
NPY
BV
BV
A
250µm
E16
NPY
B
250µm
E16
NPY
BV
BV
C
100µm
E16
NPY
D
50µm
E16
NPY
E
50µm
E16
NPY
F
50µm

3.2.4.3 Pregnancy day 16 (E16) : Figure 3.18

The density of NPY innervation was lower at E16 than at E14. The middle segments of E16 uterine horns had fewer NPY-immunoreactive axons than the ovarian and cervical segments, similar to TH innervation at this time point. Some NPY immunoreactive axons entered the uterus along with blood vessels. The number of blood vessels innervated and the innervation density around blood vessels was lower at E16 than at E14 (Figure 3.18A). Only a few blood vessels received a sparse NPY innervation. At E16, rare thick nerve bundles containing a few NPY-immunoreactive axons were present but they only occurred in one middle and one ovarian segment). This observation is in contrast to innervation revealed by TH-immunoreactivity, where thick nerve bundles containing TH-stained axons were present throughout the E16 uterus. The myometrium contained fewer single NPY-immunoreactive axons at E16 than at E14. The E16 uterus did not contain the circular muscle plexus containing fine varicose NPY axons observed in the circular muscle in the mesometrial side at oestrus. There was no difference in the NPY innervation of the linea uteri between different regions of the uterus. This observations contrasted with the findings for TH innervation at this time point, i.e., there were more TH-immunoreactive axons in the linea uteri at the ovarian ends of uterine horns from two E16 rats. Very rare NPY-immunoreactive axons travelled from plexuses around blood vessels into the endometrium. Areas lacking any innervation by NPY-immunoreactive axons were more common in E16 uterine horns than in E14 horns (Figure 3.18B).

NPY axons showing signs of degeneration were present throughout the E16 uterus (Figure 3.18C,D,E&F). They were present in the ovarian, middle and cervical

segments and the mesometrial and anti-mesometrial sides. Degenerating axons were regular in occurrence in the E16 uterus.

3.2.4.4 Pregnancy day 18 (E18)

Uterine horns at E18 had many fewer NPY-immunoreactive axons than E14 or E16 horns and the number of NPY-positive axons appeared to be lower than the number of TH-immunoreactive axons at this time point. The number of blood vessels innervated and the innervation density of the blood vessels was much lower at E18 than at E16. There was sparse NPY innervation of a few blood vessels in the ovarian and cervical segments of E18 uterine horns. In the middle segment, NPY-immunoreactive axons ran beside blood vessels but did not appear to be associated with their perivascular plexuses. In the cervical segment in one rat, some parts of blood vessels were slightly more innervated by NPY-immunoreactive axons. Most of the NPY axons present in the E18 uterus were not associated with blood vessels. There were no thick nerve bundles containing NPY axons in the E18 uterus. The NPY innervation of the myometrium was much lower at E18 than at E16. The linea uteri did not receive any NPY-immunoreactive axons at E18 in any region of the uterus. There were no fine varicose NPY-immunoreactive axons in the circular muscle. No NPY-immunoreactive axons were present in the endometrium. Most of the E18 uterus did not receive any NPY-immunoreactive axons in contrast to E16 when NPY-positive axons were present throughout the uterus.

Degenerating axons were frequently observed at E18. These axons were present across the different regions (ovarian, middle, cervical, mesometrial and anti-mesometrial) of the E18 uterus.

FIGURE 3.19: NPY-IMMUNOREACTIVE INNERVATION OF THE PREGNANT RAT UTERUS AT E20

A, Whole mount preparation of a strip from the cervical region of a 20-day pregnant uterine horn. Letters indicate the location of the micrographs shown in B-D. Bar, 5 mm. B, An NPY-immunoreactive axon (arrowhead) becomes thicker, non-varicose and more intensely immunoreactive before it terminates. Other axons (double arrowhead) are varicose and faintly stained. Bar, 50 μm. C, An NPY-immunoreactive axon with a swollen varicosity (arrowhead). The other varicosities on the axon are variably sized, variably stained and occur at irregular intervals. D, An cervical area that contains no NPY-positive innervation. Bar, 250 μm. E, Whole mount preparation of a strip from the middle region of a 20-day pregnant uterine horn. Letters indicate the location of the micrographs shown in F-H. Bar, 5 mm. F, A varicose NPY-immunoreactive axon terminates with a very large, swollen varicosity (arrowhead). Bar, 50 μm. G, The termination of a non-varicose NPY-immunoreactive axon. Bar, 100μm. H, An area from the middle region that contains no NPY-positive innervation. Bar, 250 μm. I, Whole mount preparation of a strip at the ovarian end of a 20-day pregnant uterine horn. Letters indicate the location of the micrographs shown in J-L. Bar, 5 mm. J, An NPY-positive axon has a thickened section with more intense immunoreactivity and swollen varicosities. Bar, 100 μm. K, A thick, intensely immunoreactive NPY-positive axon has a swollen varicosity (arrowhead) just before its termination. Bar, 100 μm. L, A small blood vessel (BV) that has a sparse plexus of NPY-immunoreactive axons around it. Bar, 100 μm.

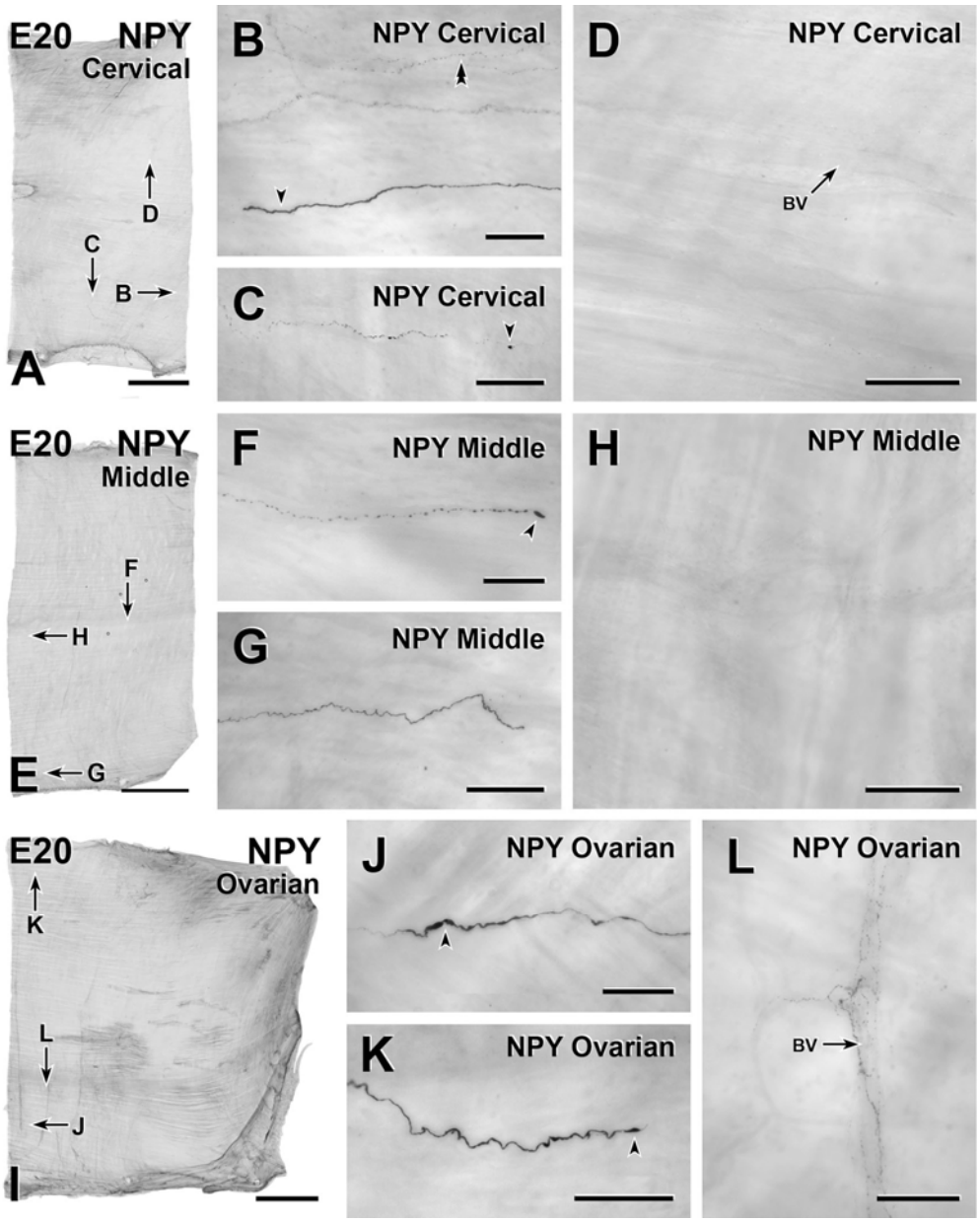
E20 NPY
Cervical
D
C
B
A
B NPY Cervical
C NPY Cervical
D NPY Cervical
BV
E20 NPY
Middle
F
H
E
G
F NPY Middle
G NPY Middle
H NPY Middle
E20 NPY
Ovarian
K
L
J
I
J NPY Ovarian
K NPY Ovarian
L NPY Ovarian
BV

3.2.4.5 Pregnancy Day 20 (E20) : Figure 3.19

My Master's thesis gave a detailed description of the NPY innervation of the rat uterus at pregnancy day 20. In summary, E20 uterine horns are almost completely devoid of NPY-immunoreactive axons and their density was much lower than at E18. Rare NPY-immunoreactive axons entered the uterus at the mesometrium and terminated shortly afterwards. Rarely, blood vessels were innervated but they received very few NPY-positive axons. The number of blood vessels that received innervation and the density of innervation were much lower than at E18. Thick nerve bundle containing NPY-immunoreactive axons were absent from the E20 uterus. There were only rare NPY-positive axons in the myometrium and no NPY axons in the linea uteri. The circular muscle plexus was absent in the E20 uterus; these fine varicose NPY axons at the bottom of the circular muscle layer in the mesometrial side were present at oestrus but not at E20. There were no NPY-immunoreactive axons in the endometrium. There were no fine varicose NPY axons in the circular muscle like the circular muscle plexus at oestrus. No NPY-immunoreactive axons were present in the endometrium. Most parts of the E20 uterus completely lacked any innervation by NPY-immunoreactive axons.

Quite a few of the NPY axons present in the E20 uterus were degenerating. They were more frequently present in the mesometrial side.

3.2.4.6 Postpartum day 1 (P1)

At P1, the distribution of NPY-immunoreactive axons within the uterus was similar to the distribution of TH-immunoreactive axons. There were more NPY-positive axons in P1 uterine horns than in E20 horns although the innervation density at both time points was quite low. At P1, a few blood vessels received a sparse NPY

innervation. Some NPY-immunoreactive axons that entered the P1 uterus along with blood vessels travelled all the way to the anti-mesometrial side. At the ovarian end of P1 uterine horns, more blood vessels were innervated by NPY-immunoreactive axons and their innervation density was higher than in the rest of the uterus. In general, the number of blood vessels innervated and their innervation density was slightly higher at P1 than at E20. Rare thick nerve bundles containing NPY-immunoreactive axons were present in P1 uterine horns.. The innervation of the linea uteri by NPY-immunoreactive axons was similar in density to the rest of the uterine on plexus at P1. Very rare NPY axons occurred in the endometrium. Like uterine horns from rats late in pregnancy, P1 uterine horns had areas that lacked NPY innervation. Innervation-free areas were present throughout P1 uterine horns and were more common on the anti-mesometrial side.

Some NPY axons in the P1 uterus had growth cones. Thick nerve bundles contained occasional NPY-immunoreactive axons with complex growth cones. Simple growth cones occurred on axons that travelled singly and on axons associated with blood vessels.

FIGURE 3.20: NPY-IMMUNOREACTIVE INNERVATION OF THE POST-PARTUM RAT UTERUS AT P3

A, In a P3 uterine horn, two NPY-immunoreactive axons with growth cones (arrows) have diverged from the sparse NPY-positive perivascular plexus around a blood vessel NPY-immunoreactive (BV) . B, C & D, Nerve bundles in P3 uterine horns contain NPY-immunoreactive axons that are giving off growth cones.

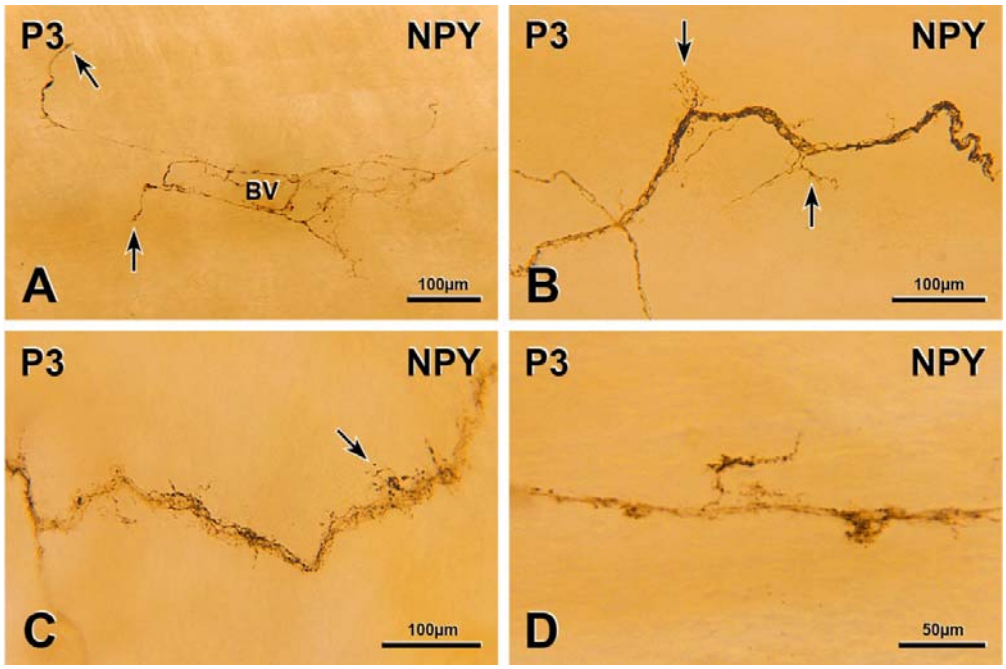
P3
NPY
BV
A
100µm
P3
NPY
B
100µm
P3
NPY
C
100µm
P3
NPY
D
50µm

3.2.4.7 Postpartum day 3 (P3) : Figure 3.20

The density of NPY-immunoreactive axons was generally higher in the P3 uterus than in the P1 uterus. More NPY-immunoreactive axons innervated blood vessels at P3 than at P1 and the density was similar to that of TH-immunoreactive axons at the same time point. At P3, rare thick nerve bundles contained NPY-immunoreactive axons. There were a few NPY-positive axons in the longitudinal and circular muscle layers. The linea uteri did not receive any NPY innervation. In the P3 uterus, there were no fine varicose axons in the location occupied by the circular muscle plexus at oestrus. Very rarely, NPY-immunoreactive axons associated with a blood vessel in the myometrium travelled to the endometrium and terminated with a growth cone. The innervation density of NPY-immunoreactive axons was higher around blood vessels and in the myometrium at P3 compared to P1. Although not as common as at P1, there were areas in P3 uterine horns that lacked TH-immunoreactive innervation. Innervation-fee areas were more common on the anti-mesometrial sides than on the mesometrial sides of P3 uterine horns.

Many of the NPY-immunoreactive axons in P3 uterine horns had growth cones, especially the NPY-positive axons that were associated with blood vessels. Axons in thick nerve bundles had some complex growth cones. Single NPY-immunoreactive axons also had growth cones.

3.2.4.8 Postpartum day 7 (P7)

P7 uterine horns had more NPY-immunoreactive axons than P3 horns. NPY innervation was denser at the ovarian end of P7 uterine horns than in the rest of the uterus. There was NPY innervation around blood vessels at P7. Some blood vessels received moderate numbers of NPY-immunoreactive axons while others received

only a few NPY-positive axons. Some NPY-immunoreactive axons followed blood vessels as they branched into smaller blood vessels as occurs in the non-pregnant uterus. Compared to P3, more blood vessels were innervated at P7 and they were supplied with more NPY-immunoreactive axons. P7 uterine horns contained a few thick nerve bundles containing NPY-positive axons. The density of NPY innervation in the myometrium and endometrium was higher at P7 than at P3. There were a few single NPY-positive axons in the myometrium. Unlike TH axons in the P7 uterus, there was no difference in the density of NPY-immunoreactive axons along the length of the linea uteri. There were no fine varicose NPY axons at the bottom of the circular muscle layer. Rare NPY-immunoreactive axons originating from blood vessels took looping courses deep into the endometrium and on rare occasions ended near glands.

At P7, uterine NPY-immunoreactive axons still exhibited growth cones. Both simple and complex growth cones were present and they occurred on axons associated with blood vessels and on axons in thick nerve bundles.

FIGURE 3.21: NPY-IMMUNOREACTIVE INNERVATION OF THE POST-PARTUM RAT UTERUS AT P14

A & B, In P14 uterine horns, blood vessels (BV) are surrounded by moderate plexuses of NPY-immunoreactive axons. There are axons with growth cones (arrows) nearby. Most of the axons with growth cones can be followed to the points (arrowheads) at which they branch off from perivascular plexuses. C, Growth cone on an NPY-immunoreactive axon. D, Sparse innervation by NPY-immunoreactive axons in the linea uteri.

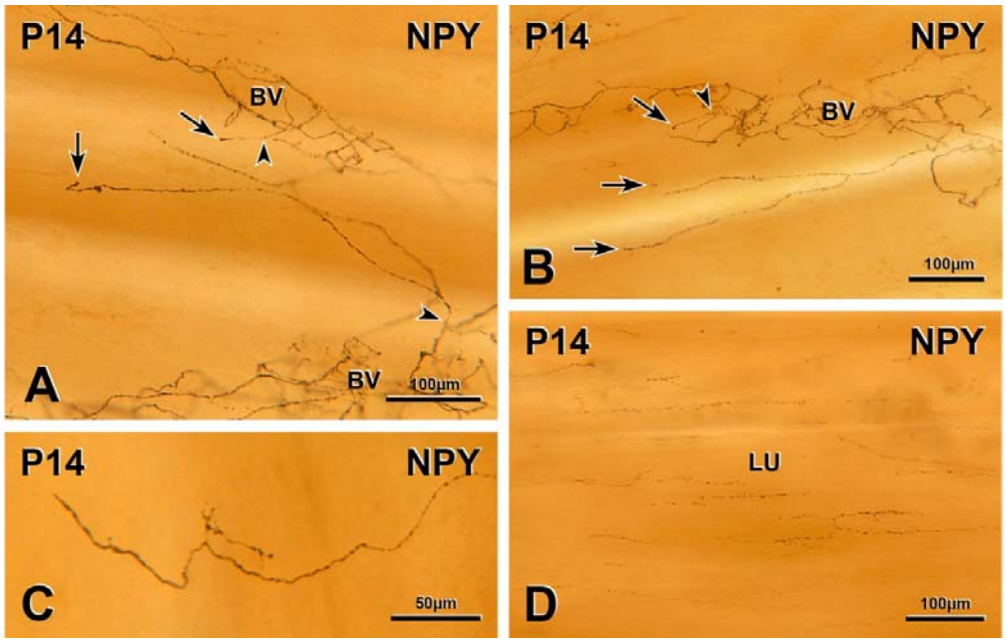
P14
NPY
BV
A
BV
100µm
P14
NPY
BV
B
100µm
P14
NPY
C
50µm
P14
NPY
LU
D
100µm

3.2.4.9 Postpartum day 14 (P14) : Figure 3.21

At P14, all layers of the uterus received more innervation from NPY-immunoreactive axons than at P7 but innervation density was still much lower than in uterine horns from non-pregnant rats at oestrus. Some NPY-immunoreactive axons entered the uterus either with blood vessels or in thick nerve bundles. NPY-immunoreactive axons provided many blood vessels with a moderate innervation while other blood vessels were only sparsely innervated. Some thick nerve bundles containing NPY-positive axons were present at P14. The density of NPY-immunoreactive axons in the myometrium was higher at P14 than at P7. A few single NPY-positive axons occurred in the longitudinal muscle layer. The fine varicose NPY-positive axons that make up the circular muscle plexus were absent at P14. In contrast to NPY-immunoreactivity at oestrus or TH-immunoreactivity at P14, no difference was observed in the NPY innervation of the linea uteri between ovarian, middle or cervical regions in the P14 uterus. Occasionally NPY-immunoreactive axons originating from blood vessels in the muscle travelled to the endometrium.

In P14 uterine horns Growth cones were still present on some NPY-immunoreactive axons that were associated with blood vessels and in thick nerve bundles. Growth cones were mostly simple.

3.2.5 SUMMARY & DISCUSSION

Staining whole mount preparations of uterine horns for either TH or NPY showed that sympathetic innervation of the uterus decreases as pregnancy advances and is almost completely absent at term. Re-innervation begins immediately after birth and is still not complete at P28. The re-innervation of the linea uteri by TH-

immunoreactive axons begins at P3 in some rats. By P28, significant re-innervation had occurred in the ovarian end of the linea uteri in all rats examined. Growth cones on sympathetic axons are abundant in uterine horns at early postpartum time points (P1, P3 and P5) and growth cones still occur on rare TH-immunoreactive axons at P28. Poisson Regression Analysis of axonal intersections showed that the density of TH-immunoreactive uterine sympathetic axons decreased from 100% at oestrus to 5.74% at E14 and 0.23% at E20. After delivery, there was a gradual increase in TH innervation density from 0.84% at P1 to 46.12% at P28. Thus, both the qualitative and quantitative studies described in this Chapter show that sympathetic innervation of the rat uterus has still not returned to normal levels by 4 weeks post-partum when uterine innervation density is only about half that at oestrus.

Chapter 4

Changes in parasympathetic innervation of the rat uterus during pregnancy and post-partum

4.1 INTRODUCTION

As Chapter 1 describes, the non-pregnant uterus receives significant parasympathetic innervation identified by ChAT- or VAChT-immunoreactivity (Gnanamanickam and Llewellyn-Smith, 2011; Papka et al., 1999). Parasympathetic nerves are found in all layers of the non-pregnant uterus and are also present around blood vessels and in the linea uteri (Gnanamanickam and Llewellyn-Smith, 2011; Papka et al., 1999). Axons immunoreactive for nNOS and axons stained for AChE were significantly reduced in the term pregnant uterus (Moustafa, 1988; Natuzzi et al., 1993). Our unpublished data from whole mount preparations of full-thickness uterine horns also show that both VAChT- and nNOS-immunoreactive axons have virtually disappeared from the pregnant rat uterus at term. There is even less known about parasympathetic re-innervation of the uterus post-partum. According to the only published study, there was a decrease in the number of AChE fibers in the post-partum uterus 1 week after delivery and the stained axons appeared to be fragmented. By 2-3 weeks post-partum, uterine horns contained large nerve trunks with AChE-stained fibers (Moustafa, 1988).

In this chapter, I have detailed and quantified parasympathetic innervation identified by immunoreactivity to VAChT in the rat uterus during late pregnancy and the first month post-partum.

4.2 RESULTS

A total of 62 rats were used in the immunohistochemical experiments for this Chapter. The same time points were examined as in Chapters 3, i.e., non-pregnant rats at oestrus (n=9), rats at pregnancy (E) days E14 (n=7), E16 (n=5), E18 (n=5) and E20 (n=4) and rats at post-partum (P) days P1 (n-4), P3 (n=4), P5 (n=4), P7 (n=4), P10 (n=5), P14 (n=6) and P28 (n=5).

I have previously described the innervation of the rat uterus at oestrus (Gnanamanickam and Llewellyn-Smith, 2011) and at E20 (unpublished data) by VAChT-immunoreactive axons in studies that used the same method as used here for immunohistochemistry in full thickness whole mount uterine preparations. The innervation patterns at these two time points found in this study were the same as described previously.

4.2.1 Changes in uterine parasympathetic innervation revealed by immunostaining for VAChT

4.2.1.1 Oestrus : Figure 4.1

The non-pregnant rat uterus at oestrus is supplied with a significant number of VAChT-immunoreactive axons. Many VAChT-immunoreactive axons entered the uterus in association with blood vessels, in thick nerve bundles or as single axons. Many blood vessels received a substantial innervation from VAChT-immunoreactive axons (Figure 4.1B). Many thick nerve bundles containing VAChT-immunoreactive axons were present throughout the non-pregnant uterus. There were also many VAChT-immunoreactive axons in the myometrium.

FIGURE 4.1: VACHT-IMMUNOREACTIVE INNERVATION OF THE NON-PREGNANT RAT UTERUS AT OESTRUS

A, Many VAChT-immunoreactive axons (arrow) in the linea uteri (LU) of the non-pregnant rat at oestrus. B, Many VAChT-immunoreactive axons innervate blood vessels (BV) and the fine varicose VAChT-immunoreactive axons in the circular muscle (CMP). Thick nerve bundle containing many VAChT-immunoreactive axons also present.

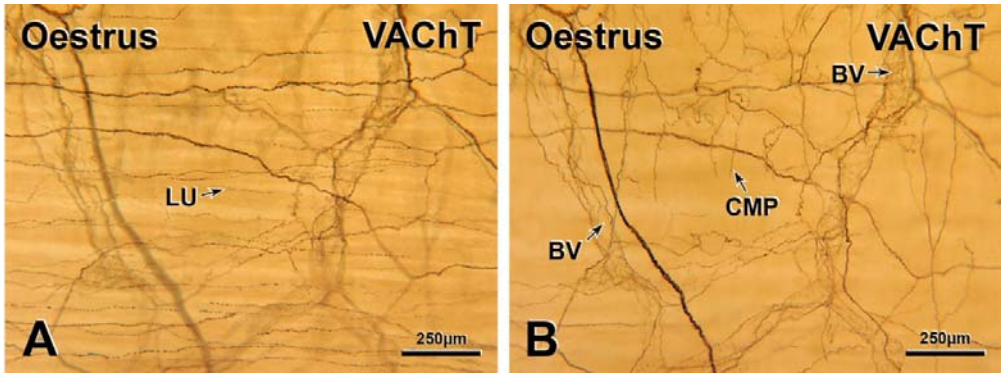
Oestrus
VAChT
LU
A
250µm
Oestrus
VAChT
BV
CMP
BV
B
250µm

The linea uteri had more VAChT-immunoreactive axons compared to the rest of the smooth muscle (Figure 4.1A). Near the bottom of the circular muscle layer, fine varicose VAChT-positive axons formed a circular muscle plexus (CMP), which followed the orientation of the circular muscle and was absent beneath the linea uteri (Figure 4.1B). Some VAChT-immunoreactive axons travelled to the endometrium from the myometrium but none were observed near glands.

4.2.1.2 Pregnancy day 14 (E14) : Figure 4.2

At E14, the pregnant rat uterus was much less innervated by VAChT-immunoreactive axons than the non-pregnant uterus at oestrus. VAChT staining in the E14 uterus was pale in spite of the higher concentration of antibody (1:2,500 dilution rather than 1:10,000 dilution) used for immunohistochemistry. In most of the rats examined, the cervical segments of uterine horns had more VAChT-immunoreactive axons compared to the middle and ovarian segments. The innervation density of the middle region was slightly lower than the cervical region. The relatively lower density of ovarian innervations was likely due to poor staining for VAChT at the ovarian end.

Few VAChT-immunoreactive axons entered the uterus as single axons or in association with blood vessels. Blood vessels received a much sparser innervation from VAChT-immunoreactive axons than at oestrus and only a small number of blood vessels were innervated (Figure 4.2B). In two rats, some of the blood vessels in the cervical segment received a few more VAChT-immunoreactive axons. In all rats, there were some blood vessels that lacked any VAChT innervation. In E14 uterine horns, thick nerve bundles with VAChT-immunoreactive axons were much less common than at oestrus and contained fewer stained fibers. The density of

VAChT innervation of the myometrium and endometrium was much lower at E14 than at oestrus. VAChT–immunoreactive axons ran through the longitudinal smooth muscle but they were very few in number. There were no VAChT-immunoreactive axons in the linea uteri. The few VAChT-positive axons in the circular muscle layer were mostly associated with blood vessels. In one portion of the cervical segment from one E14 rat and in a small portion of the middle segment in another E14 rat, there were a few VAChT-immunoreactive axons in the circular muscle on the mesometrial side in a location similar to the CMP observed at oestrus. Very rare VAChT-immunoreactive axons occurred in the endometrium but none were observed near glands. In E14 uterine horns, there were areas that were devoid of VAChT-immunoreactive axons (Figure 4.2D). Areas without VAChT innervation were present in ovarian, middle and cervical regions in all rats and were slightly more common in the anti-mesometrial side compared to the mesometrial side.

Degenerating axons were common in all regions of the E14 uterus (Figure 4.2E). These axons were identifiable because they appeared fragmented or swollen or vacuolated. Fragmented VAChT-immunoreactive axons were more common than swollen or vacuolated axons.

4.2.1.3 Pregnancy day 16 (E16) : Figure 4.3

Rat uterine horns at E16 received fewer VAChT-immunoreactive axons than E14 horns. In two rats, the cervical segment had a higher density of VAChT innervation than the middle and ovarian segments. As with the E14 uterine horns, VAChT staining was poor at the ovarian end and this could be why the cervical end was more densely innervated than the ovarian end. The middle region received slightly less VAChT axons compared to the cervical region.

FIGURE 4.2: VAChT-IMMUNOREACTIVE INNERVATION OF THE PREGNANT RAT UTERUS AT E14

A, Whole mount preparations of strips from the middle and cervical regions of an E14 uterine horn. Letters indicate the location of the micrographs in B-D. B, A sparsely innervated blood vessel (BV) in the cervical region. C, Single VAChT-immunoreactive axons in the myometrium. D, An area that is devoid of innervation by VAChT-immunoreactive axons from the middle region. E, In the middle region of an E14 uterine horn, degenerating VAChT axons occur in nerve bundles or as single axons.

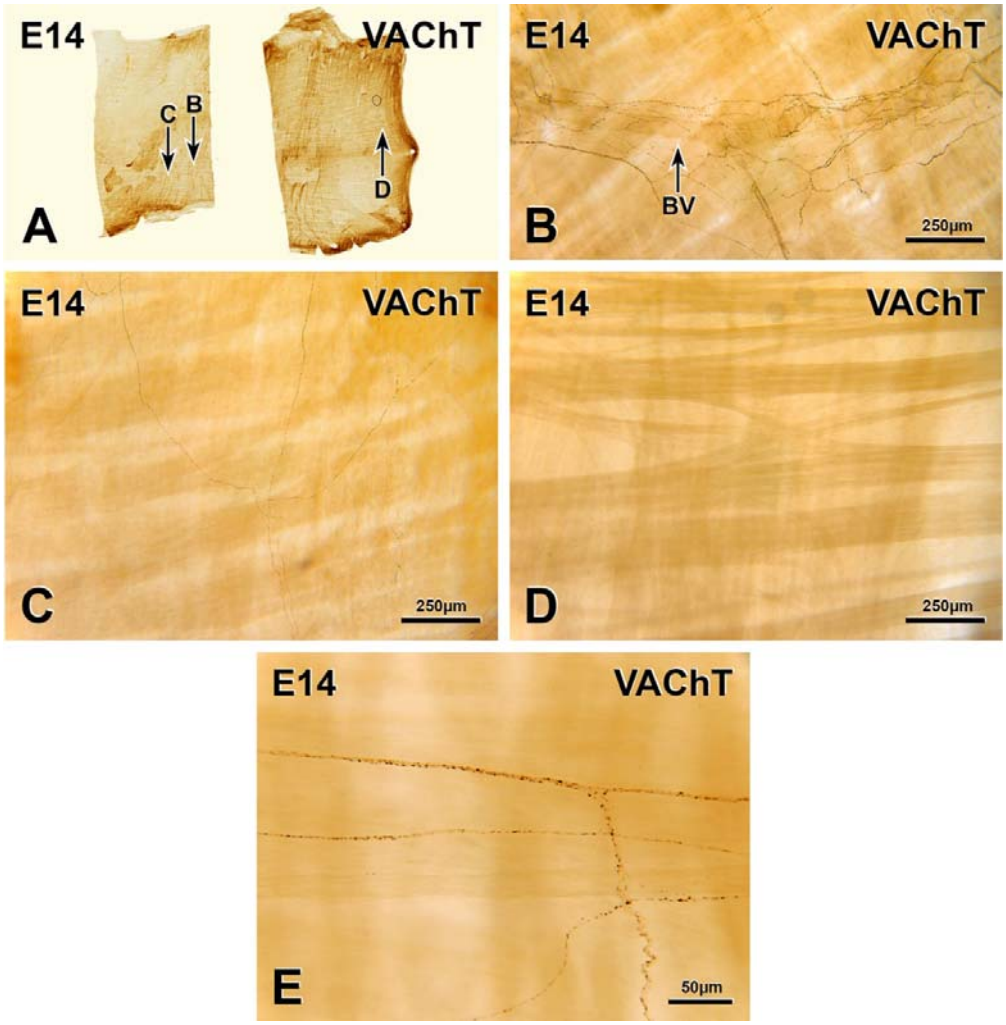
E14
VAChT
C
B
D
A
E14
VAChT
BV
B
250µm
E14
VAChT
C
250µm
E14
VAChT
D
250µm
E14
VAChT
E
50µm

At E16, a few VAChT-immunoreactive axons entered the uterus along with blood vessels or in thick nerve bundles or by themselves. Only a very few blood vessels were sparsely innervated by VAChT-immunoreactive axons (Figure 4.3A).

Blood vessels that lacked VAChT innervation were present (Figure 4.3C&D). Sometimes, there were VAChT-immunoreactive axons near blood vessels but they were not part of perivascular plexuses. E16 uterine horns had thick nerve bundles but they were very few in number and contained few VAChT-immunoreactive axons (Figure 4.3B). A few VAChT-positive axons were present in the myometrium. Rare single VAChT-immunoreactive axons travelled in the longitudinal muscle but there were no VAChT immunoreactive axons in the linea uteri. The circular muscle contained a few individual VAChT-positive axons, some axons in bundles and a few perivascular axons. At the cervical-most end in one rat, a few fine varicose VAChT-immunoreactive axons occurred on the mesometrial side in a location reminiscent of the CMP. At E16, no VAChT-immunoreactive axons were observed deep in the endometrium. There were areas in E16 horns that were not innervated by VAChT-immunoreactive axons (Figure 4.3D). These areas were present in all regions of the E16 uterus but were more common in the middle region. These areas lacking innervation were slightly more common on the anti-mesometrial side.

All regions of E16 uterine horns contained degenerating axons (Figure 4.3E).

4.2.1.4 Pregnancy day 18 (E18) : Figure 4.4

The VAChT innervation of E18 uterine horns was less dense than in E14 or E16 horns. Middle segments were less innervated than ovarian and cervical segments. Compared to E16, the density of innervation by VAChT-immunoreactive axons was lower in all uterine layers at E18. Very few VAChT-immunoreactive axons entered

the E18 uterus. Very occasional blood vessels were sparsely innervated by VAChT-immunoreactive axons and rare VAChT axons ran alongside blood vessels (Figure 4.4A&B). Many blood vessels did not receive any VAChT innervation (Figure 4.4D). Rare thick nerve bundles contained very few VAChT-immunoreactive axons. A few single VAChT-immunoreactive axons were present in the myometrium and these were rarer in the longitudinal muscle than in the circular muscle. These single myometrial axons made up the majority of VAChT-immunoreactive axons in E18 uterine horns. No fine VAChT-positive axons could be identified in the CMP. No VAChT-immunoreactive axons occurred in the endometrium. Innervation-free areas occurred in cervical, middle and ovarian regions of the E18 uterus and were more common in E18 uterine horns than in E16 horns (Figure 4.4D). These areas were also more common on the anti-mesometrial side compared to the mesometrial side. Degenerating axons were common throughout the E18 uterus (Figure 4.4E).

4.2.1.5 Pregnancy day 20 (E20) : Figure 4.5

The E20 rat uterus received many fewer VAChT-immunoreactive axons than the E18 uterus. The cervical region received the most number of VAChT-immunoreactive axons compared to the ovarian and middle regions. VAChT staining was poor in the ovarian end so it was possible to accurately determine the difference in innervation density between the ovarian and cervical regions. The very few axons that were present in the E20 uterus were mostly in the mesometrial side.

At E20, rare VAChT-immunoreactive axons entered the uterus at the mesometrium. Rarely, a VAChT-immunoreactive axon ran alongside a blood vessels but the VAChT-positive axons did not contribute to their perivascular innervation.

FIGURE 4.3: VACHT-IMMUNOREACTIVE INNERVATION OF THE PREGNANT RAT UTERUS AT E16

A, A sparsely innervated blood vessel (arrow) in the myometrium of an E16 uterine horn. B, A thick nerve bundle containing a few VAChT-immunoreactive axons travelling from the mesometrial side towards the anti-mesometrial side. C, In a sparsely innervated area in the myometrium of the ovarian region from an E16 uterine horn, a blood vessel (BV) lacks VAChT innervation. D, An area of the myometrium that is devoid of VAChT innervation. BV, blood vessels. E, Degenerating VAChT-immunoreactive axons in an E16 uterine horn are fragmenting and have some swollen varicosities.

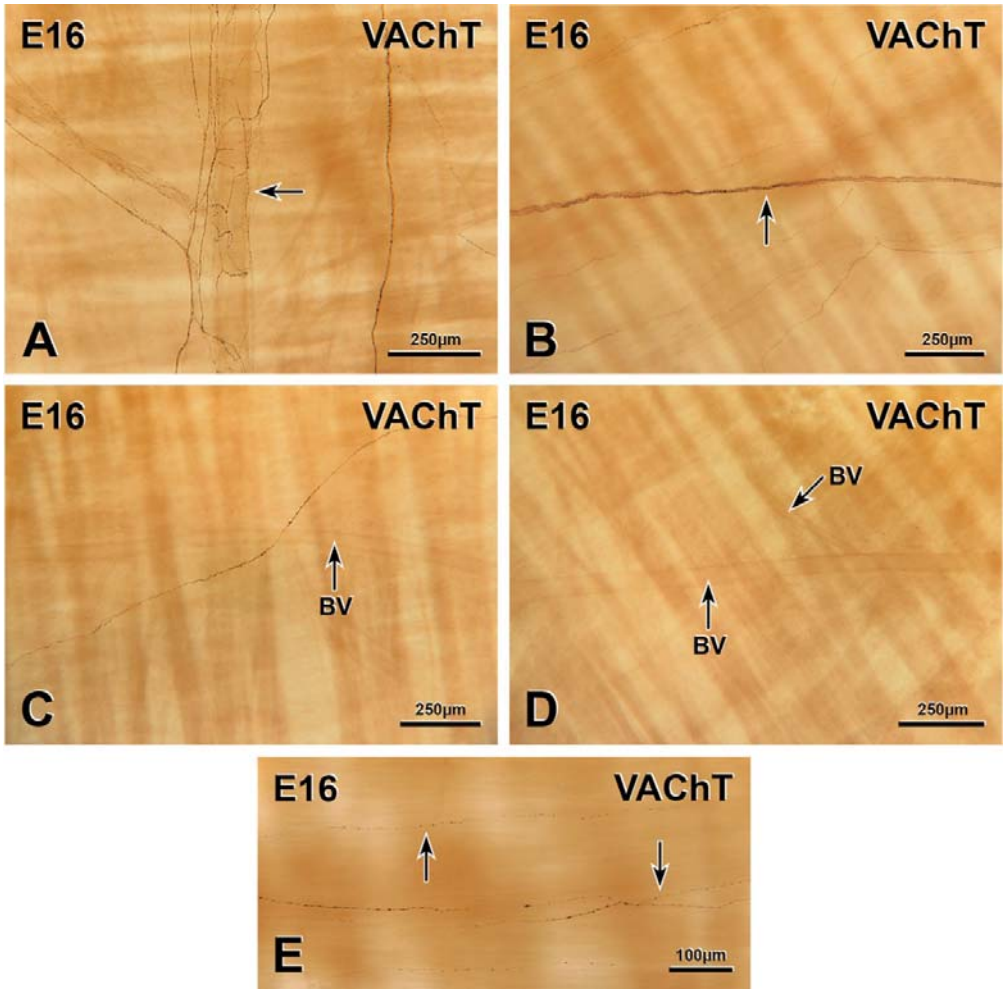
E16
VAChT
A
250µm
E16
VAChT
B
250µm
E16
VAChT
BV
C
250µm
E16
VAChT
BV
BV
D
250µm
E16
VAChT
E
100µm

FIGURE 4.4: VACHT-IMMUNOREACTIVE INNERVATION OF THE PREGNANT RAT UTERUS AT E18

A & B, in E18 uterine horns, VAChT-immunoreactive axons run near blood vessels (BV) but do not form perivascular plexuses around them.. C, Single VAChT-immunoreactive axons in the myometrium. D, An area of an E18 uterine horn without any VAChT innervation. E, A Degenerating VAChT-immunoreactive axon in an E18 uterine horn is fragmenting and has some varicosities (1-3) that appear vacuolated. Insets, vacuolated varicosities 1-3 at higher magnification.

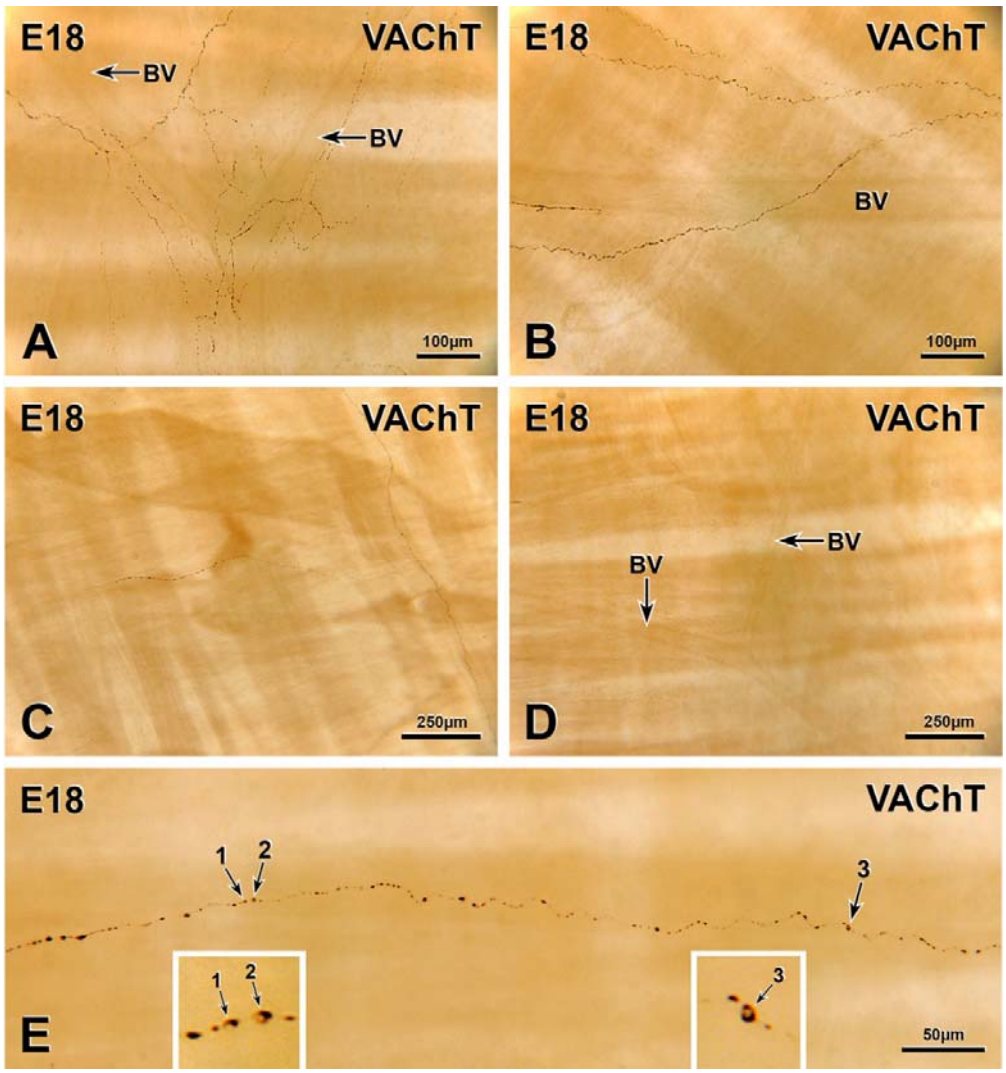
E18
VAChT
BV
BV
A
100µm
E18
VAChT
BV
B
100µm
E18
VAChT
C
250µm
E18
VAChT
BV
BV
D
250µm
E18
VAChT
1
2
3
1
2
3
E
50µm

FIGURE 4.5: VACHT-IMMUNOREACTIVE INNERVATION OF THE PREGNANT RAT UTERUS AT E20

A, A whole mount preparation of a strip from the middle segment of an E20 uterine horn. Letters indicate the location of the micrographs in B and C. B, A single fragmenting VAChT-immunoreactive axon in the myometrium. C, A blood vessel (BV) without any VAChT innervation. D & E, Degenerating VAChT-immunoreactive axons that appear fragmented and have swollen varicosities in an E20 uterine horn.

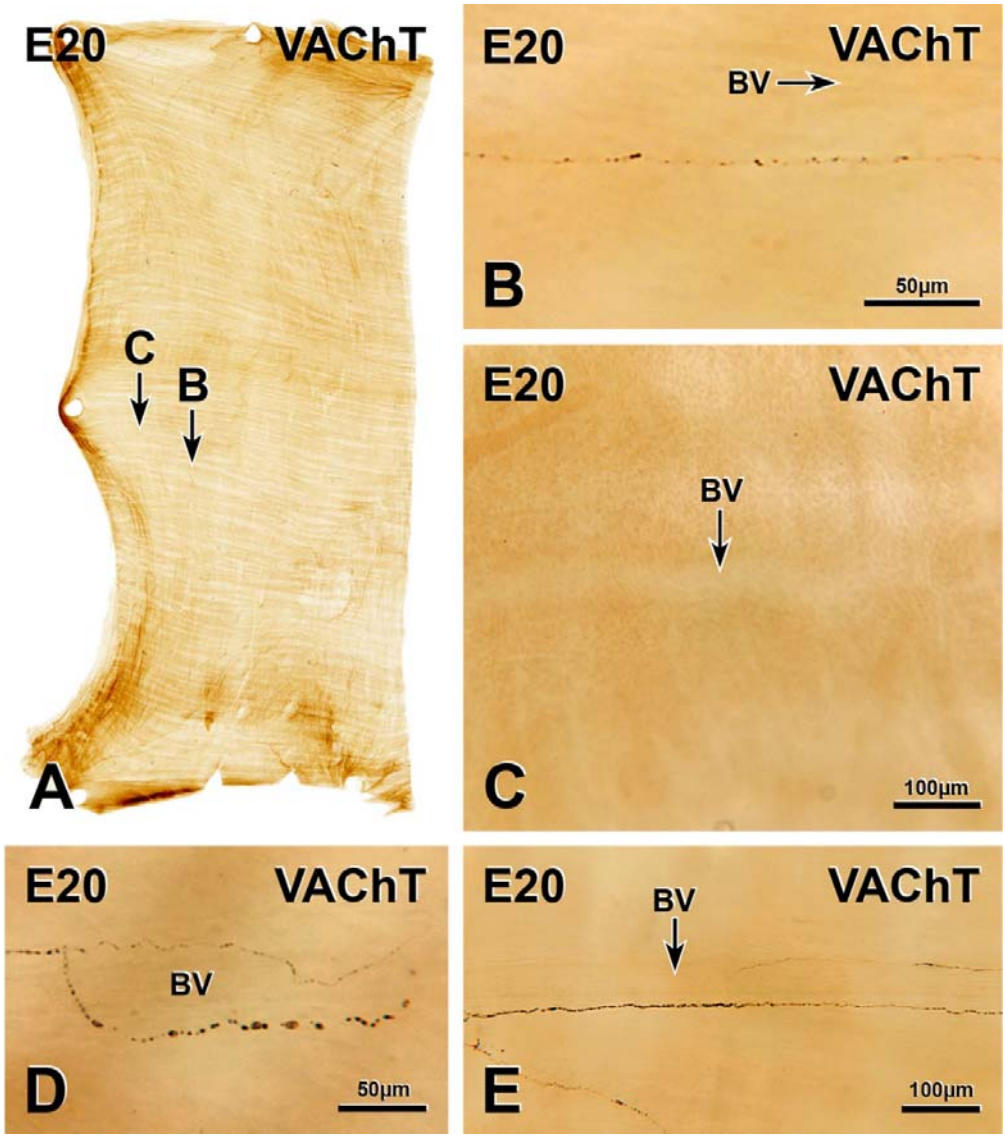
E20
VAChT
C
B
A
E20
VAChT
BV
B
50µm
E20
VAChT
BV
C
100µm
E20
VAChT
BV
D
50µm
E20
VAChT
BV
E
100µm

All blood vessels examined in the E20 uterus lacked VAChT innervation (Figure 4.5C). The VAChT-immunoreactive axons in the E20 uterus were mostly single axons in the myometrium. The linea uteri was not distinguishable and there were no VAChT-immunoreactive axons in the location where the linea uteri is normally present. There was also no evidence of fine varicose VAChT-positive axons contributing to a CMP. No VAChT-immunoreactive axons were observed in the endometrium Areas lacking innervation were more common than in the E18 uterus. In fact, most areas of the E20 uterus did not receive any VAChT-immunoreactive axons. Thus, the vast majority of all horns examined was devoid of VAChT innervation.

Among the VAChT-immunoreactive axons that were present in the E20 uterus, most were degenerating axons and these were present in all regions of the E20 uterus, including the ovarian, middle, cervical regions and the mesometrial and anti-mesometrial sides (Figure 4.5B,D&E).

4.2.1.6 Post-partum day 1 (P1) : Figure 4.6

At P1, the innervation of the uterus by VAChT-immunoreactive axons was more dense than at E20 but there was still very, very much less innervation than at oestrus. Innervation density was slightly higher in the cervical region and similar in the ovarian and middle regions. In two rats, the ovarian segment was poorly stained.

Very few VAChT-positive axons entered P1 uterine horns along with blood vessels or by themselves. Only a very few blood vessels received a sparse VAChT innervation (Figure 4.6A). The number of blood vessels innervated and the innervation density was higher at P1 than at E20. Rare thick nerve bundles were present throughout the uterus and contained only few VAChT-immunoreactive

axons. The innervation density of the myometrium was higher at P1 than at E20. Occasional individual VAChT-positive axons occurred in the myometrium but rarely in the longitudinal muscle. There was no noticeable difference in the innervation of the linea uteri by VAChT-immunoreactive axons compared to the rest of the longitudinal smooth muscle. There was no CMP at P1 and no VAChT-immunoreactive axons in the endometrium. Many areas of P1 uterine horns did not receive any innervation from VAChT-positive axons. These areas were still extensive but slightly less so than in E20 uterine horns.

Many VAChT-immunoreactive axons in the P1 uterus had growth cones (Figure 4.6B,C&D). A simple growth cone had one or two sprouts while growth cones with many sprouting finger-like processes were considered complex growth cones. Growth cones were mostly simple at P1. Often, VAChT-immunoreactive axons that travelled singly within the myometrium terminated with a growth cone. VAChT-positive axons associated with blood vessels also had growth cones.

4.2.1.7 Post-partum day 3 (P3) : Figure 4.7

The density of innervation of the rat uterus by VAChT-immunoreactive axons at P3 was higher than at P1. The ovarian and cervical regions were more densely innervated than the middle segment. Mostly, the mesometrial side was more innervated than the anti-mesometrial side.

More VAChT-positive axons entered the uterus at P3 than at P1. More blood vessels were innervated at P3 but the number of innervated blood vessels was still low overall. Blood vessels were more densely innervated than at P1 but were still surrounded by only a few VAChT-immunoreactive axons (Figure 4.7A).

FIGURE 4.6: VACHT-IMMUNOREACTIVE INNERVATION OF THE POST-PARTUM RAT UTERUS AT P1

A, A sparsely innervated blood vessel (BV) on the mesometrial side of a P1 uterine horn. Two VAChT-immunoreactive axons are beginning to form a perivascular plexus. Nerve bundles running alongside the blood vessel contain VAChT-positive axons. Red blood cells can been seen inside the blood vessel. B, C & D, VAChT-immunoreactive axons with growth cones, some of which are indicated by arrows.

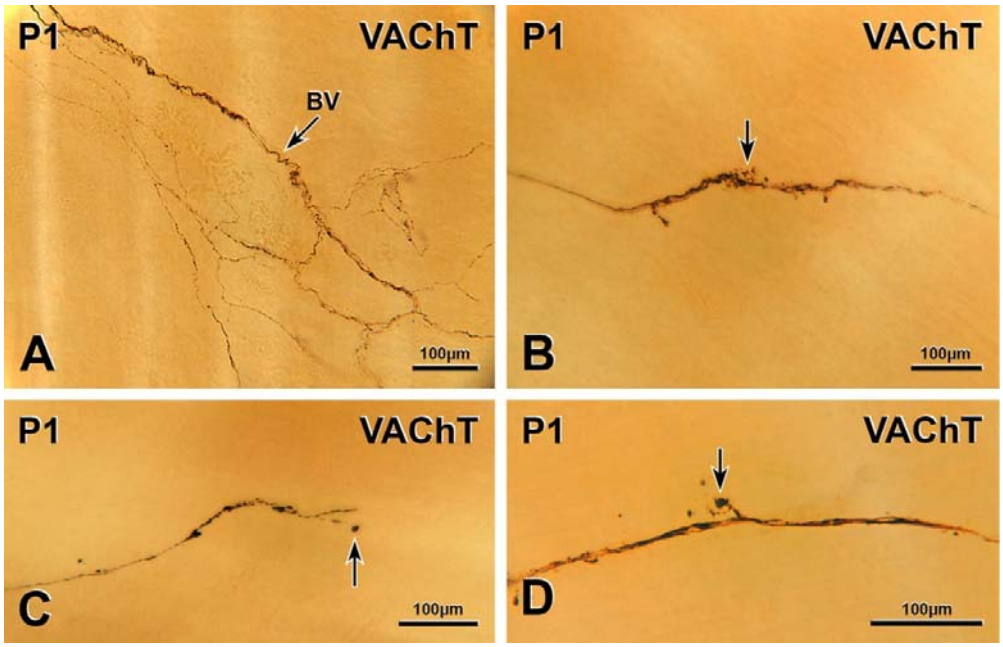
P1
VAChT
BV
A
100µm
P1
VAChT
B
100µm
P1
VAChT
C
100µm
P1
VAChT
D
100µm

Occasional thick nerve bundles containing few VAChT-immunoreactive axons were present, mostly on the mesometrial side. There were more VAChT-immunoreactive axons in the myometrium and endometrium at P3 than at P1. Both longitudinal and circular muscle layers of the myometrium contained a few single VAChT-positive axons. However, there were no VAChT-immunoreactive axons in the linea uteri in any region of P3 uterine horns and no fine varicose VAChT-positive axons anywhere in the circular muscle layer. Rare VAChT-immunoreactive axons travelled from blood vessels in the myometrium to the endometrium. There were areas of the P3 uterus that did not receive any VAChT-immunoreactive axons but they were somewhat smaller and less common than at P1.

Many more VAChT-immunoreactive axons had growth cones in the P3 than in the P1 uterus (Figure 4.7B,C&D). VAChT-positive axons in thick nerve bundles and VAChT-positive axons associated with blood vessels had simple or complex growth cones. There were also single VAChT-immunoreactive axons with growth cones. A subset of the rare VAChT-positive axons that travelled from the myometrium to the endometrium terminated with growth cones.

4.2.1.8 Post-partum day 5 (P5) : Figure 4.8

The density of VAChT-immunoreactive axons in P5 uterine horns was slightly higher than at P3. The cervical region was more densely innervated compared to the ovarian and middle regions. There was only a slight higher innervation density on the mesometrial side compared to the anti-mesometrial side.

FIGURE 4.7: VACHT-IMMUNOREACTIVE INNERVATION OF THE POST-PARTUM RAT UTERUS AT P3

A, In the myometrium of a P3 uterine horn, a blood vessel receives a sparse supply of VAChT-immunoreactive axons. B, An axon branches from a thick nerve bundle and terminates with a growth cone. C & D, VAChT-immunoreactive axons with growth cones (arrows).

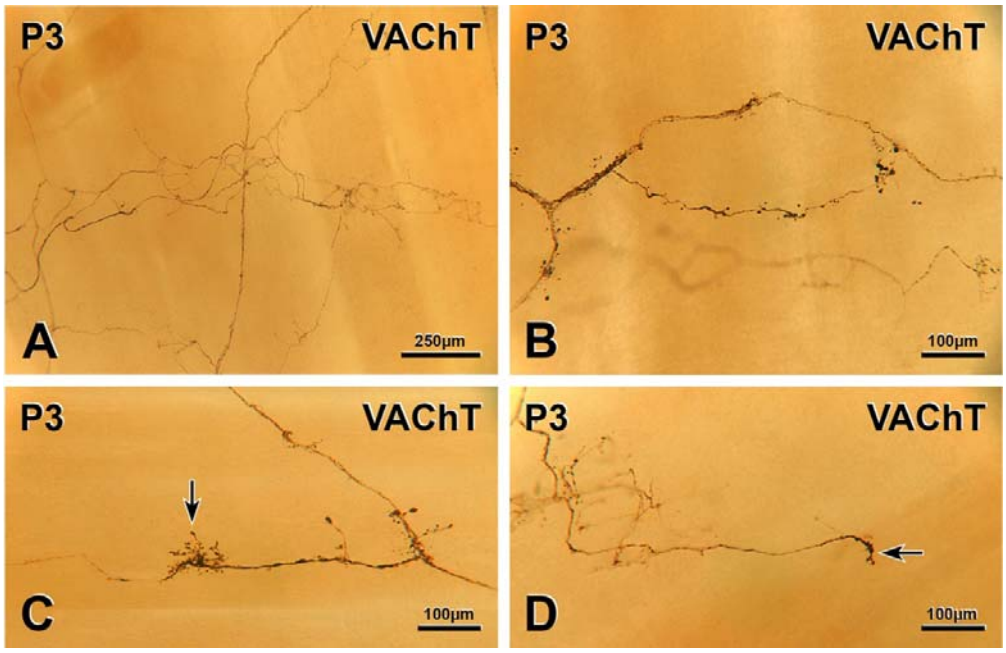
P3
VAChT
A
250µm
P3
VAChT
B
100µm
P3
VAChT
C
100µm
P3
VAChT
D
100µm

FIGURE 4.8: VACHT-IMMUNOREACTIVE INNERVATION OF THE POST-PARTUM RAT UTERUS AT P5

A, A blood vessel that entered at the mesometrium and branched receives a moderate innervation from VAChT-immunoreactive axons. B, VAChT-immunoreactive axon with growth cones (arrows). C, One of the VAChT-immunoreactive axons that has entered at the mesometrium and is travelling towards the anti-mesometrial side gives off a growth cone (arrow). D, An axon branches off a thick nerve bundle and give off a spray of growth cones (arrow).

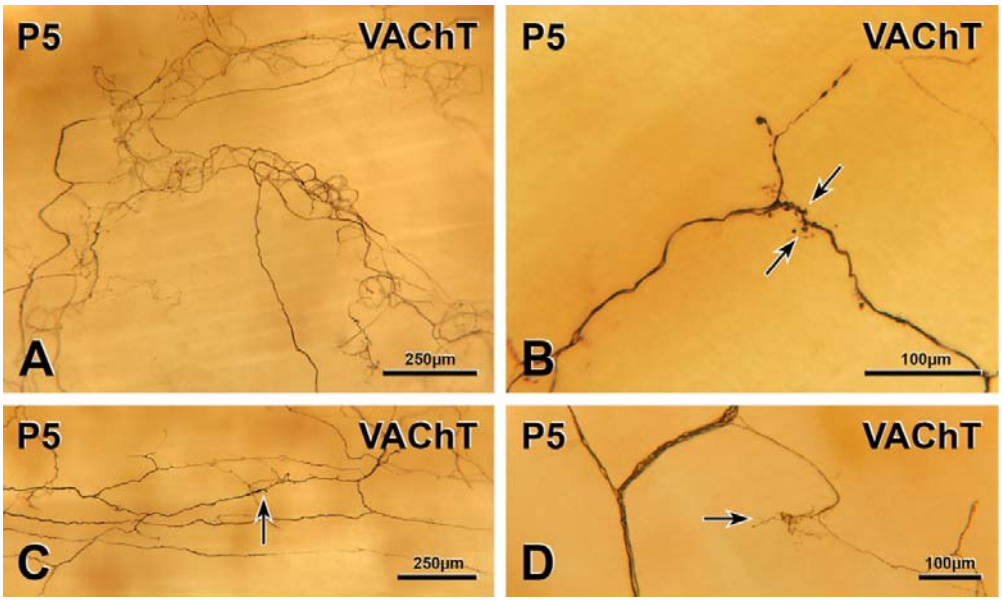
P5
VAChT
A
250µm
P5
VAChT
B
100µm
P5
VAChT
C
250µm
P5
VAChT
D
100µm

A few VAChT-immunoreactive axons entered the uterus along with blood vessels, in thick nerve bundles or rarely as single axons. Uterine blood vessels received more VAChT-immunoreactive axons at P5 than at P3 but there were still only a few VAChT-immunoreactive axons around individual blood vessels (Figure 4.8A). A few thick nerve bundles were present throughout the P5 uterus on both mesometrial and anti-mesometrial sides. These bundles contained more VAChT-positive axons than at P3. There were more VAChT axons in the myometrium at P5 compared to P3 but the innervation density of the endometrium was similar. In the myometrium, VAChT-immunoreactive axons were mostly perivascular or travelled in thick nerve bundles. Rare single VAChT-positive axons were present in the longitudinal muscle. There were no VAChT-immunoreactive axons in the linea uteri in most of the rats examined. However, in one rat, there were a few VAChT-positive axons at the ovarian end of the linea uteri but not in the rest of the uterine horn. There were no fine varicose VAChT axons in the CMP at P5. Rare VAChT axons were present in the endometrium; these axons often travelled from a blood vessel in the myometrium. P5 uterine horns contained areas that received few VAChT-immunoreactive axons and others areas where there were more VAChT-positive axons. Areas without innervation were fewer and smaller at P5 than at P3.

More growth cones were present on VAChT-immunoreactive axons in the P5 uterus than at P3 (Figure 4.8B&D). VAChT-positive axons associated with blood vessels, axons in thick nerve bundles (Figure 4.8D) and axons that travelled individually had either simple or complex growth cones. In one instance, growth cones branched off from many of the VAChT-immunoreactive axons within a thick nerve bundle.

4.2.1.9 Post-partum day 7 (P7) : Figure 4.9

P7 uterine horns were more densely innervated by VAChT-immunoreactive axons than P5 uterine horns. In all rats examined, the ovarian region had a lower density of VAChT innervation than the rest of the uterus, which may have been due to poor staining for VAChT in the ovarian region.

Small to moderate numbers of VAChT-immunoreactive axons entered the uterus along with blood vessels, in thick nerve bundles or rarely as single axons (Figure 4.9 A&B). At P7, more blood vessels were innervated than at P5, with many receiving a supply of VAChT-positive axons (Figure 4.9C). A few thick nerve bundles containing some VAChT-positive axons were present throughout the P7 uterus. These bundles were similar in number and distribution to those in the P5 uterus. Rare single VAChT-immunoreactive axons were present in the longitudinal muscle. There were no VAChT-immunoreactive axons in the linea uteri in the P7 uterus. In one small portion at the cervical end of a uterine horn from one P7 rat, VAChT-immunoreactive axons were re-appearing in the CMP near the mesometrial attachment. VAChT-immunoreactive axons in the endometrium were still rare but slightly more frequent than in the P5 uterus. At P7, there were still differences in innervation density between different areas within the same uterine horn. There were also still areas in P7 horns that lacked innervation from VAChT-positive axons. However, these areas were smaller and less common at P7 than at earlier post-partum time points. Although lower in number than in the P5 uterus, VAChT-immunoreactive axons with growth cones were still present at P7 (Figure 4.9D,E&F). Growth cones arose from many of the axons in thick nerve bundles.

FIGURE 4.9: VACHT-IMMUNOREACTIVE INNERVATION OF THE POST-PARTUM RAT UTERUS AT P7

A, in the ovarian regions of a P10 uterine horn, VAChT-immunoreactive axons proved a dense innervation entering at the mesometrium (bottom of micrograph). B, Near the mesometrium (bottom of micrograph) in the middle region of a P10 uterine horn, the VAChT innervation is less dense. . C, A blood vessel receives a moderate innervation from VAChT-immunoreactive axons. D, E & F, VAChT-immunoreactive axons with growth cones.

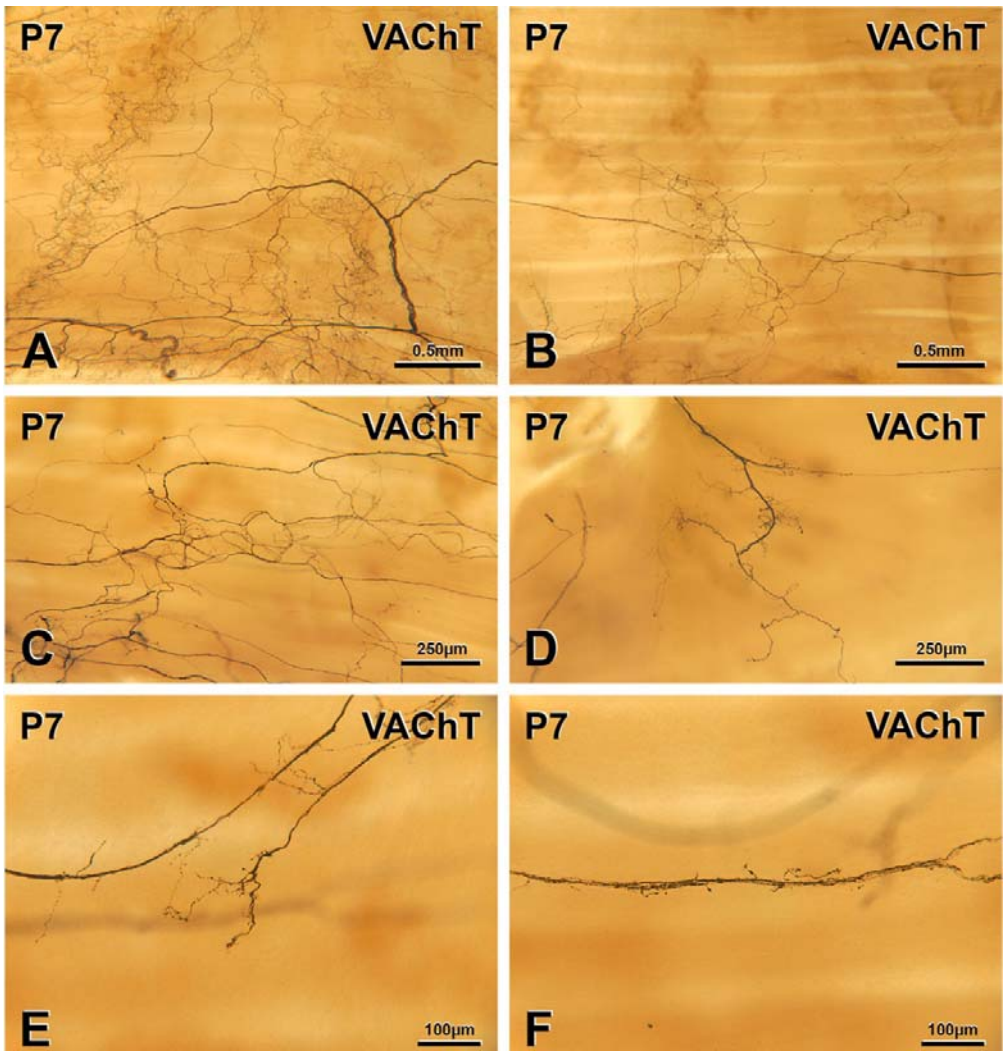
P7
VAChT
A
0.5mm
P7
VAChT
B
0.5mm
P7
VAChT
C
250µm
P7
VAChT
D
250µm
P7
VAChT
E
100µm
P7
VAChT
F
100µm

4.2.1.10 Post-partum day 10 (P10) : Figure 4.10

The density of uterine VAChT-immunoreactive axons was a little higher at P10 than at P7. In one rat, the overall density of VAChT-positive axons was higher than in the other rats. In particular, the cervical end of the uterine horn from this rat received many VAChT-immunoreactive axons (Figure 4.10A). Another two rats showed poor staining at the ovarian end so it was not possible to determine whether P10 uterine horns showed a difference in VAChT innervation density from their cervical to their ovarian ends.

At P10, some VAChT-immunoreactive axons entered the uterus along with blood vessels, in thick nerve bundles or as single axons. Similar numbers of blood vessels were innervated by VAChT-immunoreactive axons in the P10 uterus as in the P7 uterus. Most blood vessels received some VAChT-immunoreactive axons although some were only sparsely innervated (Figure 4.10D). Few thick nerve bundles containing small to moderate numbers of VAChT-immunoreactive axons were present throughout the P10 uterus. Two rats had thick nerve bundles that contained many VAChT-immunoreactive axons. There were rare single axons in the longitudinal muscle. At P10, there was variability in the innervation of the linea uteri by VAChT-immunoreactive axons. In the one rat that showed a higher density of VAChT innervation, the linea uteri had more VAChT-immunoreactive axons at its ovarian-most end. In another rat, there were very few VAChT axons at the cervical end of the linea uteri. The other rats examined had no VAChT-immunoreactive axons in their linea uteri. The VAChT innervation of the circular muscle layer consisted of perivascular axons and axons in thick nerve bundles.

FIGURE 4.10: VACHT-IMMUNOREACTIVE INNERVATION OF THE POST-PARTUM RAT UTERUS AT P10

A & B, In the cervical region of a P10 uterine horn, many VAChT-immunoreactive axons enter at the mesometrium (top of micrograph) and blood vessels have a substantial innervation C, In the middle region of a P10 uterine horn, fewer VAChT-immunoreactive axons are present at the mesometrium (top of micrograph) in D, The perivascular plexus of VAChT-immunoreactive axons around a blood vessel in the myometrium varies in density. E & F, VAChT-immunoreactive axons with growth cones.

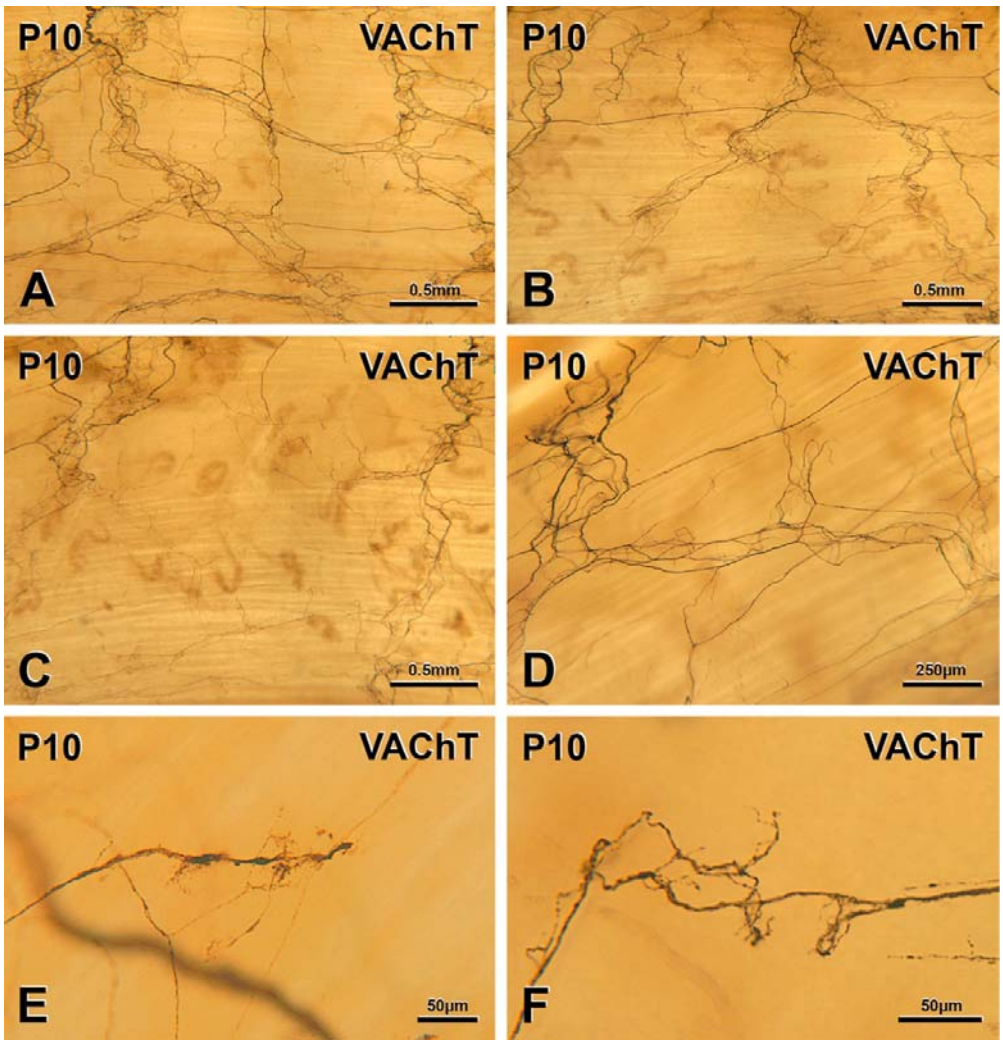
P10
VAChT
A
0.5mm
P10
VAChT
B
0.5mm
P10
VAChT
C
0.5mm
P10
VAChT
D
250µm
P10
VAChT
E
50µm
P10
VAChT
F
50µm

FIGURE 4.11: VACHT-IMMUNOREACTIVE INNERVATION OF THE POST-PARTUM RAT UTERUS AT P14

A & B, different focal planes through the same area of a P14 uterine horn. The mesometrium is at the bottom of the micrographs. A, Blood vessels receive some VAChT-immunoreactive axons, B, VAChT-immunoreactive axons in the circular muscle (arrow). C, VAChT-immunoreactive axons in the linea uteri in the middle region of a P14 uterine horn. D & E, Rare VAChT-immunoreactive axons have growth cones (arrows).

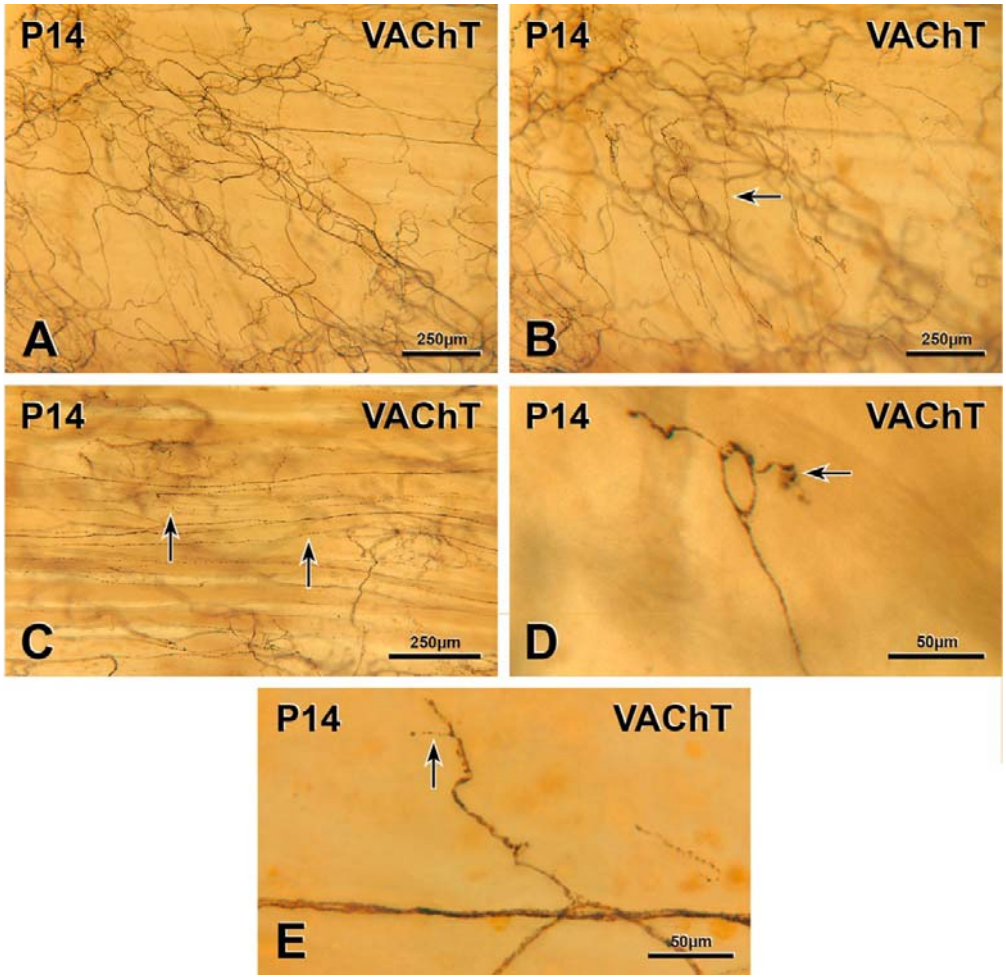
P14
VAChT
A
250µm
P14
VAChT
B
250µm
P14
VAChT
C
250µm
P14
VAChT
D
50µm
P14
VAChT
E
50µm

At P10, no single VAChT-positive axons were observed in the bulk of the circular muscle or in the region where the CMP was located at oestrus. Even at P10, there were still only rare VAChT-immunoreactive axons in the endometrium. There were areas throughout the P10 uterus without any innervation. These areas were slightly higher at the anti-mesometrial side compared to the mesometrial side.

Growth cones were present on VAChT-immunoreactive axons in the P10 uterus but there were fewer axons with growth cones than at P7 (Figure 4.10E&F). Growth cones were mostly simple. Axons in thick nerve bundles and associated with blood vessels gave rise to growth cones.

4.2.1.11 Post-partum day 14 (P14) : Figure 4.11

There were more VAChT-immunoreactive axons in the uterus at P14 than at P10. The uterine horn from one P14 rat had a higher density of VAChT-positive axons than horns from the other rats. Immunostaining for VAChT was poor at the ovarian end in two rats. The cervical region received the highest innervation density compared to the middle and ovarian regions. In some areas of the P14 uterus, the mesometrial side received more VAChT-immunoreactive axons than the anti-mesometrial side.

At P14, there were more VAChT-immunoreactive axons entering the uterus along with blood vessels and more axons in thick nerve bundles than at P10. VAChT-positive axons contributed to perivascular plexuses around many blood vessels. The innervation of blood vessels was mostly moderate in density but a few blood vessels were more heavily supplied by VAChT-immunoreactive axons (Figure 4.11A). The numbers of thick nerve bundles in P14 uterine horns was similar to P10 and there were some thick nerve bundles that contained moderate numbers of

VAChT-immunoreactive axons. In two rats, a few thick nerve bundles contained many VAChT-immunoreactive axons. VAChT-positive axons in the myometrium consisted mostly of axons associated with blood vessels and axons in thick nerve bundles. In the middle and ovarian segments from one rat, there were a few VAChT-positive axons in the linea uteri (Figure 4.11C). There were no VAChT-immunoreactive axons in the linea uteri in all other rats examined at P14. In the cervical region of the rat with the higher innervation density, there were a few VAChT-immunoreactive axons in the circular muscle but they did not have the arrangement of axons in the CMP (Figure 4.11B). Rare VAChT-immunoreactive axons were present in the endometrium at P14. There were a few areas in the P14 uterus that lacked VAChT innervation; these areas were less common compared to the earlier post-partum time points and more common on the anti-mesometrial than the mesometrial side.

VAChT-immunoreactive axons in the P14 uterus still showed growth cones but there were fewer axons with growth cones than at earlier post-partum time points (Figure 4.11D&E). Growth cones were simple and present on perivascular axons.

4.2.1.12 Post-partum day 28 (P28) : Figure 4.12

The density of uterine VAChT innervation at P28 was higher than at P14 but still lower than in the non-pregnant uterus at oestrus. VAChT immunostaining in the ovarian end of all three rats examined was sparse, probably because of poor staining in the ovarian end by the anti-VAChT antibody. The cervical region (Figure 4.12A) was more densely innervated by VAChT-immunoreactive axons than the middle region (Figure 4.12B).

FIGURE 4.12: VACHT-IMMUNOREACTIVE INNERVATION OF THE POST-PARTUM RAT UTERUS AT P28

A, In the cervical regions of a P28 uterine horn, many VAChT-immunoreactive axons enter at the mesometrium (left of micrograph) and provide a dense innervation to Blood vessels as well as innervating the myometrium B, In the middle region of a P28 horn, fewer VAChT-immunoreactive axons enter at the mesometrium (right of the micrograph). C, A blood vessel is surrounded by a dense plexus of perivascular VAChT-immunoreactive axons. D, A thick nerve bundle containing many VAChT-immunoreactive axons in the cervical region of a P28 uterine horn. E & F, Growth cones on VAChT-immunoreactive axons.

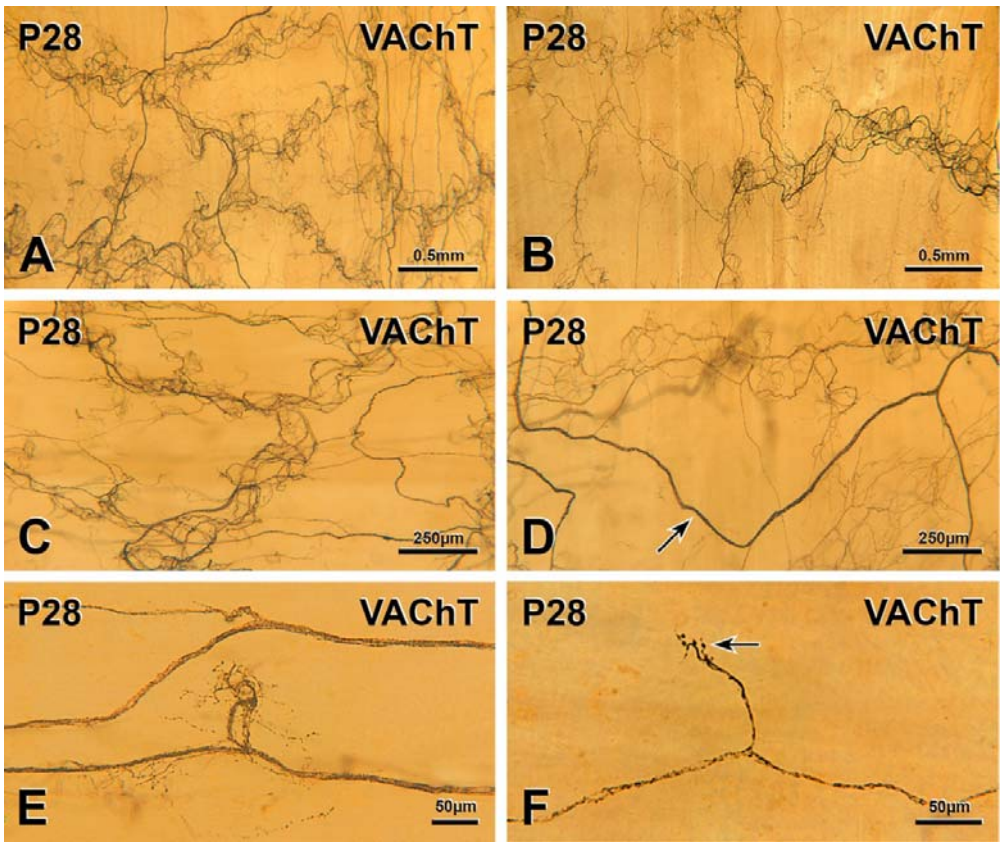
P28
VAChT
A
0.5mm
P28
VAChT
B
0.5mm
P28
VAChT
C
250µm
P28
VAChT
D
250µm
P28
VAChT
E
50µm
P28
VAChT
F
50µm

At P28, many VAChT-immunoreactive axons entered the uterus along with blood vessels, in thick nerve bundles or occasionally as single axons. Many blood vessels were innervated in the P28 uterus, with the density of their perivascular innervation being moderate to sometimes significant (Figure 4.12C). Thick nerve bundles containing many VAChT-positive axons were present throughout the P28 uterus (Figure 4.12D). Apart from one small portion in the middle of the uterine horn from one rat, the linea uteri did not receive any VAChT-immunoreactive axons. In one part of the cervical end of the horn from another rat, a few VAChT-positive axons lay near the bottom of the circular muscle layer and were arranged in a fashion similar to the CMP. Only a few VAChT-immunoreactive axons travelled from the myometrium to the endometrium and terminated there but none were observed close to glands. Areas without innervation were rare in the P28 uterus. These rare areas were mostly in the anti-mesometrial side.

Although rare, growth cones were present on VAChT-immunoreactive axons in the P28 uterus (Figure 4.12E&F). Growth cones were simple and present on axons in thick nerve bundles or axons associated with blood vessels.

4.2.2 Quantification of VAChT-immunoreactive axons in the pregnant and post-partum uterus

Four rats from each time point immunostained for VAChT were used for quantification of VAChT-immunoreactive axons. The sample of tissue in which innervation density was quantified at each time point was similar to that described in Section 3.2.3. Five squares were counted from each rat; the total number of squares counted at each time point was therefore 20.

TABLE 4.1: QUANTIFICATION OF PARASYMPATHETIC INNERVATION DENSITY BY POISSON REGRESSION ANALYSIS.

Time point	Average intersections	Incidence Rate Ratio (%)	95% Confidence Interval	P value	% innervation at OEST
OEST	286.2	Reference	-	-	
E14	54.45	11.24	3.66 – 34.57	<0.001	19.03
E16	73.75	15.26	4.97 – 46.84	0.001	25.77
E18	5.05	0.55	0.17 – 1.76	<0.001	1.76
E20	5.85	0.50	0.16 – 1.62	<0.001	2.04
P1	5.70	1.03	0.33 – 3.22	<0.001	1.99
P3	28.30	8.21	2.65 – 25.46	<0.001	9.89
P5	66.50	44.62	14.53 – 136.97	0.158	23.24
P7	91.95	62.56	20.38 – 192.00	0.412	32.13
P10	136.50	147.30	48.01 – 45.19	0.498	47.69
P14	200.10	186.88	60.92 – 573.25	0.274	69.92
P28	182.55	125.66	40.97 – 385.44	0.690	63.78

Incidence Rate Ratio is a relative measure of the effect of a particular time point on the number of intersections generated by STATA during Poisson Regression Analysis. Oestrus was considered the reference; therefore IRR=100%.

FIGURE 4.13: DENSITY OF PARASYMPATHETIC INNERVATION DURING PREGNANCY AND POST-PARTUM

The graph shows the difference in parasympathetic innervation density in uterine horns from non-pregnant rats (OEST), rats on pregnancy day 14 (E14), 16 (E16), 18 (E18) and 20 (E20) and rats on post-partum days 1 (P1), 3 (P3), 5 (P5), 7 (P7), 10 (P10), 14 (P14) and 28 (P28) uterine horns.

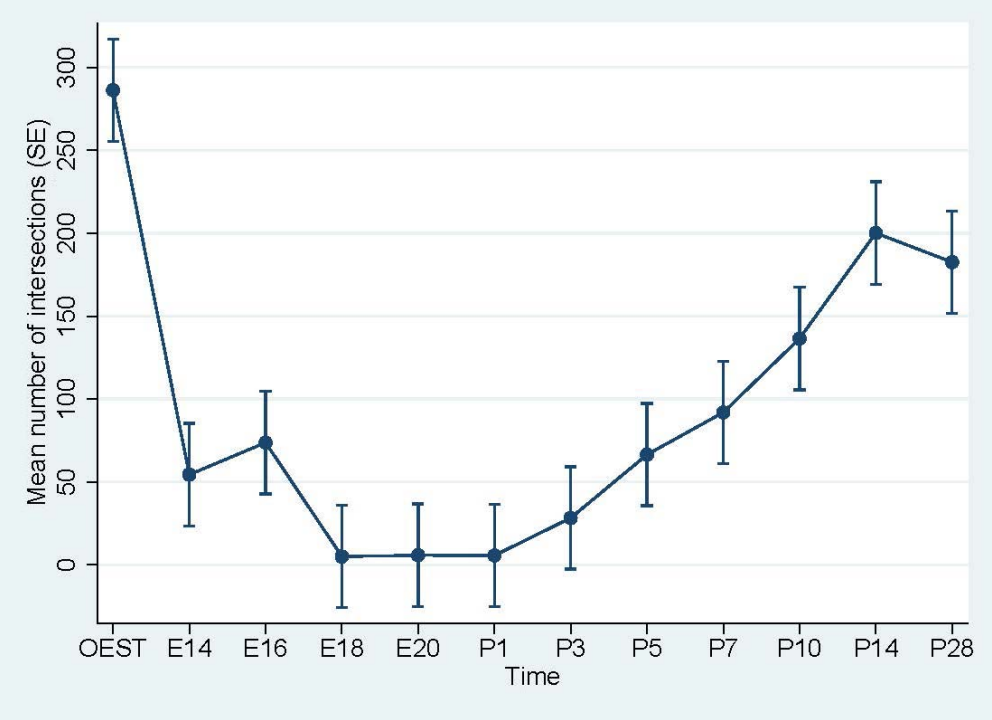
Mean number of intersections (SE)
0
50
100
150
200
250
300
OEST
E14
E16
E18
E20
P1
P3
P5
P7
P10
P14
P28
Time

Innervation was assessed at twelve time points in total: oestrus (OEST), E14, E16, E18, E20, P1, P3, P5, P7, P10, P14 and P28.

Section 2.4.5.2 in Chapter 2 contains a detailed description of the procedure for quantification. Poisson Regression Analysis was performed by Dr Shahid Ullah, Flinders Centre for Epidemiology and Biostatistics, Flinders University, and took into account the differences in the total number of squares in the locating grid for each uterine horn.

The data from the Poisson Regression Analysis are summarized in Table 4.1 and graphed in Figure 4.13. As mentioned in Chapters 2 & 3, Incidence Rate Ratio (IRR) is a relative measure of the effect of a particular time point on the number of intersections. STATA generates IRR when Poisson Regression Analysis is performed. Oestrus is the reference time point and therefore considered as 100% IRR. During pregnancy, the parasympathetic innervation density was massively reduced as evidenced by an IRR of 11.24% at E14, 15.24% at E16, 0.55% at E18 and 0.50% at E20. Compared to oestrus, there were statistically significant differences in the parasympathetic innervation density at all time points during pregnancy, i.e., E14, E16, E18 and E20. By P1, the IRR for parasympathetic innervation density had increased to 1.03% and there was a statistically significant difference in IRRs between oestrus and P1 and P3. However, the IRRs for axonal intersections at P5, P7, P10, P14 and P28 were not statistically different from the IRR at oestrus. The IRRs for P10, P14 and P28 were 147.30%, 186.88% and 125.66%, respectively, of the IRR at oestrus. However, examining the entirety of uterine horns immunostained for VAChT from these time points made it clear that parasympathetic innervation had not still returned to the non-pregnant state and was very far from being denser than at oestrus. For example, linea uteri were not completely re-innervated by P5, P7,

P10, P14 or P28. At all of these time points, the CMP was generally absent and growth cones were still present. As mentioned in Chapter 3, it is likely that low sample size and the high degree of variability in innervation density between different regions within the same uterine horn probably contributed to these unexpected results for statistical comparisons of IRRs. Another problem for the statistical analysis was that the overall density of VAChT innervation varied among rats at each time point. For example, at P14, one of the rats had a markedly higher innervation density compared to the other three rats. This variability may be why the IRR for P14 was higher than the IRR for P28. The P14 rat with the higher innervation density had one or two placental attachments less than the other P14 rats and this could be the reason for the higher innervation density. It was not possible to estimate the number of pups in the P28 uterus as some of these rats had had multiple pregnancies. Using the quantitative data we now have, we have estimated that we would have to count intersections in 270 squares per time point to generate statistically significant results. Again, because the amount of time required to count axonal intersections in one square from an area with high innervation density was at least an hour, counting 270 squares per time point, with a total of 270 squares for each marker, was beyond the scope of this project.

4.3 SUMMARY & DISCUSSION

Similar to the changes found for innervation of the uterus by TH-immunoreactive axons in Chapter 3, VAChT-immunoreactive axons also decreased as pregnancy progressed and increased progressively after delivery. The innervation density was lowest at E20 and highest at oestrus. Growth cones were abundant on VAChT-immunoreactive axons in early post-partum uterine horns, particularly at P3 and P5.

Re-innervation of the linea uteri was variable. At P28, the uterus was significantly innervated by VAChT immunoreactive axons but the density of VAChT innervation was still lower than in the non-pregnant uterus at oestrus.

There was a statistically significant difference in the parasympathetic innervation density between oestrus and E14, E16, E18, E20, P1 and P3. While there were no statistically significant differences between oestrus and the rest of the post-partum time points, i.e., P7, P10, P14 and P28, the microscopic analysis described in Section 4.1 clearly showed that the density of uterine innervation supplied by VAChT-immunoreactive axons had not returned to or exceeded normal levels. VAChT innervation of rat uterine horns gradually increased from almost nothing at E20 to about 50% of normal at P28. Hence, the re-innervation of the rat uterus by VAChT-immunoreactive axons was not complete even as late as 28 days post-partum.

Chapter 5

Changes in sensory innervation of the rat uterus during pregnancy and post-partum

5.1 INTRODUCTION

As detailed in Chapter 1, the uterus of the non-pregnant rat receives a significant sensory innervation. Many sensory nerves identified by immunoreactivity for calcitonin gene related peptide (CGRP) and substance P (SP) occur in all layers of the non-pregnant rat uterus (Gnanamanickam and Llewellyn-Smith, 2011; Shew et al., 1990; Shew et al., 1991). The linea uteri, a thick band of longitudinal muscle opposite the mesometrium, receives more sensory nerves than the rest of the uterine smooth muscle (Gnanamanickam and Llewellyn-Smith, 2011). Blood vessels are surrounded by many sensory axons and there are also many CGRP- and SP-immunoreactive axons deep in the endometrium, often lying close to uterine glands (Gnanamanickam and Llewellyn-Smith, 2011; Shew et al., 1991). However, very little is known about how uterine sensory innervation changes during pregnancy and post-partum. The aim of this chapter was to fill these gaps in knowledge by determining the distribution of CGRP-immunoreactive axons in whole mount preparations of rat uterine horns between day 14 of pregnancy (E14) and post-partum day 28 (P28) and to quantify how the density of sensory innervation changes during this period. The only neurochemical marker chosen to study sensory innervation is CGRP because in the rat uterus all CGRP-containing nerves also contain SP but not all SP-containing nerves contain CGRP (Shew et al., 1991).

5.2 RESULTS

Uterine horns were examined for their CGRP innervation at the same time points as in Chapters 3 and 4, i.e., oestrus, pregnancy (E) days E14, E16, E18 and E20 and post-partum (P) days P1, P3, P5, P7, P10, P14 and P28.

5.2.1 Changes in uterine sensory innervation revealed by immunostaining for CGRP

5.2.1.1 Oestrus : Figure 5.1

I have published a description of the sensory innervation of the rat uterus at oestrus (Gnanamanickam and Llewellyn-Smith, 2011) based on immunostaining for CGRP in whole mount preparations similar to those used here (Llewellyn-Smith and Gnanamanickam, 2011). In summary, rat uterine horns at oestrus are significantly innervated by CGRP-immunoreactive axons. CGRP-positive axons are present in every layer of the uterus, including the longitudinal and circular muscle layers (Figures 5.1A&B), the linea uteri and the endometrium. At oestrus, the linea uteri has more CGRP-immunoreactive axons than the rest of the longitudinal smooth muscle (Figure 5.1A). CGRP-immunoreactive axons are also present deep in the endometrium close to uterine glands and contribute to the perivascular plexuses around blood vessels (Figure 5.1B).

5.2.1.2 Pregnancy Day 14 (E14) : Figure 5.2

Compared to innervation density at oestrus, the E14 uterus received many fewer CGRP-immunoreactive axons. Overall, E14 uterine horns had only a few CGRP-immunoreactive axons (Figure 5.2B).

FIGURE 5.1: CGRP-IMMUNOREACTIVE INNERVATION OF THE NON-PREGNANT RAT UTERUS AT OESTRUS

A and B show different focal planes through a rat uterine horn at oestrus. A, CGRP-immunoreactive axons innervate blood vessels (BV) and the linea uteri (LU). B, CGRP-immunoreactive axons at the bottom of the circular muscle layer form the circular muscle plexus (CMP). Note that the CMP is not present under the linea uteri. Some CGRP-positive axons surround blood vessels.

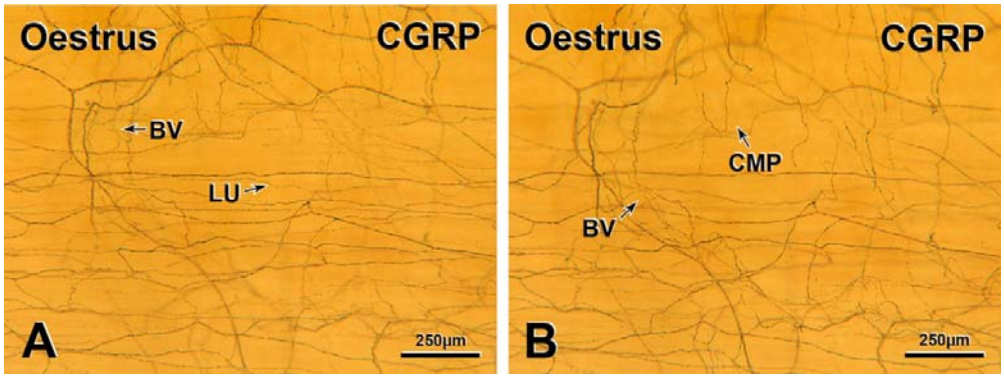
Oestrus
CGRP
BV
LU
A
250µm
Oestrus
CGRP
CMP
BV
B
250µm

FIGURE 5.2: CGRP-IMMUNOREACTIVE INNERVATION OF THE PREGNANT RAT UTERUS AT E14

A, Whole mount preparations of strips from the middle and cervical segments of an E14 uterine horn. Letters indicate the location of the micrographs in B-F. B, Sparse CGRP innervation of an E14 uterine horn. C, A few CGRP-immunoreactive axons run alongside a blood vessel. D, CGRP-immunoreactive axons in the circular muscle layer. E, A degenerating CGRP-immunoreactive axon that is fragmenting. F, An area in an E14 uterine horn that is devoid of CGRP innervation.

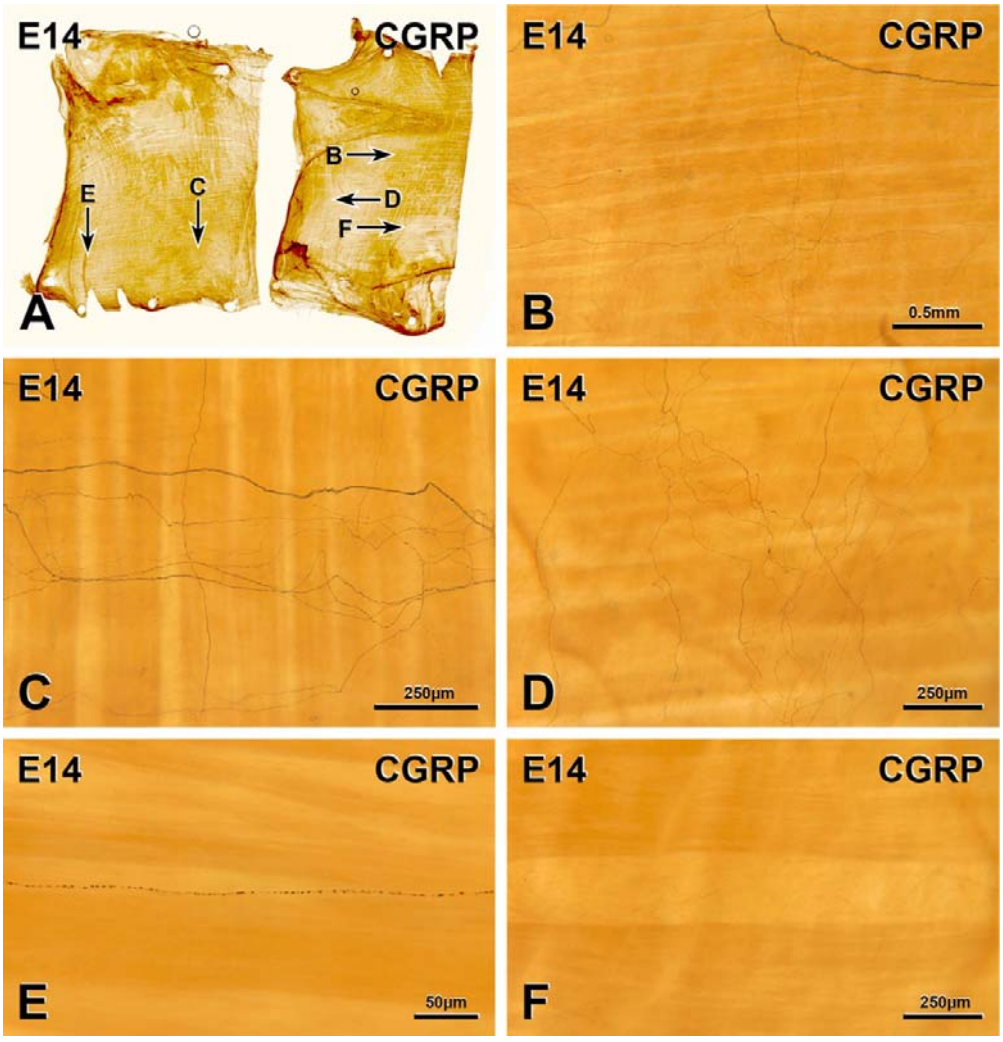
E14
CGRP
A
B
C
D
E
F
E14
CGRP
B
0.5mm
E14
CGRP
C
250µm
E14
CGRP
D
250µm
E14
CGRP
E
50µm
E14
CGRP
F
250µm

The ovarian-most end of E14 uterine horns showed the most CGRP-positive axons in all layers, followed by the cervical segment. CGRP-immunoreactive axons were fewest in the middle segment of uterine horns. At E14; the density of CGRP innervation varied among rats, with some rats having somewhat more CGRP-positive axons around blood vessels and in the myometrium than other rats.

At E14, CGRP-immunoreactive axons entered the uterus singly or associated with blood vessels or in thick nerve bundles. The number of CGRP-positive axons entering E14 uterine horns was much lower than at oestrus. In general, few blood vessels within the uterus were innervated and each innervated blood vessel was surrounded by only a few CGRP-immunoreactive axons (Figure 5.2C). The density of perivascular CGRP-positive axons was lowest in the middle portion of E14 uterine horns. Rare blood vessels near the ovarian-most ends of uterine horns received more CGRP-immunoreactive axons in some rats; some of these blood vessels had an innervation density similar to that at oestrus. All regions of the uterus contained some blood vessels that were not innervated. At E14, there were rare thick nerve bundles containing very few CGRP-immunoreactive axons in the myometrium of ovarian, middle and cervical segments of uterine horns. In the longitudinal muscle layer of the myometrium at E14, innervation density was much lower than at oestrus, with few CGRP-immunoreactive axons that ran parallel to the smooth muscle cells. In one part of the ovarian segment in one rat, there were many longitudinal CGRP-positive axons grouped together as occurs in linea uteri in non-pregnant rats. However, in all other E14 rats, linea uteri were not distinguishable because there were no areas within the longitudinal muscle layer showing a higher density of CGRP-immunoreactive axons. Compared to the CGRP innervation of the circular smooth muscle at oestrus, the innervation at E14 was much lower, with few CGRP-

immunoreactive axons occurring amongst circular smooth muscle cells (Figure 5.2D). However, in one rat, the number of axons in the circular muscle was a little higher at the ovarian-most end. On some occasions, CGRP-immunoreactive axons branched from a blood vessel in the longitudinal smooth muscle to the circular smooth muscle before returning to join the blood vessel. In the endometrium of E14 uterine horns, the number of CGRP-immunoreactive axons was much lower than at oestrus. On rare occasions, a CGRP-immunoreactive axon associated with a blood vessel left it and travelled from the muscle into the endometrium.

E14 uterine horns contained CGRP-immunoreactive axons that were fragmenting and swollen, morphological features that are indicative of degeneration (Klukovits et al., 2002; Sporrong et al., 1981). Fragmenting axons were common in all regions of E14 uterine horns (Figure 5.2E), suggesting that CGRP innervation was disappearing throughout the uterus. Swollen CGRP axons were less common in the E14 uterus. There were areas within E14 horns that lacked any CGRP-immunoreactive axons (Figure 5.2F). Areas without CGRP innervation were present across all regions of the uterus (i.e., ovarian, middle, cervical segments as well as mesometrial and anti-mesometrial sides). However, denervated areas were more common on the anti-mesometrial side, the side opposite to where axons enter the uterus. In contrast, all regions of the non-pregnant rat uterus at oestrus contained CGRP innervation and areas without innervation were never found.

FIGURE 5.3: CGRP-IMMUNOREACTIVE INNERVATION OF THE PREGNANT RAT UTERUS AT E16

A, Sparse CGRP innervation on the mesometrial side in the middle region of an E16 uterine horn. B, in the cervical region of an E16 uterine horn, a few CGRP-immunoreactive run near a blood vessel (BV) but do not innervate it. C, A blood vessel (BV) lacks CGRP innervation; although CGRP-immunoreactive axons travel nearby. D, An area lacking CGRP innervation on the anti-mesometrial side of the middle region from an E16 horn. E & F, Degenerating CGRP-immunoreactive axons that run near blood vessels (BV) are fragmenting.

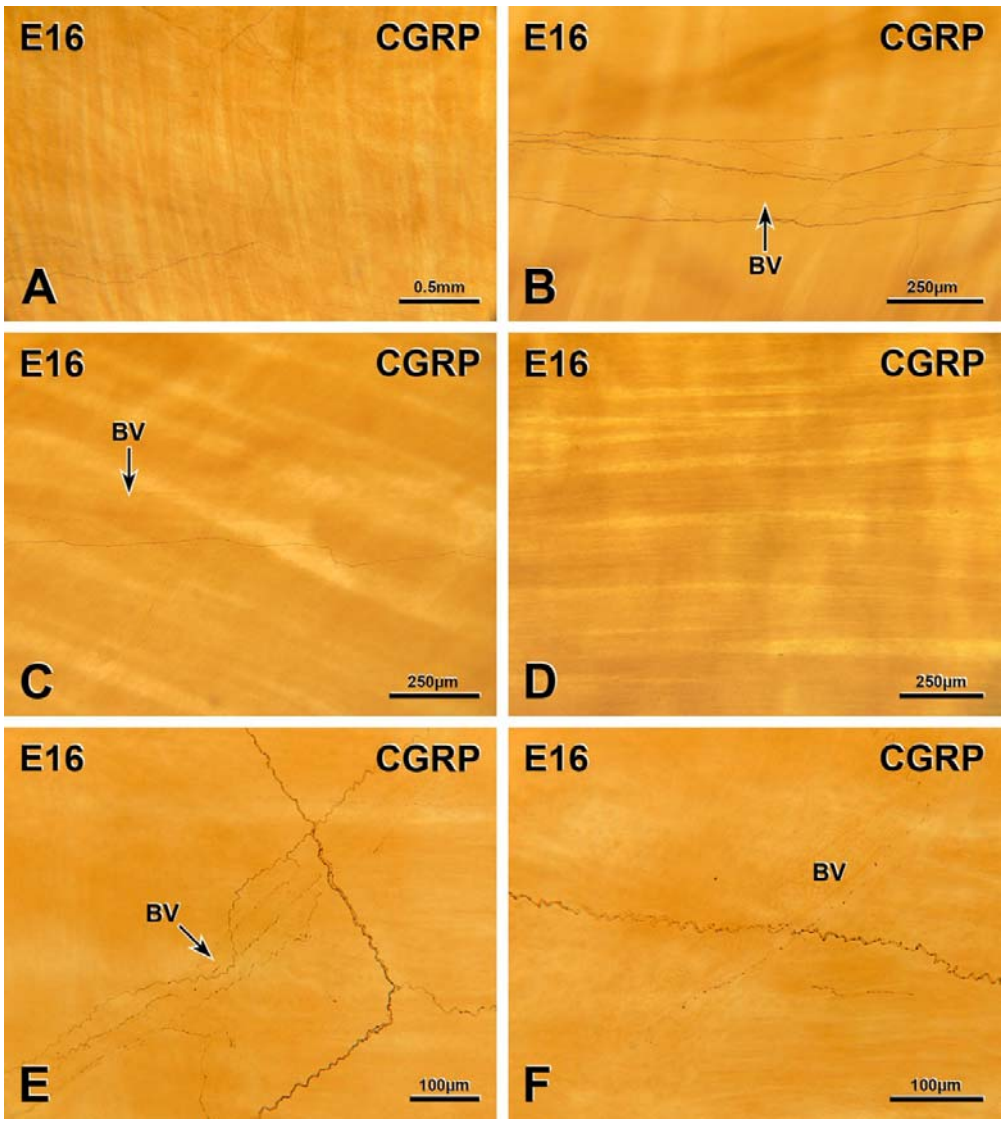
E16
CGRP
A
0.5mm
E16
CGRP
BV
B
250µm
E16
CGRP
BV
C
250µm
E16
CGRP
D
250µm
E16
CGRP
BV
E
100µm
E16
CGRP
BV
F
100µm

5.2.1.3 Pregnancy day 16 (E16) : Figure 5.3

At E16, uterine horns had fewer CGRP-immunoreactive axons than at E14. As at E14, the ovarian end was more densely innervated than the rest of the E16 uterus. In one rat, CGRP-immunoreactive innervation at the ovarian end was similar in density to that in the non-pregnant uterus at oestrus. In the middle portion of the uterus in all rats, very few CGRP-immunoreactive axons were present.

At E16, only a few CGRP-immunoreactive axons entered the uterus singly, in thick nerve bundles or associated with blood vessels. Fewer blood vessels were innervated at E16 than at E14 and these blood vessels were only sparsely innervated by CGRP-immunoreactive axons (Figure 5.3B). Many blood vessels, particularly in the middle segments of E16 uterine horns, had no CGRP innervation (Figure 5.3C). Some thick nerve bundles were present throughout the uterus and some travelled from the mesometrial side all the way to the anti-mesometrial side. Few CGRP-immunoreactive axons were present in these thick nerve bundles. CGRP-positive axons were also present in the myometrium at E16. A few axons occurred in the longitudinal and circular muscle layers and their numbers were slightly lower than at E14. Few CGRP-immunoreactive axons were present in the endometrium. On rare occasions, a CGRP-positive axon left a myometrial blood vessel to travel to the endometrium, where it terminated. Like in the E14 uterus, there were areas in the E16 uterus without any CGRP innervation (Figure 5.3D). Areas lacking innervation were more common at E16 than at E14. These areas were present across the uterus and slightly more common in the anti-mesometrial side compared to the mesometrial side.

Degenerating, fragmented CGRP-immunoreactive axons were common in all regions of E16 uterine horns (Figure 5.3E&F). Degenerating CGRP axons with a swollen appearance were rarely present.

5.2.1.4 Pregnancy day 18 (E18) : Figure 5.4

E18 uterine horns were much less innervated by CGRP-immunoreactive axons than E14 or E16 horns. The density of CGRP innervation was similar in the ovarian and cervical segments of E18 uterine horns and there was less innervation in middle segments.

A few CGRP-immunoreactive axons entered the uterus at the mesometrium, either individually or in thick nerve bundles. Nerve bundles running alongside blood vessels contained CGRP-immunoreactive axons but the blood vessels themselves were not surrounded by perivascular plexuses of CGRP-positive axons (Figure 5.4B). Many blood vessels were completely lacking in innervation and also did not have CGRP-immunoreactive axons running alongside them. Rare thick nerve bundles contained fewer CGRP-positive axons at E18 and they were fewer of these bundles than at E16. Very few CGRP-immunoreactive axons were present in the longitudinal and circular muscle layers; their numbers were lower than at E16. Most of the remaining CGRP-immunoreactive axons were present in the myometrium. There were almost no CGRP-immunoreactive axons in the endometrium. There were many areas of the E18 uterus in which CGRP-immunoreactive axons were absent (Figure 5.4E); these areas lacking innervation were more common on the anti-mesometrial side.

Fragmented, degenerating axons were present in all regions of the E18 uterus (Figure 5.4C&D) whereas swollen CGRP-positive axons were rare.

FIGURE 5.4: CGRP-IMMUNOREACTIVE INNERVATION OF THE PREGNANT RAT UTERUS AT E18

A, sparse CGRP innervation of an E18 uterine horn. B, CGRP-immunoreactive axons run near but do not innervate a blood vessel (BV). C & D, Degenerating CGRP-immunoreactive axons that are fragmenting and have swollen varicosities. E, An area in an E18 uterine horn that is devoid of CGRP innervation. .

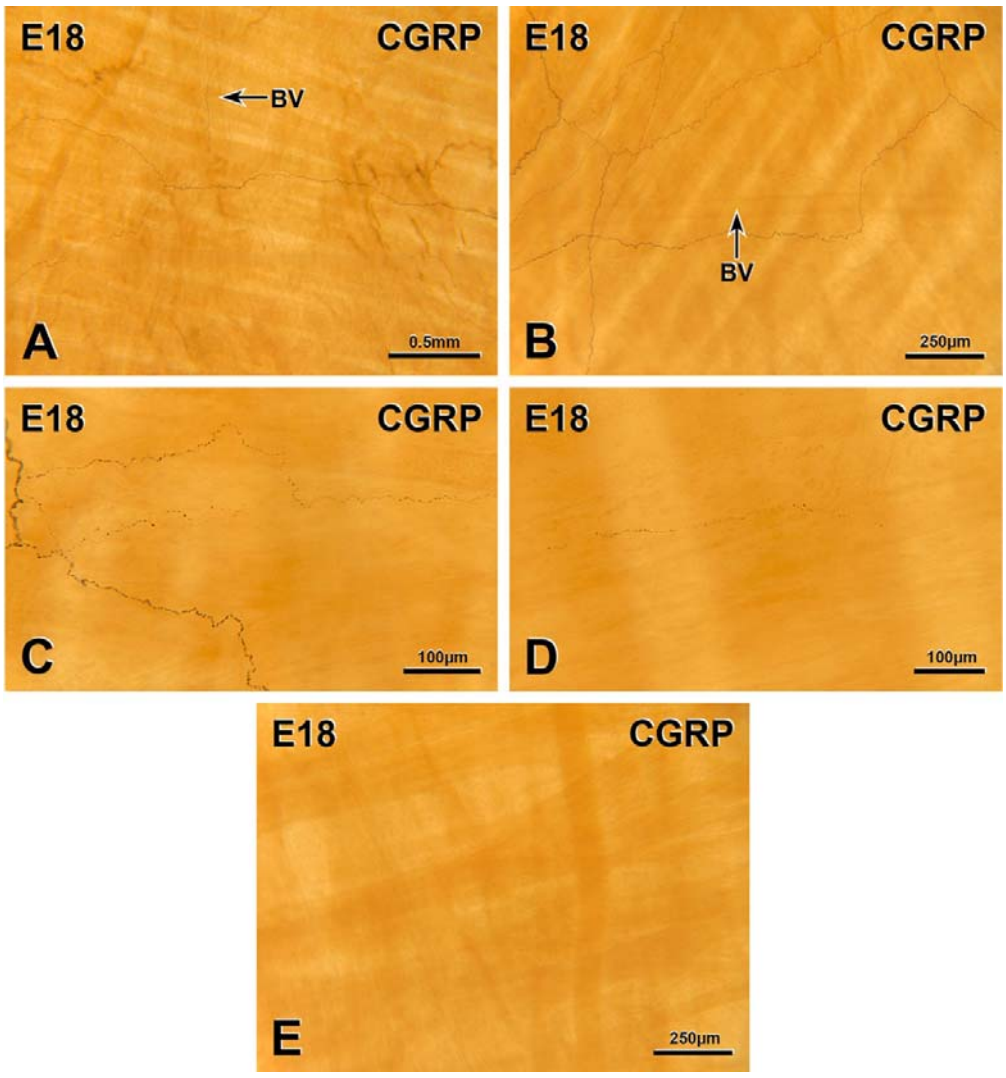
E18
CGRP
BV
A
0.5mm
E18
CGRP
BV
B
250µm
E18
CGRP
C
100µm
E18
CGRP
D
100µm
E18
CGRP
E
250µm

FIGURE 5.5: CGRP-IMMUNOREACTIVE INNERVATION OF THE PREGNANT RAT UTERUS AT E20

A, Whole mount preparation of a strip from the cervical region of a E20 uterine horn. Letters indicate the location of the micrographs shown in B-D. Bar, 5 mm. **B,** A network of varicose and non-varicose CGRP-immunoreactive axons and very small nerve bundles containing CGRP-positive axons. Bar, 250 μm. **C,** A CGRP-immunoreactive axon varies in thickness, varicosity spacing and staining intensity along its length. Bar, 100 μm. **D,** An area that contains no CGRP-positive innervation. Bar, 250 μm. **E,** Whole mount preparation of a strip from the middle region of a E20 uterine horn. Letters indicate the location of the micrographs shown in F-H. Bar, 5 mm. **F,** A wavy, looping CGRP-immunoreactive axon varies in thickness and has occasional varicosities. Bar, 100 μm. **G,** A CGRP-immunoreactive axon varies in thickness and runs close to a blood vessel. Bar, 100 μm. **H,** An area that contains no CGRP-positive innervation from the middle region of a pregnant horn. There are no CGRP-positive perivascular axons around two branching blood vessels (BV) that run through the area. Bar, 250 μm. **I,** Whole mount preparation of a strip from the ovarian region of a E20 uterine horn. Letters indicate the location of the micrographs shown in J and K. Bar, 5 mm. **J,** A nerve bundle branches and contains varicose and non-varicose CGRP-immunoreactive axons. Bar, 100 μm. **K**, A small nerve bundle contains CGRP-immunoreactive axons. A non-varicose CGRP-positive axon takes a crooked course near the small nerve bundle. Another branching nerve bundles with immunoreactive axons is mostly out of focus. Bar, 100 μm.

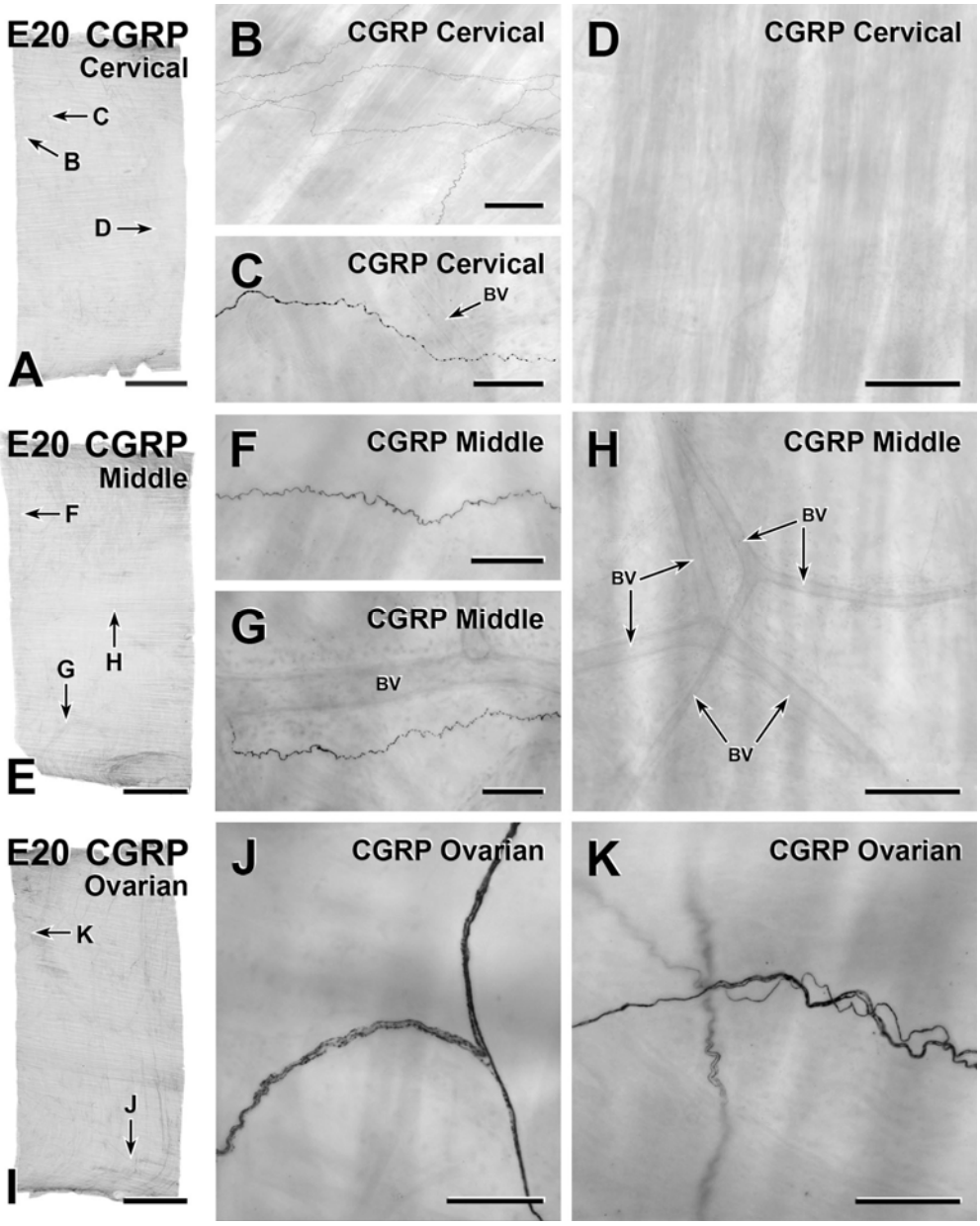
E20 CGRP
Cervical
C
B
D
A
B
CGRP Cervical
C
CGRP Cervical
BV
D
CGRP Cervical
E20 CGRP
Middle
F
G
H
E
F
CGRP Middle
G
CGRP Middle
BV
H
CGRP Middle
BV
BV
BV
E20 CGRP
Ovarian
K
J
I
J
CGRP Ovarian
K
CGRP Ovarian

5.2.1.5 Pregnancy day 20 (E20) : Figure 5.5

My Master's thesis described uterine sensory innervation at E20 in full thickness whole mount uterine preparations immunostained to reveal CGRP or SP (Gnanamanickam and Llewellyn-Smith, 2011). The innervation pattern for CGRP-immunoreactive axons found here was the same as described in my Master's thesis. E20 uterine horns had the lowest density of CGRP innervation of any of the time points examined. Almost the entire E20 uterus was devoid of CGRP-immunoreactive axons and only very few CGRP-immunoreactive axons were present (Figure 5.5).

CGRP-positive axons entered the uterus singly and often terminated on the mesometrial side. Rare CGRP-positive axons ran close to blood vessels but did not appear to be part of the perivascular plexuses of nerves that surround blood vessels in uterine horns fixed at oestrus (Figure 5.5B&G). Very rarely, CGRP-positive axons were present on the anti-mesometrial side of the uterus.

5.2.1.6 Post-partum Day 1 (P1) : Figure 5.6

One day after delivery (P1), the uterus had more CGRP-immunoreactive axons than on the day before delivery (E20) but the overall density of innervation was still very low. There were more CGRP-immunoreactive axons on the mesometrial side compared to the anti-mesometrial side of the uterus.

Only a few CGRP-immunoreactive axons entered the uterus, either singly, associated with blood vessels or in thick nerve bundles. These CGRP-positive axons did not travel far within the uterus before terminating. Rare blood vessels had occasional CGRP-positive axons associated with them (Figure 5.6A) and the density of CGRP innervation around blood vessels decreased as the blood vessels travelled towards the anti-mesometrial side of the uterus. A few thick nerve bundles

containing some CGRP-positive axons were present throughout the length of the uterus (i.e., from the ovarian end to the cervical end) but were more common on the mesometrial side compared to the anti-mesometrial side. There were very few CGRP-immunoreactive axons in the longitudinal and circular layers of the myometrium and no CGRP-immunoreactive axons in the linea uteri. Rare CGRP-immunoreactive axons travelled from the myometrium to the endometrium, where the total population of CGRP-positive axons was minuscule. No CGRP-immunoreactive axons were observed near glands.

CGRP-immunoreactive axons with growth cones were present throughout P1 uterine horns (Figure 5.6B&C). Most of the CGRP-positive axons in the P1 uterus had growth cones, which occurred on axons in the thick nerve bundles and on CGRP-positive axons associated with blood vessels in the myometrium. Growth cones were more common on axons on the mesometrial than on the anti-mesometrial side of the uterus.

Growth cones in the P1 uterus were mostly simple but rare growth cones had a complex morphology. A growth cone with one or two sprouts was considered a simple growth cone. Growth cones with many sprouting finger-like processes were considered complex growth cones.

5.2.1.7 Post-partum Day 3 (P3) : Figure 5.7

At P3, uterine horns had more CGRP-immunoreactive axons than at P1. Ovarian ends were more densely innervated than the rest of the P3 horns and there were more CGRP-immunoreactive axons on their mesometrial than anti-mesometrial sides.

FIGURE 5.6: CGRP-IMMUNOREACTIVE INNERVATION OF THE POST-PARTUM RAT UTERUS AT P1

A, CGRP-immunoreactive axons near blood vessels (arrow) near the mesometrium in a P1 uterine horn. **B & C,** Growth cones (arrows) on CGRP-immunoreactive axons on the mesometrial side.

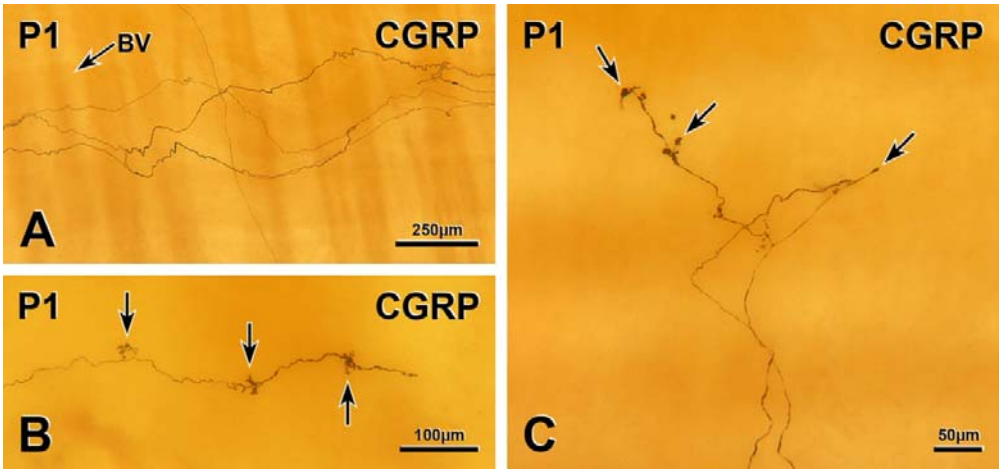
P1
BV
CGRP
A
250µm
P1
CGRP
B
100µm
P1
CGRP
C
50µm

FIGURE 5.7: CGRP-IMMUNOREACTIVE INNERVATION OF THE POST-PARTUM RAT UTERUS AT P3

A, CGRP-immunoreactive axons with growth cones (arrow) on the mesometrial side of a P3 uterine horn. **B & C,** Complex growth cones (arrows) on CGRP-immunoreactive axons close to their entry through the mesometrium.

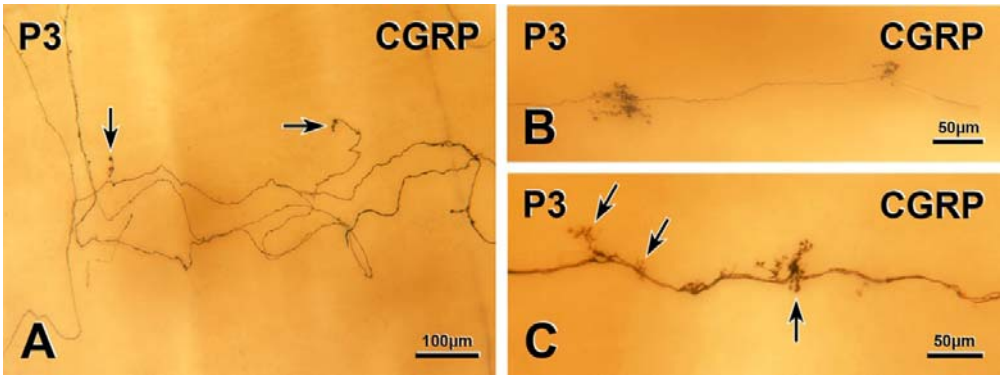
P3
CGRP
A
100µm
P3
CGRP
B
50µm
P3
CGRP
C
50µm

Some CGRP-immunoreactive axons entered the uterus through the mesometrium in the same way as at P1, i.e., either as single axons, associated with blood vessels or in thick nerve bundles. On the mesometrial side of P3 uterine horns, a few blood vessels were sparsely innervated by CGRP-immunoreactive axons (Figure 5.7A). Thick nerve bundles containing some CGRP-immunoreactive axons were present throughout the uterus. At P3, there were more CGRP-positive axons in the myometrium than at P1 and there were more CGRP-positive axons in the circular muscle layer than in the longitudinal muscle layer. Although there were no CGRP-immunoreactive axons in the linea uteri, there were CGRP-immunoreactive axons in the circular muscle layer immediately below it. Axons in the circular muscle were either single, associated with blood vessels or in thick nerve bundles. Rarely, CGRP-immunoreactive axons travelled to the endometrium from the myometrium; on one occasion, a CGRP-positive axon left a thick nerve bundle and travelled close to a gland in the endometrium and terminated with a growth cone.

Growth cones were present on many CGRP-immunoreactive axons in P3 uterine horns (Figure 5.7B&C). Axons associated with blood vessels and in thick nerve bundles in the myometrium had growth cones. There were simple and complex growth cones on many of the CGRP-positive axons that were associated with blood vessels. Many thick nerve bundles had CGRP axons with complex growth cones. Occasionally thick nerve bundles containing CGRP-immunoreactive axons with complex growth cones branching off them entered at the mesometrium. These thick nerve bundles travelled towards the anti-mesometrium and finally reduced to a single axon that terminated with a simple growth cone. Some CGRP-immunoreactive axons travelled in loops from the myometrium to the endometrium before terminating with growth cones.

5.2.1.8 Post-partum Day 5 (P5) : Figure 5.8

CGRP-immunoreactive axons were more numerous in P5 uterine horns than at earlier post-partum time points. CGRP innervation density was much higher at the ovarian most end compared to the rest of the uterus; there were also more axons on the mesometrial side compared to the anti-mesometrial side.

At P5, a few blood vessels received a sparse innervation from CGRP-immunoreactive axons; more blood vessels were innervated at P5 than at P3. Thick nerve bundles containing some CGRP-immunoreactive axons were present throughout the uterus (Figure 5.8B). CGRP-immunoreactive axons were more numerous in the circular muscle layer of P5 uterine horns whereas only a few CGRP-positive axons were present in the longitudinal muscle. In one rat, many CGRP-immunoreactive axons were present in the linea uteri in the ovarian end of the uterus but not in the middle and cervical regions. In all other rats, there were no noticeable differences in the innervation of the linea uteri compared to the rest of the longitudinal smooth muscle. Few CGRP-immunoreactive axons were present in the endometrium. Rare CGRP-immunoreactive axons that originated from around blood vessels travelled close to uterine glands.

At P5, many CGRP-immunoreactive axons ended in growth cones and axons with growth cones were distributed throughout the P5 uterus (Figure 5.8B&C). CGRP-positive axons with many complex growth cones occurred in thick nerve bundles and in association with blood vessels in the myometrium. Axons with simple growth cones were also present around blood vessels.

FIGURE 5.8: CGRP-IMMUNOREACTIVE INNERVATION OF THE POST-PARTUM RAT UTERUS AT P5

A, CGRP-immunoreactive axons entering a P5 uterine horn at the mesometrium. **B,** A thick nerve bundle near the mesometrium contains CGRP-immunoreactive axons that are giving off growth cones. C, CGRP-immunoreactive axons with complex growth cones.

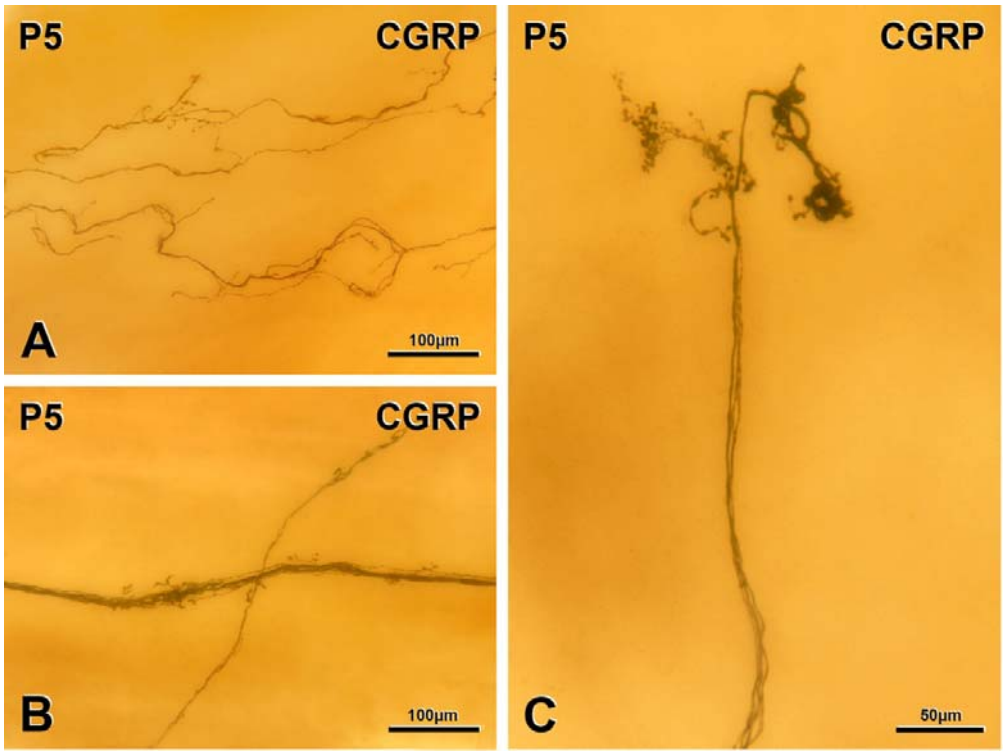
P5
CGRP
A
100µm
P5
CGRP
B
100µm
P5
CGRP
C
50µm

5.2.1.9 Post-partum Day 7 (P7) : Figure 5.9

P7 uterine horns received a heavier CGRP innervation than horns from rats at P1, P3 or P5. Again, the ovarian end contained more CGRP-immunoreactive axons than the rest of the uterus.

CGRP-positive axons entered the uterus individually, in thick nerve bundles or in association with blood vessels. The CGRP innervation of some blood vessels was low to moderate in density (Figure 5.9A). The number of blood vessels innervated was similar to P5 but there were more CGRP axons around blood vessels at P7. A few thick nerve bundles containing some CGRP-immunoreactive axons were present throughout the uterus and they entered either at the mesometrium or at the ovarian most end. Both the circular and longitudinal muscle layers of the myometrium were supplied with CGRP-immunoreactive axons at P7 but the density of innervation was slightly higher in the circular muscle layer. The myometrium in ovarian segments of P7 uterine horns was more heavily innervated by CGRP axons than the myometrium in the middle and cervical segments. In the myometrium, CGRP-immunoreactive axons were generally not associated with blood vessels and ran parallel to the smooth muscle cells of the layer in which they lay and formed a random network similar to that in the non-pregnant uterus. There were more CGRP-immunoreactive axons in the linea uteri in the ovarian segments of P7 uterine horns than in the rest of the uterine smooth muscle. A few CGRP-positive axons innervated the linea uteri of the cervical segment in only one rat. There were no CGRP-immunoreactive axons in the linea uteri in the middle region of the P7 uterus in any rats. A few CGRP axons travelled to the endometrium from the myometrium. Very rare CGRP-immunoreactive axons travelled close to uterine glands.

FIGURE 5.9: CGRP-IMMUNOREACTIVE INNERVATION OF THE POST-PARTUM RAT UTERUS AT P7

A, CGRP-immunoreactive axons enter through the mesometrium along with a blood vessel. The bifurcated axon at arrow B is shown at higher magnification in B. **B,** The bifurcated CGRP-immunoreactive axon at arrow B in A is tipped with simple growth cones. **C,** Branching CGRP-immunoreactive axons with growth cones on the mesometrial side of a P7 uterine horn. **D,** A CGRP-immunoreactive axon with growth cones near its entry through the mesometrium.

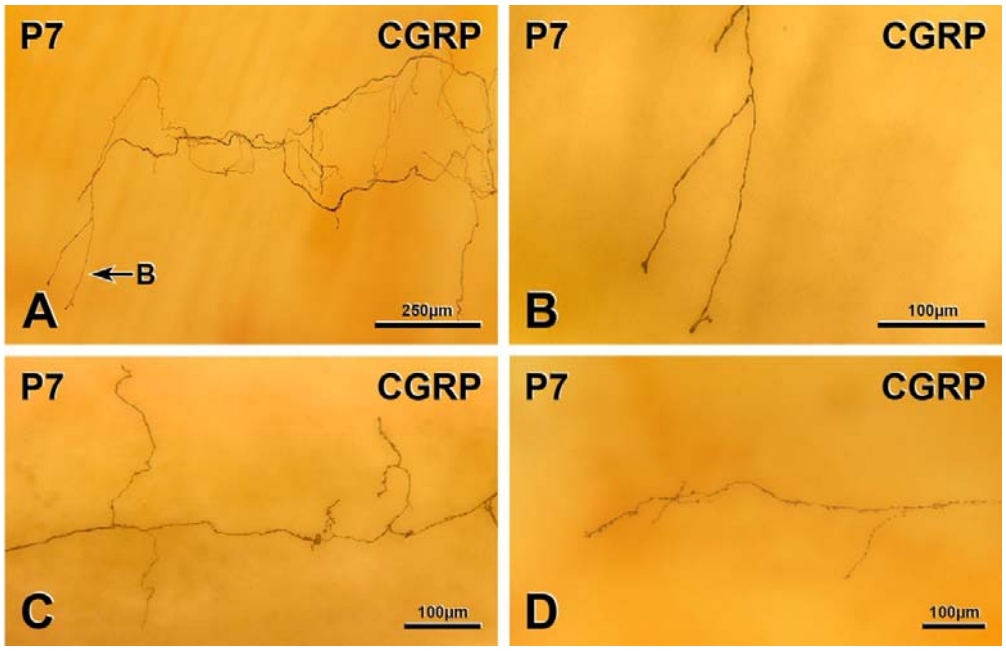
P7
CGRP
B
A
250µm
P7
CGRP
B
100µm
P7
CGRP
C
100µm
P7
CGRP
D
100µm

FIGURE 5.10: CGRP-IMMUNOREACTIVE INNERVATION OF THE POST-PARTUM RAT UTERUS AT P10

A, The ovarian-most end of a P10 uterine horn is supplied by many CGRP-immunoreactive axons, which occur around blood vessels and in the linea uteri. **B,** An area in the middle region of a P10 uterine horn receives less CGRP innervation. **C,** Another area in the middle region of a P10 uterine horn has even less CGRP innervation than the region shown in B.

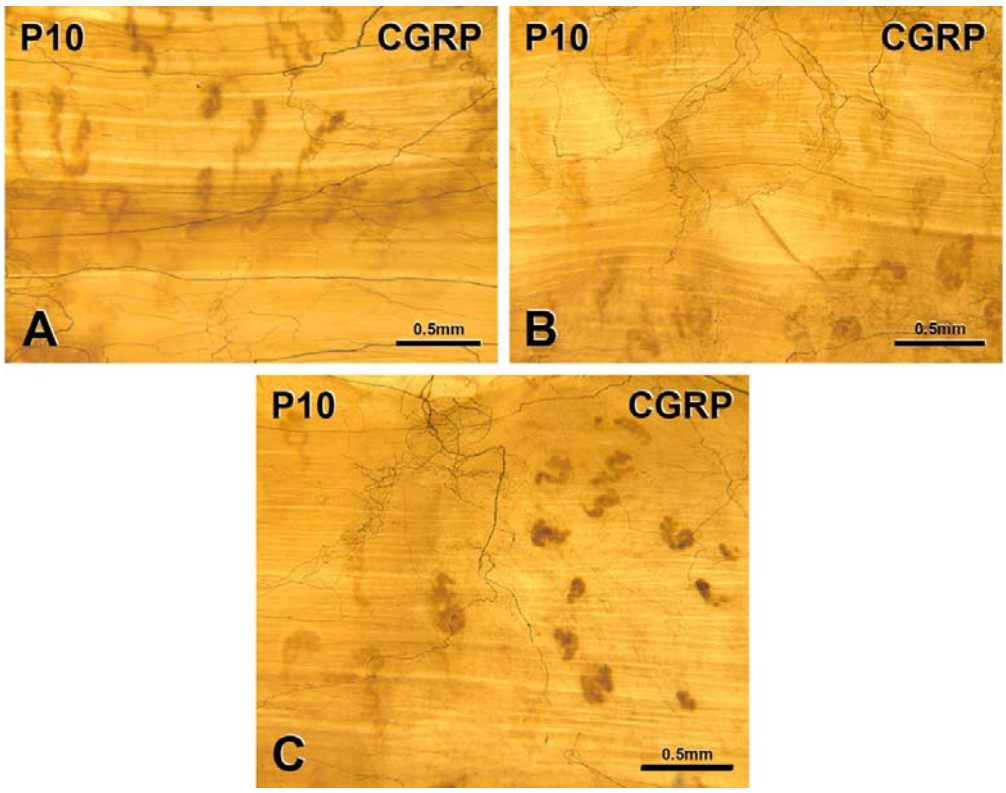
P10
CGRP
A
0.5mm
P10
CGRP
B
0.5mm
P10
CGRP
C
0.5mm

FIGURE 5.11: CGRP-IMMUNOREACTIVE INNERVATION OF THE POST-PARTUM RAT UTERUS AT P10

A, CGRP-immunoreactive axons entering the uterus surround a blood vessel. B, in the mesometrial region of a P10 uterine horn, CGRP-immunoreactive axons in a nerve bundle give rise to growth cones (arrows). C, A CGRP-immunoreactive axon bifurcates and gives rise to growth cones.

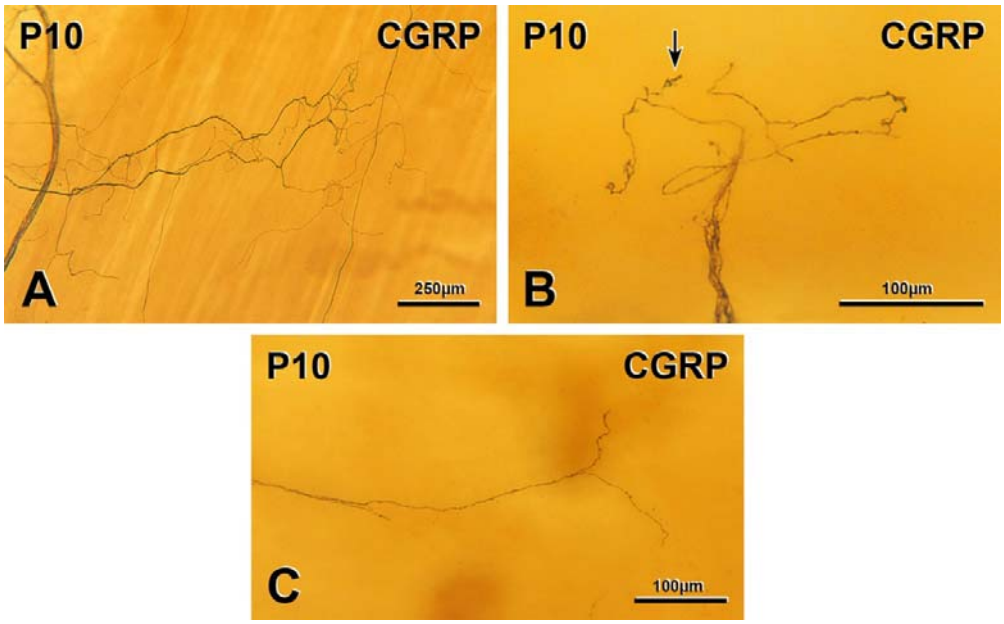
P10
CGRP
A
250µm
P10
CGRP
B
100µm
P10
CGRP
C
100µm

Growth cones were present on CGRP-immunoreactive axons in P7 uterine horns but there were fewer axons with growth cones at P7 than at P5 (Figure 5.9C&D). Growth cones occurred on axons associated with blood vessels and on axons in thick nerve bundles in the myometrium. Some axons associated with blood vessels had a few simple and complex growth cones. There were a few CGRP-positive axons in thick nerve bundles that had growth cones, which were usually complex.

5.2.1.10 Post-partum Day 10 (P10) : Figures 5.10&5.11

The P10 uterus was more heavily innervated by CGRP-immunoreactive than the P7 uterus and there were more CGRP-positive axon in the ovarian segment than in the rest of the uterus (Figure 5.10A).

Many CGRP-immunoreactive axons entered the uterus as single axons, in thick nerve bundles or in association with blood vessels. More blood vessels were innervated by CGRP-immunoreactive axons at P10 than at P7 and the density of the blood vessel innervation was moderate (Figure 5.11A). A few thick nerve bundles containing some CGRP-immunoreactive axons ran across the P10 uterus. CGRP-positive axons were more numerous in some of the thick nerve bundles in the ovarian segment than in similar bundles in the middle and cervical segments. The circular muscle layer had more CGRP-immunoreactive axons than the longitudinal muscle layer. At P10, the linea uteri had more CGRP-immunoreactive axons at its ovarian end than in the rest of its length. In one rat, only a short portion of the ovarian end of the linea uteri had an increased supply of CGRP-positive axons. Generally, the innervation of the linea uteri in the middle and cervical regions of P10 uterine horns was similar although in one rat, the cervical-most end of the linea uteri had very few

CGRP-immunoreactive axons. Occasionally, CGRP-immunoreactive axons travelled from the muscle to the endometrium.

CGRP-immunoreactive axons in P10 uterine horns still exhibited growth cones but they were few in number (Figure 5.11B&C). Rare complex growth cones were present but most growth cones at P10 were simple. Growth cones occurred on CGRP-positive axons associated with blood vessels and on CGRP-positive axons in thick nerve bundles in the myometrium.

5.2.1.11 Post-partum Day 14 (P14) : Figure 5.12

At P14, the uterus was more highly innervated compared to P1, P3, P5, P7 and P10. As at the earlier post-partum time points, the ovarian most end was more densely innervated compared to the middle and cervical regions.

CGRP-immunoreactive axons took the same routes to enter the uterus as on previous post-partum days. Blood vessels also had more CGRP innervation compared to earlier in the post-partum period (Figure 5.12A). Occasionally, axons associated with a blood vessel that entered from the mesometrium left the blood vessel and joined other CGRP-immunoreactive axons from another blood vessel. A few thick nerve bundles containing some CGRP-positive axons were present throughout P14 uterine horns. Theses bundles were similar in number to those present at P10. The myometrium contained some CGRP-immunoreactive axons that were not associated with blood vessels or thick nerve bundles; most of the myometrial CGRP-positive axons were in the circular muscle layer. Aside from those in the linea uteri, very few CGRP-immunoreactive axons supplied the longitudinal muscle layer.

FIGURE 5.12: CGRP-IMMUNOREACTIVE INNERVATION OF THE POST-PARTUM RAT UTERUS AT P14

A, CGRP-immunoreactive axons near their entry point through the mesometrium along with a blood vessel. B, on the mesometrial side of a P4 uterine horn, a CGRP-immunoreactive axon that branched off a blood vessel gives off a growth cone. C, CGRP-immunoreactive axons in the linea uteri at the ovarian-most end of a P14 uterine horn. D, A CGRP-immunoreactive axon branches in the longitudinal muscle layer and gives off growth cones.

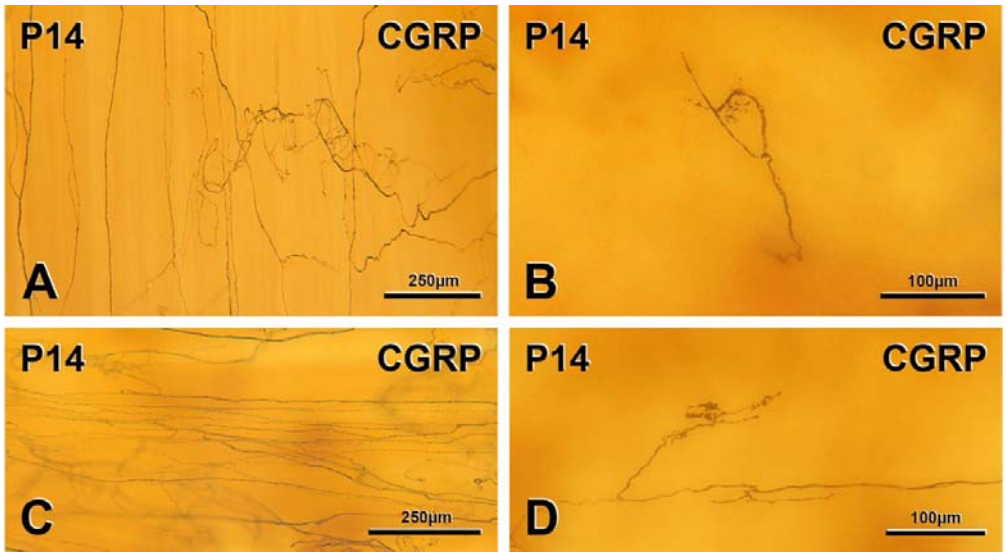
P14
CGRP
A
250µm
P14
CGRP
B
100µm
P14
CGRP
C
250µm
P14
CGRP
D
100µm

FIGURE 5.13: CGRP-IMMUNOREACTIVE INNERVATION OF THE POST-PARTUM RAT UTERUS AT P28

A, At the ovarian most end of a P28 uterine horn, CGRP innervation is dense. CGRP-immunoreactive axons occur around blood vessels and in thick nerve bundles. B, The middle region of a P28 uterine horn is less densely innervated by CGRP-immunoreactive axons L. C, A blood vessel (arrow) receives a moderate innervation from CGRP-immunoreactive axons. D, CGRP-immunoreactive axons (arrow) in the linea uteri at the ovarian end of a P28 uterine horn. E, CGRP-immunoreactive axons enter at the mesometrium. One axon terminates with a growth cone (arrow). F, A CGRP-immunoreactive axon travels deep into the endometrium close to an uterine gland.

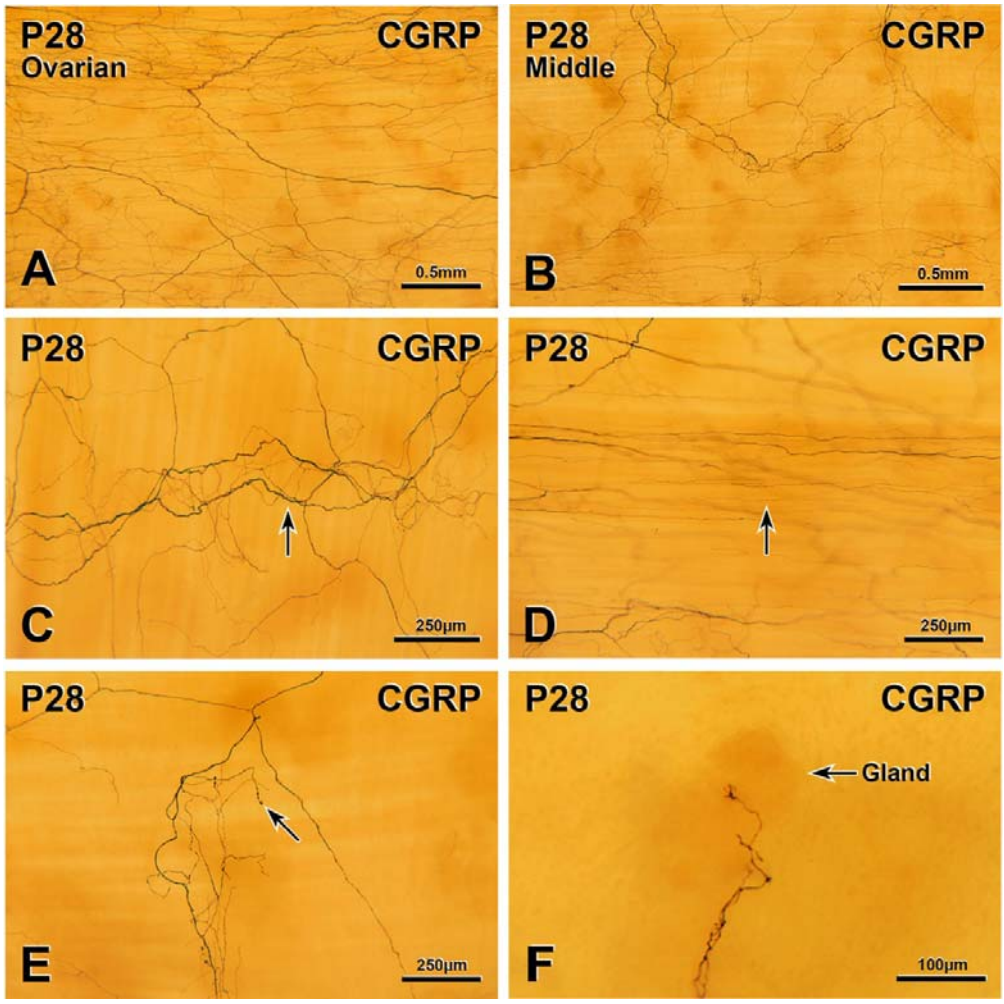
P28
Ovarian
CGRP
A
0.5mm
P28
Middle
CGRP
B
0.5mm
P28
CGRP
C
250µm
P28
CGRP
D
250µm
P28
CGRP
E
250µm
P28
CGRP
Gland
F
100µm

In three rats, the linea uteri had more CGRP-immunoreactive axons in the ovarian end compared to the rest of the uterine smooth muscle (Figure 5.12C). In two rats the innervation of the linea uteri was present in the ovarian end and in another rat, the line uteri was innervated in the cervical end. Deep in the endometrium, there were a few CGRP-immunoreactive axons that could be followed travelling from blood vessels in the myometrium.

At P14, growth cones were still present on CGRP-immunoreactive axons but they were rare and simple (Figure 5.12B&D).

5.2.1.12 Post-partum Day 28 (P28) : Figure 5.13

At P28, uterine horns contained a significant number of CGRP-immunoreactive axons. The ovarian-most end was more densely innervated by CGRP-immunoreactive axons than the middle and cervical regions (Figure 5.13A&B).

As at previous post-partum time points, many CGRP axons entered the uterus with blood vessels, in thick nerve bundles or by themselves. The number of blood vessels innervated by CGRP-immunoreactive axons was much higher than at P14. The density of CGRP innervation around blood vessels was also higher than at P14 (Figure 5.13C). Many blood vessels had a significant CGRP innervations but the density of CGRP innervation around individual blood vessels varied. Rare, sparsely innervated blood vessels were still present at P28. CGRP-immunoreactive axons associated with blood vessels often left the blood vessel and joined other axons associated with another blood vessel. Thick nerve bundles with many CGRP-immunoreactive axons were present throughout the P28 uterus. Some thick nerve bundles contained as many CGRP-immunoreactive axons as thick bundles in non-pregnant uterine horns at oestrus. Both the longitudinal and circular muscle layers of

the P28 myometrium received many CGRP-immunoreactive axons. However, the linea uteri was still only innervated by CGRP-immunoreactive axons at its ovarian-most end, where there were more CGRP-immunoreactive axons than in the rest of the uterine smooth muscle (Figure 5.13D). The innervation of the linea uteri did not differ from the rest of the myometrium in the middle and ovarian regions of P28 uterine horns. Some CGRP-immunoreactive axons were present deep in the endometrium but these rarely came close to uterine glands (Figure 5.13F). The CGRP-positive axons in the endometrium arrived there by travelling from the myometrium.

There were growth cones on rare CGRP-immunoreactive axons at P28 (Figure 5.13E).

5.2.2 Quantification of CGRP-immunoreactive axons in whole mount preparations of the uterus

CGRP-immunoreactive axons were quantified in whole mount preparations of uterine horns at all time points that were examined to provide the descriptions of innervation in Section 5.1: OEST, E14, E16, E18, E20, P1, P3, P5, P7, P10, P14, P28. Section 3.2.3 describes the sample of tissue in which TH innervation density was quantified and a similar sample of tissue was used for quantification of the density of CGRP innervation at each time point.

Poisson Regression Analyses were performed using the statistical package, STATA, by Dr. Shahid Ullah, Flinders Centre for Epidemiology and Biostatistics, Flinders University. The Incidence Rate Ratio (IRR), a relative measure of the effect of a particular time point on the number of intersections, was generated by STATA during Poisson Regression Analysis. Because the area in which intersections could

be quantified (i.e., the total number of squares in the locating grids that covered the counting areas for all four uterine horns at each time point) differed substantially between the different time points, the statistical analysis took into consideration the total number of locating grid squares in each counting area.

The results of the Poisson Regression Analysis for intersections of CGRP-immunoreactive axons with the bars of the 500μm x 500μm counting grid are summarised in Table 5.1. From an average number of intersections of 199.95 at oestrus, there was a massive decrease in intersections to 0.50 at E20. By P28, the average number of intersections had increased to 85.50.

Figure 5.13 shows the changes in the density of CGRP innervation from the non-pregnant state at oestrus (OEST) through pregnancy days 14 (E14), 16 (E16), 18 (E18), 20 (E20), and then through post-partum days 1 (P1), 3 (P3), 5 (P5), 7 (P7), 10 (P10), 14 (P14) and 28 (P28). Oestrus is the reference time point and considered as 100% IRR. As pregnancy progressed, the innervation density decreased to 15.25% at E14, 1.31% at E16, 1.37% at E18 and a very low 0.05% at E20. There were statistically significant differences in innervation density between oestrus and all time points during pregnancy. From P1 to P28, CGRP innervation density increased from 0.74% to 54.95% of that at oestrus. There were statistically significant differences in the innervation density between oestrus and the early post-partum time points, P1, P3, P5 and P7. Although the density of the CGRP innervation at P10, P14 and P28 was much lower than at oestrus, counts of intersections at these time points were not statistically significantly different from counts at oestrus.. This is probably due to the low sample size.

TABLE 5.1: POISSON REGRESSION ANALYSIS OF INTERSECTIONS OF CGRP-IMMUNOREACTIVE AXONS DURING PREGNANCY AND POST-PARTUM

Time point	Average intersections	Incidence Rate Ratio (%)	95% Confidence Interval	P value	% innervation at OEST
OEST	199.95	Reference	-	-	-
E14	67.60	15.25	3.74 – 62.17	0.009	33.81
E16	17.70	1.31	0.31 – 5.52	<0.001	8.85
E18	8.00	1.37	0.33 – 5.64	<0.001	4.00
E20	0.50	0.05	0.01 – 0.27	<0.001	0.25
P1	4.70	0.74	0.17 – 3.15	<0.001	2.35
P3	21.40	12.32	3.01 – 50.42	0.004	10.70
P5	31.70	18.62	4.56 – 76.10	0.019	15.85
P7	31.60	12.31	2.99 – 50.71	0.004	15.80
P10	52.15	44.07	10.81 – 179.72	0.253	26.08
P14	60.85	58.37	14.32 – 237.93	0.453	30.43
P28	85.50	54.95	13.49 – 223.84	0.403	42.76

Incidence Rate Ratio is a relative measure of the effect of a particular time point on the number of intersections generated by STATA during Poisson Regression Analysis. Oestrus was considered the reference; therefore IRR at oestrus =100%.

FIGURE 5.14: DENSITY OF SENSORY INNERVATION DURING PREGNANCY AND POST-PARTUM

The graph shows the density of CGRP-immunoreactive sensory innervation in uterine horns from non-pregnant rats at oestrus (OEST), rats at pregnancy days 14 (E14), 16 (E16), 18 (E18), 20 (E20), and rats at post-partum days 1 (P1), 3 (P3), 5 (P5), 7 (P7), 10 (P10), 14 (P14) and 28 (P28).

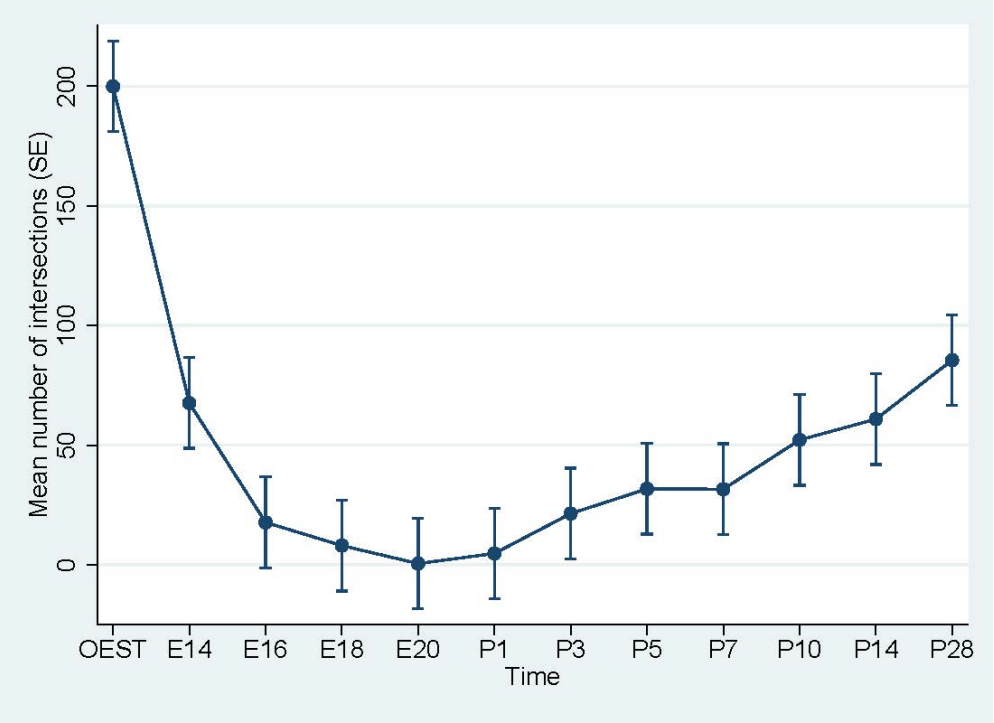
Mean number of intersections (SE)
0
50
100
150
200
OEST
E14
E16
E18
E20
P1
P3
P5
P7
P10
P14
P28
Time

Since this is the first study to quantify innervation density in whole mount preparations, we are now able to calculate the required sample size (number of grid squares to count for each rat) to achieve statistically significant results. This required sample size for sensory innervation density is 57 squares per time point. In this study, a total of 20 squares were counted at each time point. There were practical limitations to counting more squares; for example, counting one square in an area of the uterus with high innervation density took at least an hour. Therefore, counting 57 squares per time point for three different markers was more than this project could achieve. The number of CGRP intersections was also affected by variability in the density of axons between different parts of the same uterine horn as was found for horns stained for TH (see Figure 3.10). The high degree of variability in the density of CGRP innervation across each uterine horn also resulted in the large confidence intervals.

5.3 SUMMARY AND CONCLUSIONS

Sensory denervation and re-innervation of the rat uterus during pregnancy and post-partum follows the same pattern as sympathetic and parasympathetic denervation and re-innervation. The uterus gradually denervates as pregnancy progresses. The density of CGRP-immunoreactive innervation progressively decreased from 15.25% of the normal density at E14 to 0.05% of the normal density at E20. Thus, at E20, the uterus is almost completely devoid of sensory nerves. The uterus gradually re-innervates as time after delivery increases. Re-growth of CGRP-immunoreactive sensory axons is apparent on the day after delivery (P1), when the density of CGRP innervation has increased from the E20 value of 0.05% to 0.74% of normal. However, sensory re-innervation of different structures within the uterus does not

occur with the same time-course. Re-innervation of the linea uteri only began at P5. The density of CGRP-positive sensory axons in the uterus progressively increases with time after delivery. Growth cones were present on CGRP-immunoreactive axons at all the post-partum time points examined in this study. Growth cones were most numerous at P3 and P5 and rare at P14 and P28. By P28, significant re-innervation of the uterus by CGRP-immunoreactive axons had occurred Nevertheless, the density of CGRP-positive axons at P28 is only about half (54.95%) that found in the non-pregnant uterus at oestrus.

Chapter 6

Expression of microRNAs in the major pelvic ganglia during pregnancy and post-partum

6.1 INTRODUCTION

As described in Chapter 1, microRNAs (miRNAs) are a class of non-coding RNAs that are 18-22 nucleotides long (Bicker and Schratt, 2008). They regulate gene expression by degrading mRNA. MicroRNAs along with RISC complexes bind to specific base pairs in mRNA; the mRNA translation is then prevented and sometimes mRNA is degraded by nucleases in the RISC (Alberts et al., 2014a). MicroRNAs are involved in the normal functioning of the nervous system (Christensen and Schratt, 2009; Weishaupt et al., 2012) and also change in disease states (Bicker and Schratt, 2008). MicroRNAs are also important in the normal functioning of the reproductive system (Hawkins et al., 2012). Given the role of miRNAs in the regulation of gene expression, their differential expression in different diseases and their roles in nervous system and reproductive function, it is possible that miRNAs may contribute to changes in the innervation of the rat uterus during pregnancy and post-partum.

As a first step towards investigating mechanisms that might underlie innervation changes in the uterus during pregnancy and post-partum, this chapter aimed to determine if there were any alterations in the expression levels of miRNAs in the major pelvic ganglia (MPG), which is one of the main sources of sympathetic and parasympathetic innervation of the rat uterus (Owman and Stjernquist, 1988). MicroRNA expression was compared between non-pregnant rats at oestrus (OEST), late term pregnant rats at E20 and post-partum rats at P5 and P14. Total RNA from

MPGs from rats at OEST, E20 and P5 were sent for microarray analysis. Relative quantification reverse transcription polymerase chain reaction (RT-PCR) was then done to confirm the changes in miRNA expression levels that had been identified by microarray analysis. In the RT-PCR experiments, miRNAs extracted from rats at a third time point, P14, were also tested.

6.2 RESULTS

6.2.1 RNA extraction

Total RNA was extracted from individual MPGs using methods detailed in Chapter 2. Total RNA concentration and yield were quantified using a Nanodrop 8000 and quality was assessed using a Bioanalyser at the Adelaide Microarray Centre. Total RNA yield per MPG varied from 430ng to 2330ng.

6.2.2 Microarray analysis

Affymetrix miRNA v4 arrays were used for the microarray analyses, which were performed by Mark van der Hoek at the Adelaide Microarray Centre. Affymetrix miRNA v4 arrays were based on miRBase v20 and provided 5,214 mature human, rat and mouse miRNAs. The microarray results were visualized by generating a principal component analysis (PCA) plot using Partek Express software (Figure 6.1). The PCA plot shows the difference in microRNA expression between different samples within the same group and also the differences between sample groups. Expression data from each MPG is represented as a dot in three-dimensional space so they can be compared with each other. Samples with similar gene expression are expected to cluster together. In Figure 6.1, the blue dots represent miRNA samples

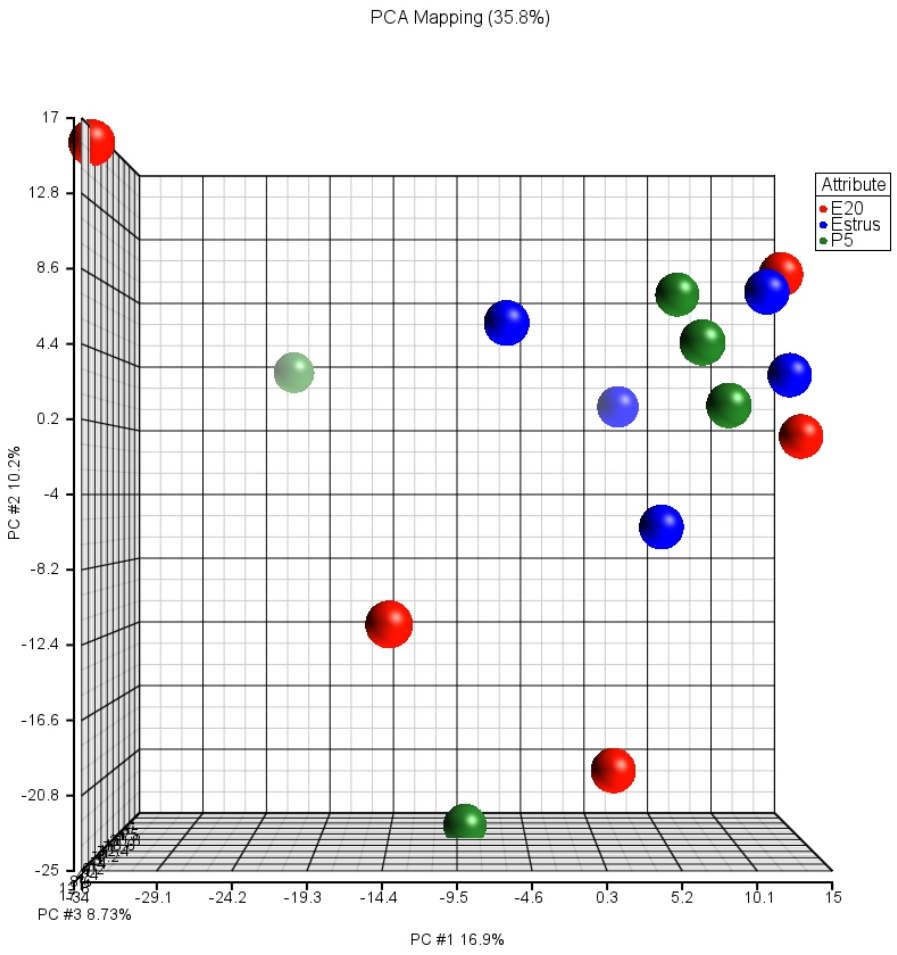

FIGURE 6.1: PRINCIPLE COMPONENT ANALYSIS

Principle component analysis (PCA) plot of microRNA expression levels in major pelvic ganglia from rats at oestrus (blue), pregnancy day 20 (E20; red) and post-partum day 5 (P5; green).

from rats at oestrus; the red dots, samples from rats at E20 and the green dots, samples from rats at P5. The samples did not cluster together, indicating that expression of miRNAs across the samples was variable. The expression of miRNAs in samples within the groups was different and also overlapped between groups. The variation in the expression of miRNAs within groups was similar to the variation between groups. This made it hard to identify differentially expressed miRNAs with this data.

Analysis of the microarray results by ANOVA showed that the expression levels of two microRNAs were reduced in MPGs from rats at P5 compared to MPGs from rats at oestrus. The two microRNAs whose expressions levels changed were miR-221-3p and miR-222-3p; the nucleotide sequences for these miRNAs are shown in Table 6.1. The reduction in expression for both miRNAs was 1.4 fold. ANOVA showed that these differences were significant at $P<0.05$. miR-221-3p and miR-222-3p had similar sequences as shown in Table 6.1. The microarray data were normalised the RMA normalisation method with mean probeset summarisation.

6.2.3 Relative Quantification Reverse Transcription PCR

The expression of the two miRNAs, miR-221-3p and miR-222-3p, was determined by relative quantification reverse transcription PCR. RNA samples extracted from one MPG from each of 8 rats at oestrus, each of 8 rats at E20, each of 8 rats at P5 and each of 8 rats at P14 were examined in the PCR analysis. Total RNA extracted from the hypothalamus of one non-pregnant rat at oestrus was used for the preparation of standard curves.

TABLE 6.1: NUCLEOTIDE SEQUENCES OF MIRNAS THAT ARE DIFFERENTIALLY EXPRESSED IN MPGS BETWEEN NON-PREGNANT RATS AT OESTRUS AND POST-PARTUM RATS AT P5

MiRNA	Sequence
rno-miR-221-3p	AGCUACAUUGUCUGCUGGGUUUC
rno-miR-222-3p	AGCUACAUCUGGCUACUGGGU

6.2.4 Housekeeping gene

Because this was the first study to examine the expression of miRNA in MPGs, it was necessary to define a housekeeping gene against which to compare the expression levels of the two miRNAs that microarray analysis had identified as showing changes during pregnancy and post-partum. Studies examining the expression of miRNAs in various neuronal tissues had used U6snRNA, Sno234 or U87 as housekeeping genes (Natera-Naranjo et al., 2010; Strickland et al., 2011; Zhang et al., 2011a). Housekeeping genes were first tested on dilutions of RNA from the hypothalamus of a non-pregnant rat at oestrus followed by RNA from MPGs. Serial dilutions of the RNA from the hypothalamus were used to generate standard curves. The standard curve provided the amplification efficiency which enabled Qgene to normalize the expression of miRNA even if the amplification efficiencies were different. Each serial dilution of RNA from the hypothalamus and the samples (RNA from MPGs) was always tested in triplicate. U6snRNA was the first housekeeping gene tested for use in the current study. The cycle threshold (Ct) value is the number of the cycles required for the fluorescent signal to exceed threshold/background. High Ct values indicate that the amount of nucleic acid in the sample is low and low Ct values indicate the amount of nucleic acid in the sample is high. The cycle threshold (Ct) values for U6snRNA across all the samples (Total RNA from MPGs) tested varied from 25 to 38 cycles. Because the expression of U6snRNA varied markedly across the samples, it was not suitable for use as a reference gene. Sno234 was assessed next but had Ct values between 34 and 38 cycles in dilutions of RNA from the hypothalamus.

TABLE 6.2: MEAN NORMALIZED EXPRESSION OF MIR-221 ACROSS ALL MPG SAMPLES

Rat #	Time	Mean Normalized Expression
A1316 RHS	OEST	0.385155 ± 0.038084
A1464 RHS	"	0.550147 ± 0.019517
A1465 RHS	"	0.376748 ± 0.045954
A1466 RHS	"	0.303367 ± 0.012284
A1467 RHS	"	0.361307 ± 0.007478
A1306 RHS	"	0.380176 ± 0.026754
A1307 LHS	"	0.479147 ± 0.044208
A1309 RHS	"	0.370647 ± 0.039368
A1456 RHS	E20	0.754389 ± 0.052143
A1444 LHS	"	*3.214167 + 0.178718*
A1448 RHS	"	0.313439 ± 0.032844
A1458 RHS	"	0.499268 ± 0.043215
A1472 RHS	"	0.410324 ± 0.042908
A1383 LHS	"	0.249488 ± 0.005811
A1442 RHS	"	0.411413 ± 0.044037
A1447 RHS	"	0.111828 ± 0.018937
A1342 RHS	P5	0.359998 ± 0.042555
A1451 RHS	"	0.462466 ± 0.016855
A1452 RHS	"	0.332367 ± 0.026443
A1454 RHS	"	0.80244 ± 0.017394
A1455 RHS	"	0.750166 ± 0.039288
A1432 LHS	"	0.708798 ± 0.035458
A1437 LHS	"	0.404486 ± 0.015118
A1459 RHS	"	0.573132 ± 0.041391
A1340 LHS	P14	0.529629 ± 0.038378
A1349 RHS	"	0.480143 ± 0.046493
A1350 LHS	"	0.601333 ± 0.019956
A1356 LHS	"	0.920435 ± 0.038463
A1358 RHS	"	0.450215 ± 0.030019
A1385 LHS	"	0.500101 ± 0.026219
A1388 LHS	"	0.390225 ± 0.009896
A1407 RHS	"	0.206906 ± 0.009519

LHS = left hand side; RHS = right hand side

TABLE 6.3: MEAN NORMALIZED EXPRESSION OF MIR-222 ACROSS ALL MPG SAMPLES

Rat #	Time	Mean Normalized Expression (± SE)
A1316 RHS	OEST	0.027099232 ± 0.002628
A1464 RHS	"	0.031899780 ± 0.002368
A1465 RHS	"	0.032714308 ± 0.003498
A1466 RHS	"	0.027120014 ± 0.001508
A1467 RHS	"	0.044478511 ± 0.002947
A1306 RHS	"	0.030088749 ± 0.001228
A1307 LHS	"	0.027122531 ± 0.003516
A1309 RHS	"	0.052160891 ± 0.006366
A1456 RHS	E20	0.069923267 ± 0.003817
A1444 LHS	"	*0.110706411 ± 0.012677*
A1448 RHS	"	0.024516762 ± 0.001681
A1458 RHS	"	0.02660004 ± 0.002441
A1472 RHS	"	0.030323581 ± 0.003881
A1383 LHS	"	0.014901126 ± 0.000284
A1442 RHS	"	0.020828284 ± 0.003136
A1447 RHS	"	0.007627069 ± 0.001492
A1342 RHS	P5	0.035861737 ± 0.003077
A1451 RHS	"	0.052050249 ± 0.00291
A1452 RHS	"	0.02725983 ± 0.002189
A1454 RHS	"	0.073877974 ± 0.002621
A1455 RHS	"	0.043909034 ± 0.001558
A1432 LHS	"	0.048566324 ± 0.002668
A1437 LHS	"	0.02098566 ± 0.001673
A1459 RHS	"	0.061676462 ± 0.003204
A1340 LHS	P14	0.044037184 ± 0.000864
A1349 RHS	"	0.030412293 ± 0.003939
A1350 LHS	"	0.037466827 ± 0.002089
A1356 LHS	"	0.081298719 ± 0.004457
A1358 RHS	"	0.038255384 ± 0.002142
A1385 LHS	"	0.050888507 ± 0.003662
A1388 LHS	"	0.048477836 ± 0.003524
A1407 RHS	"	0.028176426 ± 0.001617

LHS = left hand side; RHS = right hand side

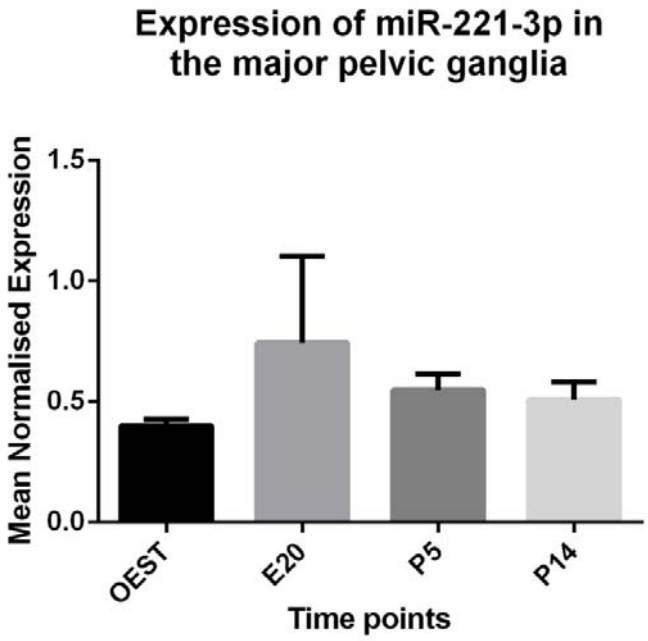

FIGURE 6.2: EXPRESSION OF MIR-221-3P IN INTACT MAJOR PELVIC GANGLIA FROM RATS AT OESTRUS (OEST), PREGNANCY DAY 20 (E20), POST-PARTUM DAY 5 (P5) AND POST-PARTUM DAY 14 (P14).

MicroRNA expression was analysed by quantitative real time polymerase chain reaction and normalised to U87. Data are expressed as normalized mean ± SE (error bars) (n=8).

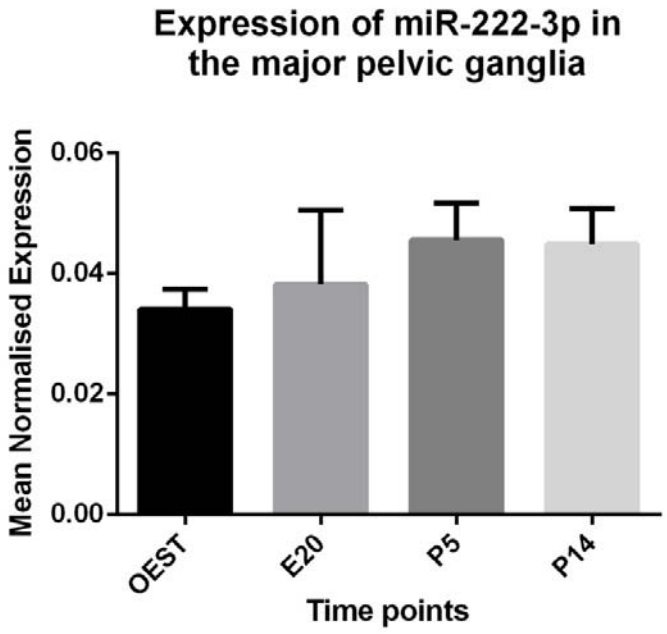

FIGURE 6.3: EXPRESSION OF MIR-222-3P IN INTACT MAJOR PELVIC GANGLIA FROM RATS AT OESTRUS (OEST), PREGNANCY DAY 20 (E20), POST-PARTUM DAY 5 (P5) AND POST-PARTUM DAY 14 (P14).

MicroRNA expression was analysed by quantitative real time polymerase chain reaction and normalised to U87. Data is expressed as normalized mean ± SE (error bars) (n=8).

These high Ct values meant that there was very low expression of sno234 in the control tissue, making it unsuitable as a housekeeping gene. The third housekeeping gene tested, U87, had Ct values between 19 and 25 cycles. Out of the 32 samples, 29 had Ct values between 19 and 21. The low Ct values meant that U87 was expressed in larger amounts compared to the other housekeeping genes and showed minimal variation across the samples (see Appendix 2). U87 was therefore chosen as the housekeeping gene and qRT-PCR results were normalized to U87. U87 is a small nucleolar RNA (Gogolevskaya et al., 2002).

6.2.5 qRT-PCR

The mean normalized expression of miR-221 and miR-222 from each rat are summarised in Tables 6.2 and 6.3.

Student t tests showed no statistically significant difference in the expression of either miR-221-3p (Figure 6.2) and miR-222-3p (Figure 6.3) between any of the time points examined, i.e., OEST vs E20, OEST vs P5, OEST vs P14, E20 vs P5, E20 vs P14 and P5 vs P14. There was aberrant expression of both miR-221-3p and miR-222-3p in one sample, A1444 LHS (italicised in Tables 6.2 and 6.3) at E20. There was no difference to statistical significance even if this sample was removed.

6.3 SUMMARY AND DISCUSSION

The experiments described in this chapter have shown that miRNA expression in the intact MPG does not change during pregnancy and post-partum. Microarray analyses suggested that two microRNAs extracted from intact MPGs, miR-221-3p and miR-222-3p, were downregulated at P5 compared to oestrus.

TABLE 6.4: STATISTICAL ANALYSIS OF THE EXPRESSION OF MIR-221-3P IN MPGS

Time points tested	P value
OEST vs E20	0.3548
OEST vs P5	0.0561
OEST vs P14	0.1771
E20 vs P5	0.5996
E20 vs P14	0.5307
P5 vs P14	0.6926

TABLE 6.5: STATISTICAL ANALYSIS OF THE EXPRESSION OF MIR-222-3P IN MPGS

Time points tested	P value
OEST vs E20	0.7512
OEST vs P5	0.1244
OEST vs P14	0.1330
E20 vs P5	0.6021
E20 vs P14	0.6319
P5 vs P14	0.9395

However, results from qRT-PCRs showed that there were no statistically significant differences in the expression of these miRNAs at any of the time points compared (OEST, E20, P5 & P14).

6.3.1 Technical considerations

This is the first study to examine the expression of miRNA in major pelvic ganglia of rats. Although there were no statistically significant differences in the expression of miRNAs in the whole MPG, this finding does not exclude the possibility that miRNAs specifically in sympathetic and parasympathetic post-ganglionic neurons are involved in changes to uterine innervation during pregnancy and post-partum. In this project, RNA was extracted from the entire MPG but not all of the neurons in the MPG project to the uterus (Owman and Stjernquist, 1988). The percentage of neurons that project to the uterus and cervix is probably lower than 25% (Gu et al., 1984). Many neurons in the pelvic ganglia can be retrogradely labelled from the female reproductive organs; but in all of the published studies the tracers were injected into the cervix as well as the uterus (Gu et al., 1984; Houdeau et al., 1995; Serghini et al., 1997). Hence, the sample of uterus-projecting neurons in an entire MPG is likely to be very small and any miRNAs occurring in these neurons would represent only a tiny fraction of total miRNA extracted from an intact MPG. This dilution problem would be overcome by using a method like laser capture microdissection (Alldred et al., 2015; Subramanian et al., 2014) or *in situ* hybridization for miRNAs (Tam et al., 2011). These methods could precisely target expression of miRNAs in uterus-projecting neurons and would provide results that more accurately reflect the effects of pregnancy and parturition on miRNA

expression. It is probable that pregnancy-related changes in miRNA expression, if any, occur only in the uterine projecting neurons of the MPG.

Both miR-221-3p (Natera-Naranjo et al., 2010) and miR-222-3p (Zhou et al., 2012) are expressed in neurons. miR-222 has been shown to promote axonal growth in dorsal root ganglia following sciatic nerve transection in rats (Zhou et al., 2012). miR-222 downregulates the expression of phosphatase and tensin homolog deleted on chromosome 10 (PTEN). PTEN inhibits the $P1_3K$ (phosphoinositide 3-kinase) pathway, which is significant for axonal growth (Zhou et al., 2012). In cultures of sympathetic neurons from superior cervical ganglia of 3 day old rats, miRNA-221 is more abundant in sympathetic axons than in cell bodies (Natera-Naranjo et al., 2010); but its role in axonal growth remains to be investigated. In light of these observations, it would be worthwhile to investigate whether the expression of these two miRNAs changes during pregnancy and post-partum specifically in uterus-projecting neurons in the MPG.

Chapter 7

General Discussion

In this project, I have confirmed that sympathetic nerves completely disappear from the uterus during pregnancy and slowly re-innervate the uterus post-partum beginning immediately after delivery. I have also provided the first comprehensive account of what happens to parasympathetic and sensory nerves over the same time period. For the first time, I have quantified the changes in the density of uterine sympathetic, parasympathetic and sensory innervation during pregnancy and post-partum in whole mount preparations. Whole mount preparations provide the most accurate representation of innervation patterns. They allow us to visualize every layer of the uterus and track axons from where they enter the uterus to where they terminate whereas sections only give information about a small sample of a uterine horn. I have previously described in detail the sympathetic, parasympathetic and sensory innervation of the non-pregnant rat uterus using whole mounts (Gnanamanickam and Llewellyn-Smith, 2011). In that study, whole mount preparations of the uterus enabled me to identify the differential innervation of the linea uteri in the non-pregnant uterus for the first time (Gnanamanickam and Llewellyn-Smith, 2011).

7.1 CHANGES TO SYMPATHETIC INNERVATION OF THE RAT UTERUS DURING PREGNANCY AND POST-PARTUM

7.1.1 Sympathetic denervation during pregnancy

Studies using glyoxylic acid fluorescence or immunohistochemistry for TH or NPY in rats, guinea pigs and humans have confirmed that pregnancy induces sympathetic denervation of the uterus (Alm et al., 1988; Chavez-Genaro et al., 2006; Fried et al., 1986; Fried et al., 1985; Haase et al., 1997; Klukovits et al., 2002; Sporrong et al., 1981; Thorbert et al., 1979). In this project, I have shown that the numbers of both NPY and TH-immunoreactive axons dramatically decline during pregnancy. The decrease in sympathetic innervation density is progressive. TH and NPY axons were substantially reduced at E14 but at E20 they had almost completely disappeared.

Previous studies on the rat uterus during early pregnancy (day 5 and 10) have shown that sympathetic innervation is similar in density to the non-pregnant state (Chavez-Genaro et al., 2006; Klukovits et al., 2002). At day 15, degeneration of axons had begun; at day 18 very few axons were present and by day 22 almost all innervation had disappeared (Klukovits et al., 2002). The current study was done on whole mount preparations of uterine horns from rats on days 14, 16, 18 and 20 of a 21-22 day pregnancy and the results were similar to the findings above. At all pregnancy time points from E14 to E20, the uterus was significantly denervated compared to the non-pregnant uterus. The differences in innervation density as measured by intersections of TH-immunoreactive axons with a counting grid were statistically significant compared to oestrus at all time points during pregnancy. At E14, uterine innervation density was 5.74% of that in the non-pregnant rat uterus. Innervation density decreased to 3.3%, 1.56% and 0.23% of the non-pregnant density

at E16, E18 and E20, respectively. The number of blood vessels innervated and the extent of their innervation also decreased as pregnancy progressed.

7.1.2 Sympathetic re-innervation post-partum

As discussed in detail in Chapter 1, only a few studies have been published on sympathetic re-innervation of the post-partum uterus in rats (Chavez-Genaro et al., 2006; Haase et al., 1997; Moustafa, 1988), guinea pigs (Alm et al., 1977; Alm et al., 1988; Owman et al., 1980; Thorbert et al., 1978) and sheep (Sigger et al., 1986). This study is, therefore, the first to detail the progressive sympathetic re-innervation of the rat uterus after delivery and to quantify the increase in the density of TH-immunoreactive axons in whole mount preparations. In agreement with previously published work (Haase et al., 1997), I found that TH-immunoreactive axons were present in the uterus by post-partum day 1 (P1) . At P1, the density of TH-immunoreactive axons was very low compared to the non-pregnant uterus but was a little higher than in the E20 uterus. TH-positive axons occurred near blood vessels, in thick nerve bundles and also travelled into the uterus by themselves. There were growth cones on TH-immunoreactive axons in the P1 uterus but they were much more numerous at P3 and P5. Growth cones were present on TH-immunoreactive axons at all post-partum time points examined, even in the P28 uterus although they were rare by this time. Re-innervation of the linea uteri began at P3 and was also not complete at P28. In general, the density of sympathetic innervation was higher at the ovarian end compared to the rest of the uterus. Quantification of axonal intersections and Poisson Regression Analysis confirmed that the number of TH-immunoreactive axons progressively increased from P1 to P28. At P1, the number of TH-immunoreactive axons measured by axonal intersections was 99.16% lower than in

the non-pregnant uterus. At P28 TH innervation density was 54% lower than the non-pregnant uterus.

7.2 CHANGES TO PARASYMPATHETIC INNERVATION OF THE RAT UTERUS DURING PREGNANCY AND POST-PARTUM

7.2.1 Parasympathetic denervation during pregnancy

Previous studies have found a reduction in nNOS-containing and AChE-positive axons detected by immunohistochemistry, NADPH-diaphorase staining or the Karnovsky and Roots method in rat uterus during pregnancy (Moustafa, 1988; Natuzzi et al., 1993; Papka et al., 1995; Riemer et al., 1997). Unpublished results from our laboratory have also found a massive reduction in the parasympathetic innervation of the rat uterus at E20 using immunohistochemistry for nNOS and VAChT. In this study using immunostaining for VAChT in whole mount preparations, I have provided a detailed description of parasympathetic denervation and re-innervation of the rat uterus during pregnancy and post-partum. As it did for sympathetic nerves, pregnancy caused a significant reduction in the parasympathetic innervation of the rat uterus. At E14, the density of VAChT-immunoreactive axons was very much reduced compared to the non-pregnant uterus. VAChT-positive axons were still present around some blood vessels but the perivascular innervation was only moderate. At E16, the density of parasympathetic nerves was even lower than at E16 and by E18 there were only a few parasympathetic nerves present. As I described previously (unpublished observations), the E20 uterus had almost no VAChT-immunoreactive axons. Rare axons entered the uterus and ran near blood vessels but did not surround them.

By E14, the parasympathetic innervation density had decreased to 11.24% and by E20 this was further decreased to 0.50%. There was a statistically significant difference in the parasympathetic innervation density between oestrus and all pregnancy time points examined – E14, E16, E18 and E20.

7.2.2 Parasympathetic re-innervation post-partum

Only one previous study has reported on parasympathetic re-innervation of the post-partum uterus using the non-specific method of AChE staining on sections of rat early post-partum uterus (3 and 10 days) and later (15 days and 3 weeks) in the post-partum period (Moustafa, 1988). The early post-partum uterus was found to be less innervated by AChE axons and the fibers that persisted were fragmented. In late post-partum rat uterine horns, AChE fibers were more darkly stained and occurred in large nerve trunks (Moustafa, 1988).

This thesis presents the first detailed description and quantification of parasympathetic re-innervation of the rat uterus post-partum using whole mount preparations and an immunohistochemical marker that unequivocally demonstrates cholinergic nerves, VAChT. In rat uterine horns, parasympathetic re-innervation also began at P1. There were a few VAChT-immunoreactive axons in the P1 uterus and some VAChT axons had growth cones. Growth cones on VAChT-positive axons were more numerous at P3 and P5 and occurred at all subsequent time points, becoming rare at P28. Parasympathetic re-innervation of the linea uteri began at P5 in one rat but there were no VAChT-immunoreactive axons in the linea uteri in P7 uteri. At P10, there was one rat that had more axons in the linea uteri at the ovarian end but none of the rats in P14 or P28 showed any difference in the innervation of the linea uteri along the length of a uterine horn. The ovarian end of the rat uterus did

not receive a higher density of VAChT-immunoreactive axons as was the case for TH-immunoreactive axons. This could be due to the faint staining of VAChT antibody in the ovarian end of the post-partum uteri. A few experiments were repeated by pinning down the ovarian end in the crystallizing dish but ovarian ends still did not stain well for VAChT axons.

The parasympathetic innervation density as revealed by staining for VAChT increased from 1.02% at P1 to 125.66% at P28. The unusually high innervation densities at P10 (147.29%), P14 (186.87%) and P28 (125.66%) are possibly due to the low sample size and the variability in innervation density across each individual uterine horn. The variability between rats as discussed in Chapter 4 could also have contributed. Nevertheless, there were statistically significant differences in parasympathetic innervation density between oestrus and P1 and P3.

7.3 CHANGES TO SENSORY INNERVATION OF THE RAT UTERUS DURING PREGNANCY AND POST-PARTUM

7.3.1 Sensory denervation during pregnancy

A decrease in the concentration of SP measured by radioimmunoassay has been reported in the uteri of 14 day and 19 day pregnant rats (Traurig et al., 1984). In the late pregnant guinea pig, no SP- or CGRP-immunoreactive axons were present in uterine sections (Alm and Lundberg, 1988). Previous unpublished data from our laboratory has also found a massive reduction in SP- and CGRP-immunoreactive axons in the E20 rat uterus. In this study, I used immunoreactivity for CGRP to identify sensory innervation of the rat uterus. Since all CGRP-immunoreactive uterine axons in the rat also contain SP (Shew et al., 1991), only immunoreactivity

for CGRP was studied. CGRP-immunoreactive axons were present in E14 uterine horns but their density was much lower than in the non-pregnant uterus. CGRP-positive axons provided a moderate innervation to a few blood vessels; only rarely was a blood vessel significantly innervated. By E16, the CGRP innervation density was further reduced. Some blood vessels in the middle regions of uterine horns did not receive any innervation. At E18, uterine horns received fewer CGRP-immunoreactive axons than at E16 and by E20; the uterus was almost completely devoid of CGRP-positive axons. These observations are consistent with a study on the guinea pig uterus, which did not find any CGRP- or SP-immunoreactive axons at term but only a few sections of the uterus were examined (Alm and Lundberg, 1988). The analysis of my counts of VAChT-positive axonal intersections showed that the differences in VAChT innervation were statistically significant at all pregnancy time points compared to the non-pregnant uterus at oestrus. The densities of uterine sensory innervation at E14, E16, E18 and E20 were reduced by 85%, 98.7%, 98.64% and 99.95% of the innervation density of the non-pregnant rat at oestrus.

7.3.2 Sensory re-innervation post-partum

This is the first study to describe in detail the sensory re-innervation of the rat uterus post-partum. Haase et al (1997) reported that CGRP-immunoreactive axons were present in the early post-partum rat uterus at 24 to 48 hours after delivery (Haase et al., 1997) but there is no information about sensory innervation of rat uterine horns later in the post-partum period. The results from this study agree with those of Haase et al. At P1, I found a few CGRP-immunoreactive axons in the rat uterus and most of them had growth cones. Many more growth cones were present on CGRP-immunoreactive axons at P3 and P5. Similar to sympathetic innervation revealed by

staining for TH and parasympathetic innervation revealed by staining for VAChT, the density of sensory innervation revealed by staining for CGRP increased from P1 to P28. However, the density of CGRP innervation had still not returned to the density at oestrus by P28. . Sensory re-innervation of the linea uteri began at P5 but was also not complete at P28.

This study is also the first to quantify CGRP-immunoreactive axons in the post-partum rat uterus. At P1, the number of CGRP-positive axons as assessed by axonal intersections with a counting grid was 99.03% of that at oestrus. By P28 the density of CGRP-immunoreactive axons had increased to 54% that at oestrus. Thus, like sympathetic and parasympathetic nerves, sensory nerves have still not completely re-innervated the rat uterus by 4 weeks after delivery.

7. 4 COMPARISON OF SYMPATHETIC, PARASYMPATHETIC AND SENSORY DENERVATION AND RE-INNERVATION DURING PREGNANCY AND POST-PARTUM

The non-pregnant rat uterus at oestrus receives significant numbers of sympathetic, parasympathetic and sensory nerves. The average number of axonal intersections at oestrus was 321.95 for sympathetic nerves, 286.20 for parasympathetic nerves and 199.95 for sensory nerves was. During pregnancy, there was a progressive decrease in uterine innervation across all three types of nerves, which occurred with quite similar time courses. Re-innervation by sympathetic, parasympathetic and sensory nerves began at P1 and innervation density progressively increased to roughly 50% for the innervation density at oestrus by P28. Thus, re-innervation by all three classes of nerves was not complete at P28.

Sympathetic axons first appear in the linea uteri at P3 while parasympathetic and sensory axons first appear in the linea uteri at P5 in the ovarian-most end. By P28, there were a few sympathetic and sensory axons in the linea uteri in the ovarian most end. Due to faint staining of the VAChT-immunoreactive parasympathetic axons in the ovarian ends of uterine horns, it was not possible to confirm the re-innervation pattern of the linea uteri by parasympathetic nerves in that region. The denervation and re-innervation in the middle, cervical, mesometrial and anti-mesometrial sides were similar in all three classes of nerves.

The density of innervation provided by sympathetic, parasympathetic and sensory nerves was not homogeneous along the length of rat uterine horns. The ovarian region of a uterine horn was in general more densely innervated than the middle and cervical regions. The middle region received the lowest number of sympathetic, parasympathetic and sensory axons. The mesometrial side was in general more innervated during pregnancy and post-partum compared to the anti-mesometrial side for all three types of nerves. The re-innervation pattern of the longitudinal and circular muscle layers was similar as was the re-innervation of the endometrium. The densities of sympathetic and sensory innervation in the ovarian region were similar, but parasympathetic innervation in the ovarian end was slightly less dense. This apparent variation in parasympathetic innervation could be related to the antibody as quite a few post-partum uteri were faintly stained in the ovarian end even when horns from the same rats were re-stained.

7. 5 QUANTIFICATION OF CHANGES IN UTERINE INNERVATION DENSITY

This study is the first to quantify the density of sympathetic, parasympathetic and sensory nerves in the rat uterus during pregnancy and post-partum using whole mount preparations. My results show that for all nerve types in the uterus, there is a progressive decrease in innervation as parturition approaches and a progressive increase in innervation as time increases after delivery. Using whole mounts was an advantage for my project because they allowed me to count all of the axons in all of the different layers of the uterus using photographs at different focal planes. There was some variability in the counts, which depended on where the squares randomly-chosen for counting happened to fall. The density of the TH-, VAChT- and CGRP-immunoreactive innervation could vary greatly between different areas of a pregnant or post-partum uterine horn. This variability meant that there were areas in each uterine horn where there were few or no axons but other areas where innervation density was high. In contrast, non-pregnant uterine horns were more densely innervated and innervation density was less variable across each horn. Consequently, wherever a random square happened to fall in a non-pregnant horn, at least a few axons were present. In the pregnant and post-partum uterine horns, however, there were squares in which 0 or very few intersections were counted as well as squares in which many intersections were counted, leading to large difference in the numbers of intersections between squares in the same rat. This variability in uterine innervation and the small sample size (counting intersections in 5 squares in each of 4 rats at each time point) resulted in the large confidence intervals for the data. The large confidence intervals also affected the P values. Future studies with a

larger sample size (i.e., intersections counted in more squares in each rat) will be required in order to overcome these limitations.

The high degree of variability I found in innervation density within the same uterine horn calls into question the reliability of studies in which innervation was examined or quantified in sections of pregnant and post-partum uteri. In these studies, it would have been impossible to know whether axons were being quantified in areas where some innervation or no innervation was present. The heterogeneous distribution of axons across a pregnant uterine horn could explain why Chavez-Genaro et al. (2006) found no sympathetic axons in the pregnant rat uterus at day 19 whereas Klukovits et al. (2002) found rare degenerating axons at day 22. In contrast, my statistical analysis of axonal intersections counted in randomly-selected areas of immunostained whole mount preparations provides for the first time a reliable estimate of the sympathetic, parasympathetic and sensory innervation density of the uterus during pregnancy and post-partum.

7.6 CHANGES TO miRNA EXPRESSION LEVELS IN MAJOR PELVIC GANGLIA DURING PREGNANCY AND POST-PARTUM

My immunohistochemical studies on whole mount preparations established conclusively that the rat uterus denervates as pregnancy progresses and re-innervates as time after delivery increases. Since microRNAs regulate the expression of genes that control the retraction and regrowth of axons (Dajas-Bailador et al., 2012; Strickland et al., 2011; Wu et al., 2012), I wanted to determine whether changes in miRNA expression levels might be involved in the changes to uterine innervation during pregnancy and post-partum. As a first step towards answering this question, I examined miRNA expression in major pelvic ganglia (MPGs) since some of the

neurons in the MPG project to the uterus (Owman and Stjernquist, 1988) For the first time, I determined the expression levels of miRNAs in MPGs from non-pregnant rats at oestrus, near-term pregnant rats at E20, early post-partum rats at P5 and late post-partum rats at P14. This is also the first study on the expression of miRNAs in MPGs. Microarray analysis of RNA extracted from MPGs indicated that there was an approximately 1.5 fold decrease in the expression levels for Mir-221-3p and miR-222-3p at P5 compared to oestrus. However, when quantitative RT-PCRs were done, there were no statistically significant differences in miR-221-3p and miR-222-3p across all time points. The lack of statistically significant differences in the results from the RT-PCR experiments could have several explanations. MPGs are very small ganglia and only a small amount RNA could be extracted from them. Because of the low concentration of RNA, that Nanodrop may have measured the amount of RNA inaccurately, which could have led to loading discrepancies. Nevertheless, microarrays are semi-quantitative and the decrease in expression of miR-221-3p and miR-222-3p was only small at P5 compared to oestrus. It is therefore not surprising that RT-PCR showed no change in miRNA expression levels at any of the time point examined.

Despite the negative results from my miRNA expression study, the possible influence of miRNAs on uterine innervation changes during pregnancy and post-partum cannot be ruled out. In this study, total RNA was extracted from the entire MPG while only a portion of the neurons in the MPG project to the uterus (Owman and Stjernquist, 1988). Retrograde labelling has shown that many neurons in the MPG innervate the female reproductive organs. However, in most of these studies tracers were injected into the cervix and the uterus (Gu et al., 1984; Houdeau et al., 1995; Serghini et al., 1997). It is likely that less than 25% of the neurons in the MPG

innervate the uterus and cervix (Gu et al., 1984). The number of neurons innervating the uterus is therefore relatively low and in this study total RNA was extracted from the entire MPG. It would be worthwhile to use methods like laser capture microdissection or *in situ* hybridisation for miRNAs. These methods would allow the uterus-projecting neurons to be precisely targeted so that their expression of miRNAs could be assessed without contamination by other functional types of MPG neurons.

MiRNAs have been reported to promote axonal growth and regeneration (Dajas-Bailador et al., 2012; Strickland et al., 2011; Yu et al., 2011; Zhang et al., 2011b; Zhou et al., 2012) and to guide axonal growth cones (Han et al., 2011) so it would be worthwhile to examine miRNAs and their roles in pregnancy-induced uterine denervation and re-innervation in more detail. It is quite possible that miRNAs that regulate axonal growth and retraction are present in axons in the uterus since miRNA have been found in axons in rat superior cervical ganglia (Natera-Naranjo et al., 2010). It is also possible that during pregnancy and after delivery, miRNAs change in neuronal cell bodies in other ganglia that supply innervation to the uterus, such as the inferior mesenteric ganglia (IMG) or dorsal root ganglia (DRG). Future studies assessing miRNA expression levels in the IMG, DRG and the uterus could provide valuable information about the role of miRNAs in uterine innervation changes during pregnancy and post-partum.

7.7 OTHER FACTORS THAT COULD CAUSE CHANGES IN UTERINE INNERVATION

There are other possible mechanisms that could be responsible for the changes in uterine innervation that occur during pregnancy and post-partum. Neurotrophic

factors, such nerve growth factor (NGF), brain derived neurotrophic factor (BDNF), vascular endothelial growth factor (VEGF), neurotrophin 3 and neurotrophin 4/5 may contribute to uterine innervation changes during pregnancy and post-partum. NGF is a neurotrophic factor for sympathetic and sensory neurons (Sofroniew et al., 2001) and BDNF is a neurotrophic factor for sensory neurons (Landreth and ., 2006). There are conflicting reports about the presence of NGF in the uterus. In one study, NGF and NGF mRNA in the uterus were increased in mid and late pregnancy when adjusted for uterine weight changes (Varol et al., 2000), results that are incompatible with the loss of sympathetic and sensory innervation during pregnancy. However, western blotting for NGF-β protein in the rat uterus indicated that there was a decrease in NGF during mid and late pregnancy and at 1 day post-partum (Lobos et al., 2005). Measuring NGF during pregnancy and at various times post-partum might give more information about its possible role in the retraction and regrowth of sympathetic and sensory axons. When the dorsocaudal region of the MPG from male rats at 6 months and 24 months of age was treated with BDNF and VEGF, these growth factors were found to promote growth of axons in the MPG in 6 month old rats but growth was reduced in rats over 12 months of age (Lin et al., 2010). Since the uterus receives some of its innervation from the MPG (Owman and Stjernquist, 1988), it worth investigating the role of BDNF and VEGF in the uterine innervation changes during pregnancy and post-partum.

Hormonal changes could also contribute to uterine denervation and re-innervation. Estrogen influences the density of sympathetic nerves in the rat uterus during the oestrus cycle (Zoubina and Smith, 2000). Sympathetic innervation of the uterus was also reduced in ovariectomized mice after treatment with estrogen (Zoubina and Smith, 2001) and absent after estrogen administration in 28 day old

rats (Brauer et al., 2002). In addition, estrogen has been shown to stimulate the expression of NGF in the uteri of hamsters (Shi et al., 2006). Progesterone may also play a role in changes in uterine innervation during pregnancy and post-partum. When placed in the uterus of guinea pigs, pellets containing progesterone cause a decline in the density of catecholaminergic nerves identified by fluorescence histochemistry. After initially starting around the pellet, this decrease in catecholaminergic innervation had spread to both horns by 10 days (Bell and Malcolm, 1978). Furthermore, injections containing both estradiol and progesterone injection caused a moderate decrease in fluorescent catecholaminergic nerves in guinea-pig uterine horns (Thorbert et al., 1978b). In contrast, uterine catecholaminergic innervation did not change in response to either implantation of pellets containing estradiol or subcutaneous and intramuscular injections of progesterone in guinea-pigs (Bell and Malcolm, 1978; Thorbert et al., 1978b).

The mechanical stretch of the uterus has also been shown to contribute to degeneration of axons within the uterus. When porcelain pellets were inserted in the uteri of virgin guinea pigs, there was a reduction in the number of TH-, DBH-, NPY-, NF-, NSE- and PGP-IR nerves in the myometrial tissue around the pellets compared to tissue that distant from a pellet. Pellets placed in the uterine horns of 25- to 35-day pregnant guinea pigs also decreased innervation density (Lundberg et al., 1989).

Evidence also suggests that the myometrium may a role to play in changes to uterine innervation during pregnancy. The myometrium itself may also contribute to the innervation changes during pregnancy. When samples of myometrium from virgin and early post-partum (2 to 7 days) guinea-pigs were transplanted into the anterior eye chamber of virgin guinea-pigs, myometrial samples from the virgin animals were re-innervated by sympathetic post-ganglionic axons from the superior

cervical ganglia but there was no reinnervation of post-partum samples after 3 weeks (Brauer et al., 1998).

Other factors, such as neurotrimin, semaphorins, neuropilins and bone morphogenetic protein 4 (BMP4) may also contribute to pregnancy-induced changes in uterine innervation. Neurotrimin is a neural cell adhesion molecule that can influence both sensory and sympathetic innervation; it inhibits outgrowth of sympathetic neurites and stimulates outgrowth of sensory neurites . (Monica and Smith, 2015) Neurotrimin is present in the smooth muscle cells of the rat myometrium. Immunostaining of uterine tissue sections over the estrous cycle has shown lower levels of neurotrimin in the longitudinal and circular smooth muscle when sympathetic axon density is high and vice versa. Neurotrimin is also regulated by estrogen (Krizsan-Agbas et al., 2008). Semaphorins are a family of secreted, transmembrane and membrane-anchored proteins that also inhibit sympathetic neurite outgrowth (Monica and Smith, 2015). Semaphorin 3A is present in the connective tissue between smooth muscle layers and around blood vessels in the rat myometrium; treatment with estrogen increases Semaphorin 3A in the rat myometrium (Richeri et al., 2011). BMP4 is a member of TGFβ family of cytokines and morphogens and has been shown to stimulate sensory nerve growth in cultured smooth muscle cells from the rat vagina (Monica and Smith, 2015). In the mouse uterus, BMP4 occurs in the endometrial glandular and luminal epithelium, in the connective tissue and in the myometrium (Tanwar and McFarlane, 2011) but it is unknown whether BMP4 has a similar effect on uterine smooth muscle cells in vivo.

Finally, it is possible that a combination of factors such as growth factors and miRNAs could cause innervation changes during pregnancy and post-partum. For example, there is evidence that the neurotrophic factor, BDNF, controls the

expression of miR-132, which in turn regulates axonal branching by regulating the expression of the protein p250GAP in retinal ganglion cells (Marler et al., 2014). MicroRNA 132 is the same miRNA that stimulates axonal growth in DRG explants from E13 mice (Hancock et al., 2014). Also interestingly, a protein called neurotrimin, which regulates outgrowth from sympathetic neurons in the SCG, is induced by estrogen in uterine smooth muscle cells (Krizsan-Agbas et al., 2008). Hence, it is possible that combinations of such factors are responsible for the uterine innervation changes during pregnancy and post-partum.

7.8 TECHNICAL CONSIDERATIONS

While every effort was made to ensure that the whole mounts were immunostained well, it was impossible to validate that every single axon present in the uterine horns was visualized. Nevertheless, the method visualized immunostained axons very reproducibly in uterine whole mounts so we are confident that the results in this thesis provide a reliable estimate of the density of uterine innervation during pregnancy (E14-E20) and post-partum (P1-P28).

Similarly while single immunoreactive axons were present, it is not possible say of absolute certainty that these were not part of a bundle of axons without the use of electron microscopy. When viewed with a x40 objective on a light microscope, many axons appeared to be single but it is possible that some of the axons judged to be single were in fact small axon bundles.

It is also possible that rare small axon bundles were counted as “one” in the quantification studies. All axonal intersections were counted at very high magnification in Photoshop (x400 using the zoom tool). Every single axonal intersection was counted as “one”. When axonal bundles were encountered, every

clearly visible axon was counted separately. Consequently, the number of small axon bundles mistaken to be single axons and counted as "one" is likely to be very low. This study quantified uterine innervation using whole mounts for the first time and, compared to previous studies on sections, counted axons in a much larger sample of tissue from each uterine horn studied. These factors make the data reported here the most reliable estimate of uterine innervation density to date.

7.9 FUTURE DIRECTIONS

The future directions of this project include assessing and quantifying how sympathetic, parasympathetic and sensory innervation of the uterus change in rat models of pre-eclampsia using the same immunohistochemical techniques on whole mount preparations as used in this project. The results of this project provide basic information about changes to uterine innervation during pregnancy and post-partum and will be the foundation for further investigations one pregnancy related disorders that may be affected by these changes. As detailed in Chapter 1, denervation of the pre-eclamptic uterus is incomplete compared to a normal pregnant uterus (Fried et al., 1986). Quantifying the innervation of the pre-eclamptic rat uterus using whole mount preparations would be useful in understanding the link between uterine nerves and pre-eclampsia. It would be valuable to know whether there are similar or maladaptive innervation changes in the uterus in gestational hypertension and in rats that normally develop hypertension, such as SHR rats. Whether or not pregnancy causes denervation of other maternal organs could also be investigated. It would also be interesting to know whether innervation of the post-partum uterus ever returns to non-pregnant levels since those levels have not been reached a month after delivery. Subject to the availability of tissue, it would also be important to examine and

quantify the sympathetic, parasympathetic and sensory innervation of the pregnant, post-partum and pre-eclamptic human uteri. It would also be interesting to determine what happens to A delta afferents also during pregnancy and whether they degenerate during pregnancy and re-innervate post-partum with the same time course as unmyelinated afferents.

More work needs to be done on the mechanisms that underlie pregnancy-induced denervation of the uterus and its re-innervation post-partum. The roles that neurotrophic factors play in changes to uterine innervation remain unknown. Determining the expression levels of miRNAs in other neurons that provide innervation to the uterus and in the uterus itself during pregnancy and post-partum would provide valuable knowledge. It would also be worthwhile to investigate whether hormones, including hormones that are important in pregnancy, have any influence on the denervation and re-innervation of the uterus during pregnancy and post-partum. The effect of neurotrophic factors such as artemin, NGF, BDNF, VEGF or neurturin could be tested on uterine-projecting neurons using *in vitro* neurite outgrowth assays. Artemin is known to have neurotrophic effects on neurons in the DRG (Wong et al., 2015) whereas BDNF, VEGF and neurturin have neurotrophic effects on MPG neurons in male rats (Lin et al., 2010; Wanigasekara and Keast, 2005).

Appendix 1

Solutions

Calcium Free Krebs Solution

Double-strength Ca^{+2} free Krebs solution:

NaCl	26.88 g
KCl	1.4 g
Na_2HPO_4	0.6 g
$NaHCO_3$	8.4 g
$MgCl_2$ and	4.8 g
D-glucose	8 g

The solution was made up to 2 litres with distilled water.

Single-strength Ca^{+2} Krebs solution was prepared by diluting Double-strength Krebs solution with an equal volume of distilled water.

0.4M Phosphate Buffer, pH 7.4

Na_2HPO_4	45.42 g
NaH_2PO_4	12.48 g

The reagents were dissolved in 900 ml of distilled water

The pH was adjusted to 7.4 with NaOH

The solution was made up to 1 litre in distilled water.

0.1M Phosphate Buffer, pH 7.4

0.4 M phosphate buffer, pH 7.4	250 ml
Distilled water	750 ml

Phosphate Buffered Saline (PBS)

NaCl	9 g
0.4M phosphate buffer, pH 7.4	250 ml
distilled water	650 ml

The pH was adjusted to 7.4 with NaOH.

The solution was made up to 1 litre with distilled water.

4% Formaldehyde 0.1M Phosphate Buffer, pH 7.4

0.4M phosphate buffer	250 ml
40% Formaldehyde (Ajax FineChem Pty Ltd, Australia)	100 ml

The pH was adjusted to 7.4 with NaOH

The solution was made up to 1 litre with distilled water.

0.05% Sodium azide in 0.1M Phosphate Buffer, pH 7.4

0.4M phosphate buffer, pH 7.4	100 ml
200× Na azide	2 ml

The solution was made up to 400 ml with distilled water.

30% methanol, 1% hydrogen peroxide

Absolute methanol (Ajax Finechem Pty Ltd, Australia)	30 ml

Hydrogen peroxide (Chem-Supply, Australia)	3.3 ml

The solution was made up to 100 ml with distilled water.

Tris-Phosphate Buffered Saline (TPBS)

Trizma Base	4.844 g
0.4M Phosphate buffer	100 ml
Merthiolate	2 g
NaCl	36 g

The pH was adjusted to 7.4 with HCl

The solution was made up to 4 litres with distilled water.

Immunobuffer

Triton X-100 (Chem-Supply, Australia)	3.3 ml
Tris- phosphate buffer saline	1 litre

10% Normal Horse Serum in Immunobuffer

Normal horse serum (Gibco, USA)	5 ml
Immunobuffer	45 ml

1% Normal Horse Serum in Immunobuffer

Normal horse serum (Gibco, USA)	0.5 ml
Immunobuffer	49.5 ml

Nickel-intensified Diaminobenzidine (Ni-DAB) reaction

Pre-incubation Solution:

0.4M sodium phosphate buffer, pH 7.4	10 ml
0.4% NH_4Cl	400 µl
20% glucose	400 µl
Distilled water	27.6 ml
50 mg/ml DAB	400 µl
1% Nickel Ammonium Sulfate	1.6 ml

Reaction mix:

Pre-incubation solution	1 ml
Glucose oxidase (Sigma Aldrich, USA)	1 µl

Durcupan (Resin)

Part A (Epoxy Resin)	10 ml
Part B (Hardener)	10 ml
Part C (Accelerator 960)	0.3 ml
Part D (Dibutlyphthalate)	0.3 ml

The solution was vigorously mixed by hand for 1 to 2 minutes.

Appendix 2

Ct values of housekeeping gene used – U87

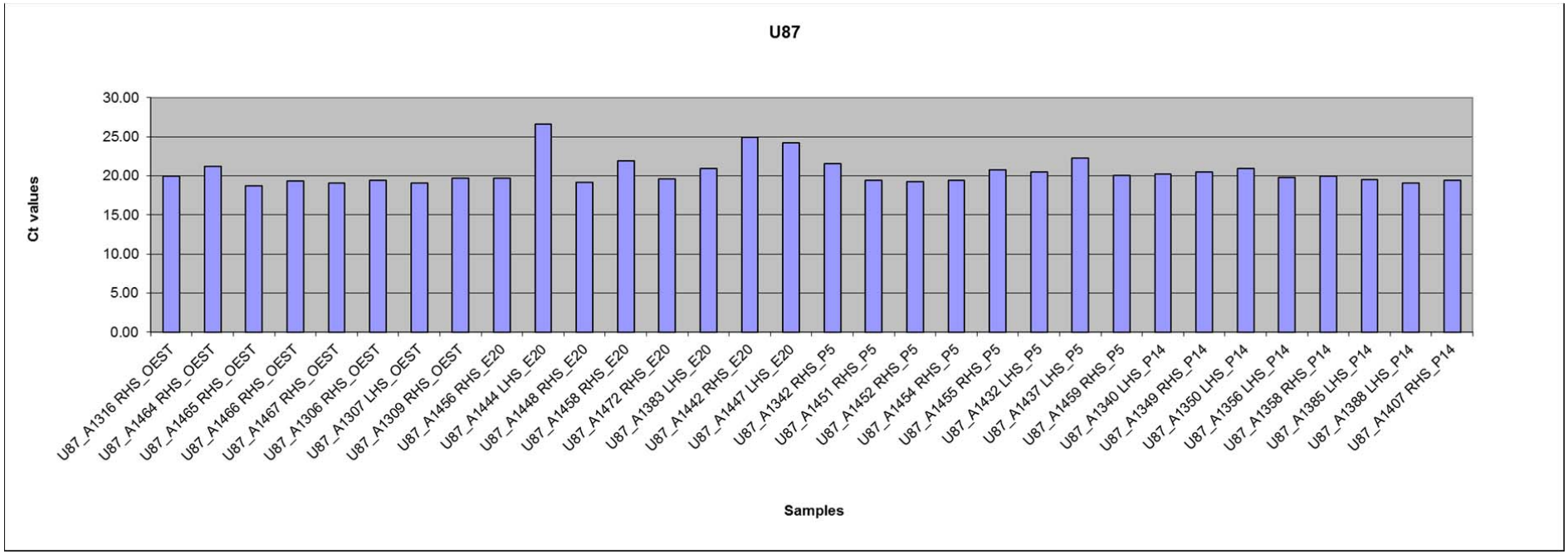

Reference List

Alberts B, Bray D, Hopkin K, Johnson A, Lewis J, Raff M, Roberts K, and Walter P. 2014a. Control of Gene Expression. In Essential Cell Biology. New York: Garland Science. p 261-287.

Alberts B, Bray D, Hopkin K, Johnson A, Lewis J, Raff M, Roberts K, and Walter P. 2014b. From DNA to Protein: How cells read the genome. In Essential Cell Biology. New York: Garland Science. p 223-259.

Alldred MJ, Lee SH, Petkova E, Ginsberg SD. 2015. Expression profile analysis of vulnerable CA1 pyramidal neurons in young-Middle-Aged Ts65Dn mice. J Comp Neurol 523:61-74.

Alm P, Bjorklund A, Owman C, Sjoberg NO, Thorbert G. 1977. Reduced tyrosine hydroxylase activity in guinea-pig uterus during pregnancy. Acta Physiol Scand Suppl 452:97-102.

Alm P, Bjorklund A, Owman C, Thorbert G. 1979. Tyrosine hydroxylase and DOPA decarboxylase activities in the guinea-pig uterus: further evidence for functional adrenergic denervation in association with pregnancy. Neuroscience 4:145-154.

Alm P, Lundberg LM. 1988. Co-existence and origin of peptidergic and adrenergic nerves in the guinea pig uterus. Retrograde tracing and immunocytochemistry, effects of chemical sympathectomy, capsaicin treatment and pregnancy. Cell Tissue Res 254:517-530.

Alm P, Lundberg LM, Wharton J, Polak JM. 1988. Organization of the guinea-pig uterine innervation. Distribution of immunoreactivities for different

neuronal markers. Effects of chemical- and pregnancy-induced sympathectomy. Histochem J 20:290-300.

Alm P, Owman C, Sjoberg NO, Stjernquist M, Sundler F. 1986. Histochemical demonstration of a concomitant reduction in neural vasoactive intestinal polypeptide, acetylcholinesterase, and noradrenaline of cat uterus during pregnancy. Neuroscience 18:713-726.

Alm P, Uvelius B, Ekstrom J, Holmqvist B, Larsson B, Andersson KE. 1995. Nitric oxide synthase-containing neurons in rat parasympathetic, sympathetic and sensory ganglia: a comparative study. Histochem J 27:819-831.

Aune B, Vartun A, Oian P, Sager G. 2000. Evidence of dysfunctional beta2-adrenoceptor signal system in pre-eclampsia. BJOG 107:116-121.

Bae SE, Corcoran BM, Watson ED. 2001. Immunohistochemical study of the distribution of adrenergic and peptidergic innervation in the equine uterus and the cervix. Reproduction 122:275-282.

Baljet B, Drukker J. 1980. The extrinsic innervation of the pelvic organs in the female rat. Acta Anat (Basel) 107:241-267.

Bastian I, Tam TS, Zhou XF, Kazenwadel J, Van der Hoek M, Michael MZ, Gibbins I, Haberberger RV. 2011. Differential expression of microRNA-1 in dorsal root ganglion neurons. Histochem Cell Biol 135:37-45.

Bicker S, Schratt G. 2008. microRNAs: tiny regulators of synapse function in development and disease. J Cell Mol Med 12:1466-1476.

Borda ES, Sterin-Borda L, Sterin-Speziale N, Gimeno MF, Gimeno AL. 1978. Functional pharmacological and morphological characteristics of two regions of rat uterine horns. Acta Physiol Lat Am 28:223-233.

Brauer MM, Chavez-Genaro R, Richeri A, Viettro L, Frias AI, Burnstock G, Cowen T. 2002. The oestrogenized rat myometrium inhibits organotypic sympathetic reinnervation. Auton Neurosci 101:13-22.

Bruce NW. 1976. The distribution of blood flow to the reproductive organs of rats near term. J Reprod Fertil 46:359-362.

Bushati N, Cohen SM. 2008. MicroRNAs in neurodegeneration. Curr Opin Neurobiol 18:292-296.

Chavez-Genaro R, Lombide P, Anesetti G. 2006. A quantitative study of rat uterine sympathetic innervation during pregnancy and post partum. Reprod Fertil Dev 18:525-531.

Cheng LC, Pastrana E, Tavazoie M, Doetsch F. 2009. miR-124 regulates adult neurogenesis in the subventricular zone stem cell niche. Nat Neurosci 12:399-408.

Chesley LC. 1975. Cardiovascular changes in pregnancy. Obstet Gynecol Annu 4:71-97.

Christensen J, Rick GA. 1987. Intrinsic nerves in the mammalian colon: confirmation of a plexus at the circular muscle-submucosal interface. J Auton Nerv Syst 21:223-231.

Christensen M, Schratt GM. 2009. microRNA involvement in developmental and functional aspects of the nervous system and in neurological diseases. Neurosci Lett 466:55-62.

Cowen T, Burnstock G. 1980. Quantitative analysis of the density and pattern of adrenergic innervation of blood vessels. A new method. Histochemie 66:19-34.

Croiset G, Nijsen MJ, Kamphuis PJ. 2000. Role of corticotropin-releasing factor, vasopressin and the autonomic nervous system in learning and memory. Eur J Pharmacol 405:225-234.

Dajas-Bailador F, Bonev B, Garcez P, Stanley P, Guillemot F, Papalopulu N. 2012. microRNA-9 regulates axon extension and branching by targeting Map1b in mouse cortical neurons. Nat Neurosci.

Davis R, Koelle GB. 1978. Electron microscope localization of acetylcholinesterase and butyrylcholinesterase in the superior cervical ganglion of the cat. I. Normal ganglion. J Cell Biol 78:785-809.

Enquobahrie DA, Abetew DF, Sorensen TK, Willoughby D, Chidambaram K, Williams MA. 2011. Placental microRNA expression in pregnancies complicated by preeclampsia. Am J Obstet Gynecol 204:178-21.

Faas MM, Schuiling GA, Baller JF, Visscher CA, Bakker WW. 1994. A new animal model for human preeclampsia: ultra-low-dose endotoxin infusion in pregnant rats. Am J Obstet Gynecol 171:158-164.

Falck B, Hillarp NA, Thieme G, Torp A. 1982. Fluorescence of catechol amines and related compounds condensed with formaldehyde. Brain Res Bull 9:xi-xv.

Fried G, Hokfelt T, Lundberg JM, Terenius L, Hamberger L. 1986. Neuropeptide Y and noradrenaline in human uterus and myometrium during normal and pre-eclamptic pregnancy. Hum Reprod 1:359-364.

Fried G, Hokfelt T, Terenius L, Goldstein M. 1985. Neuropeptide Y (NPY)-like immunoreactivity in guinea pig uterus is reduced during pregnancy in parallel with noradrenergic nerves. Histochemie 83:437-442.

Fried G, Thoresen M. 1990. Effects of neuropeptide Y and noradrenaline on uterine artery blood pressure and blood flow velocity in the pregnant guinea-pig. Regul Pept 28:1-9.

Giraldez AJ, Cinalli RM, Glasner ME, Enright AJ, Thomson JM, Baskerville S, Hammond SM, Bartel DP, Schier AF. 2005. MicroRNAs regulate brain morphogenesis in zebrafish. Science 308:833-838.

Gnanamanickam GJ, Llewellyn-Smith IJ. 2011. Innervation of the rat uterus at estrus: a study in full-thickness, immunoperoxidase-stained whole-mount preparations. J Comp Neurol 519:621-643.

Gogolevskaya IK, Makarova JA, Gause LN, Kulichkova VA, Konstantinova IM, Kramerov DA. 2002. U87 RNA, a novel C/D box small nucleolar RNA from mammalian cells. Gene 292:199-204.

Granger JP, LaMarca BB, Cockrell K, Sedeek M, Balzi C, Chandler D, Bennett W. 2006. Reduced uterine perfusion pressure (RUPP) model for studying cardiovascular-renal dysfunction in response to placental ischemia. Methods Mol Med 122:383-392.

Gu J, Polak JM, Su HC, Blank MA, Morrison JF, Bloom SR. 1984. Demonstration of paracervical ganglion origin for the vasoactive intestinal peptide-containing nerves of the rat uterus using retrograde tracing techniques combined with immunocytochemistry and denervation procedures. Neurosci Lett 51:377-382.

Guenther AE, Conley AJ, Van Orden DE, Farley DB, Ford SP. 1988. Structural and mechanical changes of uterine arteries during pregnancy in the pig. J Anim Sci 66:3144-3152.

Haase EB, Buchman J, Tietz AE, Schramm LP. 1997. Pregnancy-induced uterine neuronal degeneration in the rat. Cell Tissue Res 288:293-306.

Han L, Wen Z, Lynn RC, Baudet ML, Holt CE, Sasaki Y, Bassell GJ, Zheng JQ. 2011. Regulation of chemotropic guidance of nerve growth cones by microRNA. Mol Brain 4:40.

Hancock ML, Preitner N, Quan J, Flanagan JG. 2014. MicroRNA-132 is enriched in developing axons, locally regulates Rasa1 mRNA, and promotes axon extension. J Neurosci 34:66-78.

Harraz MM, Dawson TM, Dawson VL. 2011. MicroRNAs in Parkinson's disease. J Chem Neuroanat 42:142-156.

Hawkins SM, Andreu-Vieyra CV, Kim TH, Jeong JW, Hodgson MC, Chen R, Creighton CJ, Lydon JP, Gunaratne PH, DeMayo FJ, Matzuk MM. 2012. Dysregulation of uterine signaling pathways in progesterone receptor-Cre knockout of dicer. Mol Endocrinol 26:1552-1566.

Hebert SS, Horre K, Nicolai L, Papadopoulou AS, Mandemakers W, Silahtaroglu AN, Kauppinen S, Delacourte A, De SB. 2008. Loss of microRNA cluster miR-29a/b-1 in sporadic Alzheimer's disease correlates with increased BACE1/beta-secretase expression. Proc Natl Acad Sci U S A 105:6415-6420.

Houdeau E, Prud'homme MJ, Rousseau A, Rousseau JP. 1995. Distribution of noradrenergic neurons in the female rat pelvic plexus and involvement in the genital tract innervation. J Auton Nerv Syst 54:113-125.

Houdeau E, Rousseau A, Meusnier C, Prud'homme MJ, Rousseau JP. 1998. Sympathetic innervation of the upper and lower regions of the uterus and

cervix in the rat have different origins and routes. J Comp Neurol 399:403-412.

Jones RE and Lopez KH. 2006. The female reproductive system. In Jones RE and Lopez KH, editors. Human Reproductive Biology. China: Academic Press. p 31-72.

Kawahara H, Imai T, Okano H. 2012. MicroRNAs in Neural Stem Cells and Neurogenesis. Front Neurosci 6:30.

Kawase-Koga Y, Low R, Otaegi G, Pollock A, Deng H, Eisenhaber F, Maurer-Stroh S, Sun T. 2010. RNAase-III enzyme Dicer maintains signaling pathways for differentiation and survival in mouse cortical neural stem cells. J Cell Sci 123:586-594.

Khatun S, Kanayama N, Belayet HM, Bhuiyan AB, Jahan S, Begum A, Kobayashi T, Terao T. 2000. Increased concentrations of plasma neuropeptide Y in patients with eclampsia and preeclampsia. Am J Obstet Gynecol 182:896-900.

Khatun S, Kanayama N, Hossain B, el ME, Kobayashi T, Jahan S, Bhuiyan AB, Terao T. 1997. Increased concentrations of plasma epinephrine and norepinephrine in patients with eclampsia. Eur J Obstet Gynecol Reprod Biol 74:103-109.

Klukovits A, Gaspar R, Santha P, Jancso G, Falkay G. 2002. Functional and histochemical characterization of a uterine adrenergic denervation process in pregnant rats. Biol Reprod 67:1013-1017.

Kosik KS. 2006. The neuronal microRNA system. Nat Rev Neurosci 7:911-920.

Krizsan-Agbas D, Pedchenko T, Smith PG. 2008. Neurotrimin is an estrogen-regulated determinant of peripheral sympathetic innervation. J Neurosci Res 86:3086-3095.

Lampinen KH, Ronnback M, Groop PH, Nicholls MG, Yandle TG, Kaaja RJ. 2014. Increased plasma norepinephrine levels in previously pre-eclamptic women. J Hum Hypertens 28:269-273.

Landreth GE and . 2006. Growth Factors. In Siegel GJ, Albers RE, Brady ST, and Price DL, editors. Basic Neurochemistry. New York: Academic Press. p 471-484.

Latini C, Frontini A, Morroni M, Marzioni D, Castellucci M, Smith PG. 2008. Remodeling of uterine innervation. Cell Tissue Res 334:1-6.

Lee ST, Chu K, Im WS, Yoon HJ, Im JY, Park JE, Park KH, Jung KH, Lee SK, Kim M, Roh JK. 2011. Altered microRNA regulation in Huntington's disease models. Exp Neurol 227:172-179.

Leeman L, Fontaine P. 2008. Hypertensive disorders of pregnancy. Am Fam Physician 78:93-100.

Li Q, Dale WE, Hasser EM, Blaine EH. 1996. Acute and chronic angiotensin hypertension: neural and nonneural components, time course, and dose dependency. Am J Physiol 271:R200-R207.

Li X, Jin P. 2010. Roles of small regulatory RNAs in determining neuronal identity. Nat Rev Neurosci 11:329-338.

Li YY, Cui JG, Hill JM, Bhattacharjee S, Zhao Y, Lukiw WJ. 2011. Increased expression of miRNA-146a in Alzheimer's disease transgenic mouse models. Neurosci Lett 487:94-98.

Li Z, He X, Feng J. 2012. Dicer is essential for neuronal polarity. Int J Dev Neurosci 30:607-611.

Lin G, Shindel AW, Fandel TM, Bella AJ, Lin CS, Lue TF. 2010. Neurotrophic effects of brain-derived neurotrophic factor and vascular endothelial growth factor in major pelvic ganglia of young and aged rats. BJU Int 105:114-120.

Llewellyn-Smith IJ, DiCarlo SE, Collins HL, Keast JR. 2005. Enkephalin-immunoreactive interneurons extensively innervate sympathetic preganglionic neurons regulating the pelvic viscera. J Comp Neurol 488:278-289.

Llewellyn-Smith IJ, Furness JB, Gibbins IL, Costa M. 1988. Quantitative ultrastructural analysis of enkephalin-, substance P-, and VIP-immunoreactive nerve fibers in the circular muscle of the guinea pig small intestine. J Comp Neurol 272:139-148.

Llewellyn-Smith IJ, Gnanamanickam GJ. 2011. Immunoperoxidase detection of neuronal antigens in full-thickness whole mount preparations of hollow organs and thick sections of central nervous tissue. J Neurosci Methods 196:1-11.

Llewellyn-Smith IJ, Minson JB, Morilak DA, Oliver JR, Chalmers JP. 1990. Neuropeptide Y-immunoreactive synapses in the intermediolateral cell column of rat and rabbit thoracic spinal cord. Neurosci Lett 108:243-248.

Lobos E, Gebhardt C, Kluge A, Spanel-Borowski K. 2005. Expression of nerve growth factor (NGF) isoforms in the rat uterus during pregnancy: accumulation of precursor proNGF. Endocrinology 146:1922-1929.

Makris A, Thornton C, Thompson J, Thomson S, Martin R, Ogle R, Waugh R, McKenzie P, Kirwan P, Hennessy A. 2007. Uteroplacental ischemia results in proteinuric hypertension and elevated sFLT-1. Kidney Int 71:977-984.

Manyonda IT, Slater DM, Fenske C, Hole D, Choy MY, Wilson C. 1998. A role for noradrenaline in pre-eclampsia: towards a unifying hypothesis for the pathophysiology. Br J Obstet Gynaecol 105:641-648.

Markiewicz W, Jaroszewski JJ, Bossowska A, Majewski M. 2003. NPY: its occurrence and relevance in the female reproductive system. Folia Histochem Cytobiol 41:183-192.

Marler KJ, Suetterlin P, Dopplapudi A, Rubikaite A, Adnan J, Maiorano NA, Lowe AS, Thompson ID, Pathania M, Bordey A, Fulga T, Van Vactor DL, Hindges R, Drescher U. 2014. BDNF promotes axon branching of retinal ganglion cells via miRNA-132 and p250GAP. J Neurosci 34:969-979.

Massmann GA, Zhang J, Figueroa JP. 1999. Functional and molecular characterization of nitric oxide synthase in the endometrium and myometrium of pregnant sheep during the last third of gestation. Am J Obstet Gynecol 181:116-125.

Maynard SE, Min JY, Merchan J, Lim KH, Li J, Mondal S, Libermann TA, Morgan JP, Sellke FW, Stillman IE, Epstein FH, Sukhatme VP, Karumanchi SA. 2003. Excess placental soluble fms-like tyrosine kinase 1 (sFlt1) may contribute to endothelial dysfunction, hypertension, and proteinuria in preeclampsia. J Clin Invest 111:649-658.

Mayor-Lynn K, Toloubeydokhti T, Cruz AC, Chegini N. 2011. Expression profile of microRNAs and mRNAs in human placentas from pregnancies complicated by preeclampsia and preterm labor. Reprod Sci 18:46-56.

Melton CE, Saldivar JT. 1967. The linea uteri, a conduction pathway in rat myometrium. Life Sci 6:297-304.

Mione MC, Cavallotti C, Burnstock G, Amenta F. 1988. The peptidergic innervation of the guinea pig uterine artery in pregnancy. Basic Appl Histochem 32:153-159.

Mione MC, Cavanagh JF, Lincoln J, Milner P, Burnstock G. 1990. Pregnancy reduces noradrenaline but not neuropeptide levels in the uterine artery of the guinea-pig. Cell Tissue Res 259:503-509.

Mione MC, Gabella G. 1991. Nerve fibres in the uterine artery increase in number in pregnant guinea-pigs. NeuroReport 2:537-540.

Mitchell BS, Ahmed E. 1992. An immunohistochemical study of the catecholamine synthesizing enzymes and neuropeptides in the female guinea-pig uterus and vagina. Histochem J 24:361-367.

Morales Prieto DM, Markert UR. 2011. MicroRNAs in pregnancy. J Reprod Immunol 88:106-111.

Moustafa FA. 1988. Changes in cholinergic and noradrenergic nerves in the pregnant and postpartum uterus of the albino rat and guinea pig. Acta Anat (Basel) 132:310-316.

Nakanishi H, McLean J, Wood E, Burnstock G. 1969. The role of sympathetic nerves in control of the nonpregnant and pregnant human uterus. The Journal of Reproductive Medicine 2:20-33.

Natera-Naranjo O, Aschrafi A, Gioio AE, Kaplan BB. 2010. Identification and quantitative analyses of microRNAs located in the distal axons of sympathetic neurons. RNA 16:1516-1529.

Natuzzi ES, Ursell PC, Harrison M, Buscher C, Riemer RK. 1993. Nitric oxide synthase activity in the pregnant uterus decreases at parturition. Biochem Biophys Res Commun 194:1-8.

Nelson-Piercy C. 2003. Pre-eclampsia: The women at risk. In Critchley H, MacLean A, Poston L, and Walker J, editors. Pre-eclampsia. London: RCOG Press. p 342-353.

Noori M, Savvidou M, and Willams D. 2007. Endothelial factors. In Lyall F and Belfort M, editors. Pre-eclampsia Etiology and Clinical Practice. Cambridge, UK: Cambridge University Press. p 50-77.

Norman JE, Thompson AJ, Telfer JF, Young A, Greer IA, Cameron IT. 1999. Myometrial constitutive nitric oxide synthase expression is increased during human pregnancy. Mol Hum Reprod 5:175-181.

Oian P, Kjeldsen SE, Eide I, Norman N. 1985. Adrenaline and preeclampsia. Acta Med Scand Suppl 693:29-32.

Oliveira FS, Nessler RA, Castania JA, Salgado HC, Fazan VP. 2013. Ultrastructural and morphometric alterations in the aortic depressor nerve of rats due to long term experimental diabetes: Effects of insulin treatment. Brain Res 1491:197-203.

Ong SS, Baker PN, Mayhew TM, Dunn WR. 2005. Remodeling of myometrial radial arteries in preeclampsia. Am J Obstet Gynecol 192:572-579.

Orshal JM, Khalil RA. 2004. Reduced endothelial NO-cGMP-mediated vascular relaxation and hypertension in IL-6-infused pregnant rats. Hypertension 43:434-444.

Ortega-Villalobos M, Garcia-Bazan M, Solano-Flores LP, Ninomiya-Alarcon JG, Guevara-Guzman R, Wayner MJ. 1990. Vagus nerve afferent and efferent innervation of the rat uterus: an electrophysiological and HRP study. Brain Res Bull 25:365-371.

Osol G, Mandala M. 2009. Maternal uterine vascular remodeling during pregnancy. Physiology (Bethesda) 24:58-71.

Owman C, Alm P, Bjorklund A, Thorbert G. 1980. Extensive sympathetic denervation of the uterus during pregnancy as evidenced by tyrosine hydroxylase determinations in the guinea pig. Adv Biochem Psychopharmacol 25:313-320.

Owman C, Alm P, Rosengren E, Sjoberg N, Thorbert G. 1975. Variations in the level of uterine norepinephrine during pregnancy in the guinea pig. Am J Obstet Gynecol 122:961-964.

Owman C and Stjernquist M. 1988. Origin, distribution and functional aspects of aminergic and peptidergic nerves in the male and female reproductive tracts. In Bjorklund A, Hokfelt T, and Owman C, editors. Handbook of Chemical Neuroanatomy Volume 6: The Peripheral Nervous System. New York: Elsevier. p 445-544.

Owman C, Stjernquist M, Helm G, Kannisto P, Sjoberg NO, Sundler F. 1986. Comparative histochemical distribution of nerve fibres storing noradrenaline and neuropeptide Y (NPY) in human ovary, fallopian tube, and uterus. Med Biol 64:57-65.

Page EW. 1939. The relation between hydatid moles, relative ischemia of teh gravid uterus, and the placental origin of eclampsia. American Journal of Obstetrics and Gynecology 37:291-293.

Page KL, Celia G, Leddy G, Taatjes DJ, Osol G. 2002. Structural remodeling of rat uterine veins in pregnancy. Am J Obstet Gynecol 187:1647-1652.

Pan M, Ge Q, Li H, Yang Q, Lu J, Zhang D, Lu Z. 2012. Sequencing the miRNAs in maternal plasma from women before and after parturition. J Nanosci Nanotechnol 12:4035-4043.

Papka RE, Cotton JP, Traurig HH. 1985. Comparative distribution of neuropeptide tyrosine-, vasoactive intestinal polypeptide-, substance P-immunoreactive, acetylcholinesterase-positive and noradrenergic nerves in the reproductive tract of the female rat. Cell Tissue Res 242:475-490.

Papka RE, McNeill DL, Thompson D, Schmidt HH. 1995. Nitric oxide nerves in the uterus are parasympathetic, sensory, and contain neuropeptides. Cell Tissue Res 279:339-349.

Papka RE, Thompson BD, Schmidt HH. 1996. Identification of uterine-related sympathetic neurons in the rat inferior mesenteric ganglion: neurotransmitter content and afferent input. J Auton Nerv Syst 59:51-59.

Papka RE, Traurig HH, Klenn P. 1987. Paracervical ganglia of the female rat: histochemistry and immunohistochemistry of neurons, SIF cells, and nerve terminals. Am J Anat 179:243-257.

Papka RE, Traurig HH, Schemann M, Collins J, Copelin T, Wilson K. 1999. Cholinergic neurons of the pelvic autonomic ganglia and uterus of the female rat: distribution of axons and presence of muscarinic receptors. Cell Tissue Res 296:293-305.

Pineles BL, Romero R, Montenegro D, Tarca AL, Han YM, Kim YM, Draghici S, Espinoza J, Kusanovic JP, Mittal P, Hassan SS, Kim CJ. 2007. Distinct subsets of microRNAs are expressed differentially in the human placentas of patients with preeclampsia. Am J Obstet Gynecol 196:261-266.

Quinn M. 2005. Pre-eclampsia and partial uterine denervation. Med Hypotheses 64:449-454.

Redman CW. 1991. Current topic: pre-eclampsia and the placenta. Placenta 12:301-308.

Redman CW, Sargent IL. 2009. Placental stress and pre-eclampsia: a revised view. Placenta 30 Suppl A:S38-S42.

Richeri A, Bianchimano P, Marmol NM, Viettro L, Cowen T, Brauer MM. 2005. Plasticity in rat uterine sympathetic nerves: the role of TrkA and p75 nerve growth factor receptors. J Anat 207:125-134.

Riemer RK, Buscher C, Bansal RK, Black SM, He Y, Natuzzi ES. 1997. Increased expression of nitric oxide synthase in the myometrium of the pregnant rat uterus. Am J Physiol 272:E1008-E1015.

Roberts JM. 2003. Pre-eclampsia: A two stage disorder. In Critchley H, MacLean A, Poston L, and Walker J, editors. Pre-eclampsia. London: RCOG Press. p 66-78.

Roberts JM, Pearson G, Cutler J, Lindheimer M. 2003. Summary of the NHLBI Working Group on Research on Hypertension During Pregnancy. Hypertension 41:437-445.

Saba R, Schratt GM. 2010. MicroRNAs in neuronal development, function and dysfunction. Brain Res 1338:3-13.

Satoh J. 2010. MicroRNAs and their therapeutic potential for human diseases: aberrant microRNA expression in Alzheimer's disease brains. J Pharmacol Sci 114:269-275.

Schobel HP, Fischer T, Heuszer K, Geiger H, Schmieder RE. 1996. Preeclampsia -- a state of sympathetic overactivity. N Engl J Med 335:1480-1485.

Schratt G and Greenberg M. 2008. MicroRNA function in the nervous system. In Appasani K, editor. MicroRNAs: From basic science to disease biology. Cambridge: Cambridge University Press. p 115-128.

Schratt GM, Tuebing F, Nigh EA, Kane CG, Sabatini ME, Kiebler M, Greenberg ME. 2006. A brain-specific microRNA regulates dendritic spine development. Nature 439:283-289.

Serghini R, Prud'homme MJ, Vaudry H, Rousseau JP. 1997. Involvement of the pelvic plexus and the suprarenal ganglia in the neuropeptide Y (NPY) innervation of the cervix and the uterus of the rat. J Auton Nerv Syst 67:38-50.

Shew RL, Papka RE, McNeill DL. 1990. Calcitonin gene-related peptide in the rat uterus: presence in nerves and effects on uterine contraction. Peptides 11:583-589.

Shew RL, Papka RE, McNeill DL. 1991. Substance P and calcitonin gene-related peptide immunoreactivity in nerves of the rat uterus: localization, colocalization and effects on uterine contractility. Peptides 12:593-600.

Shew RL, Papka RE, McNeill DL. 1992. Galanin and calcitonin gene-related peptide immunoreactivity in nerves of the rat uterus: localization, colocalization, and effects on uterine contractility. Peptides 13:273-279.

Shi Z, Arai KY, Jin W, Weng Q, Watanabe G, Suzuki AK, Taya K. 2006. Expression of nerve growth factor and its receptors NTRK1 and TNFRSF1B is regulated by estrogen and progesterone in the uteri of golden hamsters. Biol Reprod 74:850-856.

Sigger JN, Harding R, Summers RJ. 1986. Changes in the innervation and catecholamine concentrations in the myometrium of pregnant and non-pregnant sheep. Acta Anat (Basel) 125:101-107.

Simon P. 2003. Q-Gene: processing quantitative real-time RT-PCR data. Bioinformatics 19:1439-1440.

Sofroniew MV, Howe CL, Mobley WC. 2001. Nerve growth factor signaling, neuroprotection, and neural repair. Annu Rev Neurosci 24:1217-1281.

Sporrong B, Alm P, Owman C, Sjoberg NO, Thorbert G. 1981. Pregnancy is associated with extensive adrenergic nerve degeneration in the uterus. An electronmicroscopic study in the guinea-pig. Neuroscience 6:1119-1126.

Strickland IT, Richards L, Holmes FE, Wynick D, Uney JB, Wong LF. 2011. Axotomy-induced miR-21 promotes axon growth in adult dorsal root ganglion neurons. PLoS One 6:e23423.

Subramanian M, Holt AG, Mueller PJ. 2014. Physical activity correlates with glutamate receptor gene expression in spinally-projecting RVLM neurons: a laser capture microdissection study. Brain Res 1585:51-62.

Sun AX, Crabtree GR, Yoo AS. 2013. MicroRNAs: regulators of neuronal fate. Curr Opin Cell Biol 25:215-221.

Sunderland N, Hennessy A, Makris A. 2011a. Animal models of pre-eclampsia. Am J Reprod Immunol 65:533-541.

Sunderland NS, Thomson SE, Heffernan SJ, Lim S, Thompson J, Ogle R, McKenzie P, Kirwan PJ, Makris A, Hennessy A. 2011b. Tumor necrosis factor alpha induces a model of preeclampsia in pregnant baboons (Papio hamadryas). Cytokine 56:192-199.

Swiet M. 2003. What are we talking about? Definitions. In Critchley H, MacLean A, Poston L, and Walker J, editors. Pre-eclampsia. London: RCOG Press. p 3-11.

Takimoto E, Ishida J, Sugiyama F, Horiguchi H, Murakami K, Fukamizu A. 1996. Hypertension induced in pregnant mice by placental renin and maternal angiotensinogen. Science 274:995-998.

Tam TS, Bastian I, Zhou XF, Vander HM, Michael MZ, Gibbins IL, Haberberger RV. 2011. MicroRNA-143 expression in dorsal root ganglion neurons. Cell Tissue Res 346:163-173.

Tang Q, Wu W, Xu X, Huang L, Gao Q, Chen H, Sun H, Xia Y, Sha J, Wang X, Chen D, Xu Q. 2013. miR-141 Contributes to Fetal Growth Restriction by Regulating PLAG1 Expression. PLoS One 8:e58737.

Tervo K, Tervo T, Palkama A. 1978. Pre- and postnatal development of catecholamine-containing and cholinesterase-positive nerves of the rat cornea and iris. Anat Embryol (Berl) 154:253-265.

Thomson AJ, Telfer JF, Kohnen G, Young A, Cameron IT, Greer IA, Norman JE. 1997. Nitric oxide synthase activity and localization do not change in uterus and placenta during human parturition. Hum Reprod 12:2546-2552.

Thorbert G, Alm P, Bjorklund AB, Owman C, Sjoberg NO. 1979. Adrenergic innervation of the human uterus. Disappearance of the transmitter and

transmitter-forming enzymes during pregnancy. Am J Obstet Gynecol 135:223-226.

Thorbert G, Alm P, Owman C, Sjoberg NO. 1977. Regional distribution of autonomic nerves in guinea pig uterus. Am J Physiol 233:C25-C34.

Thorbert G, Alm P, Owman C, Sjoberg NO, Sporrong B. 1978. Regional changes in structural and functional integrity of myometrial adrenergic nerves in pregnant guinea-pig, and their relationship to the localization of the conceptus. Acta Physiol Scand 103:120-131.

Traurig H, Saria A, Lembeck F. 1984. Substance P in primary afferent neurons of the female rat reproductive system. Naunyn Schmiedebergs Arch Pharmacol 326:343-346.

Traurig HH and Papka RE. 1993. Autonomic efferent and visceral sensory innervation of the female reproductive system: special reference to the functional roles of nerves in reproductive organs. In Maggi CA, editor. Nervous Control of the Urogenital System. Chur: Harwood Academic Publishers. p 103-142.

Traurig HH, Papka RE, Shew RL. 1991. Substance P and related peptides associated with the afferent and autonomic innervation of the uterus. Ann N Y Acad Sci 632:304-313.

VanWijk MJ, Kublickiene K, Boer K, VanBavel E. 2000. Vascular function in preeclampsia. Cardiovasc Res 47:38-48.

Varol FG, Duchemin AM, Neff NH, Hadjiconstantinou M. 2000. Nerve growth factor (NGF) and NGF mRNA change in rat uterus during pregnancy. Neurosci Lett 294:58-62.

Venkatesha S, Toporsian M, Lam C, Hanai J, Mammoto T, Kim YM, Bdolah Y, Lim KH, Yuan HT, Libermann TA, Stillman IE, Roberts D, D'Amore PA, Epstein FH, Sellke FW, Romero R, Sukhatme VP, Letarte M, Karumanchi SA. 2006. Soluble endoglin contributes to the pathogenesis of preeclampsia. Nat Med 12:642-649.

Vera PL, Haase EB, Schramm LP. 1997. Origins of the sympathetic innervation of the cervical end of the uterus in the rat. Brain Res 747:140-143.

Villar J, Say L, Gulmezoglu AM, Merialdi M, Lindheimer MD, Betran AP, and Piaggio G. 2003. Eclampsia and pre-eclampsia: A health problem for 2000 years. In Critchley H, MacLean A, Poston L, and Walker J, editors. Pre-eclampsia. London: RCOG Press. p 66-78.

Visvanathan J, Lee S, Lee B, Lee JW, Lee SK. 2007. The microRNA miR-124 antagonizes the anti-neural REST/SCP1 pathway during embryonic CNS development. Genes Dev 21:744-749.

Wanigasekara Y, Keast JR. 2005. Neurturin has multiple neurotrophic effects on adult rat sacral parasympathetic ganglion neurons. Eur J Neurosci 22:595-604.

Weishaupt N, Blesch A, Fouad K. 2012. BDNF: the career of a multifaceted neurotrophin in spinal cord injury. Exp Neurol 238:254-264.

Wong AW, Yeung KP, Payne SC, Keast JR, Osborne PB. 2015. Neurite outgrowth in normal and injured primary sensory neurons reveals different regulation by nerve growth factor (NGF) and artemin. Mol Cell Neurosci 65:125-134.

Wu D, Raafat A, Pak E, Clemens S, Murashov AK. 2012. Dicer-microRNA pathway is critical for peripheral nerve regeneration and functional recovery in vivo and regenerative axonogenesis in vitro. Exp Neurol 233:555-565.

Young BC, Levine RJ, Karumanchi SA. 2010. Pathogenesis of preeclampsia. Annu Rev Pathol 5:173-192.

Yu YM, Gibbs KM, Davila J, Campbell N, Sung S, Todorova TI, Otsuka S, Sabaawy HE, Hart RP, Schachner M. 2011. MicroRNA miR-133b is essential for functional recovery after spinal cord injury in adult zebrafish. Eur J Neurosci 33:1587-1597.

Zhang HY, Zheng SJ, Zhao JH, Zhao W, Zheng LF, Zhao D, Li JM, Zhang XF, Chen ZB, Yi XN. 2011a. MicroRNAs 144, 145, and 214 are down-regulated in primary neurons responding to sciatic nerve transection. Brain Res 1383:62-70.

Zhang J, Zhang J, Liu LH, Zhou Y, Li YP, Shao ZH, Wu YJ, Li MJ, Fan YY, Shi HJ. 2011b. Effects of miR-541 on neurite outgrowth during neuronal differentiation. Cell Biochem Funct 29:279-286.

Zhou S, Shen D, Wang Y, Gong L, Tang X, Yu B, Gu X, Ding F. 2012. microRNA-222 targeting PTEN promotes neurite outgrowth from adult dorsal root ganglion neurons following sciatic nerve transection. PLoS One 7:e44768.

Zoubina EV, Fan Q, Smith PG. 1998. Variations in uterine innervation during the estrous cycle in rat. J Comp Neurol 397:561-571.

Zoubina EV, Mize AL, Alper RH, Smith PG. 2001. Acute and chronic estrogen supplementation decreases uterine sympathetic innervation in ovariectomized adult virgin rats. Histol Histopathol 16:989-996.

Zoubina EV, Smith PG. 2000. Axonal degeneration and regeneration in rat uterus during the estrous cycle. Auton Neurosci 84:176-185.

Zoubina EV, Smith PG. 2001. Sympathetic hyperinnervation of the uterus in the estrogen receptor alpha knock-out mouse. Neuroscience 103:237-244.

Zupko I, Csonka D, Falkay G. 2005. A rat model for functional characterization of pregnancy-induced denervation and postpartum reinnervation in the myometrium and cervix: a superfusion study. Reproduction 130:743-749.

Zuspan FP, O'Shaughnessy R, Iams JD. 1981. The role of the adrenal gland and sympathetic nervous system in pregnancy. J Reprod Med 26:483-491.